Schriftenreihe IWAR

268

TECHNISCHE UNIVERSITÄT DARMSTADT

IWAR

Robert Lutze

Application of an Anaerobic Membrane Bioreactor for the Treatment of Lipid-rich Sludges

Herausgeber:
Verein zur Förderung des Instituts IWAR der TU Darmstadt e. V.

Application of an Anaerobic Membrane Bioreactor for the Treatment of Lipid-rich Sludges

Vom Fachbereich Bau- und Umweltingenieurwissenschaften
der Technischen Universität Darmstadt
zur Erlangung des akademischen Grades eines
Doktor-Ingenieurs (Dr.-Ing.) genehmigte Dissertation

von

Dipl.-Ing. Robert Lutze
aus Berlin

Erstgutachter: Prof. Dr.-Ing. Markus Engelhart
Zweitgutachter: Prof. Dr.-Ing. Jörg Krampe

Darmstadt 2021
D 17

Robert Lutze

Application of an Anaerobic Membrane Bioreactor for the Treatment of Lipid-rich Sludges.

Darmstadt, Technische Universität Darmstadt
Jahr der Veröffentlichung der Dissertation auf TUprints: 2021

URN: nbn:de:tuda-tuprints-198046
URI: https://tuprints.ulb.tu-darmstadt.de/id/eprint/19804

Hrsg.: Verein zur Förderung des Instituts IWAR der TU Darmstadt e. V.
Darmstadt: Eigenverlag, 2021
(Schriftenreihe IWAR 268)

ISSN 0721-5282
ISBN 978-3-940897-69-5

Referent : Prof. Dr.-Ing. Markus Engelhart
Korreferent: Prof. Dr.-Ing. Jörg Krampe

Tag der schriftlichen Einreichung: 25.11.2020
Tag der mündlichen Prüfung: 21.01.2021

Veröffentlichung unter CC BY-SA
https://creativecommons.org/licenses/

Alle Rechte vorbehalten. Wiedergabe nur mit Genehmigung des Vereins zur Förderung des Instituts IWAR der Technischen Universität Darmstadt e. V., c/o Institut IWAR, Franziska-Braun-Str. 7, 64287 Darmstadt.

Herstellung: Lasertype GmbH
Holzhofallee 19
64295 Darmstadt
IWAR

Vertrieb: Institut
TU Darmstadt
Franziska-Braun-Straße 7
64287 Darmstadt
Telefon: 06151 / 16 20301
Telefax: 06151 / 16 20305

Abstract

Anaerobic membrane bioreactors (AnMBRs) may provide a sustainable technological solution to overcome limitations of lipid-rich sludge digestion in industrial WWTPs. These digesters combine extensive removal of organic matter and sufficient process stability with reduced reactor volumes. However, membrane fouling and a decrease in biomass activity due to exposure to high shear forces may limit successful application.

This study characterises biological removal kinetics, limitations of anaerobic digestion of lipid-rich sludge, effects of shear stress on biomass activity and membrane performance. The study was carried out using a pilot-scale anaerobic digestion plant equipped with recuperative thickening by ceramic discs installed on a rotating hollow shaft. The membranes had a mean pore size of 0.2 µm and were operated at mean cross-flow velocities between 3.3 - 4.1 m/s. CSTRs were additionally operated for comparison of removal performance. A mixture of WAS from a municipal WWTP and flotation sludge from dairy industry was used as feed.

In AnMBR and CSTR, COD removal and methane yields followed substrate first-order kinetics. COD removal of AnMBR corresponded to the performance of CSTR at similar SRT but AnMBR was operated with higher OLRs and reduced HRT. At high COD related shares of flotation sludge over COD_{flot}/COD_{total} = 0.85, CSTR could be operated with a maximum $OLR_{COD,deg}$ = 8.3 kg COD/(m³·d) at SRT = 15 d while $OLR_{COD,deg}$ of 11.2 kg COD/(m³·d) did not lead to process instabilities using an AnMBR with HRT = 10 d and SRT = 15 d.

Process limitations, emerging inhibitions and process instabilities were clearly shown by the relationship between SMA measurements and mean COD removal rates. Activity losses of acetoclastic methanogens based on exposure to high shear required for mitigating fouling on the membranes were not observed. A decisive influence on process stability had especially the degradable lipid content in the anaerobic sludge. Inhibition on acetoclastic methanogens started at lipid contents of 50 mg lipid/ g TS while the digestion process remained stable up to 150 mg lipid/ g TS. Lower degradable lipid content in the anaerobic sludge can be achieved with elevated SRT or reduced shares of lipid-rich substrates. Hence, AnMBR can offer a higher process stability compared to CSTR at even HRT when extending the SRT. Common design criteria such as the OLR or the lipid-related sludge load did not assure a stable or efficient digestion process. Owing to the limitations on the applicability of existing design parameters, a generally valid design criterion for lipid-rich digestion – the maximum degradable lipid content in the anaerobic sludge – was elaborated. This criterion refers to the current state of knowledge on LCFA inhibition that inhibition of methanogens is initiated by the LCFA concentration related to the TS content in the sludge.

In the field of sludge digestion, membrane performance in terms of the critical flux depends in particular on the apparent dynamic viscosity as decisive sludge (characteristic) parameter. A higher apparent viscosity reduces the flux. The characteristic sludge parameters TS, VS and CST did not exhibit a clear correlation to the critical flux but showed correct tendencies. The correlation between apparent viscosity and critical flux can be significantly improved by integrating the present shear rate on the membrane surface (R^2 = 0.9). Filtration performance can be improved by increasing the rotational speed of the membrane and adding Fe salts (here $FeCl_2$) to the sludge, as they affect shear stress on the membrane disc and apparent dynamic viscosity, respectively. An increase of mean cross-flow velocity from 3.8 to 4.1 m/s improved

the critical flux by 20 %. The addition of Ferric salts (70 L $FeCl_2$ 20 % per t TS) improved the critical flux up to 30 %. A maximum critical flux up to 17 L/(m²·h) was achieved when filtrating sludge with TS ≈ 3.2 %. At TS ≈ 4.0 % and TS ≈ 4.6 %, critical fluxes of around 9 L/(m²·h) and 7 L/(m²·h) were observed.

In order to realise an economic advantage of AnMBR using rotating disc filters, specific membrane costs need to decrease noticeably. Membrane operation with higher net flux corresponding to less membrane surface required and lower costs results in case of lower TS concentration of the anaerobic sludge. This effect is especially pronounced in applications treating high shares of easily degradable substrates such as flotation sludge. Compared to conventional digesters additional energy demand for membrane rotation was around 1.0-2.5 kWh_{el}/m^3 filtrate at TS concentration of 3.5 % but can be compensated by advantages of lower heat loss based on smaller digester volumes.

Kurzfassung

Anaerobe Membranbioreaktoren (AnMBRs) können eine nachhaltige technologische Lösung bei der Schlammfaulung fettreicher Substrate auf industriellen Kläranlagen darstellen, indem sie einen weitgehenden Abbau organischer Substanz und eine ausreichende Prozessstabilität bei reduziertem Reaktorvolumen ermöglichen. Einschränkungen der Membranleistung durch Fouling und Einschränkungen der Abbauleistung durch Abnahme der Biomasseaktivität aufgrund hoher Scherkräfte im Membranmodul können hingegen den Nutzen reduzieren.

In dieser Studie wurden die Kinetik des biologischen Abbauprozesses in einem Faulreaktor mit Schlammrückhalt, mit der Behandlung von fetthaltigen Substraten verbundene Einschränkungen und Auswirkungen der Scherbeanspruchung auf die Biomasseaktivität und die Membranleistung untersucht. Dabei wurde ein Anaerobreaktor im Pilotmaßstab eingesetzt, bei dem der Schlammrückhalt durch einen Rotationsscheibenfilter mit Keramikmembranen realisiert wurde. Die Membranen hatten eine mittlere Porengröße von 0,2 µm und wurden bei mittleren Überströmungsgeschwindigkeiten zwischen 3,3 - 4,1 m/s betrieben. Ein Vergleich der erzielten Abbauleistung erfolgte mit konventionellen Reaktoren (CSTR). Alle Reaktoren wurden mit Mischungen aus Überschussschlamm und Flotatschlamm aus der Milchindustrie beschickt.

In beiden Reaktortypen folgte der CSB-Abbau einer Kinetik 1. Ordnung in Bezug auf das partikuläre Substrat. Die Abbauleistung im AnMBR entsprach der eines CSTR bei gleicher Feststoffverweilzeit (SRT). Der AnMBR konnte jedoch mit höheren Raumbelastungen betrieben werden. Bei hohen CSB-bezogenen Anteilen von Flotatschlamm über 0,85 konnten CSTRs mit $B_{R,CSB,abb}$ = 8,3 kg $CSB_{abb}/(m^3 \cdot d)$ bei SRT = 15 d betrieben werden, während Raumbelastungen von 11,2 kg $CSB_{abb}/(m^3 \cdot d)$ bei einem AnMBR mit HRT = 10 d und SRT = 15 d erzielt wurden.

Prozessgrenzen, -instabilitäten und eintretende Hemmungen wurden durch die Auswertung des Verhältnisses von SMA zur mittleren Acetatumsetzungsrate im Faulbehälter sicher detektiert. Aktivitätsverluste von methanogenen Organismen aufgrund hoher Scherbelastungen infolge des Betriebs der Membran konnten nicht festgestellt werden. Maßgeblichen Einfluss auf die Prozessstabilität hatte die verbleibende, nicht-abgebaute Lipidkonzentration im Anaerobschlamm. Beginnende Hemmungen wurden ab 50 mg Lipid/g TR beobachtet, während der Abbauprozess bis zu Konzentrationen von 150 mg Lipid/g TR stabil blieb. Längere SRT oder reduzierte Anteile an lipidreichen Substraten reduzieren die Lipidkonzentration im Anaerobschlamm. Folglich kann durch den Betrieb eines AnMBR im Vergleich zum CSTR eine höhere Prozessstabilität bei Verlängerung der Faulzeit erreicht werden. Auslegungskriterien wie die CSB-Raum- oder Schlammbelastung gewährleisteten keinen stabilen oder effizienten Faulprozess. Aufgrund der Einschränkungen der Anwendbarkeit bestehender Auslegungskriterien für die Faulung mit fettreichen Substraten wurde ein allgemeingültiges Auslegungskriterium – der abbaubare Lipidgehalt im anaeroben Schlamm - entwickelt. Dieses Kriterium bezieht sich auf den derzeitigen Wissenstand zur LCFA-Hemmung, dass die Hemmung der methanogenen Organismen durch die Konzentration der langkettigen Fettsäuren in Verbindung mit dem Feststoffgehalt im Schlamm initiiert wird.

Im Bereich der Schlammfaulung hängt die Leistung der Membran basierend auf dem kritischen Flux maßgeblich von der scheinbaren Viskosität des Anaerobschlamms ab. Eine höhere Viskosität reduziert den kritischen Flux. Die charakteristischen Schlammparameter TR, oTR und CST wiesen hingegen keine eindeutige Korrelation zum kritischen Flux auf aber richtige Tendenzen. Die Korrelation zwischen kritischem Flux und scheinbarer Viskosität kann zusätzlich durch Einbeziehung der Scherbelastung an der Membranoberfläche (R^2=0.9) verbessert werden. Der kritische Flux konnte gesteigert werden, indem die Rotationsgeschwindigkeit erhöht oder die scheinbare dynamische Viskosität des Schlamms reduziert wurde, z.B. durch Zugabe von Eisensalzen. Eine Steigerung der mittleren Rotationsgeschwindigkeit von 3,8 auf 4,1 m/s verbesserte den kritischen Flux um ca. 20 %. Eine Dosierung von Eisensalzen (70 L $FeCl_2$ / t TR) verbesserte den kritischen Flux um 30 %. Als kritischer Flux bei der Filtration von Schlamm mit TR ≈ 3,2 % wurden 17 L/(m²·h) erreicht. Bei TR ≈ 4,0 % und TR ≈ 4,6 % reduziert sich die Leistung auf etwa 9 L/(m²·h) und 7 L/(m²·h).

Ein wirtschaftlicher Vorteil von AnMBRs mit rotierenden Scheibenfiltern kann nur erreicht werden, wenn die spezifischen Membrankosten deutlich sinken. Anderenfalls wären AnMBRs zur Schlammfaulung auf Anwendungen bei geringen TS-Konzentrationen (z.B. beim Einsatz nahezu vollständig abbaubarer Substrate) zur Reduzierung der erforderlichen Membranfläche und Investitionskosten begrenzt. Der zusätzliche Energiebedarf für die Membranrotation betrug etwa 1,0-2,5 kWh_{el}/m^3 Filtrat bei TR-Konzentrationen von 3,5 % und kann durch geringere Wärmeverluste aufgrund kleinerer Reaktionsvolumina kompensiert werden.

Danksagung

Die vorliegende Arbeit ist im Rahmen des Forschungsprojekts „ESiTI“ während meiner Tätigkeit als wissenschaftlicher Mitarbeiter am Fachgebiet Abwassertechnik (Institut IWAR) der Technischen Universität Darmstadt entstanden. Die Untersuchungen wurden zum größten Teil gefördert durch das Bundesministerium für Bildung und Forschung sowie die Fritz-und-Margot-Faudi-Stiftung. Wenngleich fordernd habe ich die Zeit am Institut genossen und mich fachlich und persönlich weiterentwickeln können. Dafür bin ich allen Wegbegleitern dankbar.

Zunächst möchte ich mich herzlich bei Herrn Prof. Markus Engelhart für seine Unterstützung und die vielen hilfreichen Diskussionen zu den Themen meiner Arbeit bedanken. Herrn Prof. Jörg Krampe danke ich trotz der langen Wartezeit bis zur Fertigstellung der Arbeit für die Übernahme des Korreferats. Großer Dank gilt auch Prof. Christian Schaum, der in mir erst das Interesse für die Faulung und ihr Potential zur dynamischen Belastung geweckt hat. Herrn Prof. Martin Wagner möchte ich ebenfalls für seine Unterstützung danken, die die vielen Reisen zu Konferenzen und umfangreichen Messprogramme erst möglich gemacht haben. Herrn Prof. Cornel gilt mein Dank für die Unterstützung und die fachlichen Diskussionen in den ersten Jahren meiner Tätigkeit am Institut.

Ein großer Dank gilt insbesondere allen Mitarbeitern des Teams Eberstadt, die mich tatkräftig an den Pilotanlagen unterstützt haben: Herbert Schmitt, Ewa Freitag, Christian Georg und auch Eva John (EnviroChemie) haben jederzeit dafür gekämpft die Pilotanlage am Laufen zu halten, während Anita Curt, Sylvia Borsch und Ute Kopf doch einige Messprogramme über sich haben ergehen lassen müssen. Danke auch an alle Spender von Schlammproben ohne die diese Arbeit nicht möglich gewesen wäre.

Besonderer Dank gilt auch allen Studierenden (insbesondere an Christine Scherrer, Eva Grünewald, Daniel Luley, Helena Voit, Simon Rincke, Stefan Kaulbarsch und Stephen Paul), die im Rahmen von HiWi-Tätigkeiten und/oder Abschlussarbeiten zur Wissensbildung beigetragen und mich mit unheimlich großem Engagement unterstützt haben.

Meinen Kollegen am Fachgebiet danke ich für die schönen Jahre kollegialer Unterstützung, die Aufrechterhaltung einer angenehmen Arbeitsatmosphäre trotz der typischen (Un-)Motivationsdynamiken und für die vielen (fachlichen und nicht fachlichen) Diskussionen. Herauszuheben sind hier die „Anaerobkollegen“ Johannes Rühl, Dorothee Lensch und Tobias Blach sowie Kai Wißbrock und Thomas Fundneider als „externe“ Berater.

Meinen Freunden danke ich für die Ablenkung und das Verständnis, wenn ich wieder mal eine Verabredung absagen musste.

Ich danke meiner Familie und besonders meiner Mutter, meiner Schwester und meinem Bruder für den Rückhalt und die nie enden wollende Unterstützung.

Von ganzem Herzen danke ich meiner Frau Jessica und meiner Tochter Josefin. Ihr habt mir immer den Rücken freigehalten, mich immer wieder motiviert und seid mir mit unglaublichem Verständnis begegnet. Ich freue mich darauf, dass wir zukünftig wieder deutlich mehr freie Wochenenden für gemeinsame Stunden haben werden.

“What the world of tomorrow will be like is greatly dependent

on the power of imagination in those who are learning to read today. “

(Astrid Lindgren)

Contents

1. Introduction

1.1. Background and objectives

The careful use of globally available resources, known as resource efficiency, is a central challenge for economy and society. In the field of industrial wastewater treatment, the focus is on water and energy resources. Energy is initially required for the treatment and transport of wastewater. However, wastewater itself contains energy in the form of chemically bound energy, potential energy and thermal energy (Lensch *et al.*, 2017).

Organically loaded wastewater from the dairy industry can preferably be treated by activated sludge processes in combination with flotation and anaerobic pre-treatment such as expanded granular sludge bed (EGSB) reactors for the reduction of energy costs (Cervantes *et al.*, 2006; Londong and Rosenwinkel, 2013). Concerning sludge management, the highly caloric flotation sludge and the waste activated sludge (WAS) of the aerobic post-treatment are generally disposed of as co-substrates to municipal wastewater treatment plants (WWTP) or biogas plants. On-site anaerobic treatment of these energy-rich residues along with a combined heat and power unit (CHP) offers major benefits. Disposed sludge volumes are reduced, and methane generation is increased up to 50 % of overall energy efficiency in case of integration of waste heat usage of CHP units in industrial production.

However, operation of anaerobic digestion (AD) with major shares of flotation sludge (over 80 % chemical oxygen demand, COD), which notably consists of lipids, is challenging. Successful examples of lipid-fed digestion have been reported using various lipid-rich substrates but also stating inhibition especially related to intermediate products of anaerobic lipid digestion (Mata-Alvarez *et al.*, 2014). Generally, process control of AD focuses on maintaining optimum conditions for methanogens. Nevertheless, substrate overloads frequently occur in conventional anaerobic digesters on the basis of continuous stirred-tank reactors (CSTR). In practice, CSTRs offer few adjustment options, and load changes are the preferred option for adaptation to fluctuations in flow and substrate characteristics or observed inhibition.

The efficiency and process stability of anaerobic digesters for sludge treatment with major shares of lipids can be especially improved by

- decoupling of solids retention time (SRT) and hydraulic retention time (HRT) by implementation of an anaerobic membrane bioreactor,
- elaboration of a generally valid design criterion that sufficiently covers causes of inhibition and
- improvement in process control by introducing biomass activity measurements.

Extension of CSTRs with a unit for solid-liquid separation to recycle particulates/biomass, known as recuperative thickening, has been developed for digestion of high-strength organics (Torpey and Melbinger, 1967) but hardly followed up for lipid-rich sludge treatment. Centrifuges, flotation devices, belt filter presses, screw thickeners or membranes may serve for separation of sludge (Batstone *et al.*, 2015). Membranes are especially promising as they provide a solid capture rate of 100 %, a separation without addition of polymers for phase separation and limited release of methane during operation.

Anaerobic membrane bioreactors (AnMBRs) especially offer the following advantages compared to CSTRs:

- reduction of digester volume at comparable methane yield
- lower heat loss and, possibly, lower energy demand for mixing
- adjustable sludge load
- higher process stability based on higher biomass concentration in the reactor
- capacity increase for existing digesters

In lab-scale, higher process stability, higher COD loading rates but contradictory results on methane yields compared to CSTRs have been observed at similar SRT (Dagnew *et al.*, 2012; Yang *et al.*, 2015; Romero-Flores *et al.*, 2017). Experiences with AnMBR in pilot scale and for treating lipid- and particulate-rich flotation sludge are limited. Drawbacks of AnMBR are high capital costs and high required shear forces for mitigating deposits which adsorb and accumulate on the membrane surface during operation, i.e. fouling (Drews, 2010). Comprehensive studies on fouling have already been conducted for aerobic MBRs or AnMBRs treating mainly solids-free substrates (Huang *et al.*, 2009; Drews, 2010; Judd, 2011). However, data on fouling in application of AnMBR for sludge treatment, especially on the influence of bulk characteristics on cake-layer formation at high solid concentrations (> 30 g/L), are rarely published.

Against this background, the aim of this study is to overcome limitations of sludge digestion operated with lipid-rich flotation sludge by implementation of an AnMBR in pilot scale. A generally valid design criterion needs to be elaborated and advanced process control in continuously operated digesters on the basis of methanogenic activity needs to be introduced. The AnMBR is further investigated with regard to degradation and filtration performance, long-term stability of methane activity and energy consumption.

Therefore, the following main questions are to be answered within this study:

- How does the COD removal in the AnMBR compare to that in the CSTR as a function of SRT and HRT?
- Can common standard kinetic models of sludge digestion be used to describe the performance of an AnMBR?
- How do increasing shares of flotation sludge and operating conditions such as SRT affect COD degradation and process stability of digesters?
- Does the AnMBR offer advantages to overcome limitations of digestion fed with lipid-rich flotation sludge when compared to conventional co-digestion processes?
- Which parameters describe process stability of sludge digestion and indicate slight declines before occurrence of process failure or significant inhibition?
- Does monitoring of specific acetoclastic methanogenic activity allow for a quantitative adaptation of COD load to a continuously operated digester?
- Which key parameters affect the filterability of digestates?
- Is the methane activity affected by shear forces induced for membrane operation in long-term pilot-scale?

1.2. Structure of the thesis

The answers to the abovementioned questions and the required fundamentals are given in the following chapters.

Chapter 2 introduces kinetics of AD of complex substrates and the AnMBR process.

Chapter 3 deals with the evaluation of kinetics of recuperative thickening using an AnMBR. It focuses especially on COD degradation regarding sludge and hydraulic retention times as well as process stability. Moreover, AnMBR and CSTR are compared in terms of treating solely WAS.

Chapter 4 focuses on the technical feasibility of anaerobic treatment of WAS and flotation sludge from the dairy industry as an example of on-site sludge treatment of industrial WWTPs. Process limitations based on increasing fractions of flotation sludge as well as different sludge retention times are investigated using an AnMBR and CSTR. A generally valid design criterion for lipid-rich sludge treatment is elaborated. Specific methanogenic activity (SMA) is integrated to indicate changes in process stability due to inhibitions and as design assistance.

Chapter 5 extends previously introduced findings of process stability by the integration of SMA for a dynamic process control in continuously operated reactors and for the quantification of free digester capacity at the current status of the AD process. Limitations of inlet fluctuations and spare capacities are elaborated.

Chapter 6 covers the impact of anaerobic sludge characteristics on the critical flux. Possibilities for increasing the critical flux are elaborated.

Chapter 7 discusses the economic feasibility of AnMBR for sludge treatment with regard to capital costs for the membrane units as well as the energy balance of an AnMBR compared to CSTRs.

In Chapter 8, main conclusions are summarised and the scope for future research is discussed.

2. Anaerobic membrane bioreactor for digestion of complex particulate organic and lipid-rich matter

2.1. Anaerobic digestion of complex particulate organic matter

2.1.1 Process fundamentals

Anaerobic processes are defined as processes where neither oxygen nor nitrate are present (Henze *et al.*, 2002). These processes are carried out by various groups of microorganisms living in symbiotic relationships. In sludge treatment, depending on the substrate, solids contents range between 1-15 %. In the field of industrial and municipal wastewater sludge treatment, WAS from aerobic biological treatment steps, sludge from solid-liquid separators such as flotation units or sedimentation units (primary sludge on municipal WWTP, lipid-rich flotation sludge from the food processing industry) as well as organic liquid waste (such as food leftovers) are generally used (Metcalf and Eddy, 2004; Mata-Alvarez *et al.*, 2014). Although substrates differ significantly, organic constituents can be classified into standard substrates: proteins, lipids and carbohydrates. A characterisation of standard substrates and associated theoretical maximum biogas yields are summarised in Table 1 based on Roediger *et al.* (1990), Alves *et al.* (2009), Linke *et al.* (2011) and Poggio *et al.* (2016).

Table 1. Characterisation of standard substrates and their theoretical maximum biogas yields

Biochemical Compound	COD [g COD/g VS]	Nitrogen content [g N/g VS]	Biogas yield [L/kg VS]	CH_4 [%]
Carbohydrates	1.1-1.25	0	750-900	50
Lipids	2.86-2.88	0	1,200-1,400	68-72
Proteins	1.2-1.3	0.137	700-800	60-71

The major aim of anaerobic sludge treatment is the reduction of particulate organic matter as a result of conversion to biogas (mainly carbon dioxide and methane) (Metcalf and Eddy, 2004). The AD process can be divided into five steps: disintegration, hydrolysis, acetogenesis, acidogenesis and methanogenesis (Figure 1). Each step is performed by a specific trophic group of microorganisms that convert products of the previous step into “smaller” compounds (Henze *et al.*, 2002). All 5 steps take place simultaneously in the digester (Zehnder, 1978).

Disintegration describes the lysis of biological sludge and complex organic material by physical processes and non-enzymatic decay (Batstone *et al.,* 2002). According to Pavlostathis and Gossett (1986), this is the rate-limiting step in the degradation of WAS. Disintegration manages a breakdown of organic compounds into the biodegradable and standard substrates mainly comprising carbohydrates, fats and proteins (Schlattmann, 2011).

During hydrolysis, complex molecules are converted into small, directly degradable substances, especially monomers or dimers (Henze *et al.*, 2002; Batstone *et al.*, 2002). The process is catalysed by enzymes, which are likely produced by the organism directly benefiting from the soluble products.

According to Vavilin *et al.* (1996) and Sanders *et al.* (2000), hydrolysis can take place as follows:

- The organisms secrete enzymes into the bulk liquid, where the enzymes adsorb onto a particle or react with a soluble substrate.
- The organisms attach to a particle, produce enzymes in the vicinity of the particle and benefit directly from soluble products released by the enzymatic reaction.

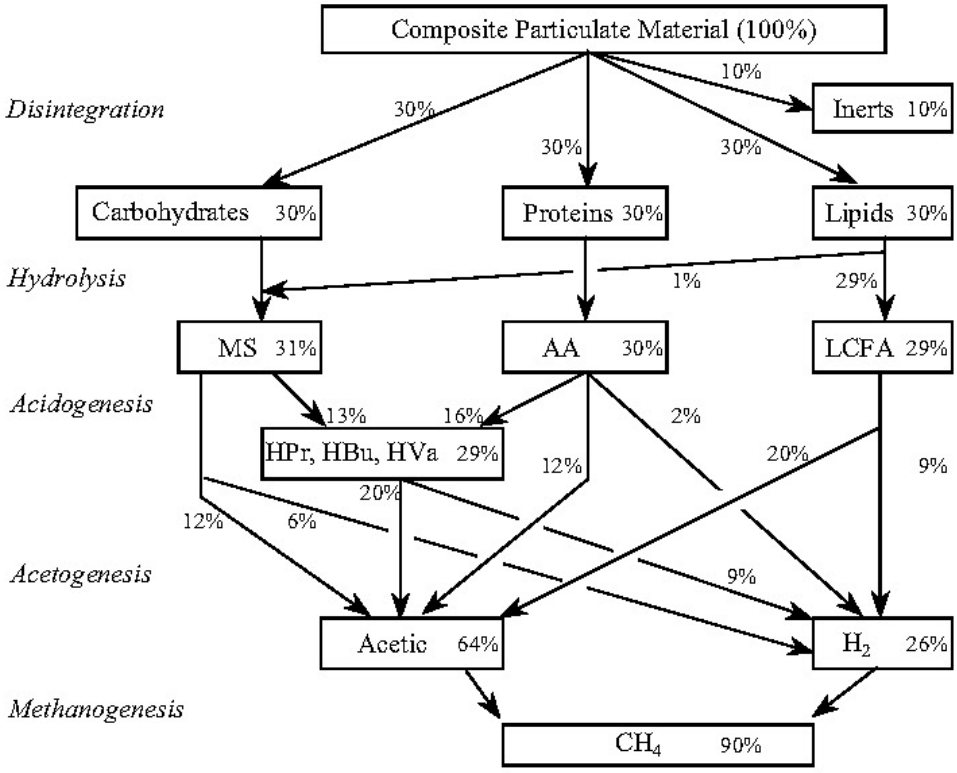

Figure 1. Anaerobic degradation chain using the example of a particulate substrate consisting of 30 % carbohydrates, 30 % proteins, 30 % fats and 10 % inert particulate matter (Batstone *et al.*, 2002)

Products of hydrolysis have a size that allows them to pass through cell membranes (Roediger *et al.,* 1990). In case of lipids, the rate of hydrolysis depends on the degree of emulsification and the distribution in a liquid (Weichgrebe, 2015). Lipids are mainly converted into long chain fatty acids (LCFA) by lipases (Madigan *et al.*, 2003). Other intermediates such as glycerol, alkanes, alcohols and aldehydes are also formed but are of negligible importance (Madigan *et al.*, 2003). Free LCFAs may cause severe inhibition of methanogens and, consequently, of the whole degradation process (Angelidaki and Ahring, 1992; Cirne *et al.*, 2007).

In the acidogenesis step, amino acids and sugars formed in the hydrolysis step are largely intracellularly fermented to organic acids (acetate, propionate and butyrate), alcohols, hydrogen and carbon dioxide. The LCFAs hydrolysed from lipids are only partially soluble and strongly adsorb onto the biomass in the reactor and/or to other surfaces (Sanders, 2001). LCFAs are oxidised to short-chain acids via the ß-oxidation pathway by electrochemical coupling of acidogenesis/acetogenesis with methanogenesis (Madigan *et al.*, 2003; Oh and Martin, 2010).

Organic acids or alcohols, which are formed in acidogenesis and cannot be used directly in methanogenesis, are converted into acetate, CO_2 and H_2 in acetogenesis (Gallert *et al.*, 2015).

Under standard conditions, these conversions are thermodynamically unfavourable. Energy gains are only possible if hydrogen partial pressures are low, as it shifts the balance of reaction towards the products (Schnürer, 2016; Dolfing, 1988). Since hydrogen is generated during acetogenesis, the hydrogen partial pressure can only be kept low if hydrogen is immediately consumed by methanogens (Schlattmann, 2011; Mata-Alvarez *et al.*, 2014). Therefore, acetogenesis and methanogenesis are interdependent and cannot be spatially separated (Schlattmann, 2011; Mata-Alvarez *et al.*, 2014). At hydrogen partial pressures between 10^{-6}-10^{-4} bar, acetogenesis and methanogenesis can take place with energy gain within this thermodynamic gap (Grepmeier, 2002). In conclusion, high hydrogen partial pressures inhibit the acetogenic bacteria (Batstone *et al.*, 2002).

In the last phase of AD (methanogenesis), acetic acid, carbon dioxide and hydrogen are converted into methane and water by archaic microorganisms. Based on the substrate, two parallel groups of organisms are responsible for the conversion into methane. About 70 % of methanogens use acetate as a substrate, and about 30 % are hydrogen-reducing methanogens, which also consume carbon dioxide for generating methane (Batstone *et al.*, 2002; Siegrist *et al.*, 2002; Metcalf and Eddy, 2004).

2.1.2 Degradation kinetics

The overall conversion rate of particulate organic matter into methane and carbon dioxide by AD results from the slowest conversion step of the AD chain. Usually, in the case of complex particulate organic matter, hydrolysis/disintegration is the rate-limiting step (Pavlostathis and Giraldo-Gomez, 1991; Batstone *et al.*, 2002; Henze *et al.*, 2002). The second slowest step is generally the methanogenesis (Henze *et al.*, 2002).

As a particular feature of methanogenesis, the concentration of organic acids (acetate) is directly proportional to the conversion rate of acetate into methane. Simply put, low disintegration/hydrolysis rates lead to lower concentrations of organic acids (especially acetic acid) and hydrogen compared to situations with higher disintegration/hydrolysis rates at comparable biomass concentration in the reactor. High concentrations of organic acids along with low pH values can also inhibit methanogens (see Section 2.1.2.2). In these cases of substrate overload or strongly inhibiting environments for methanogens, methanogenesis may become the rate-determining step (Henze *et al.*, 2002).

In the following sections, kinetics and factors influencing the degradation rate of the crucial steps of the AD, i.e., disintegration/hydrolysis and methanogenesis, are introduced in more detail.

2.1.2.1 Disintegration/ Hydrolysis

Several models describe the conversion rate of disintegration and/or hydrolysis. Basically, the following approaches are used to describe disintegration and hydrolysis:

- substrate first-order kinetics
- substrate surface-based kinetics
- biomass activity-related kinetics

The most common model of AD is the Anaerobic Digestion Model No. 1 (ADM1) (Batstone *et al.,* 2002). ADM1 follows a substrate first-order kinetics approach assuming two separate

steps: disintegration and hydrolysis. The most important models of these three approaches are discussed below in more detail. More complex models often do not clearly distinguish between hydrolysis and disintegration. Therefore, these models are commonly used for both steps (without additional disintegration). Overviews of additional models are given in He *et al.* (2007) and Vavilin *et al.* (2008).

In all introduced models hydrolysis also depends on external factors such as pH (Lokshina *et al.*, 2003; Pind *et al.*, 2003; Vavilin *et al.*, 2008), temperature (Pavlostathis and Giraldo-Gomez, 1991; Grady *et al.*, 1999;) and possibly also on the concentration of organic acids (acetate; Veeken and Hamelers, 2000; Vavilin and Angelidaki, 2005). These factors primarily influence used constants for modelling. Within the scope of this thesis, sludge treatment processes differ mainly in the concentration of solids and respective biomass concentrations. Therefore, the influence of these external factors is of minor importance and not introduced in more detail.

Substrate first-order kinetics

Disintegration according to Anaerobic Digestion Model No. 1 (ADM1) (2002) and Pavlostathis (1985)

The consideration of disintegration as a sole step apart from hydrolysis is based primarily on the work of Pavlostathis (1985), who describes disintegration as a substrate first-order reaction. In the well-accepted ADM1 as well, disintegration is modelled as a substrate first-order reaction. The authors assume that the degradation rate depends on the concentration of the substrate and a disintegration constant and is given as follows:

$$\frac{dX}{dt} = -k_{dis} \cdot X \qquad (2.1)$$

Where, $\frac{dX}{dt}$: degradation rate $(kg/(m^3 \cdot d))$

k_{dis}: disintegration constant $(1/d)$

X: substrate concentration (kg/m^3)

According to Batstone *et al.* (2002), the first-order kinetics approach has been supported by observations. The diversity of disintegration processes does not allow for a different, more fundamental approach in a generic model (Batstone *et al.*, 2002). Although ADM1 was mainly developed for modelling sewage sludge digestion using substrate specific disintegration constants, it can be used for other substrates as well (Batstone *et al.*, 2002; Schlattmann, 2011; Wichern, 2010).

Hydrolysis as substrate first-order reaction according to Eastman and Ferguson (1981) and ADM1 (Batstone et al., 2002)

Hydrolysis rate is also described as a substrate first-order reaction by ADM1. But, hydrolysis rate is determined individually for each component (carbohydrate, fat, protein) instead of a combined conversion rate of the mixed substrate, as proposed for the disintegration rate. Consequently, the hydrolysis rate of each component depends on its own hydrolysis constant and concentration.

$$\frac{dX}{dt} = -k_{hyd} \cdot X \qquad (2.2)$$

Where, $\frac{dX}{dt}$: degradation rate $(\mathrm{kg/(m^3 \cdot d)})$

k_{hyd}: hydrolysis constant for carbohydrates, proteins or fats $(1/\mathrm{d})$

X: substrate concentration (carbohydrates, proteins or fats; $\mathrm{kg/m^3}$)

According to Rusdi *et al.* (2005) and Feng *et al.* (2006), simplifications in ADM1 seem appropriate only if the disintegration rate of composite material is much lower than the hydrolysis conversion rate, i.e. if it is rate determining. Vavilin *et al.* (1996) and Batstone *et al.* (2002) compared a few models for hydrolysis and concluded that models based on the substrate first-order and Contois kinetics approach (Contois, 1959) are as good at fitting as the most complex model - the two-phase model (Vavilin et al., 1996).

Modifications of ADM1 for modelling digestion of different substrates

To model two substrates that differ in composition and degradation behaviour (e.g. co-digestion of sewage sludge or WAS with food waste), Esposito *et al.* (2011) suggest modelling disintegration rate for each substrate independently. Different disintegration rate constants of the substrates can be considered by this approach. They further include the possibility of separating each product of the disintegration process (carbohydrates, proteins and lipids) into two fractions: readily biodegradable and slowly biodegradable. Both fractions have different hydrolysis rate constants. This allows further differences in raw materials to be considered.

When tannery residuals (Polizzi *et al.*, 2017) and food waste (Garcia-Gen, 2015) are used as substrates for AD, the authors also split raw substrates into rapidly and slowly degradable fractions to achieve a better fit to measured data of batch tests. Both fractions are modelled with a separate disintegration process and their own disintegration rate constants.

AgriADM1 (Schlattmann, 2011)

Schlattmann (2011) adapted ADM1 for digestion of agricultural substrates in biogas plants. Disintegration and hydrolysis are still assumed to be following substrate first-order kinetics. However, unlike ADM1, increasing biomass concentration is considered to have a positive effect on conversion rate of hydrolysis in AgriADM1. Higher biomass concentrations increase the likelihood of an enzyme encountering a substrate particle. The likelihood of a microorganism hitting and adhering to a substrate particle to hydrolyse it increases as well. This exponential increase of likelihood leads to an increase in the hydrolysis rate until a certain upper limit (UL) of hydrolytic biomass concentration $X_{BM,hyd,UL}$ is reached in the reactor. Concentrations

above this UL do not further increase the conversion rate of hydrolysis. This approach is implemented by adjusting the hydrolysis constant k_{hyd} depending on the hydrolytic biomass concentration, as shown in Figure 2. Adjustment of k_{hyd} follows observations from batch experiments which showed higher hydrolysis rates at higher biomass concentration.

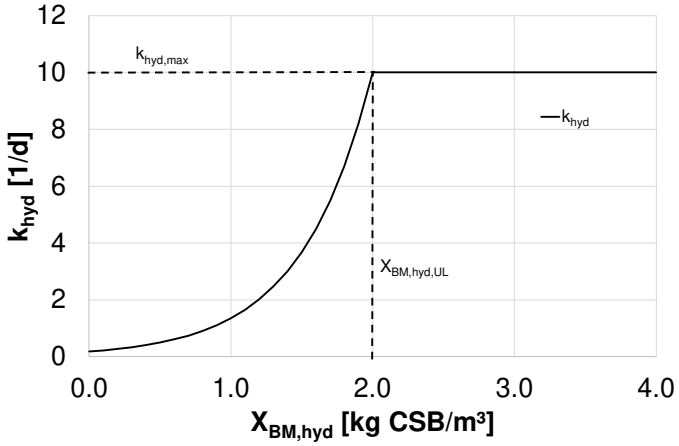

Figure 2. k_{hyd} as a function of concentration of hydrolytic biomass (Schlattmann, 2011)

The maximum hydrolysis constants correspond to values of ADM1. The UL of hydrolytic biomass concentration X_{UL} is assumed to be 2 g/L. The hydrolysis constant at lower biomass concentrations can be calculated as follows:

$$k_{hyd} = k_{hyd,max} \cdot e^{k_{hyd,exp} \cdot \left(1 + \frac{X_{BM,hyd} - 2 \cdot X_{BM,hyd,UL}}{X_{BM,hyd,UL}}\right)} \quad (2.3)$$

Where, $k_{hyd,max}$: maximum hydrolysis constant $(1/d)$

$k_{hyd,exp}$: exponential factor for hydrolysis constant; ≈4 (-)

$X_{BM,hyd}$: hydrolytic biomass concentration (kg/m^3)

$X_{BM,hyd,UL}$: upper limit of hydrolytic biomass concentration (kg/m^3)

The exponential factor $k_{hyd,exp}$ is not further defined by Schlattmann (2011) but has a value of around 4 based on own evaluation of provided data by Schlattmann (2011).

Substrate surface-based kinetics

Shrinking core model (Negri et al., 1993)

Negri *et al.* (1993) postulate that during metabolism the radius of particulate matter decreases with on-going hydrolysis. The hydrolysis rate is supposed to be proportional to the surface of particulate matter as well as the amount of hydrolytic enzymes present, which is considered proportional to the concentration of hydrolytic microorganisms. The model implies that particulate matter is spherical or has a uniform diameter.

The model was developed for the AD of municipal waste and is described as follows:

$$\frac{dX}{dt} = -K' \cdot A \cdot X_{BM,hyd} \quad (2.4)$$

Where, K': hydrolysis constant (m/d)

A: surface of particulate matter (m^2)

$X_{BM,hyd}$: concentration of hydrolytic biomass (kg/m^3)

X: particulate substrate concentration (kg/m^3)

Surface-based kinetics (Sanders, 2000)

According to Sanders (2000), the available surface area of particulate substrates A is decisive for hydrolysis rate. The particle size and shape are not important but affect the available surface. Additionally, Sanders (2000) assumes that hydrolytic enzymes are excessively present in wastewater. Hence, the concentration of hydrolytic biomass is no longer significant. The model was verified using particulate starch with defined particle sizes in batch experiments. According to Sanders (2000), changes of the substrate mass M can be calculated as follows:

$$\frac{dM}{dt} = -k_{SBK} \cdot A \quad (2.5)$$

Where, $\frac{dM}{dt}$: removal rate of substrate mass (kg/d)

M: substrate mass (kg)

k_{SBK}: surface-based hydrolysis constant ($kg/(m^2 \cdot d)$)

A: surface of particulate matter (m^2)

For co-digestion of sewage sludge or WAS along with food wastes, Esposito *et al.* (2011) and Zhao *et al.* (2019) suggest modelling hydrolysis and disintegration for both substrates independently with different biodegradation kinetics. The disintegration rate equation for sewage sludge is kept consistent with the original ADM1. The disintegration process of food waste is modelled with substrate surface-based kinetics as suggested by Sanders (2000).

Two phase model according (Vavilin et al., 1996)

The two-phase model by Vavilin *et al.* (1996) is an advancement of the surface-related kinetics approach. It considers the colonisation of particles by hydrolytic bacteria as well as the degradation of the colonised particles. The first phase is bacterial colonisation, in which hydrolytic bacteria cover the surface of solids. Bacteria on or near the particle surface release enzymes and produce the monomers that are utilised by the hydrolytic bacteria. It is assumed that a direct enzymatic reaction as the intermediate step of the total two-phase process may be quick in comparison with the stages of bacterial colonisation and surface degradation. When an available surface is covered with bacteria, the surface degrades at a constant depth per unit of time (second phase).

Therefore, the hydrolysis rate can be calculated as follows:

$$\frac{dX}{dt} = -(\frac{dX}{dt})_{max} \cdot \frac{X_{BM,hyd}}{K_B + X_{BM,hyd}} \cdot \frac{X}{K_x + X} \quad (2.6)$$

Where, K_B: equilibrium constant equal to the ratio between adsorption and desorption rate constants in the Langmuir function (kg/m^3)

$X_{BM,hyd}$: hydrolytic biomass concentration (kg/m^3)

X: particulate substrate concentration (kg/m^3)

K_X: half-saturation coefficient for the volatile solid waste concentration X (kg/m^3)

Biomass activity-based kinetics

This approach is based largely on observations of high rates of hydrolysis at high biomass to substrate ratios (Fernandez *et al.*, 2001).

Contois kinetics (Contois, 1959)

This approach is based on the observation that at high biomass concentration, the hydrolysis rate is presumably reduced by the limited substrate surface area. In systems where biomass to substrate ratios are low enough to be rate-limiting (e.g. in batch digestion), Contois kinetics could be used to adequately describe hydrolysis rates (Vavilin *et al.*, 1996). The Contois kinetics model is as follows:

$$\frac{dX}{dt} = -k_{hyd} \cdot X_{BM,hyd} \cdot \frac{\frac{X}{X_{BM,hyd}}}{K_x + \frac{X}{X_{BM,hyd}}} \quad (2.7)$$

Where, k_{hyd}: hydrolysis constant ($1/d$)

$X_{BM,hyd}$: hydrolytic biomass concentration (kg/m^3)

K_X: half-saturation coefficient for the volatile solid waste concentration X (kg/m^3)

X: particulate substrate concentration (kg/m^3)

Chen-Hashimoto kinetics (Chen and Hashimoto, 1980)

Chen and Hashimoto (1980) found a strong dependence of the half-saturation constant K_x on the degree of degradation of the substrate respectively its degraded concentration. Therefore, they suggest amending the abovementioned Contois kinetics:

$$\frac{dX}{dt} = -k_{hyd} \cdot X_{BM,hyd} \cdot \frac{X}{K_x \cdot (X_0 - X) + X} \quad (2.8)$$

Where, k_h: hydrolysis constant ($1/d$)

$X_{BM,hyd}$: hydrolytic biomass concentration (kg/m^3)

K_X: half-saturation coefficient for the volatile solid waste concentration X (kg/m^3)

X_0: starting concentration of substrate X (kg/m^3)

In batch experiments for the degradation of polysaccharide-rich particulates, this approach provides a much better approximation than other kinetic approaches (He *et al.*, 2007).

Half-order biomass kinetics (Rozzi and Verstraete, 1981)

Rozzi and Verstraete (1981) developed an empirical model based on the evaluation of various experimental data of the AD of sewage sludge. It shows the dependency of the hydrolysis rate on the concentration of hydrolytic biomass and substrate concentration. The model is as follows:

$$\frac{dX}{dt} = -K \cdot (X_{BM,hyd})^{0.5} \cdot X \qquad (2.9)$$

Where, X: particulate substrate concentration $(\mathrm{kg/m^3})$

$X_{BM,hyd}$: hydrolytic biomass concentration $(\mathrm{kg/m^3})$

K: hydrolysis constant $((\mathrm{m^3/kg})^{0.5}/\mathrm{d})$

A-order biomass kinetics (Valentini et al., 1997)

On the basis of the half-order biomass kinetics approach given by Rozzi and Verstraete (1981), Valentini *et al.* (1997) proposed a more general relationship, which considers the influence of different hydrolytic biomass concentrations by varying its exponent A.

Valentini *et al.* (1997) proposed as follows:

$$\frac{dX}{dt} = -K_{H,A} \cdot (X_{BM,hyd})^{A} \cdot X \qquad (2.10)$$

Where, X: particulate substrate concentration $(\mathrm{kg/m^3})$

$X_{BM,hyd}$: hydrolytic biomass concentration $(\mathrm{kg/m^3})$

$K_{H,A}$: hydrolysis constant $((\mathrm{m^3/kg})^{A}/\mathrm{d})$

A: order of influence of hydrolytic biomass concentration (-)

Valentini *et al.* (1997) recommend A-values between 0.42-0.67, based on batch experiments in lab scale using cellulose as the substrate.

Approach of substrate fractionation (Rojas et al., 2010)

Rojas *et al.* (2010) classify substrate into degradable, easy degradable and very easily degradable fractions for considering differences in particle size and type. The authors state that the fractionation is especially important when different substrates (sludges) are digested simultaneously in the same reactor. Substrates already present as monomers do not undergo disintegration. These are regarded as very easily degradable. Conversely, degradable and easily degradable substrates undergo disintegration. Rates are modelled by Contois kinetics with different constants. The subsequent hydrolysis in which even the very easily degradable fraction is added, is modelled using a half-order biomass kinetics approach, as suggested by Rozzi and Verstraete (1981). As an example, the biodegradable content of a lipid-rich sludge is divided into 40 % very easily degradable and 60 % easy degradable matter. Depending on

the degradability of the substrate, either hydrolysis or disintegration process is rate-limiting.

2.1.2.2 Methanogenesis

Substrate degradation for methane production by acetoclastic and hydrogenotrophic methanogens is usually described by Monod kinetics (e.g. Batstone *et al.*, 2002; Siegrist *et al.*, 2002).

$$\frac{dS}{dt} = \frac{\mu_{max}}{Y_{max}} \cdot \frac{S}{S+K_S} \cdot X_{BM,methanogens} \qquad (2.11)$$

Where, S: concentration of substrate (kg/m^3)

μ_{max}: maximum specific growth rate of biomass ($1/d$)

Y_{max}: maximum yield (g VSS/ g COD)

K_S: substrate half-saturation coefficient (kg/m^3)

$X_{BM,methanogens}$: methanogenic biomass concentration ($kg\ VSS/m^3$)

The rate of substrate conversion is thus dependent on the biomass concentration X_{BM}, substrate concentration S, affinity for the substrate K_S and microorganism-specific maximum growth rate μ_{max}. Inhibition or nutrient deficiency can be considered by adding inhibition factors to the abovementioned equation (Batstone *et al.*, 2002). The parameters K_S, Y_{max} and μ_{max} also depend on the temperature. Common values are given in Table 2.

Table 2. Kinetic parameters for methanogens

Process		Acetoclastic methanogenesis		Hydrogenotrophic methanogenesis	
Substrate		acetate		H_2/CO_2	
T	[°C]	35	37	35	33
μ_{max}	[1/d]	0.37	0.298	2.0	1.4
Y_{max}	[g $COD_{biomass}$/g $COD_{removed}$]	0.025	0.038	0.045	0.056
K_S	[mg COD/L]	40	213	$1 \cdot 10^{-3}$	0.6
Reference		[a]	[b]	[a]	[c]

[a] Siegrist *et al.* (2002)
[b] Vavilin *et al.* (1996)
[c] Gujer and Zehnder (1983)

2.1.2.3 Inhibition on anaerobic digestion

Anaerobic degradation can also be influenced by inhibiting the microorganisms involved. Kroiss and Svardal (2015) distinguish between inhibition and toxicity. Inhibition is described as the lowering of conversion processes rather than a complete stop (which is described by toxicity) and is usually reversible. It can lead to a shift in the rate-determining step from disintegration/hydrolysis to methanogenesis. A variety of factors can cause inhibition of anaerobic biological processes. In the following section, only inhibitions that have been shown to exert a significant effect on biological degradation within the frame of this thesis are elaborated in detail. These are, in particular, the pH value and concentration of organic acids (volatile fatty acid, VFA), long chain fatty acids (LCFA), free ammonia and hydrogen sulphide (H_2S).

Henze *et al.* (2002), Chen *et al.* (2014) and Weichgrebe (2015) present inhibition related to other substances, in particular metals and heavy metals, that are not considered to be relevant within the frame of this work.

Acidic or alkaline pH far from the physiological optimum value significantly affects the growth of bacteria. As cell wall structures can be damaged, the functionality of enzymes is compromised and hydrogen ion gradient-related mechanisms are disrupted (Madigan *et al.*, 2003). Siegrist *et al.* (2002) observed a decline in methanogenic activities by 50 % when the pH value dropped from 7 to 6. Duarte and Andersen (1982) observed a 50 % reduction in methane production at pH = 6.2. Batstone *et al.* (2002) state that acetate-utilising methanogens will be completely inhibited below pH values of 6.0 and not inhibited above pH values of 7.0.

Regarding concentration of organic acids, concentrations above 3,000 mg/L cause complete inhibition of methanogenesis (Weichgrebe, 2017). However, analogous to hydrogen sulphide and ammonium, it is believed that the inhibition is dependent on the concentration of the undissociated fraction. The relative fraction of undissociated acids depends on the pH value. Share of undissociated fraction increases with decreasing pH (Kroiss and Svardal, 2005). As the concentration of organic acids is analysed in total, threshold values are also usually provided based on the total concentration of organic acids. Shares of undissociated acids are neglected in common recommendations. For stable operation, standard works recommend threshold values around 500 mg HAc/L (Henze *et al.*, 2002; DWA M-368, 2014).

Inhibition related to nitrogen is based particularly on free ammonia concentration. Free ammonia concentration is also dependent on the pH value, affecting dissociation equilibrium between ammonium and ammonia in the aqueous phase. pH values greater than 7.4 are to be avoided, since in this case, equilibrium weight is on the side of the free ammonia concentration (McCarty, 1964; Kroiss, 1986). Analogous to the use of recommended values for organic acids, simplified limit values of a stable process are given as total ammonia NH_4-N, as it is easier to analyse. Kroiss (1986) describes the permissible NH_4-N concentration as a function of the pH value and different temperatures for a stable process in the anaerobic reactor, as shown in Figure 3.

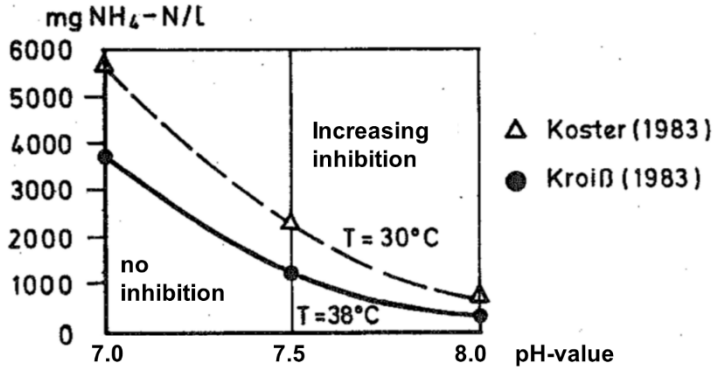

Figure 3. Permissible NH_4-N concentration for a stable anaerobic process as a function of pH and temperature (Kroiss, 1986)

Inhibition caused by non-dissociated H_2S tends to occur at low pH values. At pH = 7, 50 % of H_2S remains non-dissociated. Parkin *et al.* (1983) report that free sulphide concentrations of 50 mg/L are toxic to unadapted methanogens. Maillacheruvu and Parkin (1996) observed that H_2S inhibited acetoclastic methanogens much more than hydrogenotrophic methanogens. Yamaguchi *et al.* (1999) reported that half maximum inhibitory concentration (IC50) of H_2S for acetoclastic and hydrogenotrophic methanogens was 160 and 220 mg/L, respectively. Kroiss and Svardal (2015) recommend using threshold values of H_2S in the biogas by considering the

equilibrium in the aqueous phase at neutral pH and equilibrium between the aqueous and gaseous phases at low pressures. Concentration above 1 % H_2S in the biogas might lead to inhibition of methanogens (Kroiss and Svardal, 2015).

LCFAs can be inhibitory to anaerobic degradation even at low concentrations (Henderson, 1973; Hanaki *et al.*, 1981; Roy *et al.*, 1985; Koster and Cramer, 1986; Rinzema *et al.*, 1989; Angelidaki and Ahring, 1992). LCFA inhibition is mainly depicted as a non-competitive inhibition on the lipolytic, acidogenic or methanogenic activities. Adaptation to high concentrations in the feed is related to efficient LCFA degradation (in an adapted culture), which readily removes LCFAs as soon as they are released from the hydrolysis of lipids (Batstone *et al.*, 2002). To avoid high transient concentrations of LCFAs, gradual acclimatisation is required (Batstone *et al.*, 2002). Batstone *et al.* (2002) summarised the proposed mechanisms of LCFA inhibition:

- growth inhibition by competitive inhibition of the synthesis of LCFA essential to the structure of new bacteria,
- uncoupling of the electron transport chain from the proteins involved in ATP regeneration or transport of essential nutrients into the cell (Sheu and Freese, 1972) and
- adhesion to the bacterial cell wall and restriction of the passage of essential nutrients (Henderson, 1973).

Hence, inhibition is a result of LCFA adsorption on the cell surface. The ratio of cell surface area to LCFA concentration has a major influence on the adsorption (Hwu *et al.*, 1996).

Nevertheless, most threshold values reported for inhibition are bulk concentrations of LCFA, which also depend on the LCFA type (Silvestre *et al.*, 2014). Shin *et al.* (2003) reported IC50 of around 1,500 mg/L and 1,100 mg/L for oleate and palmitate, respectively. Silvestre *et al.* (2014) found strong inhibition at LCFA concentrations of around 1,300 mg/L containing 80 % oleate and 20 % palmitate. Chen *et al.* (2008) and Angelidaki and Ahring (1992) detected negative impacts due to stearic and oleic acid concentrations at around 200 mg/L to 500 mg/L.

Pereira *et al.* (2002) compare effects of equal oleic acid concentrations on granulated and suspended sludge and show that the adsorption capacity is decisive for the expression of inhibition and not just the LCFA concentration. This is also why heavy inhibition is irreversible (i.e. toxic), as recovery cannot be affected by a decrease in influent LCFA concentrations (Angelidaki and Ahring, 1992; Hwu *et al.*,1996). Ziels *et al.* (2016) report total solids-related inhibition at around 100 mg LCFA/g TS in the reactor using cooking oil as synthetic fat, oil and grease (FOG) source. Zonta *et al.* (2013) consider the surface area of existing biomass and possible cell membrane damage due to LCFA when modelling inhibition.

2.1.3 Design parameters of anaerobic reactors for sludge treatment

CSTR is the standard reactor for sludge treatment. CSTRs operate in fill-and-draw mode, in which the inlet flow always equals the outlet flow (see Figure 4). Concentrations of chemical compounds in the outflow correspond with concentrations in the reactor. Sludge or biomass retention time (SRT) and hydraulic retention time (HRT) are equal.

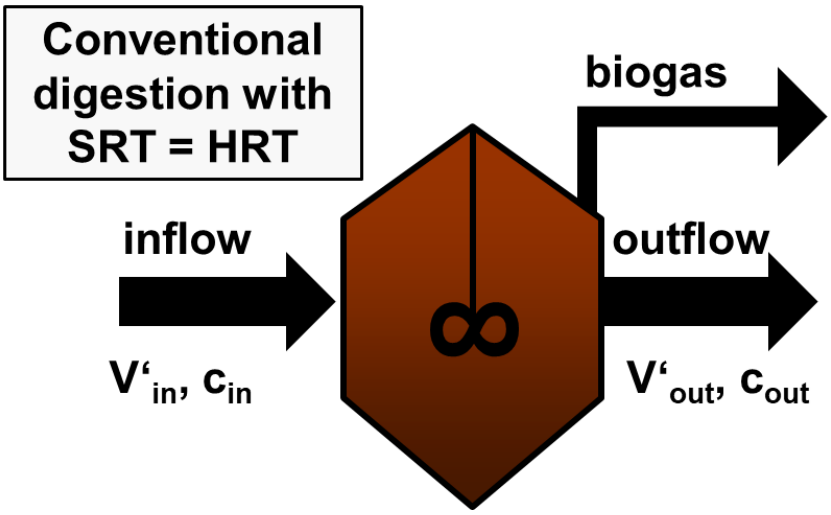

Figure 4. CSTR as standard reactor used for digestion of complex particulate organic matter

The design of required digester volume for sludge treatment is mainly based on a requested removal of organic matter and its respective COD. The degradation performance can be described based on a general mass balance, as provided in the annex (see Appendix A). The COD removal η_{COD} for a steady state following a substrate first-order reaction can be expressed as follows:

$$\eta_{COD} = 1 - \frac{c_{out}}{c_{in}} = \frac{k_{dis} \cdot t}{1 + k_{dis} \cdot t} \qquad (2.12)$$

Where, η_{COD}: COD removal (-)

c_{out}: outflow concentration (mg/L)

c_{in}: inflow concentration (mg/L)

k_{dis}: disintegration constant for substrate first-order kinetics volume flow (1/d)

t: reaction time (d)

The reaction temperature and required removal of organic matter are usually the basis of design. For economic reasons, a removal of 80 % based on degradable organic matter is commonly applied (DWA M-368, 2014). The required reaction time (SRT = HRT in CSTRs) as a function of the substrate-specific disintegration constant can be determined using above-described formula (see Figure 5; WEF/ASCE, 1992; DWA M-368, 2014). The required digester volume can be calculated as a product of substrate flow and SRT. On municipal WWTPs, required SRTs are between 12 and 25 days (WEF/ASCE, 1992; Metcalf and Eddy, 2004; DWA M-368, 2014).

In addition to achieving a specific COD removal, the survival of methane-producing microorganisms is obligatory (Henze *et al.*, 2002). A minimum SRT must be attained, which depends on growth rates of the slowest growing microorganisms, usually the acetoclastic methanogens. When maintaining organic acids at recommended concentrations of 500 mg/L (Henze *et al.*, 2002) and reaction temperatures of 35°C, growth rates μ are around 0.28 d^{-1} applying common kinetic parameters (see Table 2). This leads to minimum required sludge retention time SRT_{min} = 4 d in the digester.

$$SRT_{min} = \frac{1}{\mu} = (\mu_{max} \cdot \frac{S}{S+K_S})^{-1} = (0.37\ d^{-1} \cdot \frac{500}{500+40})^{-1} \approx 4d \qquad (2.13)$$

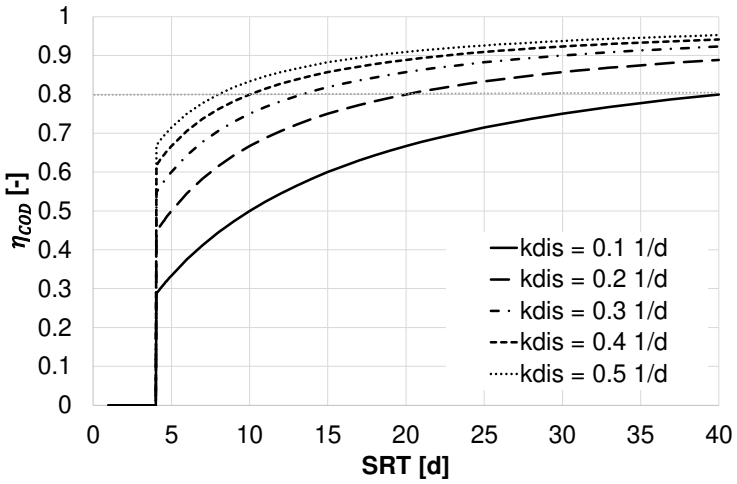

Figure 5: Influence of k_{dis} on COD removal as a function of SRT (right)

Regarding process stability of biological processes, sludge loads related to biomass are more decisive (Henze *et al.*, 2002). However, in CSTRs, a decoupling of substrate load from biomass concentration is not possible. Thus, a sludge loading rate cannot be adjusted independently but results from the biomass growth, depending on the mass of removed organic matter and SRT.

The sludge loading rate (SLR) is defined as follows:

$$SLR = B_{VS} = \frac{V'_{in} \cdot X_{in}}{X_{BM} \cdot V_{reactor}} \qquad (2.14)$$

Where, SLR, B_{VS}: sludge loading rate (kg /(kg biomass·d))

V'_{in}: inflow (m^3/d)

X_{in}: particulate matter in the Inflow (g/L)

X_{BM}: biomass concentration (g biomass/L)

$V_{reactor}$: reactor volume (m^3)

Neglecting biomass concentration, the organic loading rate replaces sludge load as the design parameter, especially in cases where differentiation of biomass and particulate residues becomes difficult (e.g. during sludge treatment).

The organic loading rate is defined as follows:

$$OLR = \frac{V'_{in} \cdot X_{in}}{V_{reactor}} \qquad (2.15)$$

Where, OLR: organic loading rate (kg /(m^3·d))

In sludge treatment organic loading rates are obtained mathematically from the substrate composition and the required SRT. Generally, they are not used for reactor design, but literature provides empirical data on limits or recommendations of maximum organic loading rates. Limits result from substrate inhibition or operation conditions such as foaming, which is related to exceeding specific biogas generation per surface area (Mata-Alvarez, 2015).

2.1.4 Process control in anaerobic digestion

The kinetic balance of AD processes with two slow steps, disintegration/hydrolysis (first) and methane production (last), and a fast intermediate step (acid production) will normally not cause any operational problems if a “complete” COD degradation into methane occurs (Henze *et al.*, 2002). However, disturbances that are mainly based on influent fluctuations occur even in normal operation, resulting in serious consequences to the performance of the processes (Jimenez *et al.*, 2015).

For safe operation of AD processes, close-loop automated control systems require a combination of efficient monitoring and decision support systems (Olsson *et al.*, 2005; Jimenez *et al.*, 2015). Close-loop automated control systems commonly use the feed flow as a manipulated variable (Olsson *et al.*, 2005). PID controllers, fuzzy control, neuronal networks or model supported tools are used as decision support systems (Liebetrau, 2008; Garcia-Gen, 2015; Jimenez *et al.*, 2015). Hence, for monitoring AD processes the focus is on the methanogenesis, as operational problems mainly originate from insufficient methanogenesis because of substrate overloads, washout of methane bacteria and inhibition of biomass (Henze *et al.*, 2002; Jimenez *et al.*, 2015). Inhibition related or leading to accumulation of VFA are especially the focus of monitoring. Typically measured variables for monitoring AD processes are pH value, concentration of organic acids (and partly also the acid spectrum), alkalinity (and its ratio with the concentration of organic acids), biogas composition, methane yield or flow and hydrogen concentration (Henze *et al.*, 2002; Olsson *et al.*, 2005; de Lemos Chernicharo, 2007; Alferes *et al.*, 2008; Kujawski and Steinmetz, 2009). Functionalities and drawbacks of these parameters are introduced in the following paragraphs.

Drops in pH are mainly induced by VFA accumulation in the reactor and directly affect microbial growth rates. However, decrease of pH depends on alkalinity of the treated sludge and can only be considered as an indicative process parameter (Murto *et al.*, 2004; Olsson *et al.*, 2015). The pH value is also subject to feedstock-related variations, and the state of the digestion cannot always be accurately indicated (Bischofsberger *et al.*, 2005).

VFAs are the most important intermediates in the AD process, since their accumulation is directly connected to the conversion rate of acetate into methane and indicates the slowest step of the AD chain. High concentration may lead to process failures (see Section 2.1.2.3). The ratio of propionic acid to acetic acid can also be used for the early detection of disorders (Olsson *et al.*, 2005; Boe *et al.*, 2007). As degradation of propionate is only possible at low hydrogen partial pressure, a sufficient use of released hydrogen as a substrate by methanogens is required. Therefore, the inhibition of hydrogenotrophic methanogens is always associated with a rapid increase in propionic acid concentration (Bischofsberger *et al.*, 2005; Olsson *et al.*, 2005; Boe *et al.*, 2007). Angelidaki *et al.* (1993) and Mata-Alvarez *et al.* (2015) argue that it is not possible to define distinct VFA concentrations to indicate the state of each anaerobic process, as different systems have their own concentration levels of VFA during normal and stable operation. Trends of VFA concentration show a good correlation with the state of the methanogenic step (Olsson *et al.*, 2005).

Low concentration of hydrogen associated with low partial pressure is required for an undisturbed anaerobic degradation process. Hydrogen concentration in the reactor strongly depends on the state of the methanogenic step (Furumai, 1997; Inanc *et al.*, 1999; Huang *et al.*, 2000). Olsson *et al.* (2005) recommend using trends instead of measured concentrations as fixed threshold values.

Alkalinity refers to the buffer capacity of water against pH changes that would make the water more acidic, for example, in the case of accumulation of fatty acids (de Lemos Chernicharo, 2007). The alkalinity is based on the concentration of total inorganic carbon (TIC). For process control, the ratio VFA/TIC should typically be less than 0.2-0.3 (Bernard *et al.*, 2001; Olsson *et al.*, 2005). A higher ratio reduces the pH and makes inhibition of methanogens more likely. Due to inaccuracies in determining both parameters, Weichgrebe (2015) recommends using trends for assessment of process stability based on alkalinity. Alkalinity also depends on the substrate characteristics and the gas volume flow (due to the influence of generated carbon dioxide on the carbonate balance), which makes evaluation under dynamic operation and changing substrates nearly impossible (Olsson et al., 2005).

Decreasing methane content or lower yields may be caused by substrate overload or inhibition of the anaerobic process (Bischofsberger *et al.*, 2005; Liebetrau, 2006). Increased load first enhances methane production before substrate overload might lead to process failure with corresponding lower methane ratios and/or biogas rates (Nielsen *et al.*, 2007). Methane yield and ratio also strongly depend on the substrate characteristics (see Table 1). “Normal” changes occur based on usual variations of feedstock especially in the field of industrial wastewater treatment.

The abovementioned parameters as a single device are not enough to evaluate and assess proper operating conditions of AD plants, which is why simplified PID control loops are not sufficient for comprehensive process control (Jimenez *et al.,* 2015). Therefore, approaches for close-loop automated control require at least one of the following: comprehensive expertise on the process, data, a reliable model and a comprehensive study for fitting (Ward *et al.*, 2008). For example, Garcia-Gen (2015) defined the current spare capacity of a digester by comparing the current methane flow with a fixed maximum achievable methane flow for a given substrate. The maximum achievable methane flow of an optimised feeding was previously modelled based on a detailed substrate or substrate mixture characterisation. Transferability to other digestion processes or the use of other substrates is limited (Garcia-Gen, 2015). Current experiences are summarised by Olsson *et al.* (2005), Garcia-Gen (2015), Jimenez *et al.* (2015) and Nguyen *et al.* (2015). Further, the values of the parameters introduced above change significantly only when methanogenesis has already replaced the disintegration/hydrolysis as the rate-determining step and/or is inhibited.

Slight changes in the methanogenic step, such as slight inhibition, are usually not observed by previously introduced approaches for process control.

Measurement of biomass activity (especially methanogenic called specific methanogenic activity; SMA) has shown to be advantageous for evaluating current process stability but is (until now) not measurable online (Ince *et al.*, 1995; Liebetrau, 2006; de Lemos Chernicharo, 2007; Mata-Alvarez *et al.*, 2015). Owing to high growth rates of hydrogenotrophic methanogens, methane activity of the acetoclastic methanogens is of major importance (see Table 2; Mata-Alvarez *et al.*, 2015). In batch tests of biomethane potential of organic substrates, SMA is well-

established for the determination of the right food-to-microorganism ratio (Angelidaki *et al.*, 2009). SMA is often also used for determination of inhibition on biomass growth, for example, by LCFAs (Dereli *et al.*, 2014b) or toxic concentrations of heavy metals such as zinc (Kuozeli-Katsiri *et al.*, 1988).

For evaluating process stability against substrate overload, Siegrist *et al.* (2002) defined a safety factor, SF, including acetate conversion activity as follows:

$$SF = \frac{maximum\ acetate\ conversion}{average\ acetate\ conversion} \qquad (2.16)$$

Values greater than 1.0 imply that hydrolysis/disintegration remains the rate-limiting step and provides some reliability against the accumulation of inhibiting intermediates such as organic acids. Siegrist *et al.* (2002) determined maximum acetate conversion using an unspecified pulse feeding instead of a well-defined measurement with a definite starting concentration of acetate as recommended by Angelidaki *et al.* (2009).

Siegrist *et al.* (2002) did not use SF for controlling the inflow load. However, Ince *et al.* (1995) applied SMA tests successfully during the start-up of an anaerobic membrane bioreactor (AnMBR) for treating brewery wastewater. Monteggia (1991) used SMA for the operation of upflow anaerobic sludge bed reactors (UASB). In both cases, SMA was used to determine a maximum organic loading rate. Garcia-Gen (2015) applied SMA to set limits of maximum inflow concentration in sewage sludge digestion. Nevertheless, up to today SMA is not commonly used for monitoring AD processes. The application of SMA as a “continuous” process control parameter for AD processes, especially for a dynamic operation of anaerobic digestion, still needs to be examined in detail.

2.1.5 Experiences and limitations of (co-)digestion of lipid-rich sludge

In continuation of the previously mentioned mechanisms of inhibition related to LCFA as intermediate product of lipid digestion (see Section 2.1.2.3), this chapter summarises experiences of digester operation fed with lipid-rich sludge from industrial wastewater treatment facilities.

Concentration levels of lipids and LCFAs in domestic and industrial wastewater are quite diverse (Alves *et al.* 1999). Wastewater from food processing industries such as dairies, fish canning factories, olive mills, ice cream manufacturing and slaughterhouses especially is characterised by high lipid content (Dereli *et al.,* 2014b). Total lipid concentration in dairy wastewater may vary from 0.9 to 2.0 g/L (Kim *et al.*, 2004). In wastewater from slaughterhouses, lipid concentrations in the range of 0.5 to 2.5 g/L are common (Londong and Rosenwinkel, 2013). Wool scouring and olive mill processes usually generate effluents with lipid concentrations between 5 and 25 g/L (Beccari *et al.*, 1998; Becker *et al.*, 1999).

Even higher concentrations are present in the flotation sludge of these industries. Flotation is used for removing particulate matter and fats from wastewater, with removal efficiencies around 85 % (Londong and Rosenwinkel, 2013) to protect subsequent biological steps (Cervantes *et al.*, 2006). Composition, solids content and quantity of flotation sludge are highly related to the type and production of the facility.

The compilation of studies treating lipid-rich sludge by AD in Table 3 show that substantial variations exist in lipid shares (0.1-0.7 g/g) and the associated achievable methane yield or its biodegradability.

Table 3. Examples of lipid-rich organic (industrial) wastes

Type of industrial organic waste	Lipid share [g VS/g VS]	VS [%]	COD/VS [g/g]	Methane yield [L/kg VS_{added}]	Ref.
Flotation sludge	0.30-0.35	13-18	n.d.	450-750[1]	a
Flotation fat	n.d.	~ 6-7	n.d.	680	b
Flotation sludge from food processing	n.d.	6.2 - 34.2	n.d.	960[1]	c
Flotation sludge from dairy industry	~ 0.7	n.d.	n.d.	230 L /kg COD	d
	~ 0.5	5.4	2.75	> 300 L /kg COD[1]	e
Flotation sludge from meat processing industry	0.5	8.7	2.2	1,100	f
	> 0.5	13.8	2.9	1,200	g
	n.d.	5	2.9	705	h
	~ 0.6	14.21	1.44	760	i
	~ 0.25	18.5	1.0	590	j
Cheese whey	~ 0.1	4-7	2-2.5	500-600	k
Slaughterhouse waste	~ 0.6	25	n.d.	670	l
	n.d.	20-30	1.8-2.4	590-820	m
	0.56	87 (dried)	2.2	720	n
	~ 0.65	54	2.4	680	o
Grease trap sludge from slaughterhouse	n.d.	16 - 25	n.d.	900	a
Fish oil sludge	0.3-0.5	80-85	n.d.	500-650[1]	p
Fish waste	0.35-0.5	25-40	n.d.	450-550	q
Fat, oil and grease	n.d.	n.d.	2.85	> 1,000	r
	0.5-0.8	10-40	1.2	~ 1,000	s
	0.78	40	2.9	700	t
Grease-trapped waste	0.5	14	1.0	1050	u
Corn-to-ethanol thin stillage	~ 0.3	3.7	1.9	550	v
Food waste	~ 0.24	~ 25-30	1.6	450	w
	~ 0.1-0.2	~ 12-17		390-480	x
	~ 0.13	4.7	2.0	420	y
	0.01-0.1	16-24	n.d.	430-680	z

[1]: calculated from data; n.d. not determined

References:

a. Ahring *et al.* (1992); b. Lfu (2007); c. Reipa (2003); d. Usack *et al.* (2018); e. Hubert *et al.* (2020); f. Girault *et al.* (2012); g. Battimelli *et al.* (2009); h. Creamer *et al.* (2010); i. Harris *et al.* (2017); j. Borowski and Kubacki (2015); k. Escalante *et al.* (2018); l. Pages-Diaz *et al.* (2018); m. Moukazis *et al.* (2018); n. Pitk *et al.* (2013); o. Rodriguez-Abalde *et al.* (2017); p. Luste and Luostarinen (2010); q. Kafle *et al.* (2013); r. Noutsopoulos *et al.* (2013); s. Salama *et al.* (2019); t. Kabouris *et al.* (2009); u. Zhu *et al.* (2011); v. Dereli *et al.* (2014b); w. Poggio *et al.* (2016) x. LFL (2013); y. Hu *et al.* (2018); z. Li *et al.* (2017).

Basically, lipid-rich organic residues from the food processing industry or slaughterhouses are characterised by easy biodegradability, high methane yields and high COD/VS ratios (see Table 1 and Table 3; Ahring *et al.*, 1992; Dereli *et al.*, 2014b; Mata-Alvarez *et al.*, 2014). Lipid shares in the residues of 100 % would theoretically have a COD/VS content of 2.9 g/g (see Table 1) and a maximum methane yield of approx. 1000 NL/kg VS_{added} if completely degraded to methane. As mentioned in Section 2.1.2.3, LCFA-related inhibition must be considered as it limits operational organic loading rates of lipid-rich anaerobic sludge treatment. Operational problems such as foaming and biomass flotation related to lipid-rich substrates are also reported (Pereira *et al.*, 2003; Rinzema *et al.,* 1994).

Flotation sludge is often co-digested in sludge treatment facilities of municipal WWTPs or biogas plants. In these applications, flotation sludge mostly represents a minor fraction of the organic content of the feed (< 20 %; Mata-Alvarez *et al.*, 2014). Nevertheless, higher fractions have also been successfully applied and are introduced in the following paragraphs.

Hubert *et al.* (2020) successfully treated sewage sludge (SS) and flotation sludge from the dairy industry with maximum COD-related ratios up to 43 % (with VS-related ratio up to 30 %) using a CSTR operated at SRT = 20 d in lab scale. Digesters were successfully operated with maximum OLRs of 4.4 kg COD/(m^3·d) or 2.3 kg VS/(m^3·d) (Hubert *et al.,* 2020). Flotation sludge-related OLRs of 0.7 kg VS/(m^3·d) were achieved (Hubert *et al.,* 2020). Girault *et al.* (2012) successfully treated WAS and flotation sludge from the meat processing industry with maximum COD-related ratios up to 42 % (with VS-related ratio up to 34 %) using a CSTR operated at SRT = 25 d in pilot scale. Maximum OLRs of 3.0 kg COD/(m^3·d), 1.4 kg VS/(m^3·d) or lipid-related organic loading rates of 0.2 kg VS_{lipid}/(m^3·d) were achieved (Girault *et al.,* 2012). Higher ratios initiated accumulation of LCFA (Girault *et al.,* 2012) or VFA (Hubert *et al.* 2020). Nevertheless, reactors were not fed continuously but twice a day (Girault *et al.*, 2012) or only once a day for 5 days a week (Hubert *et al.*, 2020). Therefore, transferability of the results to continuously fed reactors is questionable, as high intermediary substrate or LCFA concentrations may have negatively influenced anaerobic degradation (Batstone *et al.*, 2002).

Luostarinen *et al.* (2009) used grease trap sludge from slaughterhouses for co-digestion with sewage sludge. At SRT = 16 d, maximum organic loading rate of 3.46 kg VS/(m^3·d), grease-related OLR of 1.59 kg VS_{grease}/(m^3·d) and VS-related share of 46 % were achieved (Luostarinen *et al.*, 2009). Pitk *et al.* (2013) digested slaughterhouse wastes with sewage sludge using mixtures up to 5 % (w/w) without noticing process inhibition, corresponding to shares of slaughterhouse waste up to 68.1% of the total organic loading using a CSTR with SRT = 22.5 d. Digesters were successfully operated with maximum OLRs of 2.68 kg VS/(m^3·d) and maximum lipid-related organic loading rates of 1.0 kg VS/(m^3·d) (Pitk *et al.*, 2013).

Hamawand (2015) reviewed findings of co-digestion of slaughterhouse wastes and WAS and recommended organic loading rates of around 0.05-0.08 kg BOD/(m^3·d) at hydraulic retention times > 20 d.

The technical feasibility of co-digestion of fat, oil and grease (FOG) with sewage sludge has been documented in several studies (Suto *et al.*, 2006; Davidsson *et al.*, 2008; Kabouris *et al.*, 2009; Luostarinen *et al.*, 2009; Wan *et al.*, 2011; Ziels *et al.*, 2016). Mata-Alvarez *et al.* (2014) reviewed findings of co-digestion of sewage sludge or WAS with lipid-rich wastes and recommended an organic loading rate of 0.8 kg VS_{FOG}/(m^3·d) for maintaining a stable anaerobic digestion process. When combining lipid-rich streams with WAS, higher organic loading rates seem achievable because of lower lipid contents in WAS than in sewage sludge (Mata-Alvarez *et al.*, 2014).

The transferability of achieved maximum achievable organic loading rates for lipid-rich sludge treatment of one substrate to another is limited as shown from differences in characteristics of the lipid-rich substrates (Table 3). Ziels *et al.* (2016) chose a different parameter to define load limits, the maximum tolerable specific LCFA concentration in the reactor. Ziels *et al.* (2016) used cooking oil as synthetic FOG and achieved a maximum tolerable specific LCFA concentration of 100 mg LCFA/g TS in the reactor. This limit corresponded to a fat-related maximum

organic loading rate of around 0.75 g VS_{fat}/(L·d) (using CSTR operated at SRT = 20 d). Digesting WAS and grease interceptor waste, Wang *et al.* (2013) determined a maximum FOG-related OLR of 1.5 kg VS_{FOG}/(m^3·d).

In cases of strong inhibition related to LCFAs, Palatsi *et al.* (2009) compared different recovery strategies. The fastest reduction of inhibition was achieved by replacing 40 % of the biomass in the reactor, i.e., by increasing the biomass/LCFA ratio, or adding bentonite to the reactor (Palatsi *et al.*, 2009). The most common strategy for relieving inhibition of methanogens - the reduction or stopping of feeding - is not recommended and only led to minor recovery effects after 10 days (Palatsi *et al.*, 2009).

2.2. Membrane filtration for use in membrane bioreactors

2.2.1 Process fundamentals

The membrane process is a physical separation process characterised by the division of a feed stream into two streams by a semipermeable membrane barrier: concentrate (retentate) and permeate (filtrate) (Figure 6, left). The product of the membrane process is either the permeate or the concentrate but rarely both (Mulder, 1996). Membranes represent a selective barrier for the two phases and mainly determine selectivity of the separation process (Mulder, 1996). Separation is achieved under application of a driving force, as one component from the feed mixture is less retained by the membrane and can traverse through the membrane much faster (Figure 6, right) (Mulder, 1996).

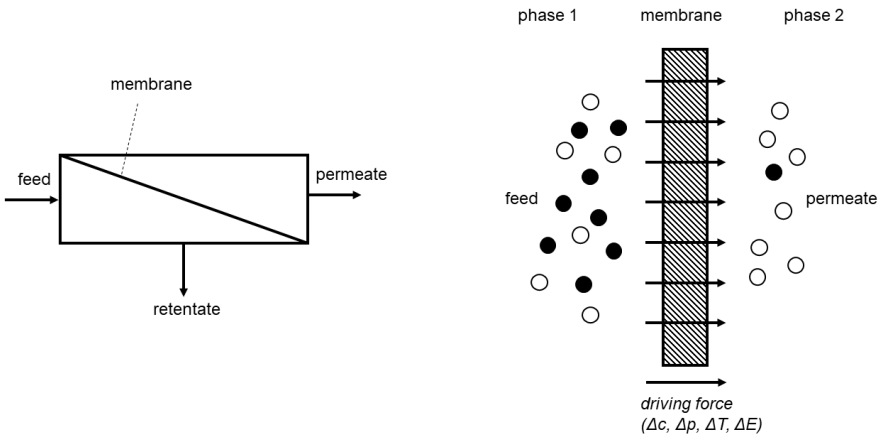

Figure 6. Principle of membrane processes (left), and a schematic representation of a two-phase system separated by a membrane (right; Mulder, 1996)

Types of membranes for microfiltration/ ultrafiltration

Ultrafiltration and microfiltration membranes are typically used when applying membranes in solid-liquid separation applications, e.g. a membrane bioreactor for separating biomass from water. The mean pore sizes of these membranes are sufficient to retain anaerobic mesophilic biomass with a typical mean particle size of around 3-140 µm (Wang *et al.*, 2018; see Table 4). Membranes with a lower molecular weight cut-off (MWCO) are generally not required in MBR applications (Dagnew, 2010). In MBRs, the driving force for the separation into solids-rich and solids-free streams is the transmembrane pressure.

Table 4. Membrane classification and typical pressures and permeability ranges (Judd, 2011; Mulder, 1996)

Membrane process	Particle size rejection [µm]	MWCO[1] [Da]	Pressure range [bar]	Permeability [L/(m²·h·bar)]
Reverse Osmosis	< 0.001	< 100	10-100	0.05-1.4
Nanofiltration	0.001-0.01	100-1,000	5.0-20	1.4-12
Ultrafiltration	0.01-0.1	1,000-500,000	1.0-5.0	10-50
Microfiltration	> 0.1	> 500,00	0.1-2.0	> 50

[1] 90% of spherical uncharged component with given molecular weight will be retained on the feed side

Regarding membrane material, both organic and inorganic membranes exist. For organic membranes, polyvinylidene difluoride (PVDF), polyethylsuphone (PES), polyethylene (PE) and polypropylene (PP) are mostly used (Dagnew, 2010). Inorganic materials are mostly ceramics, especially aluminium oxide, zirconium oxide and titanium dioxide (Baker, 2012). The advantages of ceramic membranes are their resistance to chemicals and stability at high temperatures (Baker, 2012). This enables a wide application range, especially when cleaning procedures for reducing cake formation on the membrane surface (scaling and fouling) are frequently required (Manison, 2013). Advantages of polymeric membranes are lower costs and higher package densities in modules. Ultra- and microfiltration membranes used in MBRs comprise modules of different forms: hollow fibre, flat and tubular. The rotation discs investigated in this work belong to the plate membranes. Hollow fibre membranes have the highest package density but have disadvantages in cleaning (Judd, 2011). Tubular and plate membranes have low package densities but are easy to operate, to clean and maintain turbulent flow conditions with limited pressure drop (Dagnew, 2010).

Membrane operation

In MBR applications, the cake layer control on the membrane surface is decisive in achieving a sufficient permeate flow to minimise costs (Melin and Rautenbach, 2007). Therefore, a dynamic filtration (crossflow filtration) mode is favoured over a static membrane filtration (dead-end filtration; Zeman and Zydney, 1996; Cheryan, 1998; Figure 7).

In dead-end filtration, feed flow is orthogonal to the membrane and all retained matter accumulates as a clogging layer on the membrane. During operation, the clogging layer grows over time. A maximum is reached when either the permeate flow collapses or a maximum transmembrane pressure (TMP) is reached. Consequently, filtration is interrupted, and chemical cleaning of the membrane is required (Melin and Rautenbach, 2007). In dynamic filtration mode, feed and concentrate flow tangentially to the membrane (Zeman and Zydney, 1996). The velocity of the feed flow along the membrane reduces clogging on membrane surface because of the resulting shear forces. After the start-up phase, the process reaches a quasi-steady state corresponding to a steady thickness of the clogging layer on the membrane, where deposit on the membrane from the bulk stream and particles which are removed by the stream are in equilibrium. A characteristic permeate flow rate develops and remains preferably stable over a long time. The establishment of a reasonable crossflow by a recycle flow over the membrane (module) or gas sparging is most common (Ripperger, 1993). Recycle streams also reduce concentration in the membrane module based on filtrate discharge. The membrane module investigated in this study achieves crossflow when moving membrane surface

by rotation of the microfiltration discs (see Figure 17). Gas sparging and moving membrane surfaces have the advantage of being able to set the crossflow without pumping large volumes of water for generating required shear forces. This is related to lower energy demands compared to conventional crossflow applications on the basis of pumping. However, energy demands for setting crossflow velocities remain higher compared with that of the dead-end filtration mode (Mulder, 1996; Zeman and Zydney, 1996).

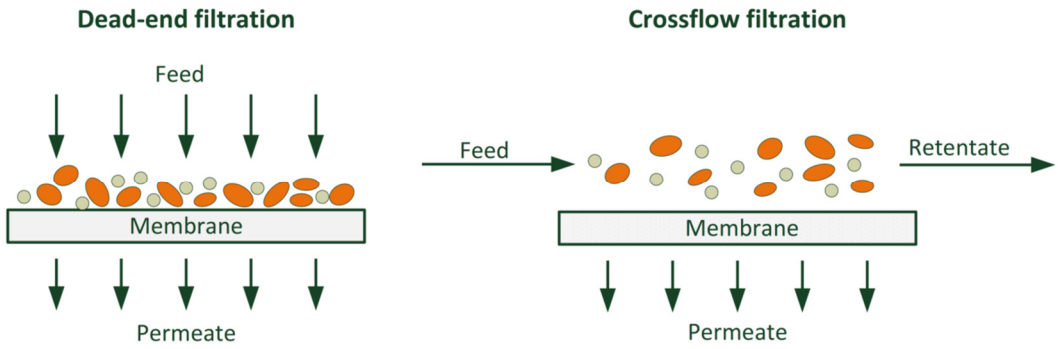

Figure 7. Principle of dead-end filtration and crossflow filtration (Düppenbecker, 2018)

For crossflow filtration, the assembly of the membrane module can either be in a side-stream or a submerged configuration (Judd, 2011). In a side-stream configuration, crossflow over the membrane surface for reducing cake formation on the membrane is achieved by a recycle stream. TMP as a driving force is employed via feed pumps or water levels in the reactor, which push liquid through the membrane (Dagnew, 2010). A filtration pump is only required in case of backflush applications. In the submerged configuration, a filtration pump is required to draw the filtrate out of the system. The membrane module can be either placed directly into the reactor tank or in a separate side-stream basin in submerged configurations. Cake layer formation can be reduced by setting crossflow velocities especially using gas bubbles (Liao *et al.*, 2006).

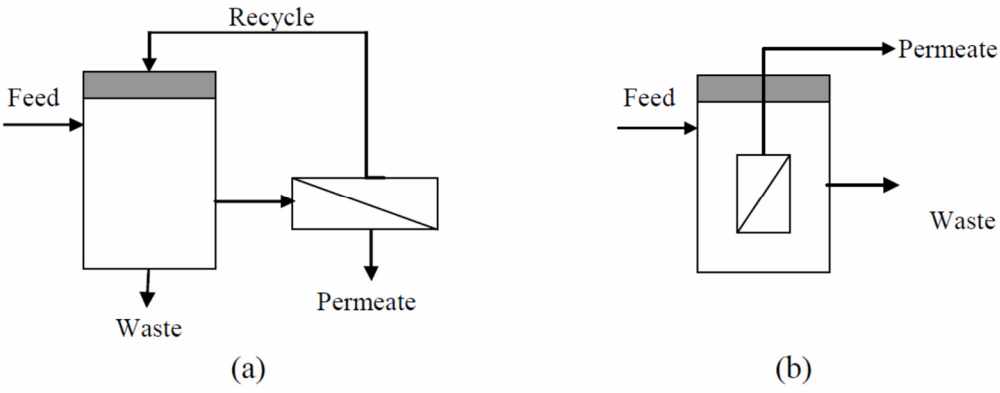

Figure 8. MBR configurations with membrane module in (a) side-stream configuration and (b) submerged configuration (Dagnew, 2010)

Nevertheless, coverage of the membrane surface by deposits accumulating or adsorbing during operation can only be controlled, not prevented. This phenomenon is called fouling. It remains the most critical issue in the operation of MBRs (e.g., Le-Clech *et al.*, 2006; Meng *et al.*, 2009; Drews, 2010; Judd, 2011).

Fouling

Membrane fouling means the restriction or blocking of membrane pores, which reduces filtration performance and permeability by increasing the filtration resistance (Judd, 2011). Therefore, fouling is characterised by a permeability loss due to flux decrease at steady TMP or TMP increase at steady flux (see Figure 10). Fouling mainly results from concentration polarisation developing a cake or gel layer on the membrane surface and/or pore blocking (Lim and Bai, 2003; Dagnew, 2010; Strathmann, 2011; Baker, 2012). Organic fouling refers to the reduction of membrane performance because of the interaction of the membrane surface with components produced by bacteria during operation and other organic dissolved or particulate feed matter (Liao *et al.*, 2006; Dagnew, 2010). Inorganic fouling (or scaling) is related to flux decline or TMP increase by inorganic chemical components. Although fouling phenomena are rather complex, common approaches for describing flux decline and the mechanism of fouling are related to simple classical models shown in Figure 9 (Bowen and Jenner, 1995; Ho and Zydney, 2006; Judd, 2011). While internal fouling (blocking and pore constriction; Figure 9 a-c) is related to components smaller than the membrane pores, cake layers are formed on the upper surface of the membrane based on lower back transport from the membrane surface to the bulk rather than transport to the membrane (external fouling; Figure 9 d).

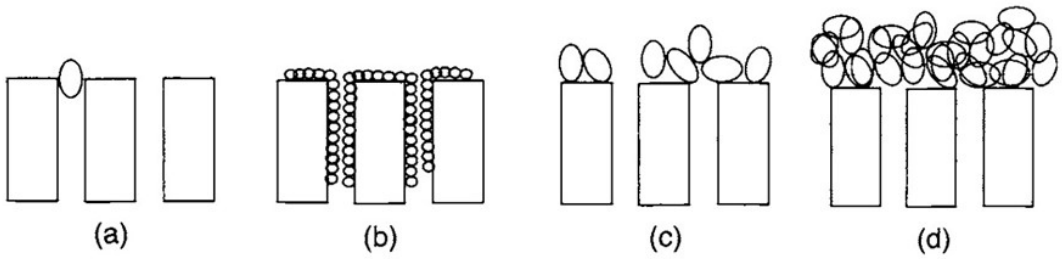

Figure 9. Fouling mechanisms: (a) complete blocking, (b) internal pore blocking, (c) intermediate blocking, (d) cake formation (Bowen and Jenner, 1995; Judd, 2011)

Drews (2010) and Kraume *et al.* (2009) divided fouling into different categories. Reversible fouling occurs due to external deposition of material (cake filtration) and is mostly removed during filtration breaks (relaxation steps) under crossflow conditions or backflush cycles. The slope of the baseline is called residual fouling and cannot be easily removed by relaxation or backflush. Maintenance clean-ups are required, which consist of intensified backflush optionally enhanced using small dosages of chemicals. Irreversible fouling (also called long-term fouling) refers to fouling that can only be removed by chemical cleaning. Irrecoverable fouling cannot be removed by any cleaning and occurs over long periods of time. Fouling rates of reversible (0.1-1 mbar/min) and residual fouling (0.01-0.1 mbar/min) are significantly higher than fouling rates of long-term fouling (0.001-0.01 mbar/min) or irreversible fouling (< 0.001 mbar/min; Drews, 2010); therefore, mitigation strategies focus on reversible and residual fouling.

A simplified representation of the general impact of design, operation, and bulk characteristics on fouling in AnMBR applications is given in Figure 11. Decisive influencing factors for mitigating fouling are membrane type, sludge characteristics and membrane operation. For predicting flux decline or TMP increase over time, simplified models were developed and summarised by Ho and Zidney (2006), Dagnew (2010) and Fonouni *et al.* (2017). As deposits on membrane surface are mainly made via convective transport and reduced by back transport into bulk,

mass transport mechanisms are presented in more detail in Section 2.2.2. General strategies for reducing fouling during membrane operation and design are introduced in Section 2.2.3. Bulk properties affecting fouling in AnMBRs are summarised in Section 2.3.

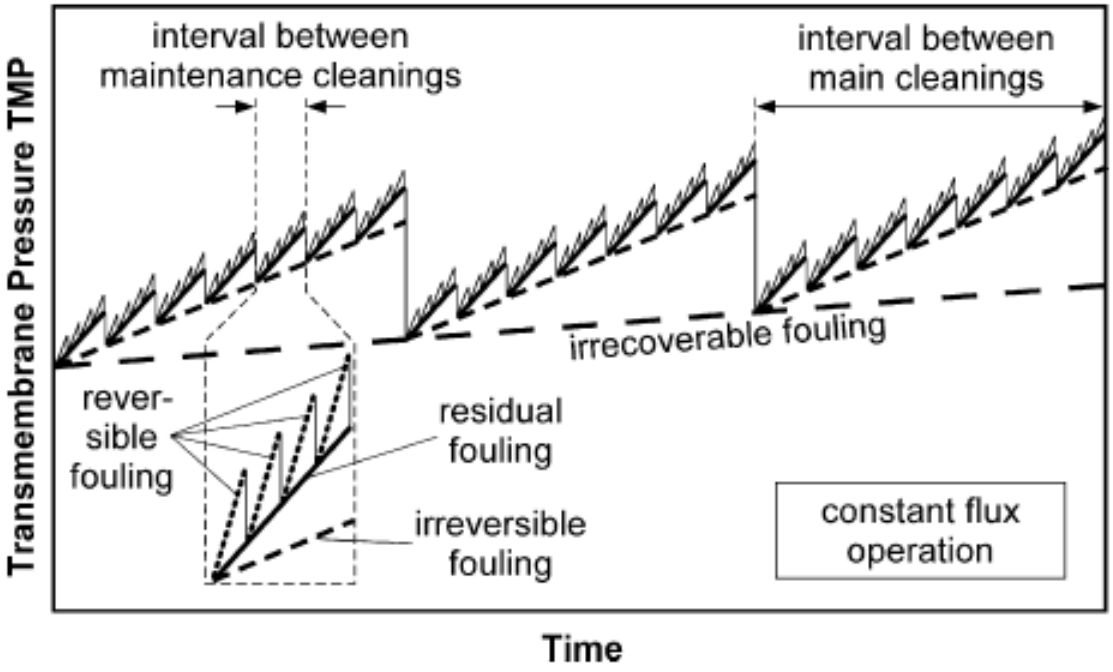

Figure 10. Schematic representation of different fouling types observed during long-term operation of full-scale MBRs at a constant flux (Kraume *et al.*, 2009)

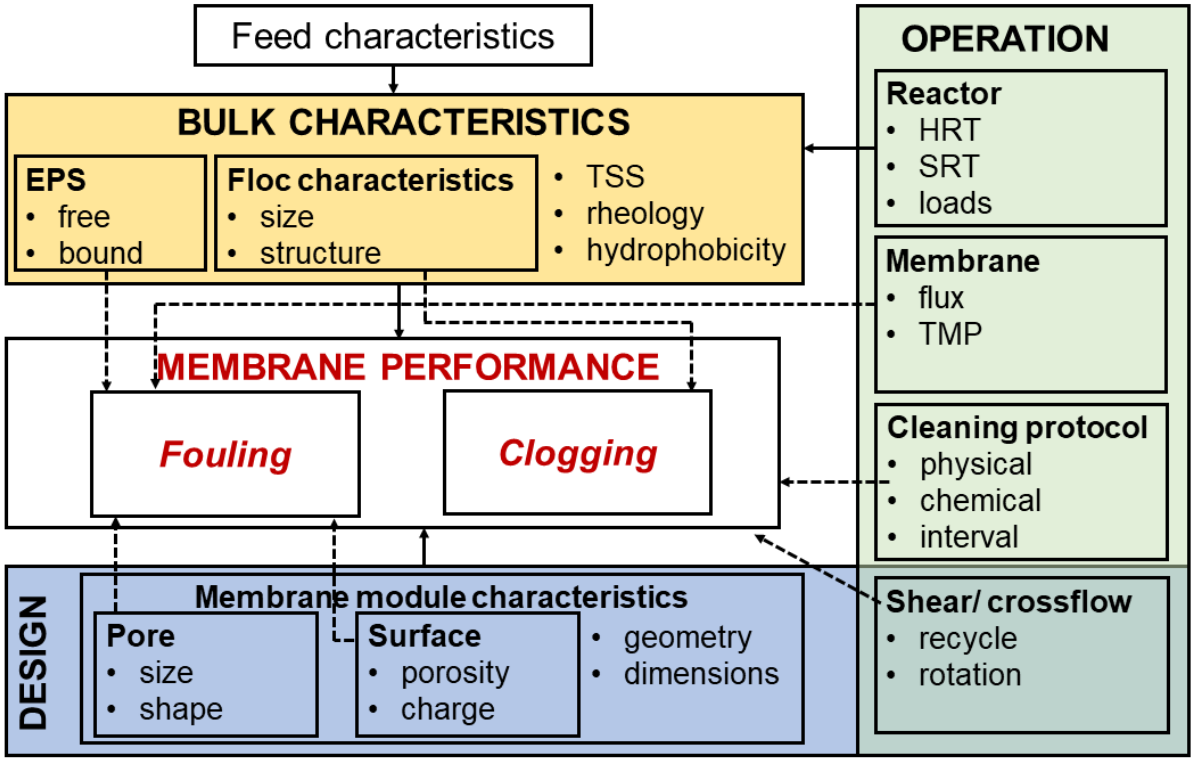

Figure 11. Interrelationship between AnMBR parameters and fouling (originally created by Judd (2006) for aerobic MBR and transferred to AnMBR)

2.2.2 Mechanisms of mass transport

Mechanisms of mass transport during filtration can be described with a mass-balance approach (Bacchin *et al.*, 2006; Jørgensen *et al.*, 2014). The net radial flux of material towards the membrane is the combination of a convective flux towards the membrane and back transport fluxes of retained compounds into the bulk stream (Bacchin *et al.*, 2006). The back transport of retained substances into bulk flow can be based on either diffusive or hydrodynamic effects (Melin and Rautenbach, 2007). The dominating effect mostly depends on the particle size. At particle sizes lower than 0.1 µm, Brownian diffusive effects dominate the back transport (Melin and Rautenbach, 2007; Bacchin *et al.*, 2006). Larger particles and colloids are more susceptible to shear-induced diffusion (Melin and Rautenbach, 2007; Bacchin *et al.*, 2006) or hydrodynamic effects. In the use of membranes to separate biomass or particles of digested sludge, the diverse size distribution, which comprises significant amounts of particles larger and smaller than 0.1 µm, must be considered. In the following paragraphs, the most common diffusion and hydrodynamic models for calculating permeate flux are introduced.

Gel polarization as the most common diffusion model

The net radial flux of material towards the membrane is a combination of convective flux and diffusive back transport fluxes of retained compounds into the bulk stream (Bacchin *et al.*, 2006; Jørgensen *et al.*, 2014; Figure 12). Under consideration of general fluid dynamic principles, a boundary layer is formed. The boundary layer is characterised by a concentration gradient of macromolecules that cannot pass the membrane (Zeman and Zydney, 1996; Cheryan, 1998; Strathmann, 2011; Baker, 2012). This phenomenon is called concentration polarisation. The theory based on boundary layer assumes that the mass transfer resistance is limited to a thin boundary layer of thickness δ (Figure 12).

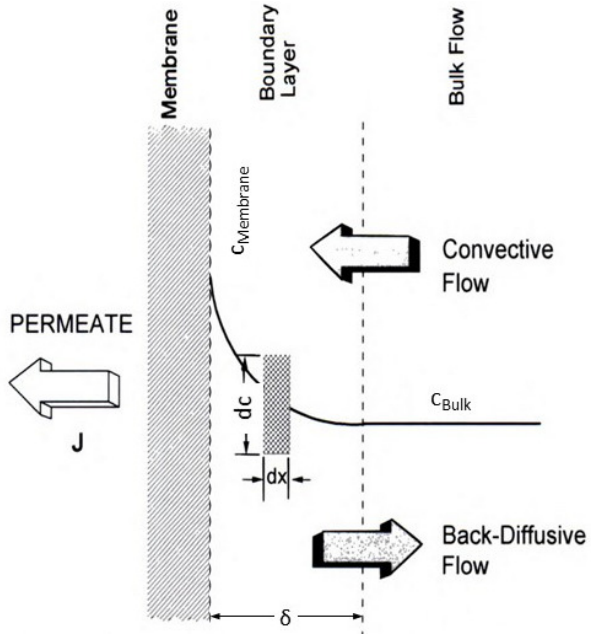

Figure 12. Schema for mass balance and concentration profile of foulants near a membrane (Cheryan, 1998)

The thickness of boundary layer δ is essentially dependent on the type of flow (turbulent or laminar, as determined by Reynolds number) and fluid characteristics. Outside the boundary

layer in the bulk stream, the concentration of the transported component is c_{Bulk}. The concentration at the membrane surface is $c_{Membrane}$. Furthermore, it is assumed that mass transport happens in direction x vertically oriented to the membrane surface.

The mass-balance equation for development of fouling is as follows (Jørgensen *et al.*, 2014):

$$\frac{d\omega}{dt} = J \cdot c_{Bulk} - D\frac{dc}{dx} \tag{2.17}$$

Where, ω: specific foulant mass on membrane surface (kg/m^2)

J: filtrate flux ($L/(m^2 \cdot h)$)

c_{Bulk}: concentration of foulant in bulk flow(kg/L)

dc: concentration change in infinitesimal boundary layer segment (kg/m^3)

dx: thickness of infinitesimal boundary layer segment (m)

D: diffusion coefficient of solute (m^2/h)

In steady state, convective transport towards the membrane and diffusive back transport must be identical, as there is no additional deposition of foulants on the membrane when interactions between the membrane and foulants are neglected. As a result,

$$J \cdot c_{Bulk} = (D\frac{dc}{dx}) \tag{2.18}$$

The gel layer model now assumes that the highly concentrated solution on the membrane surface reaches a gel-like state as a result of the continuous removal of the solvent (Blatt *et al.*, 1970). In this highly viscous layer, the directed movement of the dissolved components comes to a standstill (stagnant layer). In the theory of classical filters, the gel layer is assigned a hydrodynamic resistance and can be calculated by the formula of Kozeny-Carman or Darcy's Law (Nakao *et al.*, 1979; Karode and Kumar, 2001; Schwinge *et al.*, 2002). If the filtration pressure is changed, the thickness of the gel layer or its hydrodynamic resistance adjusts so that the steady state flux remains constant (Bacchin *et al.*, 2006; Schipolowski, 2007; Jørgensen *et al.*, 2012). Thus, the maximum permeate flow is independent of pressure and is called the limiting flux J_{lim} when related to the membrane surface.

Assuming that bulk concentration, gel layer concentration and filtrate concentration are constant, the limiting flux depends on the diffusion coefficient D and thickness of the boundary layer δ.

$$J_{lim} = \frac{D}{\delta} \cdot \ln\left(\frac{c_{gel}}{c_{bulk}}\right) \tag{2.19}$$

Apart from an increase in the diffusion coefficient, the flux also increases with lower concentrations in the bulk and reduced thickness of the boundary layer. The thickness of boundary layer reduces with higher Reynolds numbers, which result from higher crossflow velocity and/or lower viscosity of the fluid.

The diffusion expressed by the diffusion coefficient can be Brownian diffusion (D_B), shear-induced diffusion (D_S) or both (Jørgensen *et al.*, 2014), depending especially on the particle size of the foulant as stated before.

Particles smaller than 0.1 µm behave in accordance with Brownian molecular motion based on the Stokes-Einstein formula (Cussler, 2009). According to the Stokes-Einstein relationship,

increasing particle diameters and higher viscosities of the feed reduce the diffusion coefficient and limiting flux, respectively.

The equation for calculation of the Brownian diffusion coefficient is as follows:

$$D_B = \frac{k_B \cdot T}{6 \cdot \pi \cdot \eta_{feed} \cdot r_{particulate}} \quad (2.20)$$

Where, k_B: Boltzmann constant (J/K)

T: temperature (K)

η_{feed}: dynamic viscosity of feed (Pa·s)

$r_{particulate}$: mean radius of particulate matter (m)

For particle sizes larger than 0.1 µm, Brownian diffusion does not significantly affect the back transport (Fane, 1984). Zydney and Colton (1986) replaced the diffusion coefficient by a shear-induced diffusion coefficient D_S. In addition, Leighton and Acrivos (1987) introduced a dimensionless hydrodynamic diffusion coefficient D(Φ) that can be used to empirically calculate a shear-induced diffusion coefficient D_S. Zydney and Colton (1986) proposed an approximated hydrodynamic diffusion coefficient D(Φ) of 0.03.

The shear-induced diffusion coefficient can be calculated as follows:

$$D_S = \dot{\gamma}_m \cdot {r_{particulate}}^2 \cdot D(\Phi) \quad (2.21)$$

Where, $\dot{\gamma}_m$: shear rate on membrane (1/s)

$r_{particulate}$: particle radius (m)

D(Φ): hydrodynamic diffusion coefficient (-)

$$D(\Phi) = 0.33 \cdot \phi^2 \cdot (1 + 0.5 \cdot e^{8.8 \cdot \phi})$$

Φ: volume fraction of particles relative to concentration (-)

In case of particle size larger than 0.1 µm, diffusive back transport and consequently limiting flux increase with larger particle diameter of foulants and higher shear based on crossflow velocity.

Filter resistance model based on Darcy's law (Hydrodynamic model)

This model is based on the general theory that the flow of each solution component through the membrane is proportional to the ratio of driving force and transport resistance. Each membrane has its own TMP- and flux related hydraulic membrane resistance R_m. In practice, the hydraulic membrane resistance is usually experimentally determined from the water flow at a given transmembrane pressure. In case of fouling, additional filter resistances caused by cover/gel layer or adsorption effects must also be considered.

Thus, the flow can be estimated based on Darcy's law as follows (Altmann and Ripperger, 1997; Schipolowski, 2007):

$$J = \frac{TMP}{(R_m + R_{ads} + R_{gel\ layer}) \cdot \eta_{filtrate}} \quad (2.22)$$

Where, R_m: resistance of membrane (m^{-1})

R_{ads}: resistance of membrane by adsorption (m^{-1})

$R_{gel\ layer}$: resistance of membrane by gel layer (m^{-1})

$\eta_{filtrate}$: viscosity of the filtrate (Pa·s)

During filtration, the membrane resistance and the adsorption resistance are comparatively low and can be neglected. However, the gel layer resistance is decisive and is defined as follows (Melin and Rautenbach, 2007):

$$R_{gel\ layer} = \frac{\eta_{feed} \cdot c_{feed}}{\tau_w \cdot \rho} \cdot F(TMP) \quad (2.23)$$

Where, η_{feed}: dynamic viscosity of the feed (Pa·s)

τ_W: wall shear stress (Pa)

ρ: density of feed (kg/m^3)

F(TMP): pressure-depending factor ($1/(m \cdot s)$)

The TMP-dependent empirical factor F is used to fit measured values (Melin and Rautenbach, 2007).

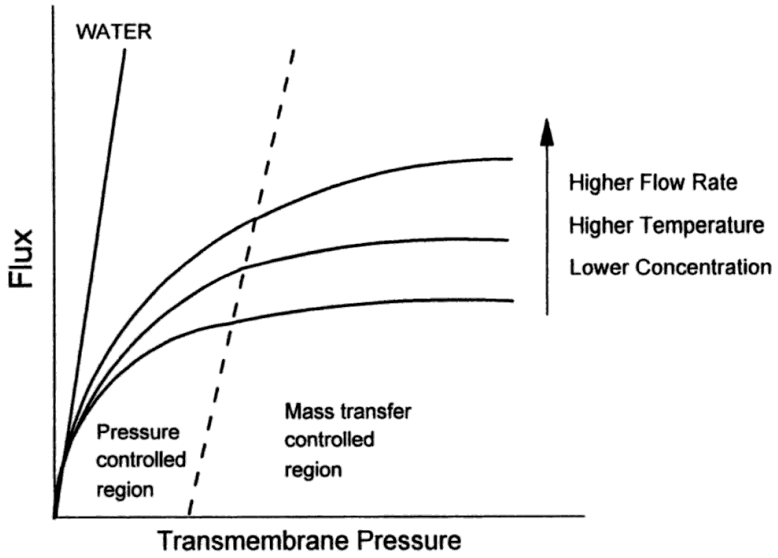

Figure 13. Simplified correlation of flux from TMP as driving force (Cheryan, 1998)

Based on the hydrodynamic model, lower resistances especially increase the achievable flux at even driving force (TMP). Within a sub-critical flux region (or for clean water), there is a linear relationship between TMP and flux. This region is called the pressure-controlled region (Cheryan, 1998). In this region, back transport is higher than the convective flux to the membrane, and there is no deposition of organic matter on the membrane surface. Here, the flux can be expressed in simple terms by a linear relationship between flux, TMP and specific

membrane resistance R_m, as additional resistances are negligible (see Figure 13). If the flow exceeds a system-dependant critical value, more substances are transported in the direction of the membrane surface than are transported back into the bulk stream. Thus, additional membrane resistances occur. This region is called the mass transfer-controlled region (Cheryan, 1998). Here, flux increases with higher flow rate and temperature and lower concentration or viscosity as bulk characteristics.

2.2.3 Design parameters for membranes in MBR

Membrane steps of membrane bioreactors are designed rather empirically because of the complexity of membrane filtration phenomena as shown in the previous section regarding mass transfer mechanisms (Drews, 2010). In addition to the general membrane selection, the flux represents the decisive design parameter. The higher the flux, the smaller the membrane surface required. However, higher flux also leads to a higher requirement of driving forces (TMP in micro- and ultrafiltration). Moreover, increased fouling rates exist due to stronger convective transport of foulants to the membrane surface. Economically, higher flux reduces capital expenditure (CapEx), while operational expenditure (OpEx) increases (Drews, 2010; Krebber, 2013). The widely accepted concept of critical flux is a practical approach for plant design (Guglielmi *et al.*, 2007; Dagnew, 2010; Drews, 2010).

Critical flux

Critical flux is defined as the flux below which minimal fouling occurs (Dagnew, 2010). This concept was introduced by Field *et al.* (1995). It describes the flux in which the convective transport of substances to the membrane surface and the diffusive back transport into the bulk stream are in equilibrium (Field *et al.*, 1995). Hence, based on a strong definition of the critical flux, operations below the critical flux show no fouling (Le-Clech *et al.*, 2003; Judd, 2011). If the flow exceeds the system-dependent critical flux, the mass flow of substances to the membrane surpasses backflow into the bulk, which leads to accumulation of particulate matter on the membrane surface. This concept results in a linear relationship between TMP and flux within the sub-critical flux region and an exponential increase in TMP above the critical flux value (Dagnew, 2010).

Critical flux cannot be theoretically predicted so far but can be estimated to be around 2/3 of the limiting flux (Field and Pierce, 2011). Lab or pilot tests must be conducted to design membrane units (Ochando-Pulido *et al.*, 2012). The flux-step method suggested by Field *et al.* (1995) is the most common method to determine the critical flux (Le-Clech *et al.*, 2003; Judd, 2011). As per the method, the flux is increased stepwise, kept constant for a certain time and the corresponding TMP in steady state is measured (Field *et al.*, 1995; Figure 46). The flux steps can then be plotted against, for example, the TMP at the end of each step (Figure 14). Field *et al.* (1995) define critical flux as the highest flux with a quasi-linear relationship between TMP and permeate flux without any increase in TMP at the end of the set flux step compared to clear water (strong form; see Figure 14). But other definitions of critical flux also exist which are based on other definitions of relevant changes in flux-TMP relationship (weak form of critical flux). The most used criteria for defining the critical flux were summarised by Le-Clech *et al.* (2003). The criteria are based on the change in relationship to flux by applying different relevant TMPs (initial, mean overstep or final) or the definition of maximum fouling rates. For

example, Le-Clech *et al.* (2003) define a critical fouling rate of 0.1 mbar/min for reversible fouling, applied in the last minutes of each step for defining the critical flux. Till date, no protocol for critical flux determination has been standardised. Step height, step duration and interval between these steps vary in publications; this influences the results of critical flux and complicates comparison (e.g. Drews, 2010; Krebber, 2013). Nevertheless, Le-Clech *et al.* (2003) report minor differences in critical flux values when comparing the most commonly used criteria. However, applying a criterion deviate from the strong form of critical flux leads to higher values of critical flux (Figure 14). Based on all criteria, critical flux mostly covers reversible fouling (short-term fouling; see Figure 10; Le-Clech *et al.*, 2003). Thus, in practical terms, critical flux is not always attainable in MBR, as other types of fouling may also be relevant to design (Judd, 2011).

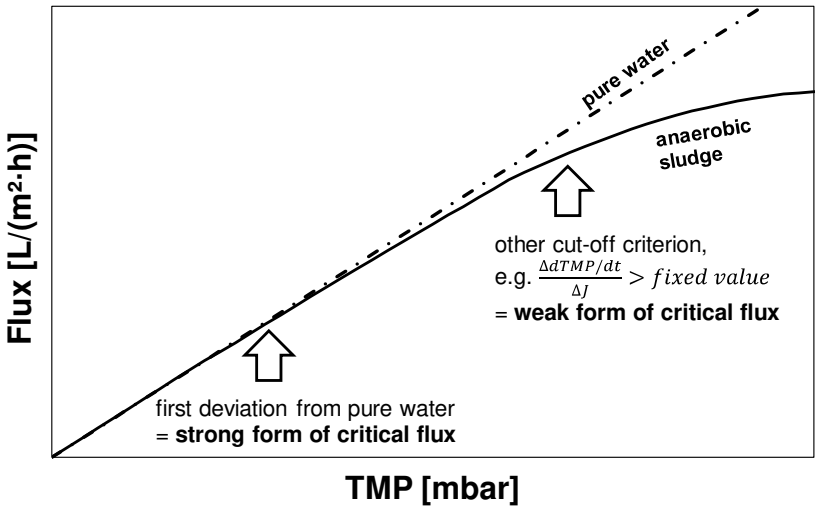

Figure 14. Schematic determination of the critical flux on applying flux-step method

Van der Marel *et al.* (2009) extended the previously introduced flux-step method for determination of residual and irreversible fouling (long-term fouling) as the criterion for critical flux. Van der Marel *et al.* (2009) included relaxation steps to develop critical flux values for membranes operated with backwash or relaxation phases, as common in practice. A relaxation phase is the filtration phase at low flux, in which reversible fouling is removed and the surface layer is reduced. When the TMP of the relaxation phase increases by a defined limit compared to the previous relaxation phase at low flux, irreversible fouling can be assumed. This critical flux is called critical flux for irreversibility. According to Van der Marel *et al.* (2009), the determination of the critical flux based on long-term fouling represents the transition to the threshold flux.

Threshold flux

The threshold flux is the maximum flux at which long-term fouling builds up at a very low and constant rate (Field and Pearce, 2011: Stoller *et al.*, 2013). Above the threshold flux, fouling increases exponentially (Stoller *et al.*, 2013). Usually, the threshold flux can only be determined in long-term tests for each investigated flux.

Sustainable flux

In practical terms, two different operational strategies of MBRs are possible:

- Intermittent operation with high flux (in the range of the critical flux), where associated high fouling rates may lead to extensive backflush or chemical cleaning.
- Sustainable permeability operation at low flux (close to threshold flux) with reduced fouling rates, which may lead to extension of chemical cleaning cycles.

While intermittent operation is related to high OpEx, sustainable permeability operation refers to low OpEx at high CapEx due to high membrane surface requirements. An extension of assessing both fluxes by economic factors is called the sustainable flux (Field and Pearce, 2011). The determination of the sustainable flux requires cost and duration of backwashing and chemical cleaning, membrane cost, flux and long- and short-term fouling rates. However, the exact determination is laborious, since long-term operations for each setting have to be carried out and economic factors additionally depend on the respective application and location.

Therefore, a subcritical range depending on the critical flux is commonly used as a design parameter for long-term operation with reasonable fouling rates (Dagnew *et al.*, 2010; Judd, 2011; Dereli *et al.*, 2014a). The sustainable flux is usually in a range of 60-80 % of the critical flux (Dagnew *et al.*, 2010; Judd, 2011; Dereli *et al.*, 2014a):

$$J_{design} = J_{sustainable} \approx (0.6 - 0.8) \cdot J_{critical} \qquad (2.24)$$

2.3. Membrane bioreactor for particulate- and lipid-rich anaerobic digestion (AnMBR)

Recuperative thickening (RT) represents an extension of CSTR as standard process for particulate-rich sludge digestion (see Section 2.1.3) with an aggregate for solid-liquid separation in order to decouple HRT and SRT as a result of partial sludge recirculation (see Figure 15) (Torpey and Melbinger, 1967).

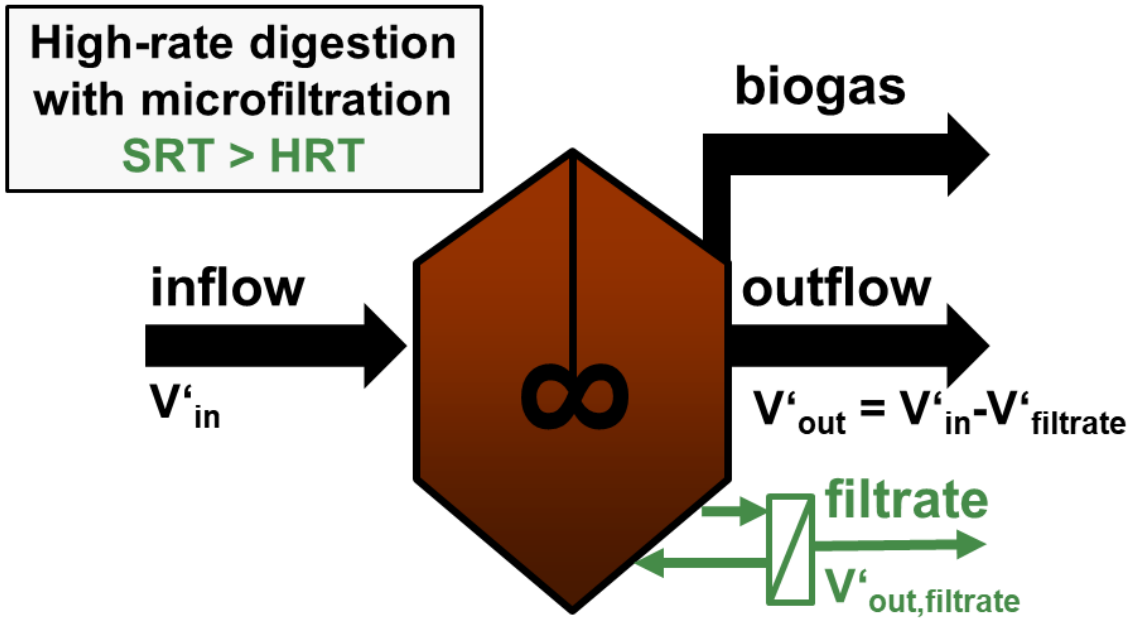

Figure 15. Simplified process scheme of recuperative thickening (RT) using a membrane in side-stream configuration

The decoupling of SRT and HRT increases the concentration of particulate matter in the reactor which contains biomass, inorganic matter and organic non-degradable and degradable matter. As a result of higher concentrations of substrate and biomass, higher reaction rates should result in RT (see Section 2.1.2.1). Centrifuges, flotation devices, belt filter presses, screw thickeners or membranes may serve to separate sludge.

RT offers especially the following opportunities:

- Reduction of digester volume at similar methane yield.
- Lower heat loss and, possibly, lower energy demand for mixing.
- Increased COD removal/methane yield at similar digester volumes.
- Higher process stability based on higher biomass concentration in the reactor.
- Upgrade of existing digesters through establishment of spare capacity for additional sludge.

Table 5. Overview of comparative studies concerning continuous-flow stirred-tank reactor (CSTR; in italics) and recuperative thickening (RT)

Substrates	OLR_{max} [g VS/L/d]	HRT [d]	SRT [d]	Dewatering unit	Scale	Performance: Methane yield	Performance: VS removal	Performance: Process stability	Ref.
WAS + PS	*1.75*	*20*	*20*	/	lab				a
(40%+60%)	3.5	10	28-30	Gravity		-	+ 10 %	(+)	
THP sludge	*4.75*	*15*	*15*	/	lab				b
	4.75	15	30	Filtration[3]		-	-	(+)	
THP sludge	*4.75*	*15*	*15*	/	lab				b
	8.58	7.5	15	Filtration[3]		-	-	(+)	
Raw sludge	*n.a.*	*15*	*15*	/	large				c
	n.a.	15	40	Centrifuges		+20 %	+22 %	(+)	
Raw sludge	*n.a.*	*20*	*20*	/	lab				d
	n.a.	20	30	Gravity		-[1]	n.a.	(+).	
WAS + PS	*1.5*	*25*	*25*	/	large				e
	4.0	10	25	Screws		-[1]	Lower	-[2]	
WAS	*0.4 - 0.5*	*30*	*30*	/	lab+				f
	0.8 - 0.9	15	30	Membrane	pilot	+ 13 %	+ 10 %	n.a.	
WAS + PS	*0.5*	*34*	*34*	/	pilot				g
	1.3	15	35	Membrane		+8 %	+ 15%	-	
WAS + PS	*0.9*	*17*	*17*	/	pilot				g
	2.5	17	25	Membrane		+40 %	+42 %	+[2]	

- means equal to CSTR
n.a. means not applicable; data was not provided
+ means reported better, but data was not provided
[1] concerning biogas yields
[2] based on VFA/alkalinity
[3] filtration over belt filter material

References:
a. Cobbledick *et al.* (2016); b. Romero-Flores *et al.*, (2017); c. Bharambe *et al.* (2015); d. Yang *et al.* (2015); e. Josse *et al.* (2017); f. Dagnew *et al.* (2013); g. Pileggi and Parker (2017).

RT is mainly considered in research and investigated in lab scale (see Table 5). Full-scale implementations are limited but do exist, for example, in Sidney (Australia) and Gloversville-Johnstown Joint Wastewater Treatment Facility (Bharambe *et al.*, 2015; Yang *et al.*, 2015).

Most research studies focus on increasing methane yield at low HRT or generating spare digester capacity without significant loss of VS reduction (e.g., Yang *et al.*, 2015; Cobbledick *et al.*, 2016).

In the comparison of degradation performance in CSTR and RT, operation at the same SRT is crucial, as SRT plays an essential role in COD removal (see Section 2.1.2.1). An extension of SRT always leads to higher COD removal regardless of reactor type if the conditions are otherwise the same. However, studies comparing performances of RT and CSTR at similar SRT but lower HRT (smaller reactor volumes) are limited. Moreover, published results are contradictory (see Table 5): Pileggi and Parker (2017) and Dagnew *et al.* (2012) observed small increase in VS removal compared to a CSTR using an AnMBR with SRT/HRT ratios greater than 2. In contrast, Berg *et al.* (2016) achieved lower specific methane yields at equal SRT using centrifuges for RT. Yang *et al.* (2015) and Romero-Flores *et al.* (2017) achieved similar methane or biogas yields using gravity thickening compared to a CSTR with similar SRT in lab scale. Cobbledick *et al.* (2016) observed similar methane yields in both reactor types using a belt filter at lab scale for RT reactors.

A higher process stability using RT is observed in most studies, although reactors were operated with higher COD loading rates and reduced HRT. However, the basis for assessing process stability or data were not provided in any of the studies compiled in Table 5.

These observations contradict published concerns in biomass activity losses due to high shear stress or oxygen exposure during dewatering or concentration of biomass (Ghyoot and Verstraete, 1997; Padmasiri *et al.*, 2007; Batstone *et al.*, 2015). Deveci (2002) found a strong impact on the viability of aerobic acidophilic organisms, particularly at solids concentrations above 10 % when using a centrifuge. Significant losses in SMA, around 54 %, were observed using centrifuges for dewatering (Batstone *et al.*, 2015). Activity losses in rotary drum thickeners remained low (0-20 %; Batstone *et al.*, 2015). No impact on biomass activity based on low oxygen exposure was observed in a belt thickener (Conklin *et al.*, 2007). Air sparging in flotation devices negatively impacted sludge activity (Conklin *et al.*, 2007). While using membrane filtration, high crossflow velocities are required for reduction of membrane fouling. In some studies, a performance reduction was observed in AD using membranes for RT, and activity losses were used as an explanation (e.g., Ghyoot and Verstraete, 1997; Padmasiri *et al.*, 2007). Dagnew (2010) and Pileggi and Parker (2017) did not observe any decline in digestion performance regarding VS removal performance in long-term investigations. However, low activity losses must not lead to performance reduction in RT reactors (especially at low recycle flows), as hydrolysis is rate-limiting mainly in sludge digestion and not affected by activity losses (Batstone *et al.*, 2015). Therefore, the question of activity losses in AnMBR application remains open.

Furthermore, when different devices for solid-liquid separation applicable in anaerobic digesters are compared, it was found that advantages of membranes especially include a capture rate of 100 % of particulate matter, which leads to a defined adjustable SRT without requiring additional flocculants (see Table 6). When using gravity thickening and centrifugation, Bharambe *et al.* (2015) and Cobbledick *et al.* (2015) reported difficulties in setting a defined solid retention time in the digester due to varying degrees of separation. Josse *et al.* (2017) achieved a steady capture of particulate matter over 98 % using a sludge screw thickener in large scale. The determination of losses of active biomass due to this incomplete capture have not yet

been investigated. Open dewatering units such as flotation devices, belt filter presses and centrifuges lead to emissions of dissolved methane due to turbulences and changes in partial pressure (see Schaum *et al.* (2015)). Berg *et al.* (2016) and Cobbledick *et al.* (2016) report higher organic matter reduction than measured as methane volume; this might indicate methane losses during solid-liquid separation. Membrane applications can be designed as closed systems with a limited release of methane during operation. All dewatering technologies except membrane filtration demand polymeric flocculants. Membranes may be successfully applied to eliminate the need for thickening polymers and to avoid their potential inhibitory effect on anaerobic biomass (Pierkiel and Lanting, 2005). However, membrane applications face a higher CapEx and additional energy expenditures, possibly leading to higher operational costs. Although membranes reliably serve for solid-liquid separation in AnMBRs (Judd, 2011), application of membranes for RT in sludge digestion are still rare (see Table 7 and Table 8).

Table 6. Most significant advantages and drawbacks of using membranes compared to other aggregates for solid-liquid separation in AnMBRs

Advantages	Drawbacks
• Capture rate of 100 % • No need of flocculants or other chemicals for solid-liquid separation • Limited release of methane during operation	• High CapEx • Higher energy consumption (?) • Require chemicals for cleaning • (no?) Activity losses based on shear for reducing fouling (?)

For sewage sludge treatment, most of the investigated membrane configurations applied sidestream tubular ultrafiltration membranes with pore sizes between 0.02 µm and 0.1 µm. Some authors used rotating ceramic discs with a mean pore diameter of 0.2 µm as in this study. Reported flux varies greatly between 5-30 L/(m²·h), which is related to variations in TMP as well as the concentration of digestates. Pierkiel and Lanting (2005) operated an AnMBR for a short period of time (7 days), which is why the reported flux of 84 L/(m²·h) is out of range. Except for the study of Brond *et al.* (2016), who also ran their reactor for a short period of time, digestate concentrations were found to be below TS = 32 g/L. According to Jahn *et al.* (2016), this range does not match the favoured operation of particulate-rich digestion on municipal WWTPs above 3 % (~30 g/L) in the digested sludge.

Reported data on using AnMBR for treating lipid-rich residuals or wastes is rare (see Table 8). There is no literature evidence regarding the use of AnMBR for digestion of lipid-rich flotation sludge from the dairy industry. Nevertheless, problems with LCFA by increased concentrations in an AnMBR were reported based on agglomeration using lipid-rich kitchen waste slurry as substrate (Xiao *et al.*, 2015). Xiao *et al.* (2015) proposed lower SRT in order to wash out inhibiting free LCFAs without providing specific threshold values. Dereli *et al.* (2014b) treated lipid-rich feed but did not notice problems based on the decoupling of HRT and SRT. At reactor concentration between 20-40 g/L (approx. 2-4 % TS), fluxes are achieved in a wide range between 1.6-80 L/(m²·h) (Table 8). Major advantages over conventional CSTRs or an operational flux that applies with a certain degree of certainty cannot be derived from these experiences.

Table 7. Comparison of membrane performance in AnMBR treating sludge from municipal WWTP

Feedstock	PS+WAS	PS+WAS	PS+WAS	PS+WAS	PS+WAS	WAS	WAS	WAS	WAS	WAS
$C_{digestate}$ (g/L)	10	30	55-60	25-40	25-40	16-20	25	32	16-20	2-36
Module type	tubular	rotating discs	rotating discs	tubular	tubular	tubular	tubular	tubular	hollow fiber	tubular
Material	TiO_2/ stainl.steel	Ceramics	Ceramics	PVDF	PVDF	PVDF	PVDF	PVDF	PVDF	PTFE
Pore size [µm]	0.1	0.2	0.2	0.02[3]	0.02[3]	0.02[3]	0.02[3]	0.02[3]	0.02	1
Surface [m^2]	1.4	1	6.8	0.2	0.2	0.2	0.2	0.2	1.07	0.015
TMP [bar]	2.4-2.8	0.2	-	0.3-0.5	0.3-0.5	0.3	0.3	0.3	<0.1	0.06
Flux [L/(m^2·h)]	84	20-30	25-30	6 - 8	6 - 8	30	21	16	11	5-11
Temperature [°C]	35	35	35	35	35	35	35	35	35	25
CFV [m/s]	5	-	-	1-1.2	1-1.2	1	1	1	1	0.1-0.7
HRT|SRT [d|d]	[1]	[2]	-	7|21	15|30	15|30	7|15	7|30	15|30	
Scale	pilot	pilot	pilot	pilot	pilot	pilot	pilot	pilot	pilot	lab
Ref.	a	b	c	d	d	e	f	f	e	g

a. Pierkiel and Lanting (2005); b. Badenova (2005); c. Brond *et al.* (2016); d. Pileggi (2016); e. Dagnew *et al.* (2013); f. Dagnew (2010); g. Ho and Sung (2009).

[1] short-term operation of around 7 days without specification of inoculum

[2] information not given

[3] MWCO = 100,000 Da

Table 8. Comparison of membrane performance in AnMBR treating lipid-rich residuals

Feedstock	Slaughter-house	Slaugh-terhouse	Kitchen waste slurry	Food waste	Food processing	Dairy waste +manure	Potato processing	Corn-based bio-ethanol plant	Swine manure
$C_{digestate}$ [g/L]	20	20-28	~ 30	20-40	23	29	40	16-28	20-40
Module	hollow fibre	tubular	tubular	flat	flat	flat	Flat	tubular	tubular
Material	Zenon ZW-10	Ceramic (Al_2O_3)		Nylon mesh		Titanium		PVDF	PVDF
Pore size	n.a.	0.2 µm	10^5 Da	50 µm	0.4 µm	0.2 µm	0.4 µm	0.03 µm	$2 \cdot 10^4$ Da
Surface [m²]	0.93	0.126	0.1	0.04		0.09			0.038
TMP [bar]	0.05	n.a.	0.23	0.01	0.03		0.03-0.04	0.05-0.2	0.4
Flux [L/(m²·h)]	1.6	5-10	7-15	2-10	2.5-4.2	40-80	0.8-5	10-14	5-10
T [°C]	38	30	39	37	33	55	35	37	37
CFV	35 L/min[2]	2-3 m/s	2.2 m/s	200 rpm	n.a.	3.3 m/s	n.a.	0.5 m/s	n.a.
HRT|SRT [d|d]	4|50	1.2|-	n.a.	7|30	29|-	23|30	<14|80	10|20-50	6|-.
Scale	pilot	lab	pilot	lab	pilot	pilot	Lab	lab	lab
Ref.	a	c	h	b	e	l	D	f	g

a. Jensen *et al.* (2015); b. Tang *et al.* (2017); c. Fuchs *et al.* (2003); d. Singh *et al.* (2010); e. Christian *et al.* (2010); f. Dereli *et al.* (2014b); g. Padmasiri *et al.* (2007); h. Xiao *et al.* (2015); i. Zitomer *et al.* (2005).

[1] mean FOG concentration of 1.8 g/L at total COD of around 10 g/L

[2] biogas sparging

In AnMBR, fouling is particularly related to the formation of cake layers on the membrane surface (Choo and Lee, 1996; Jeison and van Lier, 2008; Ho and Sung, 2009; Jørgensen *et al.* 2014; Pileggi, 2016). Compared with other applications of AnMBR that deal with treating mainly particulate-free substrates, AnMBR treating sludge faces even higher fouling potential. Fouling is associated with high concentrations of suspended solids, colloidal organic substances and soluble inorganic materials, which are partly released during digestion (Dagnew, 2010). Thus, mitigation strategies result from the reduction of negative influences especially concerning bulk characteristics and general strategies such as chemical cleaning and backwashing. The following section summarises additional experiences of influences on fouling (membrane performance), which are especially important for AnMBR in sludge treatment and which were not introduced in Sections 2.2.1 and 2.2.3

Influence of bulk characteristics on fouling

Liao *et al.* (2006), Jeison and van Lier (2008) and Huang *et al.* (2011) concluded that high concentrations of total suspended solids (TSS) lead to accelerated membrane fouling. Itonaga *et al.* (2004) showed a dependence on viscosity. Fouling is accelerated especially when TSS concentration exceeds 12 g/L as the viscosity increases exponentially above 12 g/L (Itonaga *et al.*, 2004). This contradicts Jeison and Van Lier (2008), who observed a linear reduction of the critical flux as a function of the total solids` concentration even at higher values between 25 and 50 g/L.

Smaller flocs enhance membrane fouling (Huang *et al.*, 2011; Xiao *et al.*, 2015), probably because of lower shear-induced diffusion coefficients, as shown in Section 2.2.2. Jeison and van Lier (2008) and Dereli *et al.* (2014a) reported a better filterability with an increase in volume-related median particle sizes. Dagnew (2010) reported that filterability increases with a number-related median particle size but not significantly with a volume-related median particle size. In addition, particles about the size of the membrane pores cause fouling in AnMBR by blocking the pores (Liao *et al.*, 2006; Stuckey, 2012).

The significant influence of soluble microbial products (SMP) and/or soluble extracellular polymeric substances (EPS) on fouling is well acknowledged (e.g., Drews, 2010; Judd, 2011). SMP are defined as cellular components that are released during cell lysis, diffused through the cell membrane, lost during synthesis or excreted for some purpose. An *et al.* (2009) and Lin *et al.* (2009) have found biopolymers to be especially responsible for membrane fouling. Regarding EPS and fouling, positive (Chang and Lee, 1998; Huang *et al.*, 2009), negative (Cho and Fane, 2002; Ahn *et al.*, 2006; Rosenberger *et al.*, 2006; Lin *et al.*, 2009; Dagnew, 2010) as well as no relationship (Yamato *et al.*, 2006) have been reported (Dagnew, 2010). Therefore, the relative contribution of different biopolymer fractions (carbohydrates, proteins) as well as their boundary status is complex and not fully understood (Dagnew, 2010; Judd, 2011). Divalent and trivalent cations such as iron and aluminium can neutralise the negative charge of biomass flocs and stabilise their structure (Sobeck and Higgins, 2002; Park *et al.*, 2006) which might reduce fouling. Choo *et al.* (2000) attribute reduction in fouling to the addition of divalent cations by polyaluminium chloride (PAC) because of decrease of colloidal matter. Choo and Lee (1996) report that the fine colloidal matter of the bulk is mostly responsible for cake layers, although its share in total solids is low. This explains improved critical flux after PAC addition by Choo *et al.* (2000).

In addition, precipitation of inorganic compounds, especially struvite (Yoon *et al.*, 1999; Judd, 2006; Liao *et al.*, 2006) and calcium compounds such as calcium carbonate (Kim *et al.*, 2007; Zhang *et al.*, 2007; Meabe *et al.*, 2013) were observed in AnMBR applications. Inorganic fouling because of reduced solubility of inorganic compounds is mainly caused by pH change induced by pressure changes or changes of partial pressures and CO_2 release (Kang *et al.*, 2002; Judd, 2011). It accounts to irreversible fouling and can only be reduced by chemical cleaning (see Figure 10).

More general parameters such as capillary suction time tests (CST) usually used for evaluation of dewatering ability can also be potentially used for comparing the filterability characteristics of sludge in MBR (Dereli *et al.*, 2014a). However, published results are contradictory. While some authors show a good linear correlation between CST and membrane filtration resistance (e.g., Pollice *et al.*, 2008; Laera *et al.*, 2009), Wang *et al.* (2006) show a non-linear relationship between the critical flux and CST. In other studies, no clear correlation was found (Khongnakorn *et al.*, 2007; Lyko *et al.*, 2008; Dereli *et al.*, 2014a).

Influences of AnMBR operation on fouling

Dereli *et al.* (2014a) and Dagnew (2010) observed a better filterability at lower SRT of around 20 d than at extended SRT of 30 d. Dereli *et al.* (2014a) assumed that this is related to a better washout of fine particles, as median particle size was higher at lower SRT. Dagnew (2010) also reported that the number of colloidal particles was reduced at shorter SRT.

Chen *et al.* (2017) observed that at low OLRs, fouling in an AnMBR (submerged membrane configuration with suspended biomass; PE flat sheet membrane; pore size = 0.2 µm) was caused by internal fouling induced by SMP. Kayawake *et al.* (1991) reported higher SMP concentration at lower organic loading rate. In contrast, at increased OLR, fouling was mainly attributed to the build-up of a cake layer, which was promoted by the increased concentration of highly adhesive EPS bound to biomass in the reactor (Chen *et al.*, 2017).

The operation of the membrane with subcritical flux is obligatory (see Section 2.2.3). Shimizu *et al.* (1996) and Jørgensen *et al.* (2014) show dependencies of limiting flux in aerobic MBR based on sludge concentration and shear stress. Shear rates or wall shear stress on membrane surfaces are not provided in most publications of AnMBR. Till date, no research has been done on evaluation of fouling in AnMBR based on shear comparing different membranes.

Influences of membrane design on fouling

In different studies, selection of the membrane appears to be rather arbitrary, as different membranes were used for similar applications (see Table 7). Dagnew *et al.* (2013) observed higher critical flux in tubular membranes than in hollow fiber membranes at similar mean pore size of the membranes (0.02 µm) and sludge characteristics. Negative charge of the tubular membrane surface slightly improved permeability because of lower TMPs in operation compared to a neutral charge (Dagnew *et al.*, 2013).

2.4. Summary

The literature review indicates limited research on AnMBR treating high strength particulate wastewater or sludge, especially those with high shares of lipid-rich residues, in scales larger than lab scale. Although countless kinetic models of the rate-limiting process step and membrane fouling exist, investigations on effects of membrane filtration on degradation performance of anaerobic digestion are limited.

A major concern with membrane filtration is reduction of microbial activity, as high shear stress is required for mitigating fouling. Conversely, shear forces could be advantageous for the degradation rate by reducing the particle diameter of the substrates. Published degradation performance of AnMBR in comparison to CSTRs is contradictory and was mostly obtained in lab scale with very high shear and in short test periods. Hence, a revision of existing kinetic models of AnMBR is required on the basis of long-term investigations.

Experience of the degradation performance of lipid-rich sludge is mostly limited to the standard reactor configuration, CSTR. Although limitations of the process are known, they are not transferable to other applications (substrate mixtures). A generally valid design criterion that includes the specific properties of the substrates or their mixtures and different reactor types has not been elaborated so far. Generally accepted knowledge about TS-related inhibition of LCFA during anaerobic lipid degradation have not been effectively considered so far. While in batch tests, SMA determination is used to clarify toxicities, SMA has not yet extensively been used to describe process stability in continuous AD operation.

There is extensive research and experience of fouling in aerobic MBR and partly in AnMBR treating mostly soluble substrates. However, using AnMBR for sludge treatment differs from these applications, as sludge concentrations are much higher than in common MBR and AnMBR applications treating soluble organic matter. Effects of key parameters of fouling in common MBR and AnMBR applications, such as SMP, EPS and colloidal matter on fouling could simply be outweighed by high concentration of solids and increased viscosity. The impacts of anaerobic sludge characteristics of AnMBR treating particulate-rich substrates on membrane fouling have not yet been investigated in detail.

Based on this lack of knowledge, the following topics will be discussed in this work:

Chapter 3 deals especially with the evaluation of kinetics and effects on methanogenic activity (SMA) on AD processes in an AnMBR using RT.

Chapter 4 focuses on treatment of WAS with high shares of flotation sludge from dairy industry using an AnMBR and CSTRs. A generally valid design criterion for limitations of lipid-rich sludge treatment is elaborated which allows the transferability of results regarding limitations to other applications. SMA is integrated to represent changes in process stability.

Chapter 5 deals with the integration of SMA for process control in continuously operated reactors and for the quantification of present spare digester capacity. Boundary conditions for inlet fluctuation and feeding strategy are elaborated.

Chapter 6 covers the impacts of decisive anaerobic sludge characteristics on filterability in terms of the critical flux.

3. Evaluation of kinetics in an AnMBR using recuperative thickening for anaerobic digestion of waste activated sludge

This chapter is mainly based on

Lutze, R., Rühl, J., Engelhart, M. (2017) Membrane digester as key unit of sludge treatment at changing frame conditions. In Proceedings: *IWA Specialist Conference on Sludge Management* "Sludge-Tech 2017", 09.-13.07.2017, London, UK.

3.1. Introduction

Inflow loads to municipal WWTPs in fast growing dynamic urban areas and to industrial WWTPs change constantly. This makes it difficult to maintain flexibility and expandability of sewage plant technology (Cervantes *et al.*, 2006; Tolksdorf *et al.*, 2016). These challenges also concern sludge treatment where conventionally operated digesters, characterised by slow degradation rates at high retention times, quickly reach their limits. In conventional digesters HRT equals SRT. At sudden higher sludge inflow, HRT and SRT decrease simultaneously, which can lead to overloading effects and incomplete digestion. At times with lower sludge inflow HRT and SRT increase and might reach retention times of more than 25 days. Here, methane yields do not significantly increase (see Figure 5) at the expense of energy losses for heating and mixing of the digester. Common design recommendations of HRT are between 15-20 days (DWA-M 368, 2004; Metcalf and Eddy, 2004; WEF/ASCE, 2009).

Recuperative Thickening (RT) is the process of decoupling SRT from HRT by thickening solids in the effluent of anaerobic digesters using a separation unit and returning some of thickened solids to the anaerobic digester. In this context, RT can be used for buffering varying sludge volume flows by providing flexibility in order to keep a sufficient SRT in the reactor. In this work, AnMBR was chosen as an RT system using membrane filtration as separation technology.

For sludge treatment, RT has already been researched and is implemented in a large scale (see Section 2.3). However, research data on AnMBRs shows inconsistent results concerning achieved methane yields in comparison to conventional CSTRs. At similar SRT of a digester with RT and a CSTR fed with the same sewage sludge, lower specific methane yields (e.g., Berg *et al.*, 2016, similar methane yields (e.g., Yang *et al.*, 2015; Romero-Flores *et al.*, 2017; Josse *et al.*, 2017) and higher methane yields (e.g., Dagnew *et al.*, 2012; Pileggi and Parker, 2017) were observed. At similar HRT, digesters with RT achieve higher methane yields than CSTR (see Table 5). Digesters with RT were operated at higher COD loading rates at reduced HRT while even higher process stability was reported. Comparison is usually based on limited experimental data, which focus on one or two operational settings (SRT) and do not focus on a broad evaluation of degradation kinetics. Studies invariably focused on TSS concentration below 30 g/L, which, according to Jahn *et al.* (2016), does not match the favoured operation of sludge digestion above 3 % (~30 g/L) in the digested sludge under economic and energetic aspects.

The major concern with RT is a reduction in specific methanogenic activity and microbial community due to high shear stress during dewatering. Batstone *et al.* (2015) show that low shear dewatering units do not adversely affect specific methanogenic activity. Regarding membrane filtration, high crossflow velocities are needed to reduce fouling on membranes. Reduction in

performance of anaerobic digestion is reported in some studies, especially in investigations done in lab scale (e.g., Ghyoot and Verstraete, 1997; Padmasiri *et al.*, 2007). A few long-term assessments of an AnMBR treating mixed raw sludge of a municipal WWTP conducted in a pilot scale did not observe any decline in digestion performance (Dagnew, 2010; Pileggi and Parker, 2017). Therefore, the question of activity losses in AnMBR applications remains open.

In this study, to evaluate inconsistent literature results, long-term studies of a continuously fed AnMBR treating WAS were conducted in a pilot scale. First, theoretical considerations and working hypotheses were established. These were later verified in pilot tests. Pilot tests were conducted with high total solid concentrations (> 4 %). Different HRTs and SRTs were applied. As a major aim of this study, COD removal and removal rates in AnMBR and CSTR were compared at similar and different SRTs. In the context of this aim, HRT and SRT were set below common design recommendations, since differences in methane yield and kinetics are more obvious at lower SRT. Additionally, process stability was assessed as a key indicator for tolerance against load variation. Changes in specific methanogenic activity during long-term operation of AnMBR equipped with a rotating ceramic disc filter (in a quasi large scale membrane module in terms of shear) were monitored as well.

3.2. Expected effects on removal rates by decoupling of HRT and SRT

Disintegration is usually the rate-limiting step in sewage sludge digestion (Vavilin et al., 2008). In contrast to simple assumption of first-order kinetics suggested by Batstone *et al.* (2002), other kinetic models also assume an increase in the degradation rate because of higher biomass concentration or its associated higher concentration of extracellular enzymes (see section 2.1.2). Vavilin *et al.* (1996) compared several hydrolysis kinetics for assessing degradation rates and showed that first-order models are only slightly poorer in prediction than more complex models such as the two-phase model introduced by them. A model with the Contois kinetics approach (which uses a single parameter to represent saturation of both substrate and biomass) was as good at fitting the data as the two-phase model (Batstone *et al.*, 2002).

Working hypothesis

For comparing performance of a CSTR and an AnMBR, the following working hypothesis is made:

COD removal in AnMBR and CSTR does not differ for the same SRT.

Additionally, decoupling does not affect

- substrate characteristics, its degradability and kinetic constants such as k_{dis},
- microorganisms' activity, their biomass yield and decay rate,
- microorganism population (as no shift to other species occurs).

In the following, the working hypothesis will be validated first by means of kinetic models and then by studies on a pilot scale (see section 3.4).

Concerning kinetic models, the effects of this working hypothesis on removal rates is introduced in more detail in the following. Substrate first-order model and Contois kinetics approach are used as examples as both are commonly used in AD modelling.

Effects of working hypothesis on differences in removal rates of CSTR and AnMBR taking substrate first-order kinetics into account

In general, the residual degradable COD concentration in the reactor X_{COD} in steady state can be calculated as follows:

$$X_{COD} = X_{COD,0} \cdot (1 - \eta_{COD}) \quad (3.1)$$

Where, X_{COD}: residual degradable COD concentration in the reactor (COD of effluent; g/L)

$X_{COD,0}$: inflow concentration (g/L)

η_{COD}: COD removal (-)

It can be extended through the decoupling of HRT and SRT by full retention (capture rate = 100 %) of suspended solids via, for example, microfiltration. The resulting equation is as follows:

$$X_{COD} = X_{COD,0} \cdot (1 - \eta_{COD}) \cdot \frac{SRT}{HRT} \quad (3.2)$$

While applying RT (index RT), there are decoupling ratios of SRT/HRT greater than 1. CSTRs are operated with equal SRT and HRT, leading to a decoupling ratio of 1 (index CSTR). Assuming equal COD removal at even SRT, residual degradable substrate concentration in the RT reactor can be expressed in dependence of concentration in a CSTR at similar SRT as follows:

$$X_{COD,RT} = \frac{SRT}{HRT} \cdot X_{COD,CSTR} \quad (3.3)$$

Using substrate first-order kinetics (expression 2.1 in chapter 2) for comparing removal rates, removal rates differ in the range of the decoupling ratio SRT/HRT if abovementioned working hypotheses are valid.

$$\frac{\frac{dX_{RT}}{dt}}{\frac{dX_{CSTR}}{dt}} = \frac{-k_{dis} \cdot X_{COD,RT}}{-k_{dis} \cdot X_{COD,CSTR}} = \frac{-k_{dis} \cdot \frac{SRT}{HRT} X_{COD,CSTR}}{-k_{dis} \cdot X_{COD,CSTR}} = \frac{SRT}{HRT} \quad (3.4)$$

Effects of working hypotheses on differences in removal rates of CSTR and AnMBR taking Contois kinetics into account

The daily biomass production P_x depends on the removed COD mass, SRT and microorganism-related constants such as yield and decay constant. It can be calculated as suggested by Metcalf and Eddy (2004):

$$P_x = \frac{Y \cdot \eta_{COD} \cdot Q \cdot X_{COD,0}}{(1+k_d \cdot SRT)} \quad (3.5)$$

Where, P_x: biomass production (kg VS/d)

Y: biomass yield (kg VS/kg $COD_{degraded}$)

Q: daily inflow (m^3/d)

$X_{COD,0}$: inflow concentration (g/L)

η_{COD}: COD removal (-)

k_d: decay constant (1/d)

The biomass concentration in the reactor can be calculated as follows:

$$X_{BM} = \frac{P_x \cdot SRT}{V_{reactor}} \quad (3.6)$$

Where, X_{BM}: biomass concentration (kg VS/m^3)

$V_{reactor}$: digester volume (m^3)

Considering the working hypothesis, the biomass concentration in an AnMBR (index RT) and a CSTR at even SRT can be expressed with

$$X_{BM,RT} = \frac{SRT}{HRT} \cdot X_{BM,CSTR} \quad (3.7)$$

Using Contois kinetics (see equation 2.8 in chapter 2) for comparing removal rates, removal rates differ in the range of the decoupling ratio SRT/HRT if the working hypothesis is valid.

$$\frac{\frac{dX_{RT}}{dt}}{\frac{dX_{CSTR}}{dt}} = \frac{-k_H \cdot \frac{\frac{X_{COD,RT}}{X_{BM,RT}}}{K_X + \frac{X_{COD,RT}}{X_{BM,RT}}} \cdot X_{BM,RT}}{-k_H \cdot \frac{\frac{X_{COD,CSTR}}{X_{BM,CSTR}}}{K_X + \frac{X_{COD,CSTR}}{X_{BM,CSTR}}} \cdot X_{BM,CSTR}} = \frac{\frac{\frac{X_{COD,CSTR} \cdot \frac{SRT}{HRT}}{X_{BM,CSTR} \cdot \frac{SRT}{HRT}}}{K_X + \frac{X_{COD,CSTR} \cdot \frac{SRT}{HRT}}{X_{BM,CSTR} \cdot \frac{SRT}{HRT}}} \cdot X_{BM,CSTR} \cdot \frac{SRT}{HRT}}{\frac{\frac{X_{COD,CSTR}}{X_{BM,CSTR}}}{K_X + \frac{X_{COD,CSTR}}{X_{BM,CSTR}}} \cdot X_{BM,CSTR}} = \frac{SRT}{HRT} \quad (3.8)$$

Conclusions

Following the same pattern, Table 9 summarises expected effects of other kinetic models. For the same COD removal in AnMBR and CSTR, kinetic models assume either an increase of removal rate in the range of the decoupling ratio SRT/HRT or an increase of removal rate beyond the decoupling ratio SRT/HRT. Interestingly, increased removal rates are explained by higher residual substrate concentration (e.g. substrate first-order kinetics) and alternatively by higher biomass concentration (e.g. Contois kinetics).

Higher removal rates in the range of the decoupling factor mean that in an AnMBR comparable COD removal of the substrate is achieved at comparable SRT. This is in agreement with abovementioned working hypothesis and most kinetic models (e.g. ADM 1 and Contois kinetics) but contradicts a number of publications (e.g., Dagnew *et al.*, 2012; Pileggi and Parker, 2017). For achieving an even COD removal, lower HRT is required in AnMBR. Smaller reactor volumes of AnMBRs compared to CSTRs result in the range of the decoupling factor. Thus, higher COD removal results only if SRT is extended in AnMBR compared to a CSTR.

Higher removal rates beyond the decoupling factor mean that in an AnMBR comparable COD removal of the substrate is achieved at lower SRT. This is agreement with some kinetic models (e.g. half-order biomass model proposed by Rozzi and Verstrate (1981) and Valentini *et al.* (1997)) and a number of publications (e.g., Dagnew *et al.*, 2012; Pileggi and Parker, 2017) but contradicts abovementioned working hypothesis. In this case, higher methane yields (COD removal) in AnMBR are achieved at similar SRT. Deviation from the decoupling factor can also be seen in the approach introduced by Schlattmann (2011). If the concentration of hydrolytic biomass is below a certain limit, there are higher hydrolysis/disintegration constant results for RT, which in turn increases the relative degradation rates beyond the decoupling factor.

Table 9. Increase in removal rates of AnMBR using RT compared to CSTR for different kinetic models under assumption of equal COD removal

Disintegration/hydrolysis kinetics according to	$\frac{dX_{RT}/dt}{dX_{CSTR}/dt}$
Substrate first-oder kinetics (ADM1)	$\frac{SRT}{HRT}$
Contois kinetics (Contois, 1959)	$\frac{SRT}{HRT}$
Chen-Hashimoto kinetics	$\frac{SRT}{HRT}$
Surface based kinetics (Sanders, 2001)	$\frac{SRT}{HRT}$
Half-order biomass kinetic (Rozzi and Verstrate, 1981)	$(\frac{SRT}{HRT})^{1.5}$
A-order biomass kinetic (Valentini *et al.,* 1997)	$(\frac{SRT}{HRT})^{1+A}$
Agri ADM[1] (Schlattmann, 2011)	$> \frac{SRT}{HRT}$

[1] under additional assumption that concentration of hydrolytic biomass is lower than threshold concentration

In Section 3.4.1, these theoretical considerations are examined based on the working hypothesis. Subsequently, it is shown which models most accurately describe COD removal in an AnMBR.

3.3. Material and methods

3.3.1 Experimental setup

Continuous digestion tests were performed using an anaerobic membrane digester in a pilot scale (constructed by EnviroChemie GmbH, Germany). The pilot plant has a digester volume of 2.1 m³, is fully automated, fed continuously with WAS of a municipal WWTP (20 times per day) and operated at mesophilic conditions with temperatures around 37±1 °C. A flow chart of

the pilot plant is shown in Figure 16. A detailed description is given in Engelhart *et al.* (2018) and the annex B. The buffer tanks of the pilot plant were filled once a week. The microfiltration membrane unit allows decoupling of SRT and HRT. It consists of rotating ceramic disc filters (filter ceramic disc 312 with an outer diameter of 312 mm, Kerafol GmbH, Germany) with a nominal pore size of 0.2 µm mounted on a rotating hollow shaft (see Figure 17 and Figure 18). Total membrane area of installed membrane module was $A_{Membrane}$ = 3.36 m². For reduction of fouling on the membrane rotational velocities between 250-350 rpm were applied. Corresponding crossflow velocities are given in Table 10. During filtration, gas formed in the filter and accumulated along the shaft during rotation. This interfered with the filtration process which is why rotation of the filter was stopped regularly (each 8-10 minutes) for about 30 seconds for degassing.

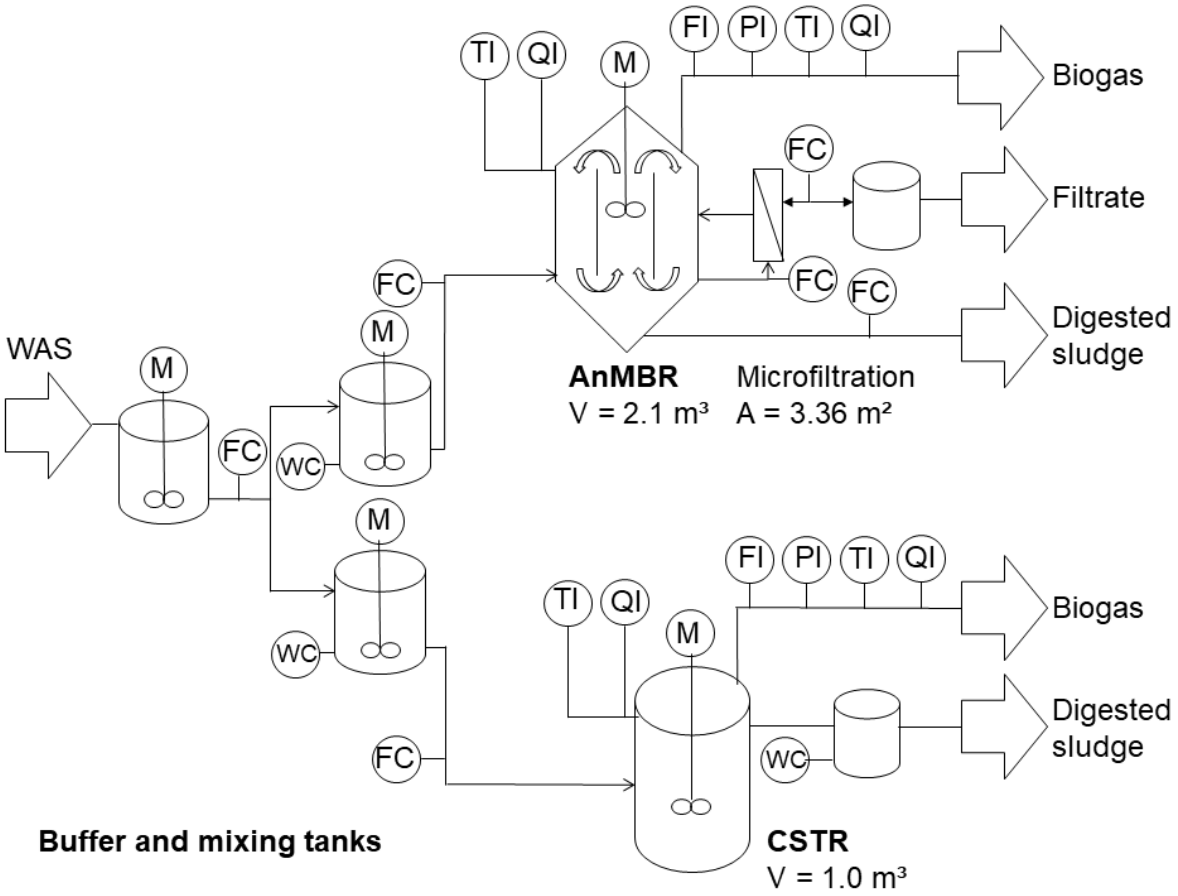

FC: Flow control, FI: Flow indication, PI: Pressure indication,
TI: Temperature indication, QI: pH indication (in digester); CH_4, CO_2 indication (in digester gas)

Figure 16. Simplified flow scheme of anaerobic membrane digester and CSTR in pilot scale

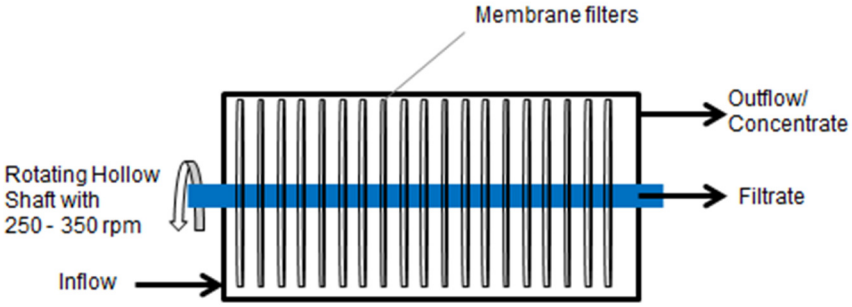

Figure 17. Scheme of rotating membrane filter

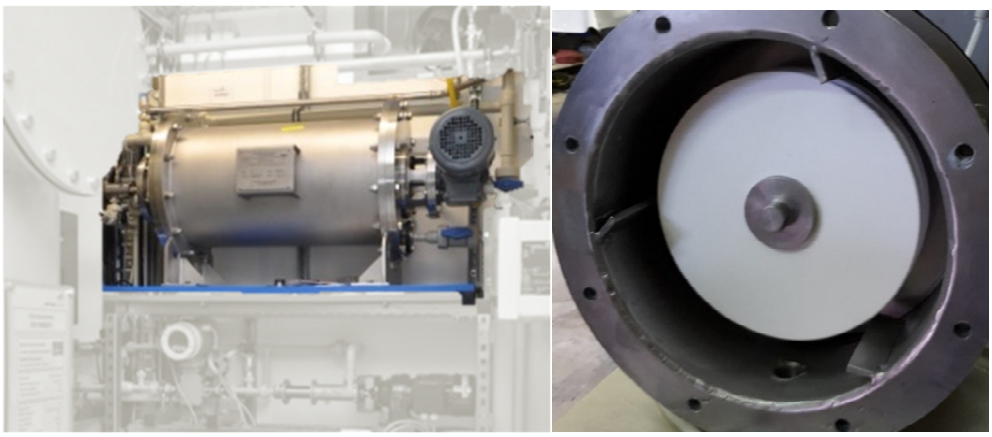

Figure 18. Membrane unit in pilot scale (left); ceramic discs installed on a hollow shaft in lab-scale (right)

Table 10. Corresponding crossflow velocities to set rotational speeds

Rotational velocity	Crossflow velocity in m/s at		
	$Ø_{min}$ = 80 mm	$Ø_{mean}$ = 225 mm[1]	$Ø_{max}$ = 312 mm
250 rpm	1.0	2.9	4.1
280 rpm	1.2	3.3	4.6
320 rpm	1.3	3.8	5.2
350 rpm	1.5	4.1	5.7

[1] mean is based on membrane surface

As reference, data regarding two conventional CSTRs were taken from Rühl (2016). These CSTRs had a volume of 1.0 m³, were operated at SRT = 20 d and SRT = 12 d at temperatures around 37±1 °C and used the same input material. A detailed description of the CSTRs is given in Engelhart *et al.* (2018) and the annex B.

3.3.2 Operating conditions

Table 11 shows the mean composition of feed WAS. This feed sludge was taken from a WWTP with 40,000 population equivalent (PE) and was used for all experiments. Different adjustments of HRT and SRT were investigated for at least three SRTs each (see Table 11). Settings were tested with decoupling ratios of SRT/HRT = 1.25 and 1.50 for different HRTs. The reference reactors with SRT = 12 and 20 d were operated over the entire period of trials. They had the same feed composition as the AnMBR in the respective periods; this is why these reactors are not separately listed here.

Table 11. Characterisation of WAS as feed (mean ± std. dev.)

Operational settings			Mean sludge composition				
HRT [d]	SRT [d]	SRT/HRT [-]	COD [g/L]	COD/ VS [-]	TS [%]	VS/TS [-]	NH_4-N [mg/L]
17.8	17.8	1.0	56.4±3.7	1.65±0.01	4.38±0.21	0.76±0.01	322±265
12.6	22.3	1.77	44.1±3.9	1.56±0.01	3.89±0.47	0.71±0.02	329±218
9.1	13.2	1.45	51.9±2.9	1.63±0.01	4.14±0.26	0.77±0.01	282±210
7.6	11.5	1.50	51.3±8.5	1.57±0.01	4.01±0.82	0.80±0.01	250±226
6.8	10.8	1.57	63.0±10.3	1.56±0.01	4,95±0.78	0.80±0.01	209±185
5.6	8.8	1.56	50.5±4.5	1.61±0.01	4.07±0.48	0.78±0.01	177±140
10.7	13.5	1.26	51.6±4.3	1.58±0.01	4.38±0.45	0.76±0.01	242±187
10.3	13.0	1.26	46.7±5.3	1.57±0.01	4.01±0.51	0.74±0.01	217±176
8.4	9.8	1.17	47.5±5.4	1.58±0.01	4.09±0.52	0.75±0.01	244±183
6.4	8.2	1.28	52.2±2.7	1.58±0.01	4.24±0.24	0.77±0.01	191±157

Reference reactors with SRT = 12 and 20 d were fed with the same feed as AnMBR in the respective periods.

3.3.3 Sampling and assays

All input and output materials were analysed in terms of TS, VS, pH value, COD, organic acids (VFA) and ammonium (NH_4-N) according to ISO or similar standards (see Table 12). Volume shares of CH_4 and CO_2 (BlueSens gas sensor GmbH, Germany) and volumetric biogas flow (Type TG1, Dr. Ing. Ritter Apparatebau GmbH & Co. KG, Germany) were measured continuously. Gas flow rates were normalised according to VDI 4630 (2006).

Table 12. Overview of analytical methods

Parameter	Standard method	Remarks/ Equipment
Total solids (TS)	DIN EN 12880 (2001)	Drying oven
Volatile solids (TVS)	DIN EN 15935 (2002)	Muffle furnace
pH-value	DIN EN 12176 (1998)	Laboratory: pH-meter pH 197 (WTW GmbH, Germany); Pilot plant: Memosens CPS171D (Endress+Hauser Messtechnik GmbH+Co.KG, Germany)
Chemical oxygen demand (COD) (sludge samples)	DIN 38414-S9 (1986)	Wet sludge sample; MPT-Titrino 98 (Metrohm Deutschland GmbH)
Chemical oxygen demand (COD) (filtrate samples)	ISO 6060 (1989) DIN 38409-H41 (1980) DIN 38409-H44 (1992)	Cuvette test LCK 514 (Hach Lange GmbH, Germany)
Organic acids (VFA)		Cuvette test LCK 365 (Hach Lange GmbH, Germany)
Ammonia (NH_4-N)	ISO 7150-1 (1984) DIN 38406-5 (1983)	Cuvette test LCK 303 (Hach Lange GmbH, Germany)
Phosphate (PO_4-P)	ISO 6878-1 (1986) DIN 38405-11 (1983)	Cuvette test LCK 350 (Hach Lange GmbH, Germany)
Methane CH_4 Carbon dioxide CO_2	Gas-phase chromatography (WLD/TCD and FID) Infrared spectroscopy	Laboratory: Agilent 6890N Gas chromatograph (Agilent Technologies, US); Pilot plant: BlueSens gas sensor (BlueSens gas sensor GmbH, Germany)

Batch tests for substrate characterisation in terms of disintegration constant

Batch tests were conducted according to VDI 4630 (2006), using the substrate and inoculum of the pilot plants and laboratory equipment by BlueSens gas sensor GmbH (Germany). CH_4, CO_2, temperature, pressure (BlueSens gas sensor GmbH, Germany) and gas volumes (Milligascounter Type MGC-1 PMMA, Dr. Ing. Ritter Apparatebau GmbH & Co. KG, Germany) were also assessed. An experimental setup of batch tests is given in Figure 19. All bench-scale tests were conducted in triplicates at a temperature of 37±0.5 °C.

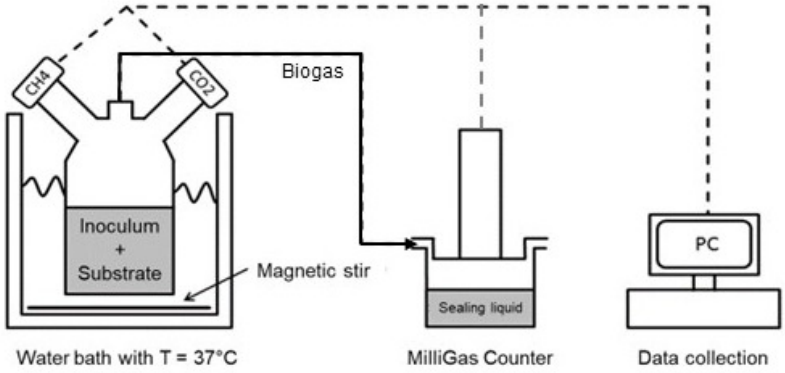

Figure 19. Experimental setup of batch tests for substrate characterisation and SMA analysis

The disintegration (hydrolysis) constant k_{dis} was determined using the approach of Angelidaki *et al.* (2009). Based on the substrate first-order kinetics approach, methane yields correspond to COD degradation and follow the given reaction in batch tests:

$$Y_{CH4} = Y_{CH4,max} \cdot (1 - e^{-k_{dis} \cdot t}) \quad (3.9)$$

Where, Y_{CH4}: methane yield (L CH_4/kg COD_{added})

$Y_{CH4,\,max}$: maximum methane yield (L CH_4/kg COD_{added})

k_{dis}: disintegration constant of a substrate first-order reaction (d^{-1})

t: time (d)

Angelidaki *et al.* (2009) defined maximum methane yield $Y_{CH4,max}$ as the cumulative methane production on the last day of the experiment in relation to the added COD. The experiment was continued until the daily gas production was less than 1 % of the total gas production, based on VDI 4630 (2006). The disintegration constant k_{dis} can be derived from the slope of plotted experimental data using the linearised equation:

$$\ln\left(\frac{Y_{CH4,max} - Y_{CH4}}{Y_{CH4,max}}\right) = -k_{dis} \cdot t \quad (3.10)$$

Batch tests for determination of specific methanogenic activity of acetoclastic methanogens (SMA)

Batch tests were conducted with the same equipment used for the determination of disintegration constants. For determination of SMA, all samples were degassed prior to tests for 24-36 h at temperatures around 20°C. Subsequently, 300 mL samples were placed in 1000 mL bottles and flushed with pure nitrogen. 1 g/L of acetic acid (glacial) 100% anhydrous for analysis (CAS-

No. 64-19-7, Merck AG, Germany) was added. After additions, all samples were closed immediately and incubated at temperatures of 37±0.5 °C. SMA was determined by the maximum slope of the curve (cumulative methane production versus time) over an integral of 1 h; it can be calculated as follows:

$$SMA = \frac{V_{CH4,2} - V_{CH4,1}}{(t_2 - t_1) \cdot m_{VS}} \cdot \frac{g\ COD_{removed}}{0.35\ L\ CH_4} \quad (3.11)$$

Where, SMA: specific methanogenic activity (g $COD_{removed}$/(gVS·d))

$V_{CH4,1}$, $V_{CH4,1}$: cumulated methane volume at t_1 and t_2 (L CH_4)

m_{VS}: mass of volatile solids in the batch (g VS)

t_1, t_2: start and end time of considered interval (h)

All batch tests were conducted in triplicates at least. At the beginning of the test, to limit other inhibition effects, an initial concentration of 1 g/L acetic acid was chosen to achieve maximum substrate uptake. Value of pH remained stable in neutral range.

Definition of process stability

Process stability is determined through a safety factor defined by Siegrist *et al.* (2002):

$$SF = \frac{maximum\ acetate\ conversion}{average\ acetate\ conversion} = \frac{\mu_{max}}{\frac{1}{SRT} + k_d} \quad (3.12)$$

Where, SF: safety factor (-)

μ_{max}: maximum growth rate of acetoclastic methanogens (d^{-1})

k_d: decay rate of acetoclastic methanogens (d^{-1})

SRT: sludge retention time (d)

Contrary to Siegrist *et al.* (2002), the maximum acetate conversion rate is determined not as a result of intermittent feeding in continuously operated reactors but by using specific methanogenic activities from batch tests. The determination of SF is carried out by comparing the SMA and the mean mass flow of $COD_{removed}$ in steady state or the last two SRTs. Furthermore, shares of COD degradation via acetoclastic methanogenesis multiplied by a factor n must be considered; this factor ranges between 0.65-0.7 according to ADM1 (Batstone et al., 2002).

Thus, the determination of SF is as follows:

$$SF = \frac{SMA \cdot m_{VS,reactor}}{n \cdot COD_{removed}} \quad (3.13)$$

Where, $m_{VS,reactor}$: mass of volatile solids added (g VS)

n: average COD conversion via acetate ~ 0.65 - 0.7

$COD_{removed}$: mass of COD removed per day (g COD/d)

Values greater than 1.0 imply that hydrolysis/disintegration remains the rate-limiting step in AD. This provides some reliability against substrate overloads, which might lead to accumulation of inhibiting intermediates such as organic acids. Assuming identical microbial populations without significant inhibition, the safety factor defined by Siegrist *et al.* (2002) does not change

with increasing OLR but with SRT. Growth-reducing effects as well as inhibiting influences on methanogenic activity lead to a reduction of the measured SMA and, thus, to a reduction of SF. Higher values of SF imply a more resilient system against substrate overload or fluctuating feed conditions and, thus, a more stable anaerobic process.

3.4. Results and discussion

3.4.1 Performance in terms of organic matter removal and methane yield

AnMBR was operated and continuously fed for more than one year at mean COD loading rates between 2.6 kg COD/(m^3·d) and 8.8 kg COD/(m^3·d) depending on operational settings (see Table 13). While organic loading rates were higher than those recommended by DWA-M 368 (2004) and Metcalf and Eddy (2004), applied HRTs and SRTs were lower than those recommended for sludge digestion. During operation, HRTs were reduced to 5.6 d. SRTs were slightly higher based on applied decoupling ratios SRT/HRT between 1.25 and 1.5. At steady state, input mass of COD to the reactor was equal to output mass of COD (comprising residual COD and produced methane). Therefore, removal-related methane yields of AnMBR and conventionally operated CSTRs approximately corresponded to a theoretical optimum value of 350 L CH_4/ kg $COD_{removed}$. COD removal was calculated from COD load in inflow and outflow and changes of COD concentration in the reactor. During operation, COD removal varied between 25 % and 42 % (Table 13). Overall, as expected, COD removal and methane yield improved with increasing SRTs.

Table 13. COD loading and COD removal performance of anaerobic membrane digester

Operational settings				Performance		
HRT	SRT	SRT/HRT	COD loading rate	COD removal[1]	Methane yield[2]	
[d]	[d]	[-]	[kg COD/m^3·d]	[%]	[L/kg COD_{added}]	[L/kg $COD_{removed}$]
17.8	17.8	1.0	3.3±0.9	41.5	131±2	314±28
12.6	22.3	1.77	4.4±0.8	32.7	108±6	353±33
9.1	13.2	1.45	5.7±1.6	37.7	121±7	348±17
7.6	11.5	1.50	6.4±1.7	41.1	139±6	331±15
6.8	10.8	1.57	7.7±2.8	38.2	124±10	343±15
5.6	8.8	1.56	8.8±1.3	28.1	98±8	350±9
10.7	13.5	1.26	5.1±1.1	28.6	97±2	348±15
10.3	13.0	1.26	4.6±1.1	26.9	87±3	343±28
8.4	9.8	1.17	5.3±2.2	26.3	105±6	355±17
6.4	8.2	1.28	7.9±1.0	25.7	91±4	335±12

[1] mean values of 7 days; [2] normalised methane yield at steady state after two sludge retention times

Although, methane yields varied only slightly (<10 %) during a setting, great variations were encountered among the individual settings from 87 to 140 L CH_4/kg COD_{added}. These variations depend not only on operation but also on seasonal changes in the degradability of WAS occurring throughout the year, as shown by variations of methane yields of the reference (CSTR with SRT = 20d; Figure 20; data was provided by Rühl (2016)).

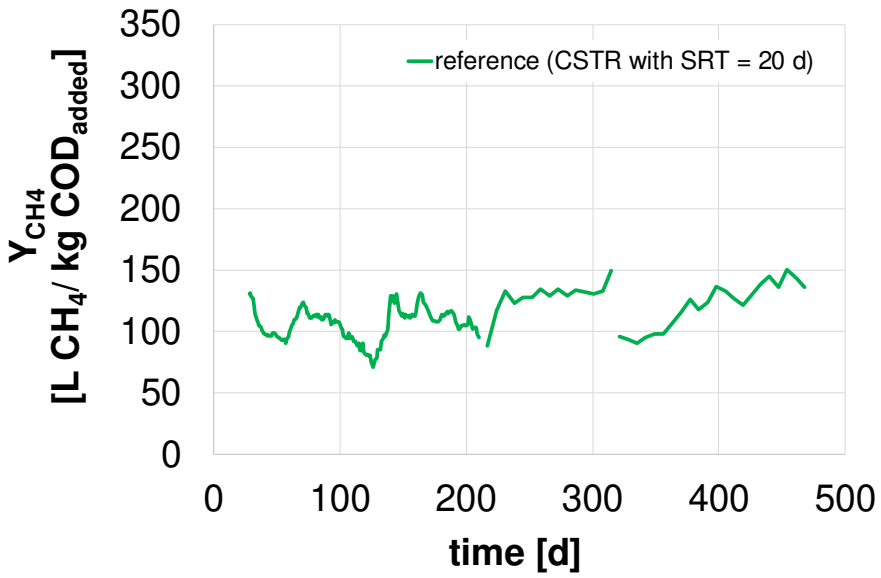

Figure 20. Methane yield of conventional digester with SRT = 20 d vs test duration (data was provided by Rühl (2016))

Therefore, for further evaluation of AnMBR performance, methane yields of the membrane digester were divided by corresponding methane yields in CSTR operated at SRT = 20 d (see Figure 21). For clarification of dependency of COD removal on SRT, methane yields of CSTRs for SRTs other than 12 and 20 days were estimated assuming disintegration as the rate-limiting step in anaerobic degradation applying a substrate first-order reaction. Disintegration constant with k_{dis} = 0.20 ± 0.02 d^{-1} was determined in batch tests irregularly over the duration of test (see further description in Section 4.2 and Table 18). A substrate first-order model was used because of its ease in determining disintegration constants and low differences between relevant models concerning COD removal for SRTs up to 10 d (Sötemann *et al.*, 2005). As already stated (see equation 2.12), COD removal η_{COD} of CSTRs can be determined as a function of HRT (= SRT) based on the kinetic coefficient from batch tests by the following expression:

$$\eta_{COD} = \frac{k_{dis} \cdot \mathrm{HRT}}{(1+k_{dis} \cdot \mathrm{HRT})} \qquad \text{with } k_{dis} = 0.20 \pm 0.02\ d^{-1} \qquad (3.14)$$

Comparing COD removal in continuously operated plants with calculated values based on batch tests, it is obvious that COD removal can be well predicted by determining kinetic constants in batch tests (Figure 21).

Comparing COD removal on the basis of relative methane yields of AnMBR and CSTR, it is clear that COD removal depends on SRT (see Figure 21). At equal SRT, significant higher COD removal (methane yields) is not achieved by RT. This is in agreement with working hypothesis ‘COD removal in AnMBR and CSTR does not differ for the same SRT’ (see section 3.2). This finding agrees with results of Romero-Flores *et al.* (2017) who used filtration in lab scale, Josse *et al.* (2017) who used screw thickeners in large scale and Yang *et al.* (2015) who used gravity thickening in lab scale. In AnMBR, similar COD removal was achieved at higher COD loading rates. This results in higher daily removed COD loads. Consequently, increased decoupling ratios boost the removal rate dX_S/dt (unit: kg $COD_{removed}/(m^3 \cdot d)$) according to the decoupling ratio but not beyond. Most kinetic models (e.g. substrate first-order, Contois kinetics and surface-related kinetics) adequately describe the COD removal and the COD removal rates in AnMBRs in comparison to CSTRs (see section 3.2 and Table 9).

Additional factors boosting COD removal, such as increased substrate degradability, higher disintegration constants or higher biomass-related constants, could therefore not be observed. Based on biomass activity-based kinetics (see section 2.1.2.1), this means that negative effects on the biomass do not significantly occur or at least do not influence COD removal. These findings regarding COD removal and removal rates agree with the previously established working hypothesis (see section 3.2).

As higher COD removal at even SRT is not observed in AnMBRs compared to CSTRs, kinetic approaches proposed by Rozzi and Verstrate (1981) and Valentini *et al.* (1997) and Schlattmann (2011) do not apply to these results. Findings also contradict the results obtained by Pileggi and Parker (2017) and Dagnew *et al.* (2012), who observed higher methane yields in AnMBRs compared to CSTRs at even SRT. However, Dagnew *et al.* (2010) observed an increase in colloidal matter and decrease in particle sizes at increasing decoupling ratios at similar SRT. Possibly, increased degradability was caused by mechanical disintegration of cells and flocs due to high shear stress caused by crossflow over the membrane surface, which boosted COD removal. In this study, differences in mean particle size between CSTR and AnMBR were not observed ($d_{50,\ CSTR}$ = 52.8±2.7 µm and $d_{50,\ AnMBR}$ = 51.0±2.0 µm; method description is given in section 6.2.3).

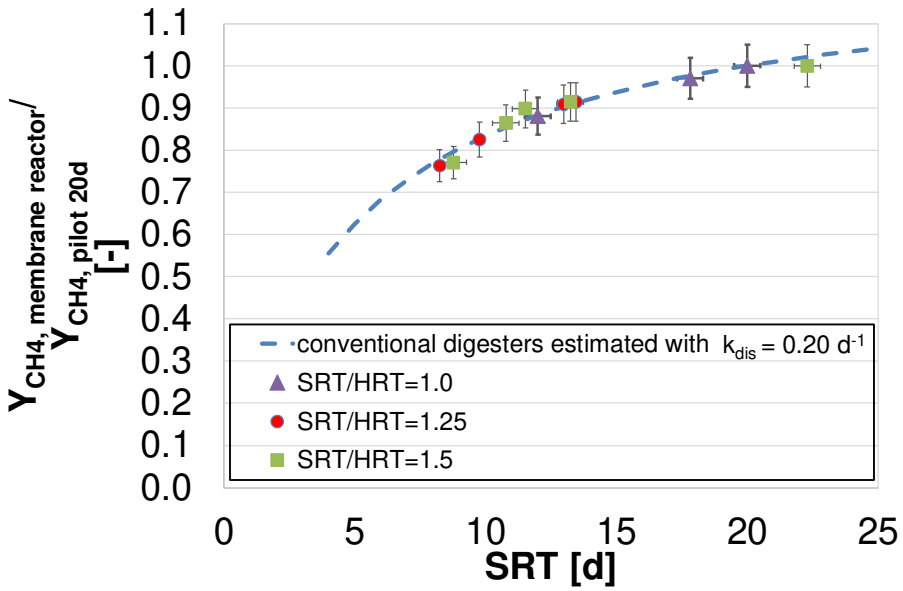

Figure 21. Methane yield in the AnMBR and CSTR compared to conventional digester operated with SRT = 20 d at various SRT when all are using WAS

When plotted against HRT, RT improves the methane yield by 10-20 % for assessed decoupling ratios and substrate (see Figure 22). To achieve a specific COD removal, the digester volume of AnMBR can be reduced in comparison to a conventional CSTR by using RT. In the case of a decoupling ratio of SRT/HRT = 1.5, the required digester volume can be reduced by 33 % lowering the required HRT from 20 to 13 days.

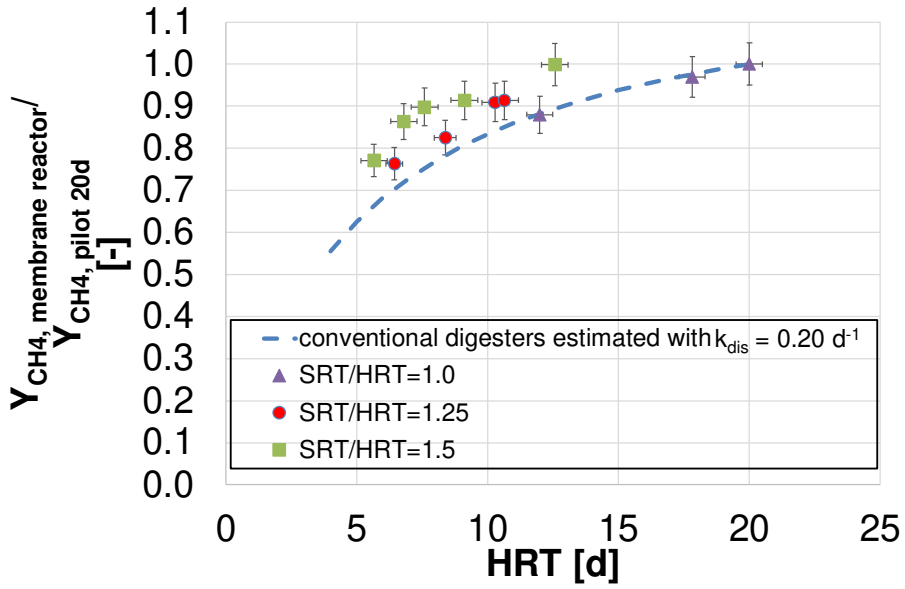

Figure 22. Methane yield in the AnMBR and CSTR compared to conventional digester operated with SRT = 20 d at various HRT when all are using WAS

Table 14. Characterisation of the digested sludge and the VS removal (mean ± std. dev.)

Operational settings			Feed	Mean digestate composition			
HRT	SRT	SRT/HRT	TS	COD	TS	VS	VS/TS
[d]	[d]	[-]	[%]	[g/L]	[%]	[%]	[-]
17.8	17.8	1.0	4.38±0.21	36.8±3.2	3.5±0.3	2.4±0.2	0.68±0.01
12.6	22.3	1.77	3.89±0.47	49.8±5.2	4.9±0.5	3.2±0.4	0.65±0.01
9.1	13.2	1.45	4.14±0.26	49.5±2.4	4.6±0.3	3.2±0.2	0.70±0.01
7.6	11.5	1.50	4.01±0.82	49.6±4.3	4.5±0.4	3.2±0.3	0.73±0.01
6.8	10.8	1.57	4,95±0.78	59.0±3.4	5.3±0.3	3.9±0.2	0.73±0.01
5.6	8.8	1.56	4.07±0.48	53.1±2.3	4.8±0.3	3.4±0.2	0.72±0.01
10.7	13.5	1.26	4.38±0.45	46.5±4.5	4.5±0.4	3.1±0.3	0.70±0.02
10.3	13.0	1.26	4.01±0.51	37.0±1.6	3.5±0.2	2.4±0.1	0.69±0.01
8.4	9.8	1.17	4.09±0.52	40.8±2.2	3.9±0.2	2.7±0.2	0.69±0.01
6.4	8.2	1.28	4.24±0.24	45.4±1.9	4.2±0.1	3.0±0.1	0.71±0.01

The membrane with a mean pore size of 0.2 µm retains all particulate matter. Therefore, TS and VS concentration in AnMBR are higher than in CSTR (see Table 14). For WAS digestion at TS_{in} = 4.0-4.5 %, SRT of 8-15 d, COD removal of around 25-30 % (see Table 13), decoupling ratio SRT/HRT of 1.25 and residual TS concentration in the reactor between 3.5-4.5 % must be considered. Higher decoupling ratio SRT/HRT of 1.5 leads to increased concentration of total solids in the reactor between 4.5-5.5 %. Owing to limited TS reduction by degradation of organic matter (see Table 13), TS concentration in the reactor even exceeds feed TS (see Table 14).

3.4.2 Process stability

In addition to being the rate-limiting step of sludge digestion along with disintegration, methanogenesis is the second key step of AD. Methanogenesis is usually controlled by monitoring the following parameters:

- pH
- organic acids concentration (VFA) and its changes
- ammonium concentration for possible inhibition at elevated pH

In the experiments, process stability gets reflected particularly through minor changes in the parameters given in Table 15. The pH value (between pH 6.9-7.2) and VFA concentration remained stable throughout the pilot trials. Slightly elevated concentration of organic acids was found at the highest COD loading rate or lowest HRT. Nevertheless, regarding inhibition of methane generation, all values were far below the critical concentrations mentioned by Weichgrebe (2015).

Table 15. Parameters for process control

Operational settings			Liquid phase in reactor			
HRT	SRT	SRT/HRT	pH	COD[1]	Organic acids	NH_4-N
[d]	[d]	[-]	[-]	[mg/L]	[mg HAc/L]	[mg/L]
17.8	17.8	1.0	7.2±0.0	1,139±283	200±41	1.237±89
12.6	22.3	1.77	7.0±0.1	1,501±462	204±29	805±85
9.1	13.2	1.45	7.0±0.0	1.247±149	247±41	972±146
7.6	11.5	1.50	7.1±0.0	1,083±210	261±60	1,108±99
6.8	10.8	1.57	7.2±0.1	1,104±296	318±58	1,101±89
5.6	8.8	1.56	7.0±0.1	1.096±534	260±54	881±38
10.7	13.5	1.26	7.1±0.1	1,226±228	212±33	930±29
10.3	13.0	1.26	6.9±0.0	1,229±323	222±40	729±44
8.4	9.8	1.17	7.0±0.1	974±304	201±104	850±58
6.4	8.2	1.28	7.0±0.0	1,104±296	246±47	881±38

[1] 0.45 µm filtered sample of the supernatant

The process stability in terms of the safety factor SF measured in steady state for some settings of AnMBR and CSTR is illustrated in Figure 23 (top). The process stability against substrate overload or accumulation of inhibiting intermediates was sufficient, as SF remained above 1.0. All measured values of SF were higher than two, which means that hydrolysis/disintegration remained the rate-limiting step. A safety margin for buffering load changes of at least 100 % with a change of rate-limiting step from disintegration to methanogenesis (SF > 2 vs. SF = 1) illustrates why the concentration of organic acids in the reactor remained low even at high OLRs (low SRT).

Results also show that the SF decreases with reduced SRT, as expected based on its definition (see Section 3.3.3). However, process stability of AnMBR reflects that SF were similar to that of CSTR at similar SRT based on kinetic parameters μ_{max} and k_d. Growth rates μ_{max} were calculated from the slope ($1/\mu_{max}$) and the intercept (k_d/μ_{max}) of the linear regression after plotting 1/SF versus 1/SRT (see Figure 23, bottom). Although estimated values of maximum growth rate μ_{max} = 0.49 d^{-1} and decay rate k_d = 0.1 d^{-1} differ from values given by Siegrist *et al.* (2002), they are in a similar range. Nevertheless, the same linear dependence of 1/SF to 1/SRT applies

to CSTR and AnMBR. Acetoclastic methanogens in AnMBR and CSTR seem to have the same growth rate and rate of decay. There is obviously no population shift to fast-growing methanogens. Therefore, values of SF are slightly lower than SF estimated by Siegrist *et al.* (2002) based on kinetic parameters (see Figure 23, top).

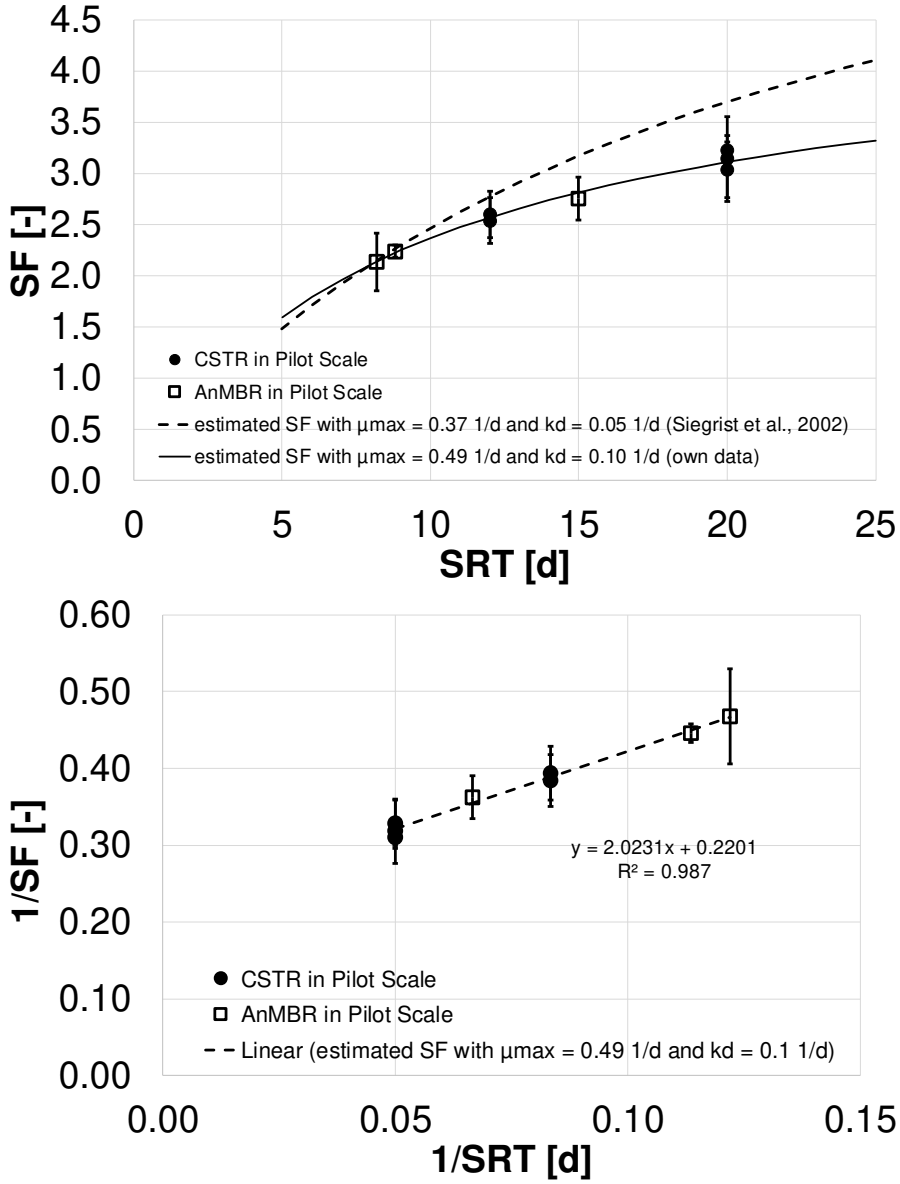

Figure 23. Comparison of process stability of AnMBR and conventional CSTR fed with WAS for different SRTs (top); maximum growth and decay rate calculated from SF and SRT (bottom)

In summary, process stability seems to depend mainly on SRT. Lower HRT and higher OLR occurring in AnMBR seem not to significantly influence SF. A negative influence on methanogens was not observed. This finding agrees with previously introduced assumptions for the working hypothesis (see Section 3.2). For the investigated system, membrane filtration had no significant effect on SMA. This conclusion is also backed by results of SF, since otherwise process stability in terms of SF would not have met expectations in long-term operations of more than 15 months. As further proof, SMA was also measured in the feed and concentrate

of the membrane unit (see Figure 24). At mean crossflow velocities of 4.1 m/s (350 rpm), activities in feed and concentrate remained constant. The SMA values of all the samples were consistent with the range suggested by Batstone *et al.* (2015), i.e., 0.2 to 0.4 g COD/(g VS·d).

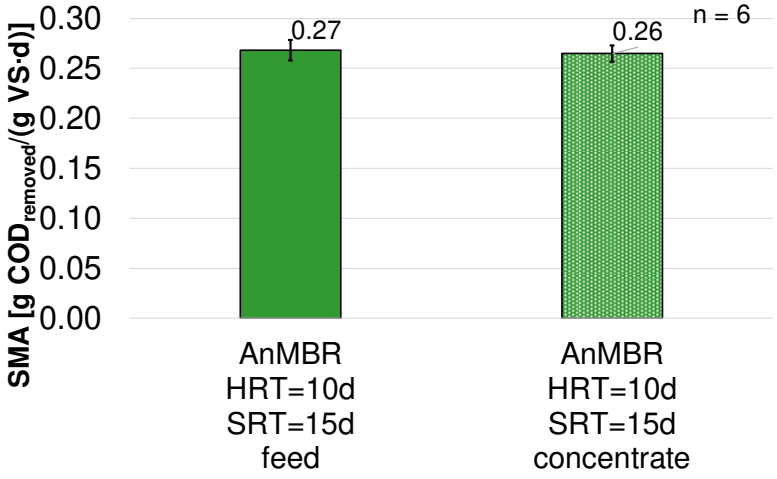

Figure 24. SMA of feed and concentrate of AnMBR at mean crossflow velocities of 4.1 m/s (350 rpm)

3.5. Conclusions

Membrane digesters treating WAS can generate smaller reactor volumes at similar methane yields or COD removal at equal SRT. Similar COD removal at even SRT is related to higher COD removal rates in AnMBRs in the range of the decoupling ratio. Additional factors boosting COD removal, such as increased substrate degradability, higher disintegration constants or higher biomass-related constants, were not significantly detected in AnMBR in pilot scale. SRT decisively determines COD removal. When SRTs are extended by membrane filtration, COD removal in AnMBR using RT is improved in comparison to CSTR.

These findings are in agreement with common AD models of complex substrates such as substrate first-order kinetics (e.g. ADM 1) or Contois kinetics. Further, a substrate-first order kinetic with integration of kinetic constants determined in batch tests was successfully used to predict COD removal using RT in AnMBR.

SMA, growth rate or decay rate were not negatively influenced by the crossflow shear of membrane filtration. Regarding process stability against substrate overload, based on the SF concept, the AnMBR behaves like a CSTR with similar SRT when operated to digest WAS. Hence, RT improves process stability in AnMBR against substrate overload and accumulation of organic acids when compared to CSTR at similar HRT. pH and organic acid concentrations remained stable even at low SRTs of 8 d.

Economically, savings in smaller reactor volumes have to be balanced against membrane costs and energy demand. Membrane costs are largely determined by the operating flux, which is why Chapter 0 deals intensively with the parameters that influence the critical flux. The energy demand of the applied system is estimated in Chapter 7.1. An economic feasibility for the application of AnMBR on municipal WWTPs treating solely WAS is discussed in Chapter 7.2.

4. Comparison of steady state performance of AnMBR and CSTR for lipid-rich sludge digestion and assessment of design criteria

This chapter is mainly based on

Lutze, R., Engelhart, M. (2020) Comparison of CSTR and AnMBR for high-solid digestion of WAS and lipid-rich flotation sludge from the dairy industry. *Water Resources and Industry*, 23, doi:10.1016/j.wri.2019.100122.

4.1. Introduction

For reduction of energy costs, highly loaded wastewater from the dairy industry (COD ≥ 1,000 mg/L) can preferably be treated by activated sludge processes in combination with flotation and anaerobic pre-treatment, such as expanded granular sludge bed (EGSB) reactors (Cervantes *et al.*, 2006; Londong and Rosenwinkel, 2013; see Figure 25). Regarding sludge management, the highly energetic flotation sludge and WAS obtained with aerobic post-treatment are generally disposed of as co-substrates to WWTPs or biogas plants.

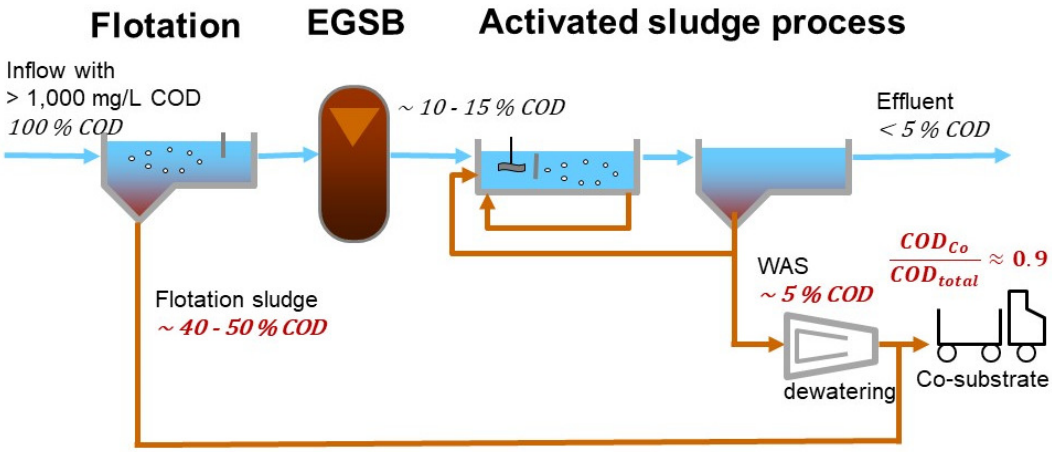

Figure 25. Exemplary state-of-the-art wastewater treatment plant of the dairy industry

In the context of further increases in resource efficiency, co-digestion strategies at municipal WWTPs or agricultural biogas plants are being increasingly criticised, since waste heat from CHP units usually is not adequately utilised on-site and additional energy expenditure is required for transportation of co-substrates; moreover, increasing regulations must be considered as well (e.g., Silvestre *et al.*, 2011; Mata-Alvarez *et al.*, 2014; Edwards *et al.*, 2017). Anaerobic treatment of these energy-rich substrates in digesters on-site (see Figure 26) combined with a CHP unit would offer major benefits, such as the reduction of disposed sludge volumes, increase of methane generation up to 50 % and increase of overall energy efficiency in the case of integration of waste heat usage of CHP units in industrial production.

However, operation of anaerobic co-digestion with major shares of flotation sludge (over 80 % COD) consisting notably of lipids is challenging. Successful examples of lipid-fed digesters using various lipid-rich substrates (Diez *et al.*, 2012; Dereli *et al.*, 2014b; Mata-Alvarez *et al.*, 2014) and lipid-related inhibition (Palatsi *et al.*, 2009; Zonta *et al.*, 2013; Mata-Alvarez *et al.*, 2014) have been reported.

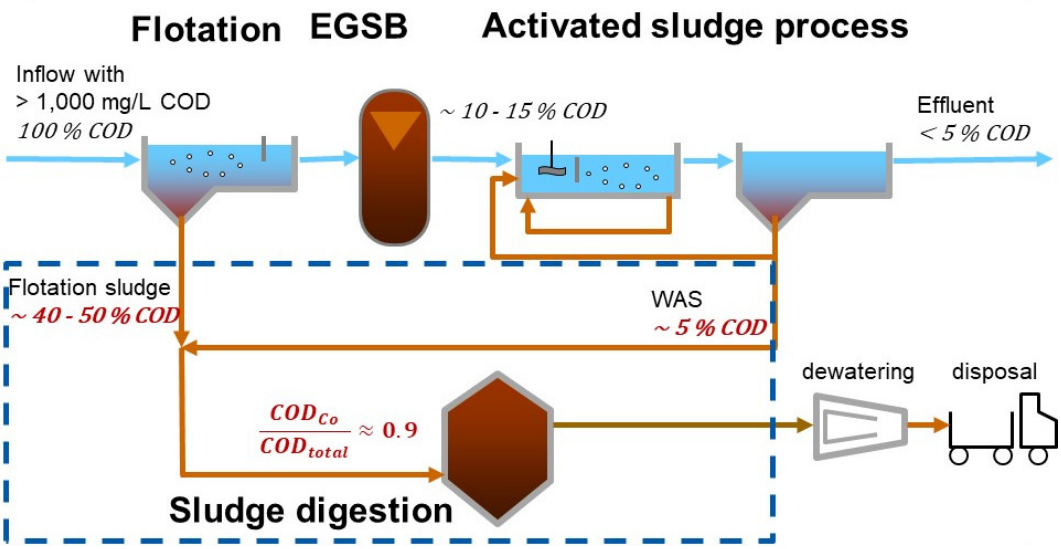

Figure 26. Overview of investigated example of industrial wastewater treatment of a dairy industry, showing on-site sludge digestion of flotation sludge and WAS

Inhibition is mostly related to accumulation of LCFAs, which are an intermediate product of anaerobic lipid degradation. Angelidaki and Ahring (1992) reported threshold concentrations for oleate as 0.2 g/L and stearate as 0.5 g/L. New publications assume that LCFA might build up layers on the biomass, which might reduce mass transfer of substrates (Hwu *et al.*, 1996; Pereira *et al.*, 2002; Dereli *et al.*, 2014b; Ziels *et al.*, 2016). Therefore, inhibition of methanogens is based on TS-related specific LCFA concentrations (Hwu *et al.*, 1996; Pereira *et al.*, 2002; Ziels *et al.*, 2016) or surface-related LCFA concentrations (Hwu *et al.*, 1996). Regarding anaerobic sludge from a treatment plant treating milk fats, Hwu *et al.* (1996) reported a 50 % loss of methanogenic activity at an oleate concentration of 32 mg/ g TS. Adding lipid-rich synthetic dairy wastewater to an AnMBR, Szabo-Corbacho *et al.* (2019) reported a loss of up to 50 % of methanogenic activity at LCFA concentration above 100 mg/ g TS, although methane yields remained stable. Ziels *et al.* (2016) provided a threshold value of 100 mg LCFA/ g TS for LCFA concentration of the sludge. Precipitation induced by divalent cations can reduce the toxic effects of LCFA at the expense of reduced biodegradability (Alves *et al.*, 2001; Pereira *et al.*, 2005). The addition of bentonite reduces the toxic effects of LCFA by providing an additional surface for adsorption in the reactor (Palatsi *et al.*, 2009) which supports the total solids related dependency of inhibiting LCFA concentration.

Maximum substrate specific volumetric loading rates (OLRs) of FOG and various lipid-rich substrates have been published as design criteria for co-digestion in CSTR. Mata-Alvarez *et al.* (2014) summarised FOG-related studies and recommended an average OLR of 0.84 kg $VS_{FOG}/(m^3 \cdot d)$ and a maximum OLR of 2.5 kg $VS_{FOG}/(m^3 \cdot d)$. Recommended OLRs for sludge digestion vary between 1.9-3.2 kg VS/(m^3·d) (WEF/ASCE, 2009), 1.6-4.8 kg VS/(m^3·d) (Metcalf and Eddy, 2004) and 2.9 kg $COD_{deg}/(m^3 \cdot d)$ (DWA M-368, 2014).

Maximum sludge loading rates are rarely published. When treating particle-free wastewaters, VSS-specific lipid loading rates range between 0.04-0.13 g lipids/(gVSS·d) (Dereli *et al.*, 2012; Szabo-Corbacho *et al.*, 2019). Although Dereli *et al.* (2012) and Szabo-Corbacho *et al.* (2019) observed a positive effect of longer SRT on methanogenic activity, SRT is not commonly used as a design parameter for digesters fed with lipid-rich substrates. Till date, there has been no

research on the flotation sludge of the dairy industry and its co-fermentation with WAS at different SRTs using AnMBRs.

This chapter deals with the technical feasibility of anaerobic co-digestion of WAS and flotation sludge from the dairy industry with COD shares of lipids up to 85 %. Steady state performance of AnMBR and CSTR are compared. The influence of SRT and shares of flotation sludge on methane yield, process stability and inhibition on acetoclastic methanogenic activity are determined. Conventional fill-and-draw CSTRs and an AnMBR were operated at HRT and SRT below common design recommendations under mesophilic conditions to investigate limitations of the loading capacity of anaerobic digesters rather than to maximise methane yields. As the introduction of additional solids can reduce inhibition, the question arises whether the joint digestion of flotation sludge with high shares of lipids and WAS with considerable amounts of non-degradable solids results in significantly lower inhibiting effects and successful operation with higher sludge loads. Finally, design criteria and potentials of AnMBR for overcoming lipid-related limitation are elaborated.

4.2. Material and methods

4.2.1 Experimental setup

The experimental setup of AnMBR and CSTR corresponds to the explanations given in Section 3.3.1. The setup was only expanded by additional buffer tanks required for flotation sludge (Figure 27). A detailed description is given in the annex B.

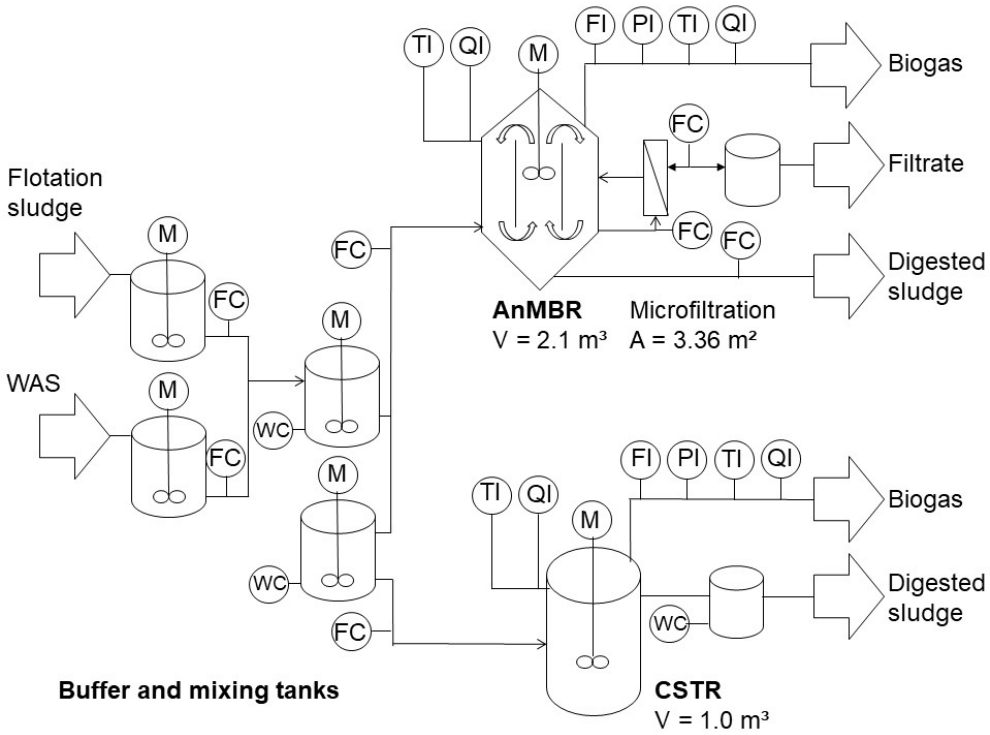

FC: Flow control, FI: Flow indication, PI: Pressure indication,
TI: Temperature indication, QI: pH indication (in digester); CH_4, CO_2 indication (in digester gas)

Figure 27. Simplified flow scheme of the anaerobic membrane digester and CSTR used for anaerobic digestion of WAS and flotation sludge in pilot scale

4.2.2 Operating conditions

Substrate sludge characteristics

WAS from a WWTP with 40,000 PE and flotation sludge from an ice cream production factory were sampled twice a week. Data on mean compositions of both substrates are given in Table 16. WAS had a mean COD concentration of around 48.2 g COD/L. The COD concentration of the flotation sludge ranged around 188.3 g COD/L.

The calculated lipid content of the flotation sludge was above 0.9 g COD_{li}/g $COD_{substrate}$.

The lipid content of the WAS was low (~ 0.2 g COD_{li}/g $COD_{substrate}$ or 0.08 g lipid/ g TS). Lipid content of WAS is slightly higher compared to other publications that found lipid contents between 0.04-0.08 g lipid/g TS in different activated sludge reactor systems (Zhu *et al.*, 2017; Liu *et al.*, 2020) but in a similar range. This might be related to the missing primary sedimentation at the WWTP used for sampling. Primary sludge usually contains higher lipid contents of 0.12 g lipid/g TS (Zhu *et al.*, 2017).

Table 16. Characterization of substrates (arithmetic mean ± standard deviation)

Parameters	WAS		Flotation sludge	
	value	n	value	n
COD [g/L]	48.2 ± 8.5	34	188.3 ± 44.9	26
Total solids [%]	4.1 ± 0.7	34	6.8 ± 1.4	26
Volatile solids [%]	3.1 ± 0.6	34	6.5 ± 1.4	26
COD/Volatile solids [g/g]	1.6 ± 0.1	-	2.9 ± 0.3	-
Nitrogen content [mg TN_b/g COD_{in}]	~ 25	10	~ 10	10
Protein content f_{pr} [g COD/g COD][a]	~ 0.25	-	< 0.1	-
Lipid content f_{li} [g COD/g COD] [a]	~ 0.2	-	> 0.9	-
carbohydrate content f_{ch} [g COD/g COD] [a]	~ 0.55	-	< 0.1	-
Lipid content [g VS/g TS][b]	~ 0.08	-	~ 0.9	-

n: number of analysis

[a] fractionation of COD was calculated based on COD/VS ratio, nitrogen content of the measured substrate and fraction specific theoretical ratios by maintaining a nitrogen, COD and mass balance suggested by Poggio *et al.* (2016). The following formulae and theoretical specific ratios were used:

$$f_{pr} = \frac{gN_{substrate}}{gCOD_{substrate}} \cdot \frac{gCOD_{pr}}{g_{pr}} \cdot \frac{g_{pr}}{gN_{pr}};$$

$$f_{pr} + f_{li} + f_{ch} = 1;$$

$$(f_{pr} \cdot \frac{g_{pr}}{gCOD_{pr}} + f_{li} \cdot \frac{g_{li}}{gCOD_{li}} + f_{ch} \cdot \frac{g_{ch}}{gCOD_{ch}}) \cdot \frac{gCOD_{substrate}}{gVS_{substrate}} = 1$$

proteins: 1.25 g COD/ g VS and a nitrogen content of 0.137 g N/ g VS
lipids: 2.87 g COD/ g VS and a nitrogen content of 0 g N/ g VS
carbohydrates: 1.18 g COD/ g VS and a nitrogen content of 0 g N/ g VS

[b] Lipid content= $f_{li} \cdot \frac{\frac{gCOD_{substrate}}{gVS_{substrate}}}{\frac{g_{li}}{gCOD_{li}}} \cdot \frac{gVS_{substrate}}{gTS_{substrate}}$

Experimental procedures

The CSTRs and the AnMBR were inoculated with digested sludge from a full-scale digester of a municipal WWTP. Mesophilic condition was maintained at temperature of around 37 ± 1°C. For comparison of both reactor types, CSTRs were operated at SRT = 10 d, 15 d and 20 d, while AnMBR was operated at HRT = 10 d and SRT = 15 d. All reactors were fed continuously. A defined mixture of WAS and flotation sludge (FS) was prepared gravimetrically at regular

intervals (3-5 times per day). The mixture composition was changed stepwise after operation of three SRTs. The ratio of investigated COD-related shares of flotation sludge (COD_{FS}) to total COD load of the inflow (COD_{FS}/COD_{total}) were 0.5, 0.6-0.7 and 0.8-0.9. OLRs are given in Table 17. After applying two SRTs without any major changes in operation, a steady state was reached. The performance in steady state was evaluated for another SRT.

4.2.3 Sampling and assays

Sampling and assays (e.g. BMP tests and SMA) correspond to the explanations given in section 3.3.3. Process stability is determined again by the approach using a safety factor proposed by Siegrist *et al.* (2002) as also given in chapter 3.3.3 (see expression 3.13). From the data of BMP batch assays, expected methane yields can be calculated for continuously fed digesters operated as CSTRs following substrate first-order kinetics (in accordance with equation 3.14 in chapter 3) with hydrolysis/disintegration as rate-determining step. The equation is as follows:

$$Y_{CH4}(SRT) = \frac{k_{dis} \cdot SRT}{1+k_{dis} \cdot SRT} \cdot Y_{max} \quad (4.1)$$

Where, $Y_{CH4}(SRT)$: Methane yield ($L\ CH_4/\ kg\ COD_{in}$)

If the degradation processes of the individual substrates do not significantly influence each other in the substrate mixture, the methane yield of the substrate mixture can theoretically be determined from the sum of the methane yields of the individual substrates. Considering COD-related shares of each substrate in the mixture, the methane yield can be calculated using their kinetic constants from batch assays as follows:

$$Y_{CH4,substrate\ mixture} = \frac{COD_{FS}}{COD_{total}} \cdot \frac{k_{hyd,FS} \cdot SRT}{1+k_{hyd,FS} \cdot} \cdot Y_{CH4,max,FS} + \frac{COD_{WAS}}{COD_{total}} \cdot \frac{k_{dis,WAS} \cdot SRT}{1+k_{dis,WAS} \cdot SRT} \cdot Y_{CH4,max,WAS} \quad (4.2)$$

Furthermore, potential maximum LCFA concentrations in the reactor were estimated by calculating the residual degradable lipids in the anaerobic sludge in order to evaluate effects on process stability. It is further assumed that removal can be described by substrate first-order kinetics (ADM1) according to previously introduced results in section 3.4.1. It is assumed that disintegration is the rate-determining step in removal of all degradable particulates in WAS which also relates to the removal of lipids. As disintegration is generally connected to degradation of WAS (Pavlostathis, 1985), it is assumed that hydrolysis is the rate-determining step in degradation of organic matter in flotation sludge.

Thus, residual degradable lipids were estimated as follows:

$$c_{res.deg.,li} = c_{li,FS} \cdot \frac{Q_{FS}}{Q_{total}} \cdot \eta_{max,FS} \cdot \left(1 - \frac{k_{hyd,FS} \cdot SRT}{1+k_{hyd,FS} \cdot SRT}\right) + c_{li,WAS} \cdot \frac{Q_{WAS}}{Q_{total}} \cdot \eta_{max,WAS} \cdot \left(1 - \frac{k_{dis,WAS} \cdot SRT}{1+k_{dis,WAS} \cdot SRT}\right) \quad (4.3)$$

Where, c_{li}: lipid concentration in the substrate ($=f_{li} \cdot COD_{substrate}/(2.87\ gCOD/gVS)$) (g VS/L)

Q_{FS}: inflow of flotation sludge (m^3/d)

Q_{WAS}: inflow of waste activated sludge (m^3/d)

Q_{total}: inflow of total feed (m^3/d)

$k_{hyd,FS}$: hydrolysis constant of the flotation sludge ($1/d$)

$k_{dis,WAS}$: disintegration constant of WAS ($1/d$)

$\eta_{max,FS}$: maximum conversion of flotation sludge to CH_4 ($= Y_{CH4} \cdot (350\ NL/kg\ COD)^{-1}$) (-)

$\eta_{max,WAS}$: maximum conversion of WAS to CH_4 ($= Y_{CH4} \cdot (350\ NL/kg\ COD)^{-1}$) (-)

In addition, OLRs of degradable matter were used and can be calculated as follows:

$$OLR_{COD,deg} = \frac{(V_{inflow,WAS})' \cdot \eta_{max,WAS} + (V_{inflow,float\ sludge})' \cdot \eta_{max,flotation\ sludge}}{V_{reactor}} \quad (4.4)$$

Where, $OLR_{COD,deg}$: organic loading rate of degradable COD ($kg\ COD_{deg}/(m^3 \cdot d)$

4.3. Results and discussion

Table 17 summarises operational performance in steady state in terms of effluent quality, methane yield and applied SRT of continuous digestion tests in pilot scale. Higher shares of flotation sludge were successfully degraded in all reactors at SRT down to 10 days. In CSTRs, highest methane yields of up to 280 L/kg COD_{in} were achieved at COD shares of lipids over 80 % and SRT = 20 d. At similar COD shares of lipids, slightly lower methane yields were obtained at SRT ≈ 10 d (see Table 17 and Figure 29). The AnMBR, operated at HRT = 10 d and SRT = 15 d, achieved methane yields higher than 280 L/kg COD_{in} at COD shares of lipids around 85 %. During the entire operational period, methane yields in relation to degraded COD always ranged between 320 and 350 L/ kg COD_{deg} in all reactors, resulting in a COD-based gap of less than 10 % in mass balance. This indicates that lipids were available for AD and did not accumulate on the liquid surface in the digester (Szabo-Corbacho *et al.*, 2019). As expected, TS and VS concentrations in the AnMBR were higher than in the CSTRs at even share of flotation sludge in the mixture. The organic acid concentrations in the reactor remained below 1,000 mg HAc/L in all operational settings. The pH value remained between 7.2-7.7 in all the settings, too.

Table 17. Steady state performances of CSTR and AnMBR fed with different feed mixtures at various SRTs (arithmetic mean ± standard deviation)

Operation		Loading					Methane yield	Effluent (reactor) composition			
SRT	SRT/ HRT	COD_{FS}/ COD_{total}	COD_{lipid}/ COD_{total}[a]	$OLR_{COD,deg.}$	OLR_{FS}	lipid related sludge load[a]	Y_{CH4}	pH	VFA	TS	VS
[d]	[-]	[-]	[-]	[kg COD_{deg}/ (m^3·d)]	[kg VS/ (m^3·d)]	[kg VS_{li}/ (kg VS·d)]	[L/kg COD_{in}]	[-]	[mg HAc/L]	[%]	[%]
CSTR											
10.2	1.0	0.47 ± 0.07	0.55 ± 0.08	5.1 ± 1.2	1.2 ± 0.2	0.08 ± 0.01	162 ± 50	7.6 ± 0.1	280 ± 139	2.7 ± 0.1	1.9 ± 0.1
11.4	1.0	0.77 ± 0.06	0.78 ± 0.06	7.7 ± 1.5	2.5 ± 0.4	0.14 ± 0.02	235 ± 8	7.2 ± 0.0	538 ± 241	2.5 ± 0.1	1.8 ± 0.1
10.3	1.0	0.86 ± 0.03	0.85 ± 0.03	10.1 ± 2.9	3.9 ± 0.9	0.23 ± 0.05	253 ± 16	7.2 ± 0.1	676 ± 280	2.4 ± 0.1	1.7 ± 0.1
15.2	1.0	0	0.2	1.4 ± 0.4	-	0.01 ± 0.00	126 ± 2	7.2 ± 0.0	200 ± 41	3.5 ± 0.3	2.4 ± 0.2
16.0	1.0	0.35 ± 0.06	0.46 ± 0.08	2.7 ± 0.6	0.5 ± 0.1	0.04 ± 0.01	171 ± 11	7.3 ± 0.0	164 ± 22	2.9 ± 0.3	2.0 ± 0.2
16.0	1.0	0.57 ± 0.10	0.63 ± 0.11	4.0 ± 0.7	1.0 ± 0.2	0.06 ± 0.01	222 ± 24	7.3 ± 0.0	181 ± 47	2.4 ± 0.1	1.7 ± 0.1
15.0	1.0	0.81 ± 0.06	0.81 ± 0.06	8.3 ± 1.4	2.7 ± 0.5	0.18 ± 0.03	264 ± 17	7.1 ± 0.2	420 ± 123	2.2 ± 0.1	1.5 ± 0.1
20.5	1.0	0	0.2	0.7 ± 0.2	-	0.01 ± 0.00	111 ± 15	7.3 ± 0.0	124 ± 10	2.6 ± 0.1	1.8 ± 0.1
20.5	1.0	0.77 ± 0.11	0.78 ± 0.11	2.9 ± 1.0	1.0 ± 0.3	0.06 ± 0.01	244 ± 16	7.2 ± 0.0	127 ± 7	2.3 ± 0.1	1.6 ± 0.1
19.5	1.0	0.86 ± 0.03	0.85 ± 0.03	2.7 ± 0.6	2.0 ± 0.4	0.13 ± 0.01	283 ± 4	7.3 ± 0.0	240 ± 8	2.3 ± 0.1	1.6 ± 0.1
AnMBR											
15.0	1.5	0	0.2	1.8 ± 1.0	-	0.01 ± 0.01	143 ± 14	7.1 ± 0.1	141 ± 54	4.1 ± 0.4	2.6 ± 0.3
16.5	1.5	0.49 ± 0.10	0.57 ± 0.12	5.6 ± 1.3	1.4 ± 0.4	0.06 ± 0.00	210 ± 25	7.2 ± 0.0	162 ± 47	4.3 ± 0.3	3.0 ± 0.1
15.3	1.5	0.59 ± 0.06	0.64 ± 0.07	6.2 ± 1.0	1.7 ± 0.4	0.08 ± 0.00	232 ± 23	7.4 ± 0.2	98 ± 83	3.4 ± 0.2	2.3 ± 0.2
15.6	1.6	0.87 ± 0.08	0.85 ± 0.08	11.2 ± 3.2	3.8 ± 1.0	0.21 ± 0.06	286 ± 30	7.7 ± 0.3	324 ± 192	2.5 ± 0.2	1.8 ± 0.1

[a] calculated total lipid content of substrate mixture with $f_{li,WAS}$ = 0.2 and $f_{li,FS}$ = 0.95

Results of BMP tests are summarised in Table 18. Based on the findings of BMP tests, the organic matter of the flotation sludge was almost completely degradable (> 0.9 g COD-CH_4/g COD_{in}) and corresponded to high methane yields of 320 L/kg COD_{in}. However, digestion of organic matter of WAS only achieved methane yields of around 154 L/kg COD_{in}. Degradation rates of organic matter of the flotation sludge are much faster than the degradation rates of WAS; this leads to a higher kinetic constant k_{hyd} for substrate first-order kinetics.

Table 18. Results of biomethane potential tests (arithmetic mean ± standard deviation)

Parameters	WAS	Flotation sludge
k_{dis} (k_{hyd}) of substrate first-order kinetics [d^{-1}]	0.20 ± 0.02	0.51 ± 0.03
Maximum methane yield $Y_{CH4,\ max}$ [L/kg COD_{in}]	154 ± 22	320 ± 15
Maximum conversion to CH_4[a] η_{max} [g COD-CH_4/g COD_{in}]	0.44 ± 0.06	0.91 ± 0.04

Each sludge was characterised 5 times by using BMP tests (results are given in the annex)

[a] $\eta_{max} = Y_{CH4} \cdot (350\ NL/kg\ COD)^{-1}$

4.3.1 Influence of substrate mixture and SRT on methane generation

In Figure 28, measured methane yields of the AnMBR operated at SRT = 15 d and with varying substrate mixtures are compared with performance of the CSTR at even SRT. Additionally, methane yields calculated from the sum of the yields of the individual substrates based on kinetic constants from batch assays are provided.

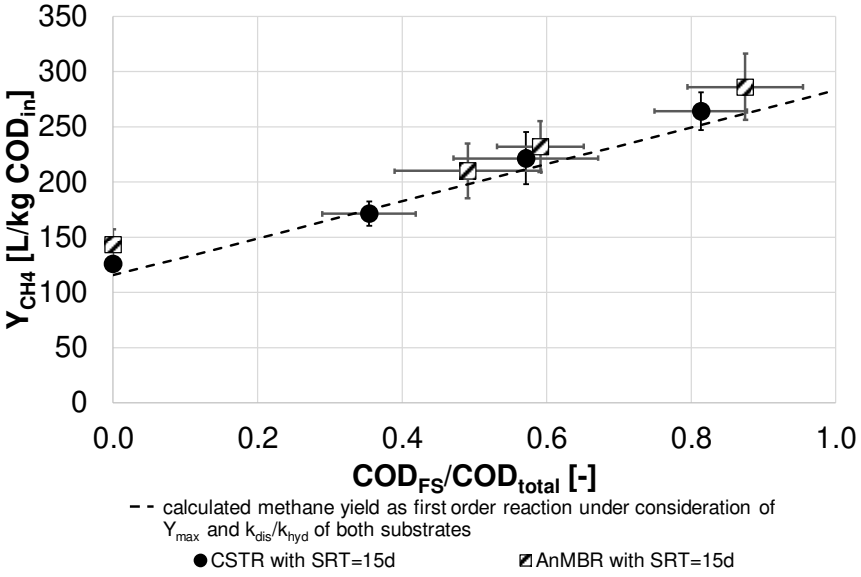

Figure 28. Methane yields of CSTR and AnMBR at SRT = 15 d compared to maximum methane yields obtained from batch tests (dashed line; represented as a function of COD-related shares of flotation sludge)

The AnMBR achieved similar methane yield as that of the CSTR operated at SRT = 15 d (Figure 28). Small differences were mainly based on minor deviations in COD shares of lipids in the substrate mixture. This finding does not agree with the findings of Xiao *et al.* (2017) who observed a positive effect on enzymatic hydrolysis activity in AnMBRs fed with lipid-rich kitchen slurry. However, these results are in agreement with previously introduced investigations of AnMBR and CSTR fed with WAS, which resulted in similar methane yields (=COD removal) at equal SRT (see Chapter 3).

Measured methane yields of continuously fed pilot plants (Table 17) meet theoretical values of methane yields (Figure 28) calculated using the abovementioned equations and kinetic constants from batch assays. Easily degradable organic matter (flotation sludge) did not limit degradation of slowly degradable organic matter (WAS), as would be the case with diauxy. Thus, in continuously fed digesters, methane generation in steady state from co-digestion of WAS and flotation sludge can be described from the sum of the yields of the individual substrates by a substrate-first order kinetics approach introduced by Batstone *et al.* (2002) as long as no significant inhibitions in the reactors occur.

The COD removal increases at elevated SRT when using the same substrate mixture as shown for mixtures with COD-related shares of flotation sludge > 0.8 in Figure 29. Even at the highest COD related shares of flotation sludge based on COD, measured methane yields of the continuously fed pilot plants meet expectations based on kinetic parameters of batch assays; no decrease in methane yields was observed. Therefore, based on COD removal, significant inhibition of AD could not be detected. Limitations of lipid-rich sludge digestion cannot be derived from this data.

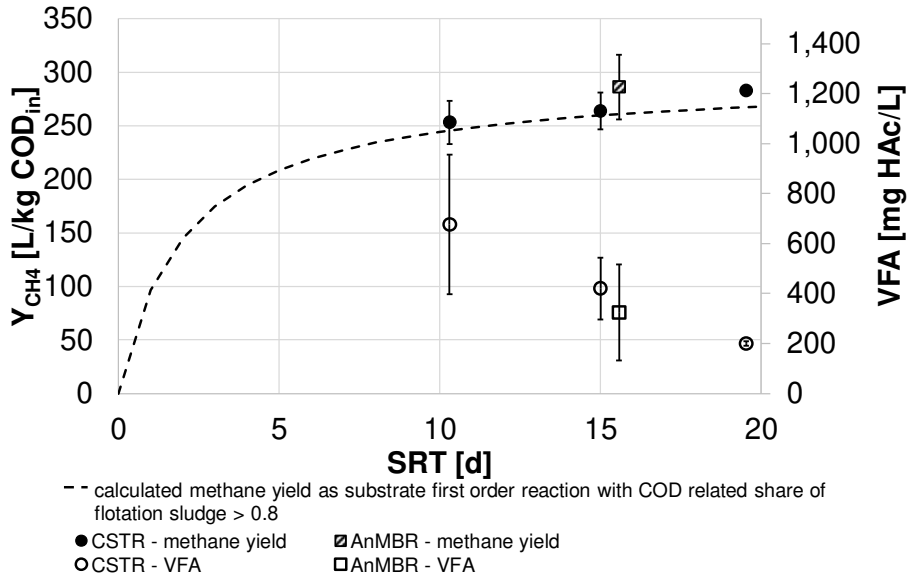

Figure 29. Methane yields of reactors fed with high-COD related shares of flotation sludge (> 0.8; represented as a function of SRT) compared to methane yields calculated as a substrate first-order reaction (dashed line)

4.3.2 Influence of substrate mixture and SRT on process stability

The concentration of volatile organic acids is an accepted criterion for defining stable operation of digesters, as instabilities are usually detected at values over 500 mg HAc/L (Henze *et al.*, 2002). In sludge treatment, low concentrations of organic acids indicate that acetoclastic methanogenesis does not determine degradation rate and events of substrate overloading are unlikely. Present results show that VFA concentrations were mostly below 500 mg HAc/L but increased with decreases in SRT at even COD shares of the flotation sludge/lipids (see Figure 29 and Table 17). VFA concentrations also increased at higher COD shares of the flotation sludge/lipids at even SRT (see Figure 28 and Table 17).

Results obtained from SMA tests show that the SF proposed by Siegrist *et al.* (2002) remained above 1.0 (see Figure 30) which is why process stability was sufficient against substrate overload.

Two factors predominantly affected SF: SRT and COD share of lipids in influent substrate.

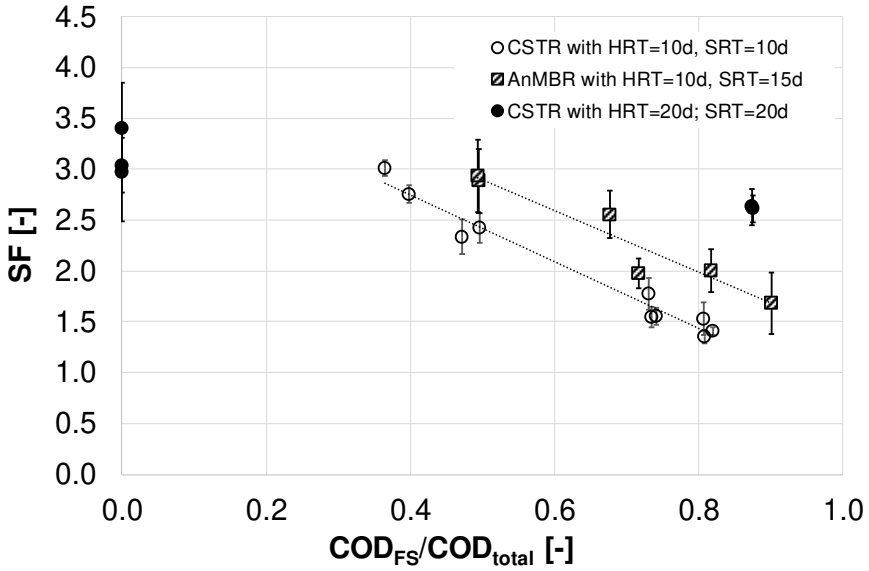

Figure 30. Safety Factor SF as function of COD-related share of flotation sludge in the feed and SRT

Lower SRT reduced safety against substrate overload. In anaerobic digesters fed with COD shares of flotation sludge > 0.8 (i.e. COD shares of lipids > 0.8 in the substrate, see Table 17), the safety factor dropped from SF = 2.5 to SF = 1.5 when SRT was reduced from SRT = 20 d to SRT = 10 d (Figure 30). This finding agrees with the definition of SF, which mentions that SF depends on SRT, maximum growth rate of acetoclastic methanogens and their decay rate. Results from Dereli *et al.* (2014b) also show a reduction of SF with reduced SRT from 30 to 20 days (SF ≈ 1.7 at SRT = 30 d and SF ≈ 1.5 at SRT = 20 d). Calculation of SF from provided data is given in Table A 4 of the annex. Ziels *et al.* (2016) also observed a dependence of methanogenic activity on SRT in digesters fed with FOG.

Safety against substrate overload also decreased in reactors fed with increasing COD shares of lipid-rich flotation sludge (Figure 30). In CSTR operated with SRT = 10 d, an increasing share of flotation sludge (and corresponding lipids) decreased SF from SF = 3 at COD_{FS}/COD_{total} = 0.4 to SF < 1.5 at COD_{FS}/COD_{total} > 0.8. Similar results were observed for digesters operated at SRT = 15 d and SRT = 20 d. In operation, this reduced safety must be accounted for by lowering variations of inflow characteristics, especially COD loads, as substrate overload might otherwise occur. When the original definition of SF is considered, a decrease of SF with increasing COD-related shares of flotation sludge indicates a reduction in growth rate of acetoclastic bacteria.

According to Siegrist *et al.* (2002), growth rate μ_{max} and decay rate k_d can be obtained by plotting 1/SF versus 1/SRT (see Figure 31). In this study, maximum growth rate could not be determined as optimum conditions were not provided in the digesters. Instead, apparent growth rate μ_{app} was determined from the data that included possible inhibition or other effects. With low shares of flotation sludge in the feed mixture, the apparent growth rate was around 0.49 d^{-1}. Values are similar to maximum growth rates obtained by some studies under optimum

conditions (e.g. Siegrist *et al.*, 2002; Batstone *et al.*, 2006). Therefore, minor inhibition can be assumed when feeding low shares of lipids. However, in digesters fed with COD shares of lipids higher than 80 %, the apparent growth rate dropped noticeably to values below 0.16 d^{-1}. Reduced apparent growth rate illustrates inhibiting influences on methanogens. As ammonium concentrations (< 1,000 mg/L) and H_2S concentrations (< 1 % in the biogas), the most common inhibitors of digestion processes, were far below critical values (Kroiss and Svardal, 2015), lipids and their hydrolysis product LCFA most likely inhibited the growth rate.

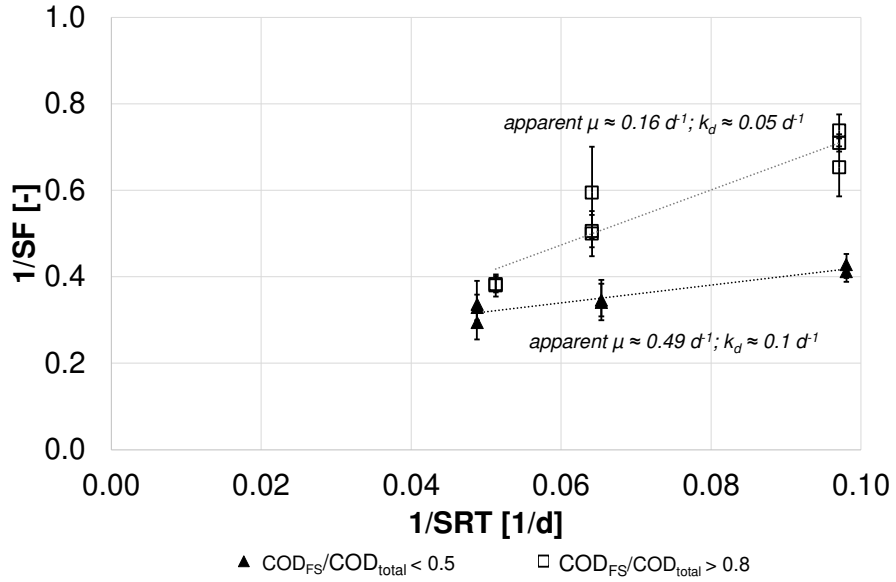

Figure 31. Apparent growth rate of acetoclastic methanogens in dependence of substrate mixture

Although there is a dependence of the concentration of organic acids on residual lipids in the anaerobic sludge (Figure 32), inhibitions are most clearly shown when measured safety factors SF are compared with safety factors calculated from non- or, at least, low-inhibited operation phases (SF_0) (see Figure 33). Concentrations of residual lipids in the anaerobic sludge were calculated using expression 4.3 in section 4.2.3 in combination with kinetic parameters and substrate characteristics in Table 16 and Table 17. Residual lipid concentrations in anaerobic sludge are higher either at lower COD removal (caused by lower SRT) or at higher feed concentration (caused by higher shares of flotation sludge) in the inlet (see expression 4.3). Safety factors from non- or, at least, low-inhibited operation phases (SF_0) were calculated using equation 3.12 using a growth rate of 0.49 d^{-1} and a decay rate of 0.1 d^{-1}, as found in reactors at $COD_{FS}/COD_{total} < 0.5$ (see Figure 31). Theoretically, a ratio of present SF and SF_0 of 1 indicates non-inhibiting conditions.

Based on the ratio SF/SF_0, an effect on degradable lipid content of the anaerobic sludge is obvious (Figure 33). Up to degradable lipid concentration of around 50 mg VS/g TS in the anaerobic sludge, ratio SF/SF_0 remained almost constant at a value of 1 indicating non-inhibiting conditions. With an increase in the content of degradable lipids to approx. 150 mg VS/gTS, the safety against substrate overload was reduced to 60-80 % in comparison to non-inhibiting conditions, which corresponds to an inhibition of 20-40 % on acetoclastic methanogens. Szabo-Corbacho *et al.* (2019) observed similar values with inhibition around 26-46 % at LCFA concentration of 120-150 mg lipid/g TSS in the anaerobic sludge when treating whole milk as synthetic dairy wastewater in anaerobic digesters. Hwu *et al.* (1996) reported higher losses of

methanogenic activity (50 %) at oleate concentration of 32 mg/g TSS. In this study, comparable stability losses of around 50 % were reached at degradable lipid contents of the anaerobic sludge above 200 mg VS/g TS.

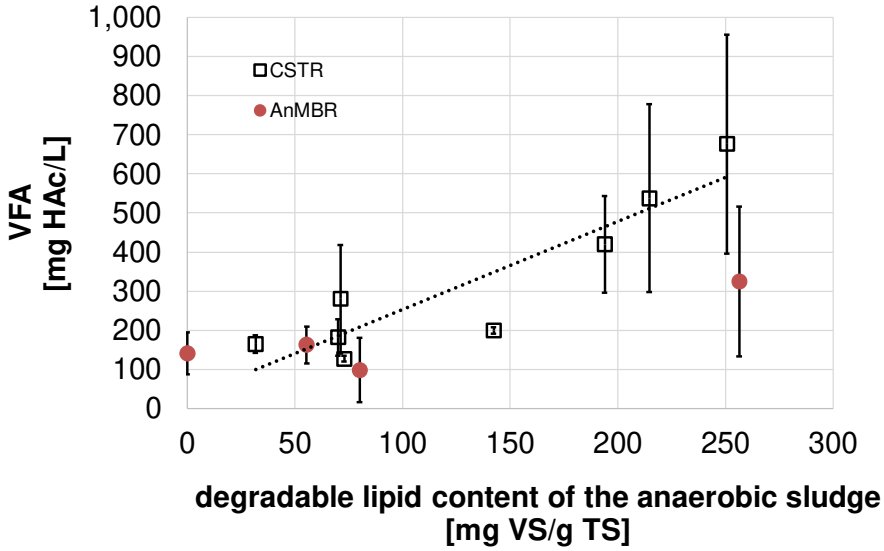

Figure 32. Concentration of volatile fatty acids plotted against degradable lipid content of the anaerobic sludge

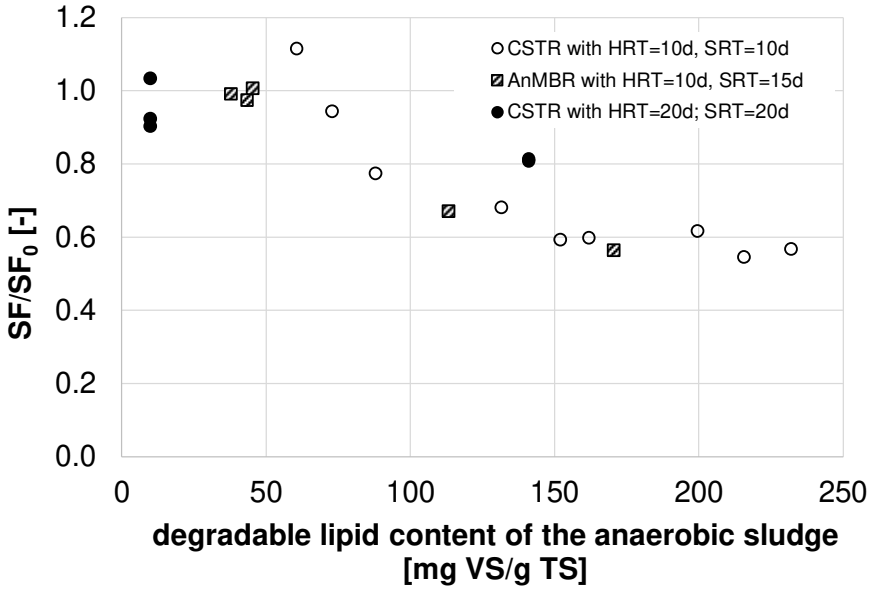

Figure 33. Changes in the safety factor corresponding to changes in degradable lipid content of the sludge

Hence, although AD performed well with respect to organic acid concentrations and COD removal at degradable lipid concentration of up to 150 mg VS/ g TS in the anaerobic sludge (see Table 17), process stability against substrate overloads was already reduced at much lower concentration. Consequently, operational fluctuations in feed may become a major concern, as substrate accumulation may occur. SF can detect microbiological causes for emerging process instabilities even before other effects such as increasing concentration of organic acids, lowering of pH or reduced methane yield are observed. This is related to the general characteristics of the multi-step anaerobic sludge digestion process that has a slow step at the start (hydrolysis, disintegration) and a slow step at the end (methanogenesis; Henze *et al.*, 2002;

Batstone *et al.*, 2006). In case of inhibition of methanogens, for example, because of substrate overloading, SMA would be reduced first; this will also be expressed by lower SFs.

4.3.3 Assessment of design criteria on the basis of reactor performances

The use of the COD loading rate represents the simplest possibility of a design criterion. In this study, a maximum COD loading rate covering all operated reactors would be around 6.0 kg COD_{deg}/(m^3·d). Limitations are especially related to the CSTR operated at lowest SRT = 11 d as variations in concentration of organic acid are highest in this CSTR. Although not critical, an increase in VFA concentration and especially their variation was observed at higher OLRs (Figure 34a). If SRT is extended to 15 days in AnMBR, organic loading rates could be increased up to OLR of 11.2 kg COD_{deg}/(m^3·d) without observing major process instabilities on the basis of VFA. In the CSTR operated at SRT = 15 d, OLR of 8.3 kg COD/(m^3·d) were successfully treated. OLRs are well above common recommendations based on degradable COD of 2.9 kg COD_{deg}/(m^3·d) by DWA M-368 (2014) but are in the range of other publications. Szabo-Corbacho *et al.* (2019) operated an AnMBRs with OLR of 4.7 kg COD_{deg}/(m^3·d) at SRT = 20 d using milk wastewater as substrate. Dereli *et al.* (2014b) operated a stable AnMBR with OLR of 8.3 kg COD_{deg}/(m^3·d) at SRT = 20 d.

Findings are similar when applying the FOG or lipid related loading rate (Figure 34b). AD processes remained stable in all reactors as long as the loading rate remained below OLR_{FS} = 2.0 kg VS/(m^3·d). With SRT = 15 d, the CSTR could be operated with a maximum corresponding to OLR_{FS} = 2.7 kg VS/(m^3·d). When using an AnMBR with HRT = 10 d and SRT = 15 d, OLR of 3.8 kg VS_{FS}/(m^3·d) did not lead to process instabilities. Higher organic loading rates in AnMBR resulted mostly from decoupling. Values achieved in this study are close to FOG-related maximum loading rate of 2.5 kg VS_{FOG}/(m^3·d) according to Mata-Alvarez *et al.* (2014) and maximum OLR up to 4.0 kg VS/(m^3·d) published by Dereli *et al.* (2014b) treating lipid-rich wastewater with an AnMBR. Maximum OLRs achieved in this study strongly exceed recommended FOG related loading rate of 0.84 kg VS_{FOG}/(m^3·d) according to Mata-Alvarez *et al.* (2014) and maximum OLR of 1.0 kg VS/(m^3·d) treating milk wastewater with an AnMBR (Szabo-Corbacho *et al.*, 2019).

Comparing the achieved maximum loads including biomass concentration in the reactor, as sludge load, specific lipid related sludge loads of up to 0.18 kg lipid/(kg VS·d) resulted in VFA concentrations mostly within the range of a stable process in this study (see Figure 34c). Literature suggests using 0.04-0.13 kg lipid /(kg VS·d) at VS/TS > 0.9 (Dereli *et al.*, 2014b; Szabo-Corbacho *et al.*, 2019). Higher values seem to have been achieved in this study, as the reactors were operated at lower VS/TS ratios of around 0.7, which was related to the inorganic contents of WAS. Higher concentrations of inorganic matter provide an additional surface for LCFA adsorption which might reduce inhibiting effects of LCFA on biomass (Palatsi *et al.*, 2009) but are not considered in definition of VS related sludge load according to Dereli *et al.* (2014b) and Szabo-Corbacho *et al.* (2019). Dereli *et al.* (2014b) and Szabo-Corbacho *et al.* (2019) used substrates with less non-degradable or inorganic matter.

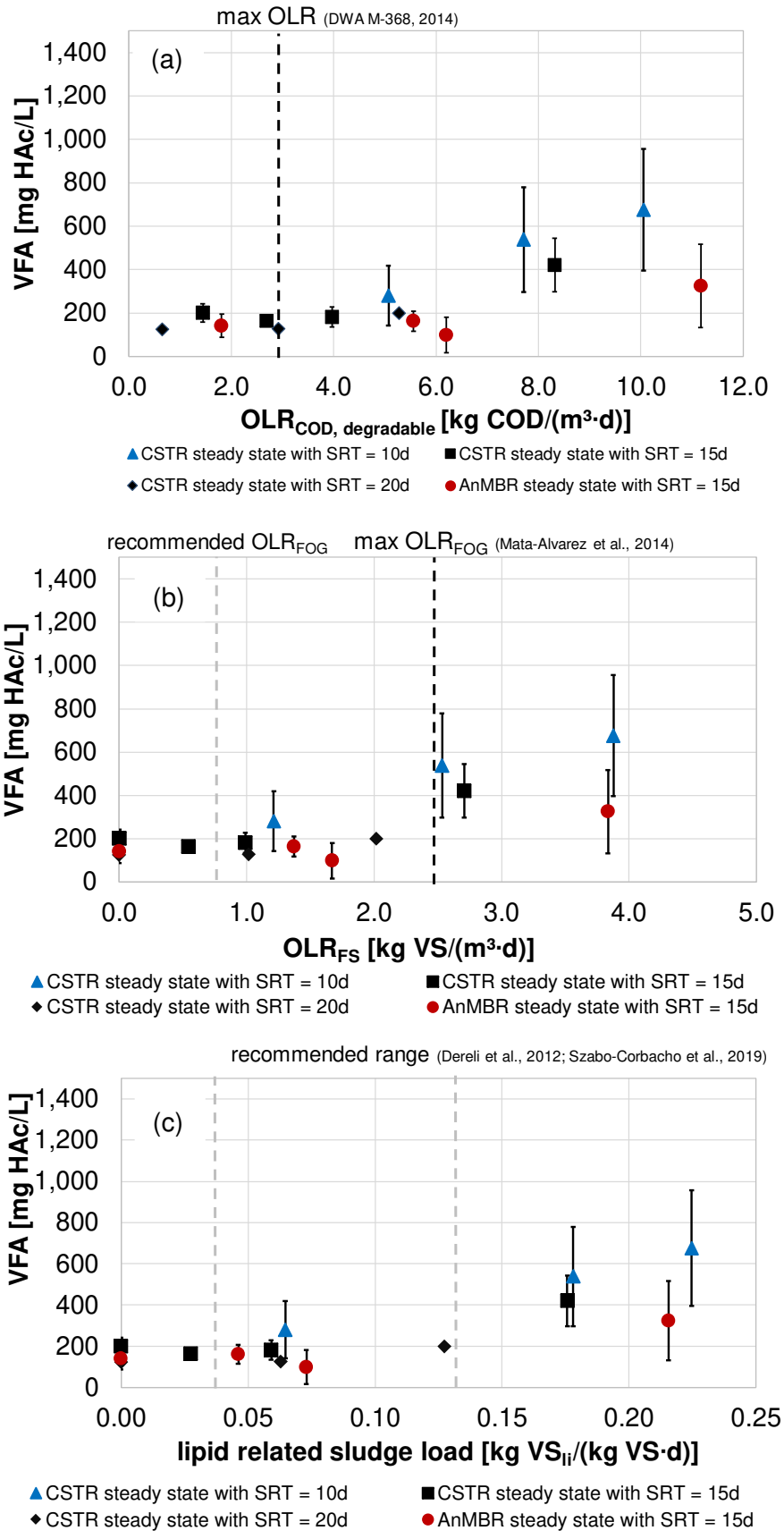

Figure 34. Organic acid concentration as a function of (a) degradable COD loading rate, (b) organic loading rate of flotation sludge and (c) lipid-related sludge load

For verifying the suitability of different design approaches, designed sludge digesters of an exemplary dairy WWTP (see Figure 26) are compared on the basis of SRT and in compliance with provision of a sufficient process stability by keeping the lipid content of the anaerobic sludge below 100 mg lipid/g TS (see section 4.3.2). The following design approaches were evaluated:

- A technical degree of degradation of 80 % based on degradable matter (Section 2.1.3),
- a maximum COD_{deg} loading rate of 2.9 kg COD/(m³·d) according to DWA-M 368 (2014),
- a FOG-related recommended loading rate of 0.84 kg VS_{FOG}/(m³·d) and a maximum loading rate of 2.5 kg VS_{FOG}/(m³·d) according to Mata-Alvarez *et al.* (2014),
- a recommended lipid-related sludge load of 0.09 kg VS_{li}/(kg VS·d) (mean value of range suggested by Dereli *et al.* (2014b) and Szabo-Corbacho *et al.* (2019)),
- a maximum degradable lipid content of 0.1 kg VS/kg TS in anaerobic sludge, and
- results of successfully conducted pilot trials: SRT_{min} = 15 d (see section 4.3.1).

The exemplary dairy WWTP has to treat a mixture of WAS and flotation sludge with a COD share COD_{FS}/COD_{total} = 0.85; both with a flow of 20 m³/d. Substrate characteristics are given in Table 16 and Table 18. COD degradation, biomass growth and lipid content of the sludge were calculated with a substrate first-order model using kinetic constants provided in Table 18. The biomass growth was calculated with a yield of 0.07 kg VS/kg $COD_{removed}$ and a decay rate of 0.03 1/d (Metcalf and Eddy, 2004). All calculations and resulting inlet and outlet concentrations are given in Table A5 of the annex. Required SRT of the designed digesters and the maximum degradable lipid content in the anaerobic sludge are summarised for the given example in Table 19.

Table 19. Minimum SRT, COD removal and lipid content of the anaerobic sludge of designed digesters on the basis of various design approaches

Design approach	SRT_{min} [d]	$\eta_{COD,degr.}$ | $\eta_{COD,total}$ [%]	$c_{deg.\ lipid}$ / $c_{TS\ in\ reactor}$ [g VS/g TS]
Tech. degree of degradation $\eta_{COD,degradable}$ > 80 %	9	80 | 60	0.16
Degradable organic loading rate $B_{degradable\ COD,\ max}$ < 2.9 kg COD/(m³·d)	34	94 | 73	0.06
FOG related loading rate			
$B_{FOG,\ rec}$ = OLR_{FS} < 0.84 kg VS_{FOG}/(m³·d)	39	94 | 74	0.06
$B_{FOG,\ max}$ = OLR_{FS} < 2.5 kg VS_{FOG}/(m³·d)	13	85 | 65	0.13
Lipid related sludge load $B_{VS,lipid}$ < 0.09 kg VS_{li}/ (kg VS·d)	18	88 | 68	0.11
Degr. lipid content of the anaerobic sludge $c_{deg.\ lipid}$ / $c_{TS\ in\ reactor}$ < 0.1 kg VS_{li}/ kg TS	20	90 | 69	0.10
Successful Pilot trials SRT = 15 d (SF = 1.8)	15	87 | 65	0.11

Based on the findings of this study, a stable AD process that allows a maximum degradable lipid content of 100 mg lipid/g TS in the sludge, requires a SRT of 20 days. In this reactor, inhibitions on methanogens are almost completely avoided (see section 4.3.2) and a quasi-maximum SF of 2.5 (depending on SRT) is provided. A quantification of acceptable inlet variations as process control is given in section 5.3.3. This approach covers minimum volumes of

anaerobic digestion reactors while assuring a stable process. CapEx and OpEx for mixing and heating are therefore limited to a minimum for the respective application.

For reaching a technical degree of degradation, i.e., η = 80 %, a SRT of around 9 days is required; however, this will not lead to a stable process as lipid content in the anaerobic sludge will be higher than 0.1 gVS/ gTS.

Designing a WWTP based on recommended values of OLR and lipid-related sludge load assures a stable digestion process. But, a maximum COD_{deg} loading rate of 2.9 kg COD/(m^3·d) according to DWA-M 368 (2014) or a recommended FOG loading rate of 0.84 kg VS/(m^3·d) according to Mata-Alvarez *et al.* (2014) will lead to large digester volumes with SRT > 30 days. High CapEx and OpEx for mixing and heating will result.

Using a lipid-related sludge load recommended by Dereli *et al.* (2014b) leads to a required SRT in a similar range of around 18 days compared to the recommended 20 days based on a tolerable degradable lipid content of 100 mg lipid/g TS in the sludge (see section 4.3.2). Designing a digester based on a maximum FOG-related loading rate of 2.5 kg VS/(m^3·d) according to Mata-Alvarez *et al.* (2014) will lead to much smaller reactor volumes with SRTs of around 15 days. In both cases, residual lipid content in the anaerobic sludge will exceed 100 mg lipid/g TS slightly. But, required SRT are in the range of successfully conducted pilot trials at SRT = 15 d. At this SRT, the AD process remained stable. Degradable lipid concentration in the anaerobic sludge stayed below 150 mg VS/ g TS. Inhibition of acetoclastic methanogens in the range of 50 % must be accepted (see Figure 33). Safety against substrate overload was reduced to SF around 1.8. Allowable inlet fluctuations are therefore reduced compared to an operation at SRT = 20 d.

In conclusion, organic loading rate and a technical degree of degradation to be achieved do not offer a precise dimensioning of digester volume for lipid-rich sludge treatment. A general transferability could only be achieved if substrate-specific values up to the integration of lipid shares in substrate mixtures were specified more precisely. Compared to the general COD loading rate, the substrate-specific loading rate is more suitable as transferable design criterion. However, recommendations with correspondingly unreported safeties worsen a precise design as shown based on recommended values on FOG treatment by Mata-Alvarez *et al.* (2014). All recommended COD loading rates for dimensioning of digesters are usually only valid for the CSTR. They have to be adjusted for the application of an AnMBR under consideration of the decoupling ratio.

The design criterion lipid related sludge load leads to a more precise design in terms of reactor volume. It includes empirical experiences on removal rates of lipids. The drawback is that much more information is required for the design. The inert components and the residual degradable components must be considered in order to calculate volatile solids concentration in the reactor. This requires substrate fractionation, kinetic constants and methane yields of all substrates. But, the inclusion of inorganic matter in the anaerobic sludge, which, however, has a significant effect in reducing inhibition on methanogens related to LCFA cannot be covered by this approach. Additional substrate specific recommendations have to be given.

The maximum degradable lipid content in the anaerobic sludge remains the most precise generally valid design criterion for lipid-rich digestion, as it considers all relevant parameters. It covers applications with different SRT, lipid shares and digester systems (CSTR or AnMBR).

As a limiting value, a content of around 50-100 mg lipid/g TS seems reasonable. In this case, inhibition on acetoclastic methanogens is limited and the AD process remains stable. Safety factors are high. This chosen design criterion is useful especially for unknown inlet fluctuations. A degradable lipid content of up to 150 mg lipid/g TS in the reactor seems to be a reasonable design criterion for AD facing low inlet fluctuations and accepting low SFs. In this case, inhibition of acetoclastic methanogens in the range of 50 % must be accepted (see Figure 33).

4.4. Conclusions

COD degradation of a mixture of WAS and lipid-rich flotation sludge from the dairy industry with high COD-related shares of lipids (> 0.9) was successfully conducted in pilot scale at SRT ≥ 15 d. The performance of AnMBR in terms of COD removal was similar to that of CSTR with similar SRT; however, AnMBR can be operated at higher OLR. These findings are in agreement with previous results provided in chapter 3. Easily degradable organic matter (flotation sludge) did not limit degradation of slowly degradable organic matter (WAS). Thus, in continuously fed digesters, methane generation in steady state from co-digestion of WAS and flotation sludge can be described from the sum of the yields of the individual substrates by a substrate-first order kinetics approach (e.g. ADM1).

Process limitations could not be observed from methane generation and only limited from concentrations of organic acids concentration but on the basis of SMA measurements. Emerging inhibition and emerging process instabilities were clearly shown when measured safety factors SF were compared with safety factors calculated from non- or, at least, low-inhibited operation phases (SF_0).

Process stability and maximum tolerable organic loads depended mainly on residual lipid concentration in the anaerobic sludge. The digestion process remained stable up to concentrations of 150 mg lipid/ g TS, although inhibition on acetoclastic methanogens started at 50 mg lipid/ g TS. At equal SRT, SF decreased with increasing shares of flotation sludge while residual lipid content in anaerobic sludge increased. Increasing SRT significantly improved this ratio and the process stability of the digestion process. Hence, AnMBR can offer a higher process stability compared to CSTR at even HRT or when extending the SRT.

Observed process limitations based on the residual degradable lipid content of the sludge corresponded well with published values of TS related LCFA inhibition. As it is a calculable parameter which covers all relevant parameters such as SRT, kinetic coefficients k_{dis}/k_{hyd}, lipid share and inorganic/inert solids in the reactor, it seems to be a promising generally valid design criterion for a precise reactor design of lipid-rich digestion. It also seems promising for transferability of results to deviating applications concerning substrate composition, degradability and fat content. As a limiting value, the degradable lipid content of the anaerobic sludge should remain between 50-100 mg lipid/g TS. Values of residual lipid content in the anaerobic sludge higher than 100 mg lipid/g TS as basis of design are recommended only in case of comprehensive preliminary studies based on laboratory or pilot tests.

Other common design criteria such as OLR or the lipid-related sludge load can provide an adequate design and a stable AD process for an investigated, specific application.Transferability of OLR and lipid-related sludge loads to other applications is limited as shown.

5. Use of SMA for process control of sludge digestion facing inlet variations

This chapter is partly based on

Lutze, R., Rühl, J., Blach, T., Engelhart, M. (2017) Facing drawbacks in process stability of anaerobic sludge treatment at high shares of energy-rich co-substrates using biomass retention by microfiltration. *In Proceedings: 15th IWA World Conference on Anaerobic Digestion "AD15"*, 17.-20.10.2017, Beijing, China.

5.1. Introduction

Industrial wastewater treatment is closely connected to production and is affected by daily or seasonal changes. This connection leads to variabilities in wastewater flow and characteristics (Cervantes *et al.*, 2006; Dereli *et al.* 2012; Dvorak *et al.*, 2015). Fluctuations in influent wastewater characteristics are usually dampened by equalising the flow (using buffer tanks) prior to the biological process (Sipma *et al.*, 2010). The buffer tank reduces shock loads but not seasonal variations in inflow composition and load (Sipma *et al.*, 2010). Consequently, spare capacity must be considered when designing industrial WWTPs (Cervantes *et al.*, 2006; Dereli *et al.* 2012; Dvorak *et al.*, 2015).

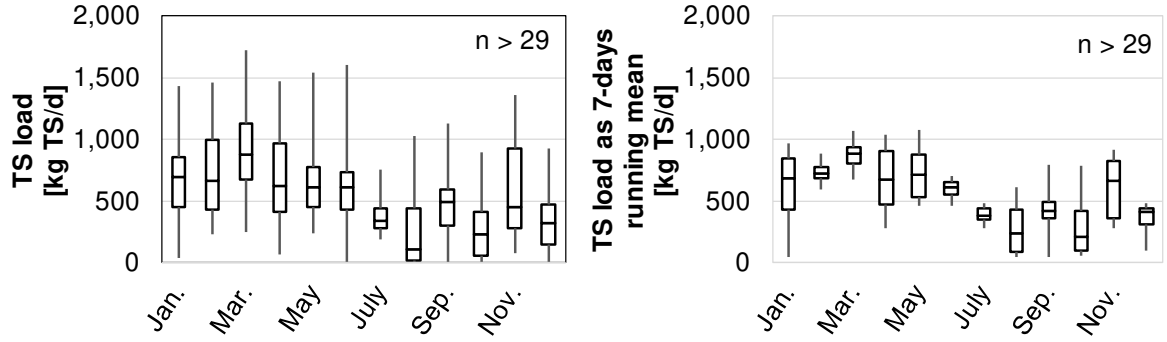

Figure 35. Variation of total solids (TS) load of flotation sludge as daily load (left) and as 7-day running mean (right) of a typical ice cream production facility

Fluctuation in wastewater composition also influences the corresponding sludge mass produced in individual processes of WWTPs (see overview of investigated example of a dairy WWTP in Figure 26 and variations of daily flotation sludge mass in Figure 35). Operators of on-site sludge digestion facilities face production-related variations in volume and substrate characteristics as well as high fractions of lipid-rich industrial sludge compared to WAS from aerobic processes on-site (Pereira *et al.*, 2005). Although buffer tanks for flotation sludge help to significantly reduce daily load fluctuations in sludge treatment, they do not provide full equalisation. Figure 35 (right) shows equalisation offered by a buffer tank with HRT = 7 d, expressed simply as 7-day running mean of TS load. In sludge treatment, CSTR with long HRT is commonly used. In practice, HRTs in buffer tanks will be shorter than 7 days in order to avoid necessary measures against odour due to starting degradation occurring in the buffer tank.

For process control, CSTR offers low adjustment options during operation. In practice, load changes remain the major option to counter fluctuation by keeping sludge load in a tolerable range. AnMBR additionally offers the possibility to adjust biomass concentration in the reactor

to counter load variations by decoupling SRT and HRT. Monitoring of AD processes is focused on methanogens, as operational problems mainly originate from insufficient conversion of the substrate into methane because of overload, washout of methanogens and inhibition (Henze *et al.*, 2002; Jimenez *et al.*, 2015). Typically measured variables to monitor AD processes are pH value, concentration of organic acids, alkalinity, biogas composition, methane yield and hydrogen concentration (Henze *et al.*, 2002; Olsson *et al.*, 2005; de Lemos Chernicharo, 2007; Alferes *et al.*, 2008; Kujawski and Steinmetz, 2009). However, these variables do not readily detect emerging inhibition of the methanogenic step (Olsson *et al.*, 2005; also see chapter 4). They only conclude on required adjustment of load or evaluate spare digester capacity in combination with empirical experience or model predictive control (e.g. based on ADM1). This requires extensive data acquisition and/or experience in operations under different process conditions. Using model predictive control needs even more fundamental knowledge about variation of microbial community, inhibition and its properties (e.g. growth rate, biomass yields and decay rates) as a result of changing process conditions (Olsson *et al.*, 2005). As an example, the variation of the apparent growth rate of acetoclastic methanogens in steady state as a result of changing share of flotation sludge was previously shown in chapter 4 (Figure 31). The consideration of all these interactions in model predictive controls is possible (e.g. Olsson *et al.*, 2005) but complex and requires a continuous adjustment with high measuring effort in practice.

Instead of using complex models or algorithms for process control, the use of advanced sensors in combination with simple process control mechanisms might be more promising. Assessment of biomass activity has been proven effective for evaluation of process stability and spare capacities against substrate overload (see section 4.3.2). Published experience is limited. Measurement focus is mainly the maximum activity of acetoclastic methanogens (SMA). SMA measurement is usually done off-line and well-established in batch tests (Angelidaki *et al.*, 2009). For process control, Siegrist *et al.* (2002) used SMA to evaluate process stability against substrate overload for sludge digestion of sewage sludge, Ince *et al.* (1995) for boosting the start-up of an AnMBR treating brewery wastewater and Monteggia (1991) for operation of UASB reactors. Garcia-Gen (2015) applied SMA for setting limits of maximum inflow concentration to sewage sludge digestion. Nevertheless, SMA is still not commonly used for monitoring AD processes.

This chapter assesses the potential of SMA as advanced sensor for a simple reliable process control loop of anaerobic sludge digestion facing load variations. Here, the sludge treatment of a production plant in the dairy industry serves as example (see description of WWTP and steady state results in Chapter 4). Findings related to pilot-scale digesters fed with WAS and lipid-rich flotation sludge are presented. Responses of common process control parameters to load changes are compared to that of SMA. Spare capacities for fluctuations in COD load are determined based on SMA.

5.2. Material and methods

5.2.1 Experimental setup

The experimental setups of the operated AnMBR and CSTR are given in Section 3.3.1.

5.2.2 Operating conditions

Data obtained from the operation of digesters with WAS and flotation sludge, introduced in Chapter 4, are used. While in Chapter 4 the focus was mostly on results in steady state, this chapter uses complete diurnal measured values from continuous operations. In this chapter, data relate to a CSTR operated at SRT = 10 d and an AnMBR operated at HRT = 10 d and SRT = 15 d. COD-related fractions of flotation sludge in feedstock mixtures range from 0 % to 90 %. Raw substrate and feedstock are given in Table 16, Table 18 and Table 17.

5.2.3 Sampling and assays

Sampling and assays correspond to procedures given in Sections 3.3.3 and 4.2.3.

5.3. Results and discussion

5.3.1 Responses of online process control variables to load changes

The Performance of CSTR operated at HRT = 10 d and responses of online process control variables to load fluctuations within the trial period are given in Figure 36. Figure 37 presents similar data regarding performance and response during AD using AnMBR at HRT = 10 d and SRT = 15 d.

In both reactors, loading rates of degradable COD were increased over time from 2 kg COD/(m^3·d) to over 12 kg COD/(m^3·d). The load increase resulted from escalating shares of flotation sludge. Higher organic load resulted in higher COD removal (Figure 36a and Figure 37a); this was because of better degradability of flotation sludge compared to WAS (see section 4.3.1, Table 18 and Figure 28). Sludge loading rates also changed over time. Starting with 0.1-0.2 kg COD/(kg VS·d), sludge loading rates reached up to 0.7 kg COD/(kg VS·d) (Figure 36a and Figure 37a). VS content in the reactor is determined by biomass growth and residual degradable and inert organic matter. Therefore, sludge load depends on loading and degradability. Lower VS content in the reactor resulted from higher degradability of a substrate (e.g., flotation sludge). Consequently, higher sludge loads were reached in the reactor at higher shares of flotation sludge. Because of sludge retention, AnMBR could be operated at lower sludge loading rates compared to CSTR at similar volumetric COD loading rate (see Figure 39).

During operation, digesters were confronted with strong variations of COD loading rates (sometimes >±100 %/d; Figure 36a and Figure 37a). Nevertheless, performance in terms of reduction of organic load remained largely stable over time. Significant process disturbances occurred in both reactors in the final 20 days of the test period. These major process disturbances were detected through increase in concentration of organic acids over 1,000 mg HAc/L (Figure 36b and 37b), followed by a drop in methane yield and methane content in biogas (Figure 36c and Figure 37c) and a slight decline in pH value in both reactors (Figure 36b and Figure 37b). Finally, COD removal in AnMBR came to a complete standstill.

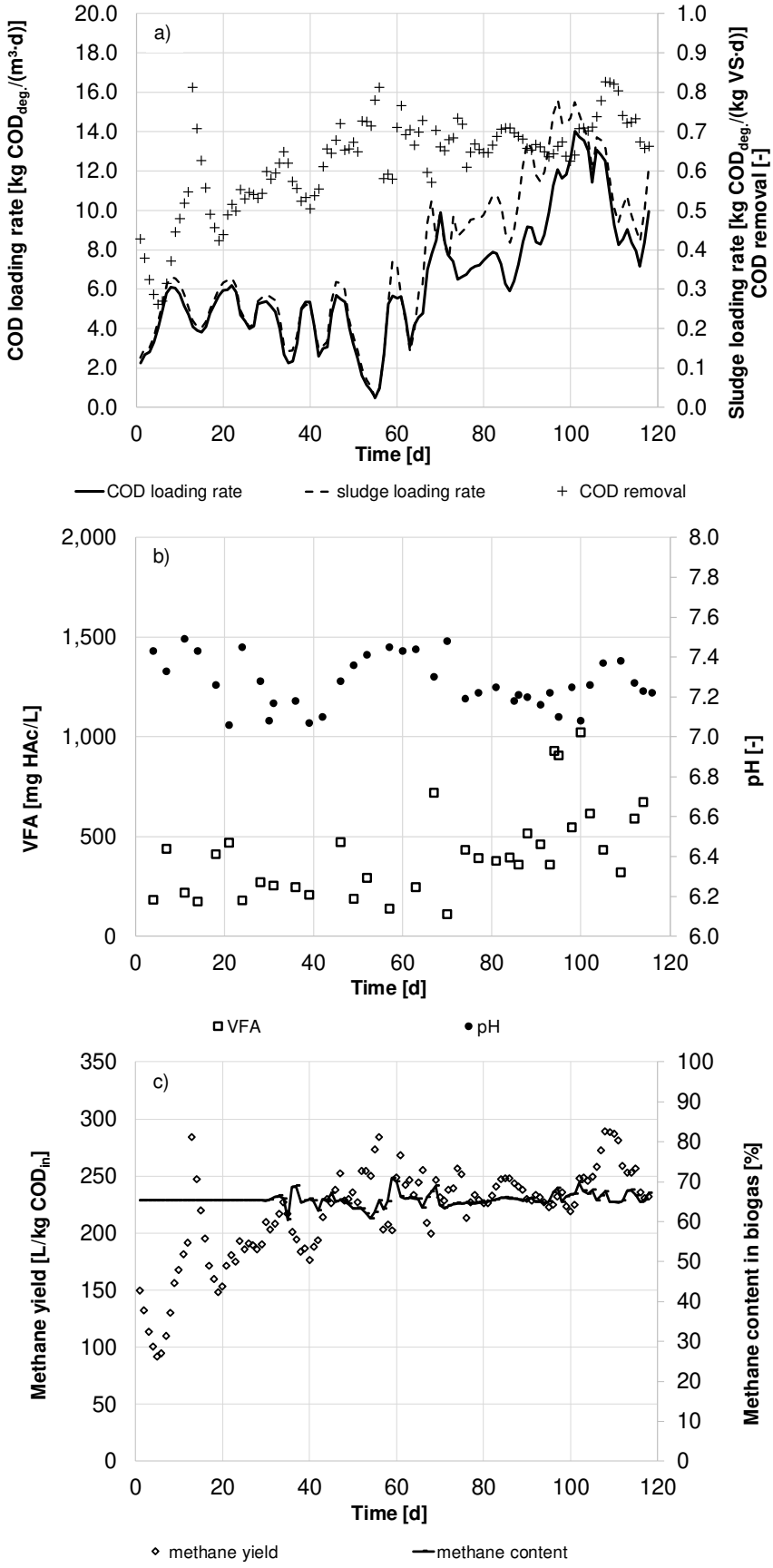

Figure 36. Performance (a) and response of process control variables (b, c) during anaerobic digestion using a CSTR with increasing shares of flotation sludge at HRT = SRT = 10 d

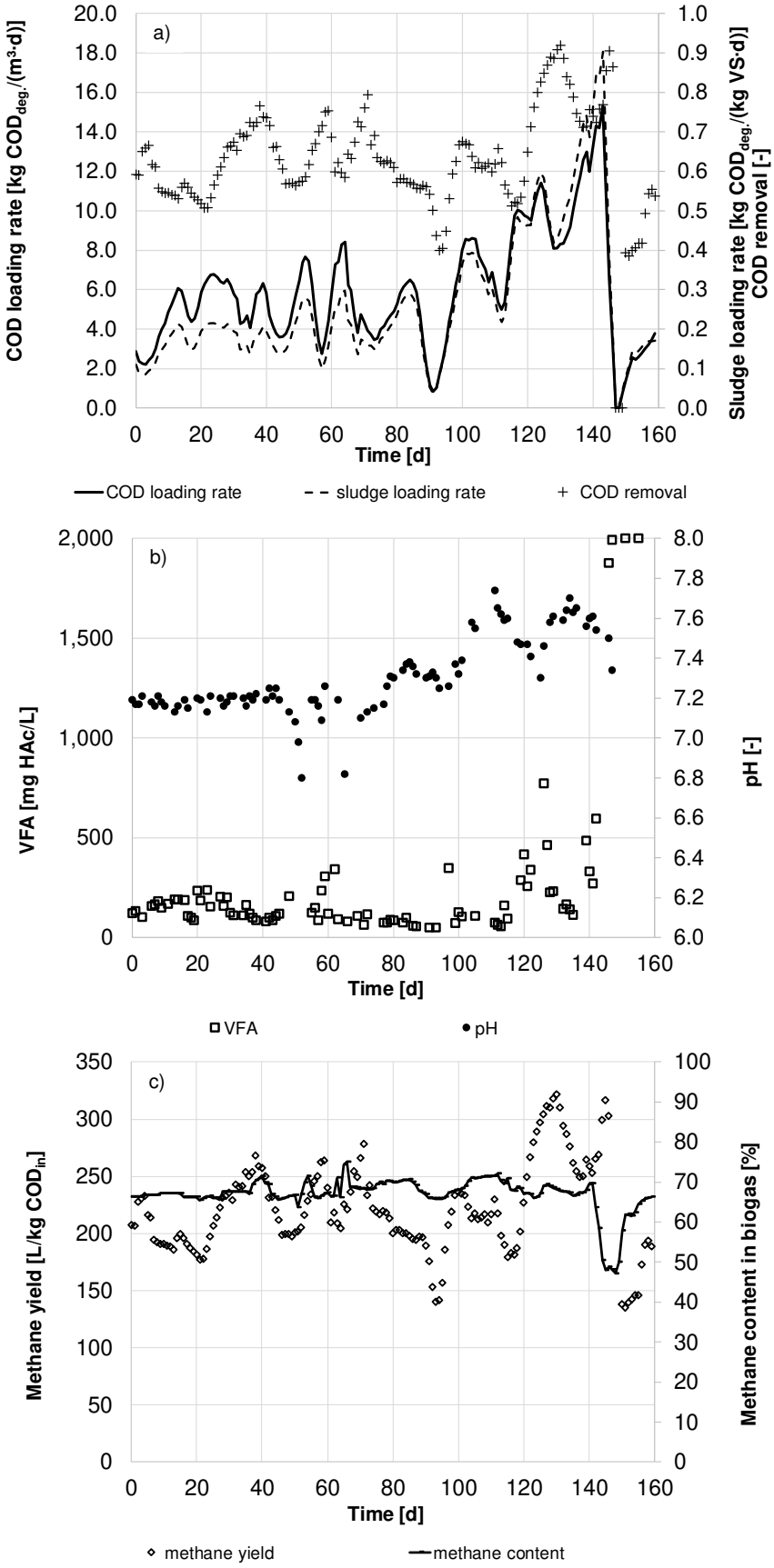

Figure 37. Performance (a) and response of process control variables (b, c) during anaerobic digestion conducted using AnMBR with increasing shares of flotation sludge at HRT = 10 d and SRT = 15 d

The concentration of organic acids seems basically applicable as a process control variable. In general, concentrations increase when acetoclastic methanogenesis replaces hydrolysis/disintegration as the rate-limiting step before a new equilibrium between the degradation rate of disintegration/hydrolysis and methanogenesis (steady state) is reached. In pilot trials, load increases over a longer period of time led to higher VFA concentrations and increased variations (especially from day 70 to 110 in CSTR operation (Figure 36b) and from day 110 to 140 in AnMBR operation (Figure 37b). Process instabilities were indicated by increases in organic acid concentrations, especially at concentrations above 1,000 mg HAc/L (Figure 36b and Figure 37b). Prior to these disturbances, the tendencies of organic acids to increase had already been observed. In the CSTR, beginning on day 70, the concentration of organic acids increased from 300 mg HAc/L to approx. 500 mg HAc/L. As feeding of the reactors was not changed, organic acid concentrations frequently rose from 500 mg HAc/L to over 1,000 mg HAc/L within one day (e.g. day 95; Figure 36). The observations of the AD process operated in AnMBR were similar. Starting at day 110, organic acid concentrations climbed from 100 mg HAc/L to 500 mg HAc/L. These outcomes agree with published findings of e.g. Olsson *et al.* (2005) that trends of VFA concentration show a good correlation with the state of the methanogenic step. However, a delayed response of VFA to load changes was obvious especially on day 140 of AnMBR operation. Although AnMBR loading was stopped at concentrations of 600 mg HAc/L, VFA concentrations continued to accumulate and rise to 2,000 mg HAc/L. This observation was mainly based on slow disintegration/hydrolysis of substrates that takes more than 24 hours for complete COD removal.

The pH value remained stable in both reactors over the test duration (Figure 36b and Figure 37b). Moreover, the buffer capacity in both reactors appeared to be sufficient over the entire period. The pH value was also subject to feedstock-related variations, and the state of the digestion could not always be accurately indicated, as already stated by Bischofsberger *et al.* (2005) and Olsson *et al.* (2005). Hence, the pH value is also unsuitable for process control in this application by controlling maximum tolerable organic loads to the reactors.

Methane yield was significantly affected by the degradability of the substrates used (see Table 1). The methane content was fairly stable over the entire period of trials (Figure 36c and Figure 37c). Current conditions of the AD process seem to be impossible to deduce. Increased loads first boosted methane production, and then substrate overload led to process failure with a corresponding lower methane yield and methane content; the same finding was reported by Nielsen *et al.* (2007) as well. Therefore, suitability of methane yield and methane content for process control in this application especially for the determination of possible maximum loads could not be confirmed by the results.

Based on the abovementioned trends of increasing VFA with increasing loads, an attempt shall be made to determine spare digester capacities on the basis of VFA for process control by a simple control loop in the following section 5.3.2. The sensors pH value, methane content and methane yield failed to show usability for evaluating spare organic loading capacities or even the current condition of the process.

5.3.2 Use of the volatile fatty acid concentration for a simple process control loop

A simple control loop for process control or determination of spare capacities consisting of VFA measurement as controlled variable and organic loading rate as manipulated variable requires a definite relationship between both variables. The relationship between VFA and both loading rates, COD loading rate and sludge loading rate, are investigated in more detail in the following paragraphs.

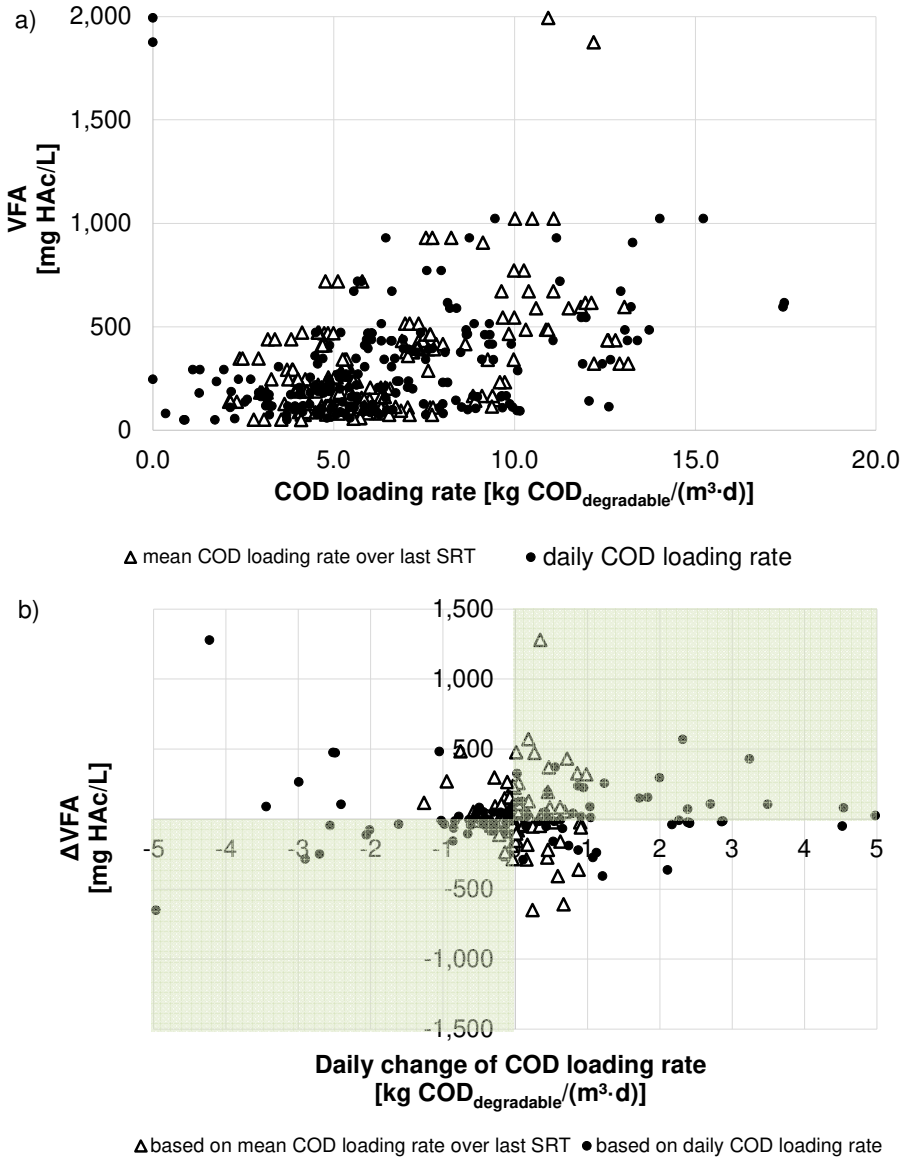

Figure 38. VFA concentration in the reactor in dependence of COD loading rate (a); changes of VFA as a function of changes of COD loading rate (expected range of values in green) (b)

The interaction between COD loading rate and organic acid concentration was monitored over duration of pilot trials by observing responses of VFA concentration to daily COD loading rates and running means of COD loading rates over one SRT (Figure 38a) and by observing changes in VFA concentration as response to changes in OLR (Figure 38b). COD loading rates based on running means were considered to account for observed delayed responses of VFA to load changes and to account for dilution effects when varying the feed.

Increasing COD loading rates cause higher organic acid concentration in the reactor (Figure 38a). VFA concentrations higher than 500 mg HAc/L only resulted from COD loading rates above 5 kg COD/(m³·d). Concentrations above 1,000 mg HAc/L only resulted from COD loading rates above 10 kg COD/(m³·d). However, a clear relationship between COD loading rate and the organic acid concentration was not observed, as a high distribution of concentration at similar COD loading rates was present. For example, a COD loading rate of 10 kg COD/(m³·d) resulted in a wide range of VFA concentration between 100-1,000 mg HAc/L in the reactor. These indistinct relationships between VFA and OLR were observed for both types of OLR: daily COD loading rate and mean COD loading rate over last SRT.

Similar findings were made regarding the relationship between the change in organic acid concentration in response to changes of COD loading rate instead of absolute values (Figure 38b). An increase of COD loading rate did not always result in an increase of organic acid concentration as expected. Higher load changes did not consequently result in higher changes of VFA concentrations compared to lower OLR changes. This is especially valid for dependencies of daily COD loading rate changes as load increases based on COD loading rate as running mean over last SRT are low (< 1 kg COD_{deg}/(m³·d)). This is in contrast to expectations that an increase in COD loading rate would always lead to an increase in the concentration of organic acids (green areas in Figure 38b); higher load changes would result in higher increases of VFA concentration.

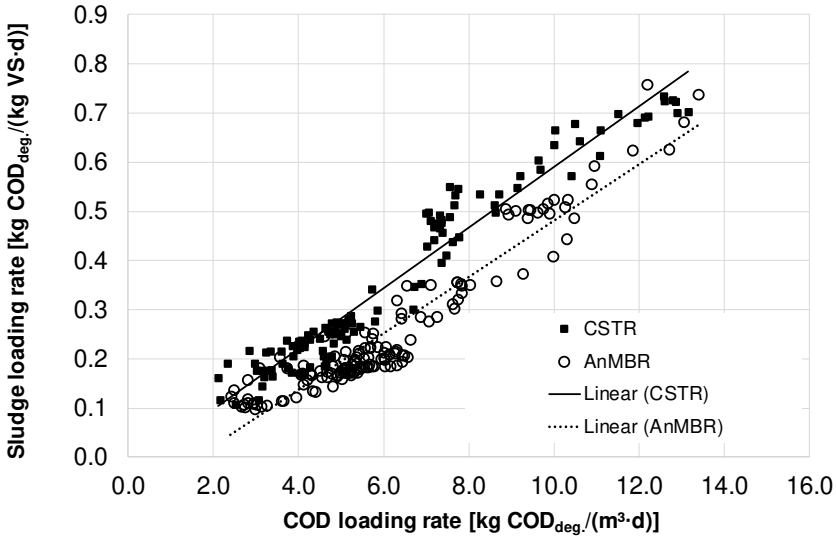

Figure 39. Comparison of CSTR and AnMBR in terms of COD and sludge loading rate

Consequently, observations did not follow an expected clear relationship between controlled and manipulated variable. Limits of load capacity based on a simple control loop consisting of organic acid concentration and the COD loading rate or its fluctuation could not be distinctly derived. The concentration of organic acids also did not provide a clear overload signal as basis for stopping feeding, since the process response was detected with a delay. Moreover, whether load changes occur at low or high COD loading rates seemed to make a difference. The biggest shortcoming in the considerations based on the COD loading rate is that the current state of the AD process and differences related to reactor configurations (AnMBR vs.

CSTR; see Figure 39) or rather existing biomass concentration in the reactor are not implemented. The use of the sludge load as manipulated variable instead seems theoretically more promising.

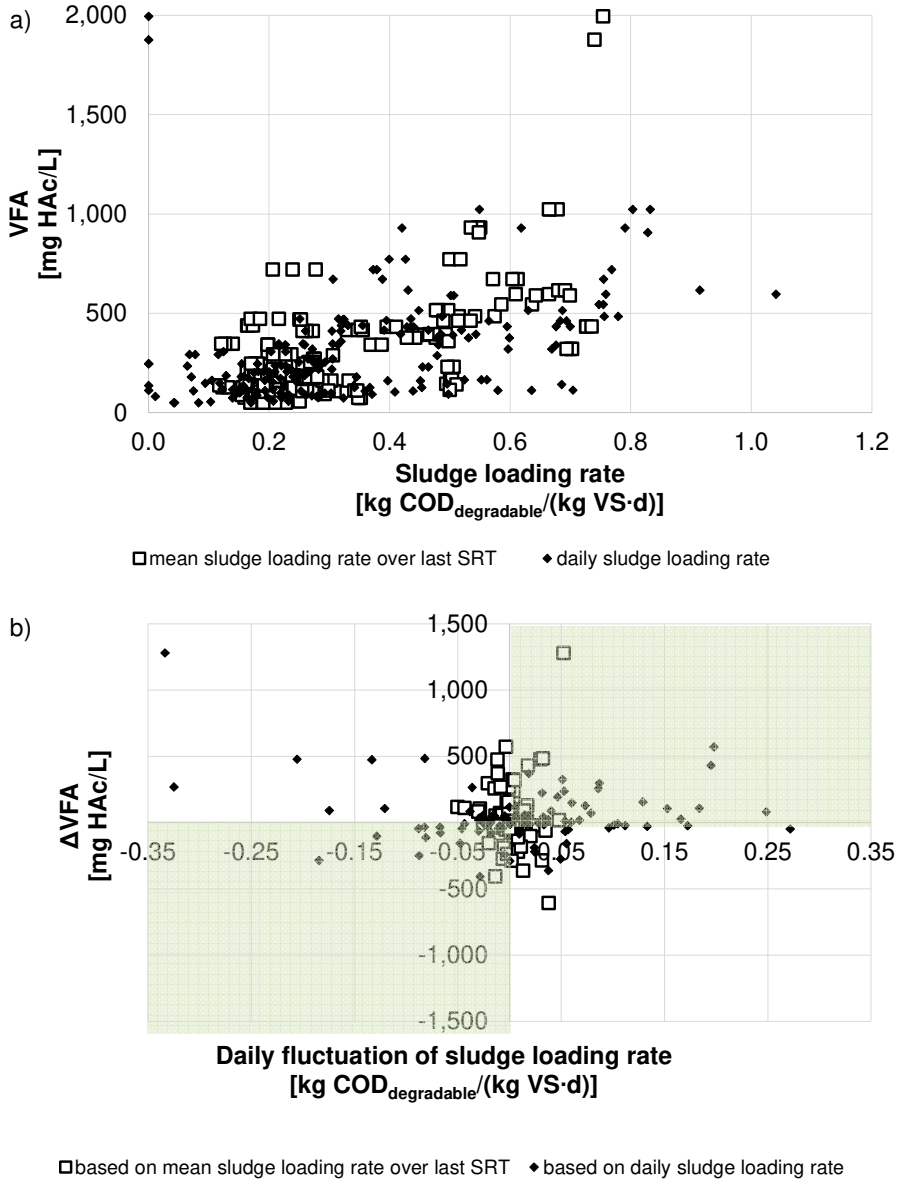

Figure 40. Concentration of VFA in the reactor in dependence of sludge loading rate (a); changes of VFA as a function of changes of sludge loading rate (expected range of values in green) (b)

VFA concentrations below 500 mg HAc/L and low variations in VFA concentration were observed at sludge loads based on running mean over last HRT below 0.5 kg COD_{deg}/(m^3·d) (Figure 40a). Sludge loads greater than 0.5 kg COD_{deg}/(kg VS·d) resulted in higher VFA concentrations and fluctuations indicating a change in process stability. Changes in sludge load did not result in a precise detectable change in concentration of organic acids (Figure 40b). Increases of sludge loads did not consequently affect an increase in VFA concentration. Same trends were observed in cases of decreasing sludge loading rates. A defined maximum tolerable load change could also not be derived from data. Most likely, the current state of the AD process or rather active existing biomass concentration and existing inhibitions in the reactor as well as delayed responses of the VFA concentration by the characteristic of the sludge

digestion limited a clear relationship between controlled (VFA) and manipulated variable (sludge loading rate).

The suitability of a simple control loop on the basis of the VFA concentration as controlled variable and the sludge loading rate as manipulated variable by calculating spare capacities is nonetheless investigated. For determination of spare capacities on the basis of VFA concentration, current state of acetate removing methanogenic step (or removal rate) must be compared to a defined maximum acetate removal rate under current conditions. The present removal rate can be theoretically derived from kinetics described by Monod kinetic (see expression 2.11 in section 2.1.2.2) taking into account the present VFA concentration in the reactor. The maximum acetate removal rate under current conditions can be defined on the basis of an acetic acid concentration of 1,000 mg HAc/L by assuming even active biomass concentration in the reactor compared to the current removal rate. The concentration was fixed at 1000 mg/L because at this concentration the removal rate is greater than 95 % of the theoretical maximum removal rate based on substrate concentration and the absence of inhibition on methanogens (Siegrist *et al.*, 2002; also see Table 2 and expression 2.11). For simplification, additional inhibitions are neglected in the following.

Spare capacities can thus be estimated as follows in a simplified manner:

$$Spare\ capacity = \left(1 - \frac{r_{vs,present}}{r_{vs,max}}\right) \cdot 100\% = \left(1 - \frac{\frac{\mu max}{Y_{max}} \cdot \frac{S_{present}}{S_{present}+K_S} \cdot X_{BM,methanogens}}{\frac{\mu max}{Y_{max}} \cdot \frac{S_{max}}{S_{max}+K_S} \cdot X_{BM,methanogens}}\right) \cdot 100\% \quad (5.1)$$

$$Spare\ capacity = \left(1 - \frac{\frac{S_{present}}{S_{present}+K_S}}{\frac{S_{max}}{S_{max}+K_S}}\right) \cdot 100\% \quad (5.2)$$

Where, Spare capacity is calculated in %

S: concentration of acetic acid (kg/m^3); S_{max} = 1,000 mg HAc/L

μ_{max}: maximum specific growth rate of biomass (g VSS/gVSS·d)

Y_{max}: maximum yield (g VSS/ g COD)

K_S: substrate half-saturation coefficient (kg/m^3)

$X_{BM,methanogens}$: methanogenic biomass concentration ($kg\ VSS/m^3$)

Lower acetic acid concentrations result in higher spare capacities of digester. In addition, the maximum tolerable sludge load can be simply calculated as long as no major changes on substrate composition (similar share over acetate path) and COD removal occur as follows:

$$B_{VS,COD,max} = B_{vs,COD,present} \cdot \left(\frac{1}{1 - \frac{Spare\ capacity}{100\%}}\right) \quad (5.3)$$

$$B_{VS,COD,max} = B_{vs,COD,present} \cdot \left(\frac{\frac{S_{max}}{S_{max}+K_S}}{\frac{S_{present}}{S_{present}+K_S}}\right) \quad (5.4)$$

Where, $B_{VS,COD}$: COD sludge loading rate (kg COD/(kg VS·d))

Theoretically, AD process remains stable as long as the new set sludge loading rate remains below the maximum tolerable sludge load

$$B_{VS,COD,new\ set} < B_{vs,COD,max} \quad (5.5)$$

In this study, however, neither acetic acid nor a complete acid spectrum was measured, but the concentration of volatile organic acids in total. For the calculation of spare digester capacities in this study, a concentration of acetic acid must be assumed. It was assumed that the relative acetate content of the total organic acids does not change and an acetic acid content of 90 % of the total VFA concentration is present as observed by Hubert et *al.* (2020) in a similar application (co-digestion of flotation sludge from the dairy industry with sewage sludge; $COD_{FS}/COD_{total} < 0.65$; SRT = 20 d). This is a strong but reasonable simplification as results discussed in the next section 5.3.3 (see Figure 42) show that the degradation rate at 1,000 mg HAc/L in the reactor corresponds to a degradation rate at 1,000 mg/L acetic acid in batch assays (SMA) using the same anaerobic sludge. Additionally, different substrate half-saturation coefficients of 40 mg/L and 213 mg/L were considered in this study (see Table 2). Responses of VFA concentration to present and maximum tolerable sludge loading rate over duration of pilot tests are given in Figure 41.

During operation of the CSTR and AnMBR with varying feeds, major process instabilities could be prevented as long as the sludge loading rate calculated as running mean over the duration of a SRT remained below the calculated maximum tolerable sludge loading rate. Individual exceedances of the daily sludge loading rate were compensated by the AD process and did not lead to a significant increase of the organic acid concentration. However, maximum tolerable sludge loading rate (and spare digester capacity) were significantly influenced by the half saturation constant and mean sludge loading rates over the last SRT. Maximum tolerable sludge loading rates strongly fluctuate each day. The dependency on the present sludge load and its changes seem too strong which is related to small changes in VFA concentrations and especially lack of changes in acetic acid concentration. Thereby, maximum tolerable sludge loading rates decreased when the reactor was not fed for several days (e.g. see day 96 of AnMBR operation). In these cases, the present sludge loading rate dropped more significantly than the concentration of organic acids. These findings contradict expectations that spare capacities must increase in case of reduced sludge loads and maximum tolerable sludge loading rates do not significantly change within 24 hours.

Further, half-saturation constant has a significant influence on the spare capacity of the anaerobic digester (Figure 41). Higher half saturation constants increase spare capacities and assessment of half-saturation constants should therefore be as accurate as possible.

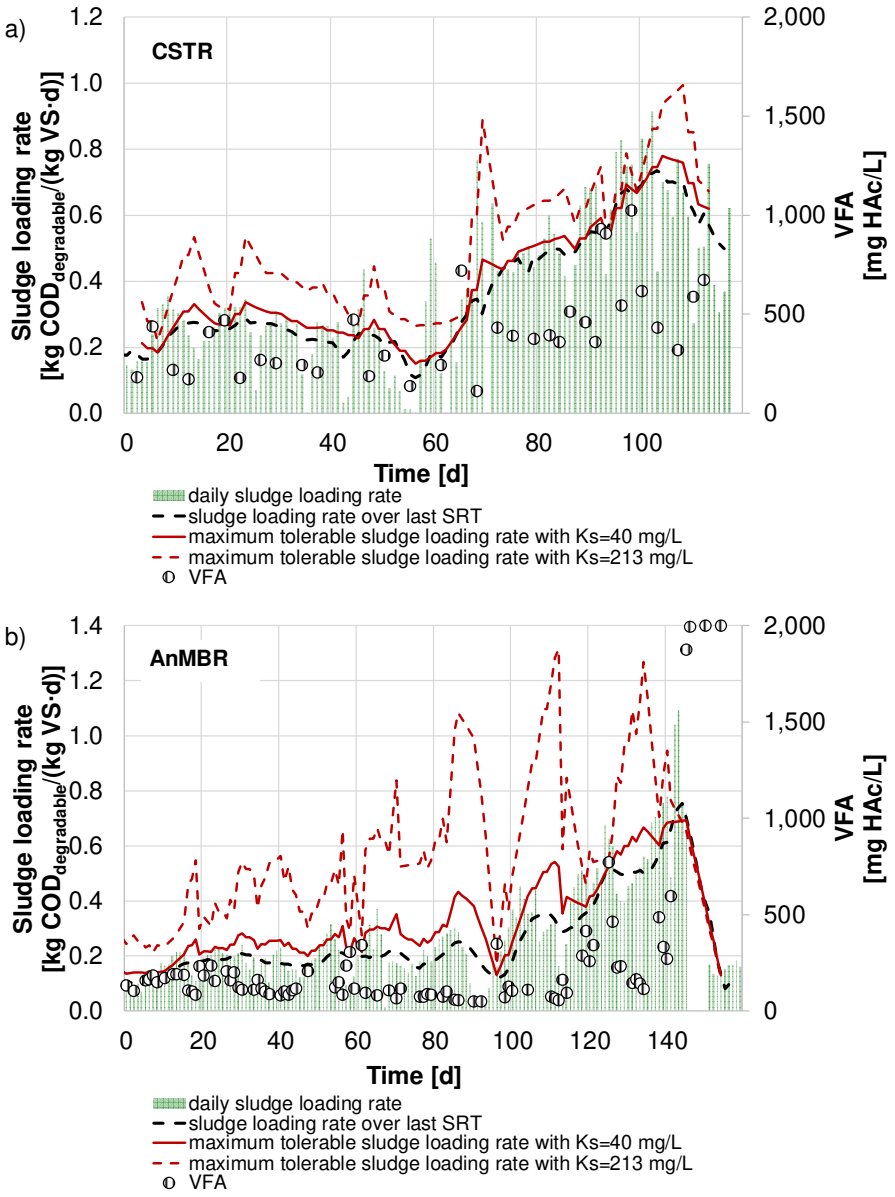

Figure 41. Present sludge loading rate and maximum tolerable sludge rate calculated on the basis of VFA concentration over duration of test of CSTR (a) and AnMBR (b)

In conclusion, this approach of a simple process control loop based on VFA concentration is limited. Possibly, this approach is more promising when acetic acid is measured and used as controlled variable instead of total VFA. Further, the half-saturation constant should be determined as precise as possible when using VFA for a process control loop. On the basis of existing data, above introduced approaches were not suitable to determine the current state of the AD process or biocenosis in the reactor.

5.3.3 Use of the SMA for a simple process control loop

In contrast to conventional process parameters, SMA explicitly describes the present condition of the methanogenic step in the reactor. Acetate-based SMA indicates the maximum possible acetoclastic COD turnover per mass of organic matter (=volatile solids; VS). It defines the maximum sludge-related COD removal rate (given as g COD/(g VS·d)) at acetate concentrations of 1,000 mg HAc/L (see Section 4.2.3) and captures present inhibitions.

Assuming that around 70 % of COD is degraded to methane via the acetate pathway (see Section 4.2.3), achieved COD removal rates and corresponding VFA concentrations in continuously fed reactors fit to predicted maximum COD removal rates measured as SMA in batch tests (Figure 42). VFA concentration in the reactors remained below 1,000 mg HAc/L as long as COD removal rates stayed below SMA. At VFA concentrations around 1,000 mg HAc/L, COD removal rates of pilot plant digesters match those measured in batch assays as SMA. VFA concentrations higher than 1,000 mg HAc/L were observed when COD removal rates in AnMBR exceeded SMA for a couple of days (see Figure 42b; day 130).

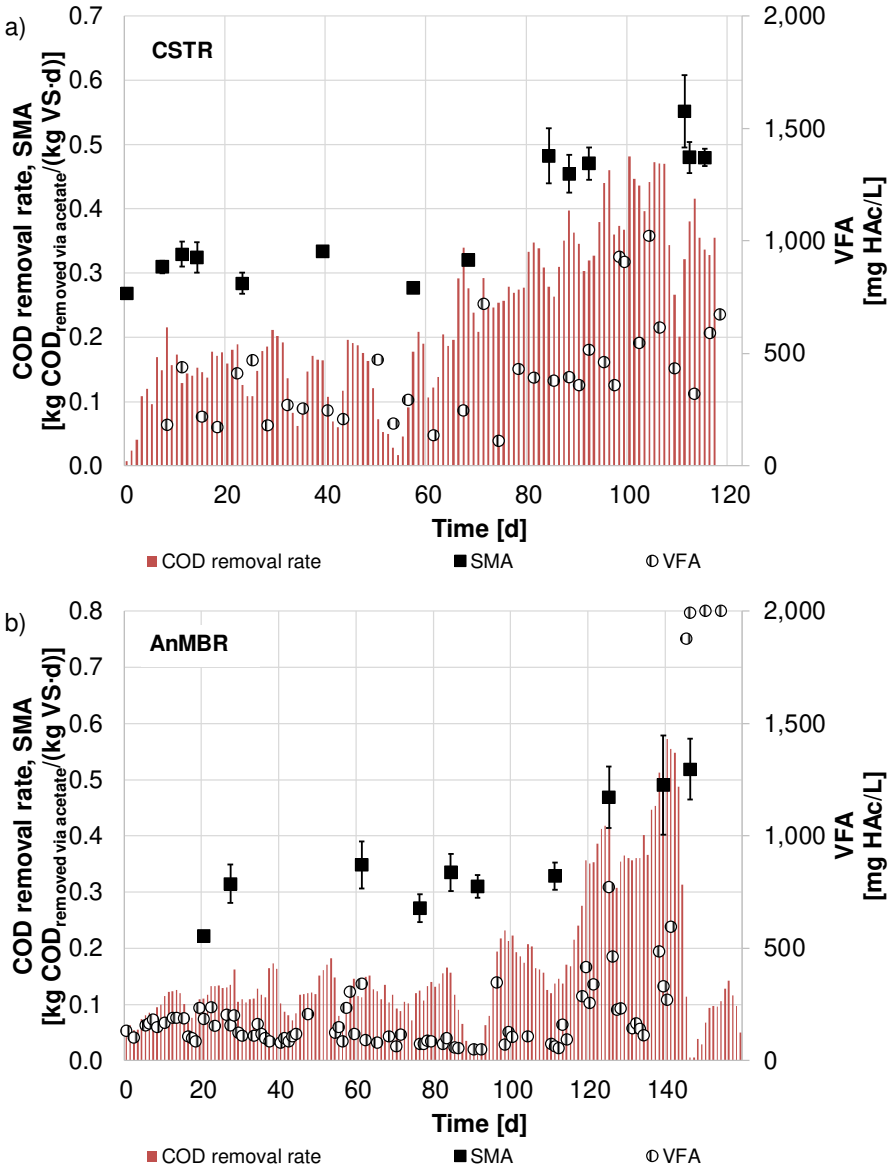

Figure 42. Comparison of COD removal rate in continuous-flow stirred-tank reactor (CSTR) (a) and anaerobic membrane reactor (AnMBR) (b) with specific methanogenic activity (SMA) and volatile fatty acids (VFA)

Consequently, SMA measurements seem to be generally suitable for determination of operational limits of anaerobic sludge digestion which is in accordance with results of other applications of AD of Monteggia (1991), Ince *et al.* (1995) and Garcia-Gen (2015).

Spare capacities can hence be determined by the ratio of present COD removal rate and the SMA as maximum tolerable COD removal rate as follows:

$$Spare\ capacity = \left(1 - \frac{COD\ removal\ rate}{SMA}\right) \cdot 100\% = \left(1 - \frac{n \cdot COD_{removed}}{SMA \cdot m_{VS,reactor}}\right) \cdot 100\% \qquad (5.6)$$

Where, $m_{VS,reactor}$: mass of volatile solids in the reactor (kg VS)

n: average COD conversion via acetate ~ 0.65 - 0.7

$COD_{removed}$: mass of COD removed per day (kg COD/d)

SMA: specific acetoclastic methanogenic activity (kg COD-CH_4/(kg VS·d))

Monteggio (1991) and Ince *et al.* (1995) were additionally able to use the ratio of daily sludge loading rate and SMA for process control, as used substrates were mainly degradable within one day. Sludge loading rate is connected with the COD removal rate as follows

$$COD\ removal\ rate = B_{vs} \cdot \eta_{COD} \qquad (5.7)$$

Where, B_{VS}: sludge loading rate (kg COD/(kg VS·d))

η_{COD}: COD removal (-)

The maximum tolerable COD removal rate corresponds to the SMA as previously shown in Figure 42. Consequently, the maximum tolerable sludge load can be defined on the basis of SMA as maximum COD removal rate and COD removal after SRT as follows

$$B_{vs,COD\ deg,max} = \frac{SMA}{n \cdot \eta_{COD,transient\ state}} \qquad (5.8)$$

Where, $B_{VS,COD\ deg,\ max}$: sludge loading rate based on degradable COD (kg COD_{deg}/(kg VS·d))

$\eta_{COD,\ transient\ state}$: COD removal in transient state (-)

In contrast to previous observations in the steady state, several subprocesses have to be considered for the determination of the COD removal in transient state. Besides disintegration, these are dilution effects due to load changes, intermediate accumulation of intermediate products (e.g. VFA) before the removal rate of e.g. methanogenesis is in equilibrium with the previous ones again. This can be simulated with hydraulic and known AD models (e.g. ADM 1), but requires high efforts in operation and many assumptions (see Introduction in section 5.1 and Olsson *et al.*, 2005). Theoretically, AD process should remain stable as long as a newly set sludge loading rate remains below the maximum tolerable sludge load which then represents the simple process control loop.

$$B_{VS,COD\ deg,new\ set} < B_{vs,COD\ deg,max} \qquad (5.9)$$

The general relationship between the sludge loading rate (daily sludge loading rate and a calculated mean over an interval of one SRT) and the SMA as decisive parameters of a simple control loop and the concentration of VFA for evaluating outcomes is shown in Figure 43. VFA concentration in the reactors remained below 1,000 mg HAc/L as long as acetoclastic sludge loading rates stayed below SMA. Major process disturbances indicated by VFA > 2,000 mg HAc/L and increasing variations in concentration occurred when the sludge loading rate over last SRT exceeded SMA, as was observed in the last 20 days of each trial.

Individual exceedances of the daily sludge loading rate could be partly compensated by the AD process as VFA concentrations mostly increased afterwards but did not lead to VFA concentrations above 1,000 mg HAc/L.

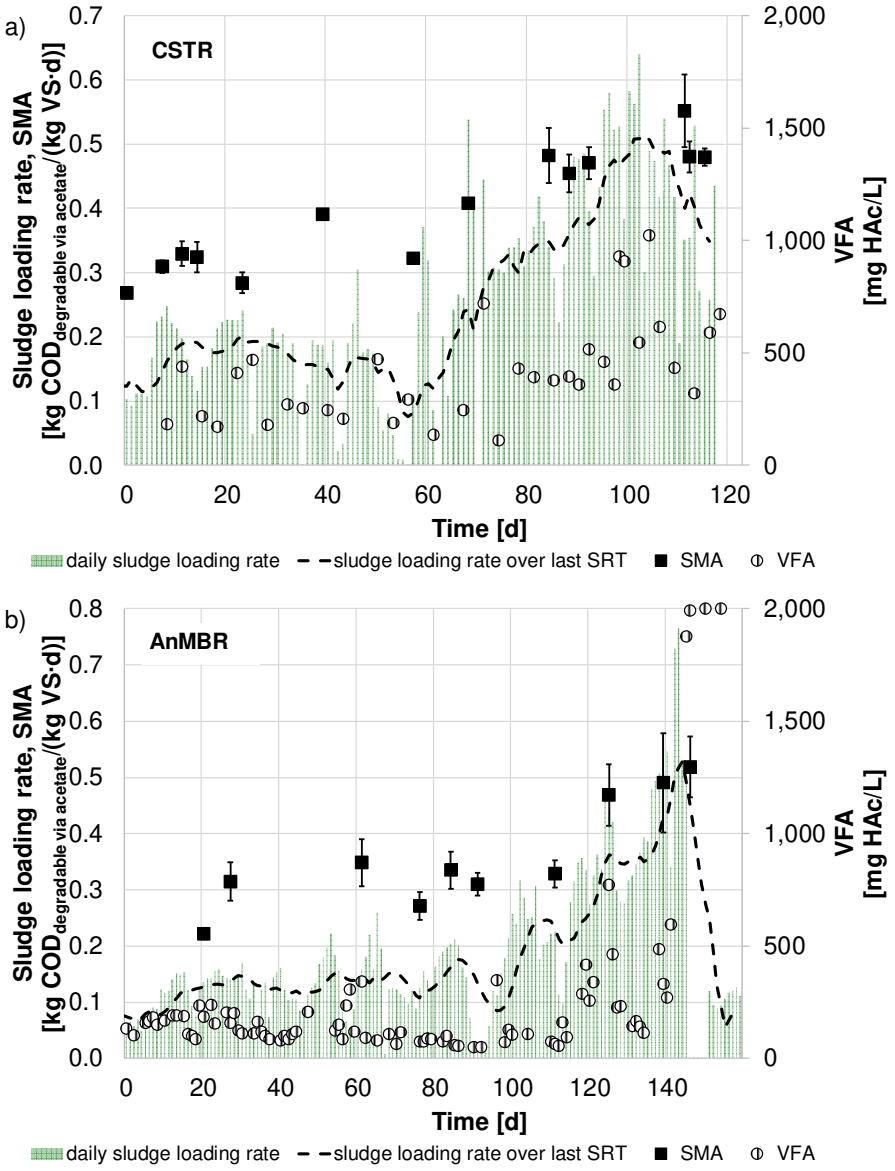

Figure 43. Process control based on sludge loading rate via acetate, specific methanogenic activity (SMA) and volatile fatty acids (VFA) in continuous-flow stirred-tank reactor (CSTR) (a) and anaerobic membrane reactor (AnMBR) (b)

In the context of this thesis a simplified process control loop is pursued to avoid the effort of comprehensive modelling for predicting the COD removal in transient state. The relationship between the sludge load and SMA is therefore extended by an empirical factor replacing the COD removal in transient state as follows

$$B_{vs,COD\ deg,max} = F \cdot \frac{SMA}{n} \qquad (5.10)$$

Where, $B_{VS,COD\ deg,\ max}$: sludge loading rate based on degradable COD (kg COD_{deg}/(kg VS·d))

F: empirical factor as substitution for COD removal in transient state (-)

To clearly assess the limits of sludge digestion, different intervals for calculating mean sludge loading rates were considered in terms of a precise response of VFA concentration for determination of the empirical factor F (Figure 44).

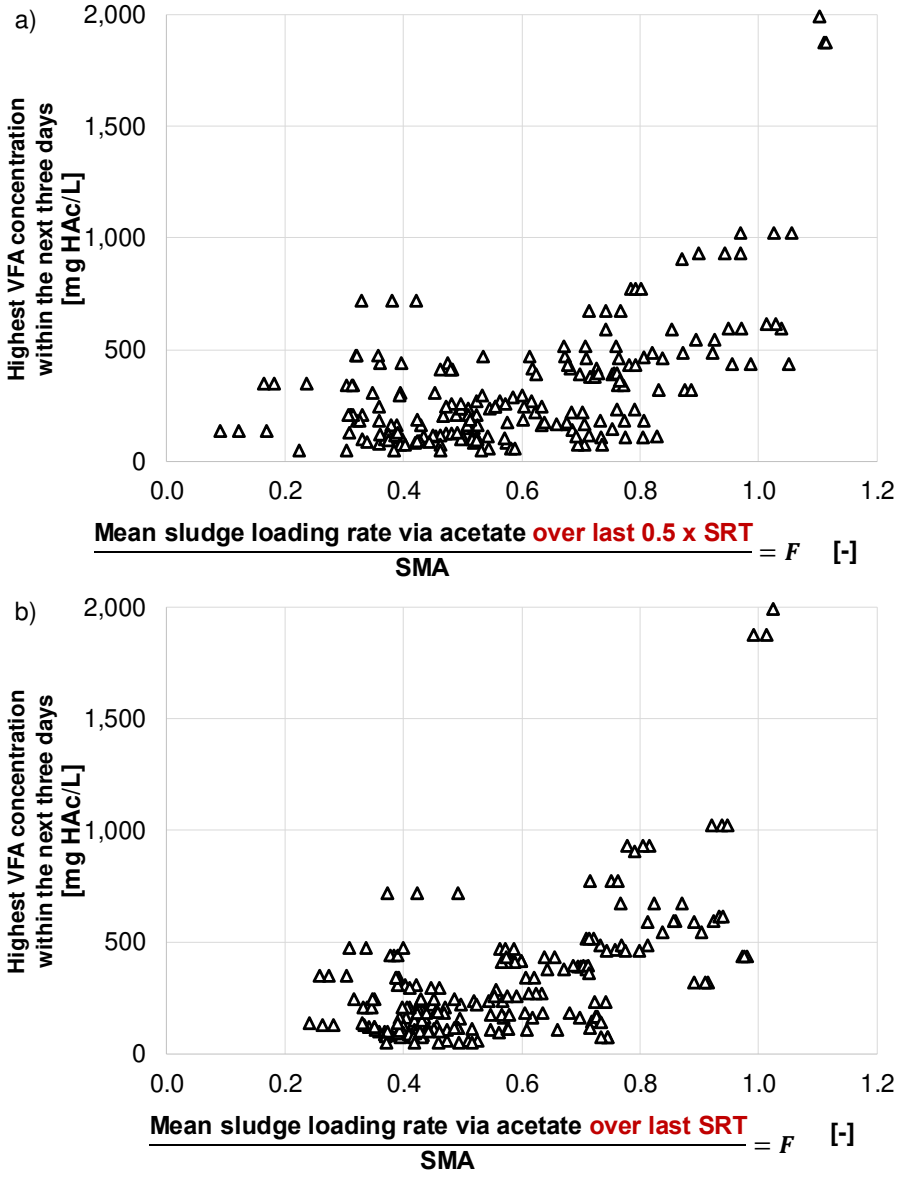

Figure 44. Organic acid concentration in the reactor as a function of the ratio of mean sludge loading rates based on various reference periods and SMA

For continuously operated anaerobic sludge digestion, it is useful to compare SMA with the mean acetoclastic sludge load of degradable COD based on last SRT (Figure 44b). At ratios B_{VS}/SMA below 0.8, organic acid concentrations always stayed below 1,000 mg HAc/L. Increase of this ratio above 0.8 resulted in accumulation of organic acids to/over 1,000 mg HAc/L and large VFA variations indicating process instability. Using 0.5·SRT as reference interval, sludge loading rate should not exceed the 0.9-fold of the SMA (Figure 44a). A one-time increase of the ratio of daily sludge loading rate to SMA to over 1.0 did not necessarily affect process stability and/or cause major increase of organic acid concentration (Figure 43) but multiple exceedances do. A one-time exceedance of the ratio of daily sludge loading rate to

SMA up to 1.5 did not necessarily affect process stability and/or cause major increase of organic acid concentration.

In conclusion, the following limitations could be identified for the investigated application treating lipid-rich flotation sludge and can be used for a simple control loop:

$$B_{VS,COD\ deg,new\ set} < F \cdot \frac{SMA}{n} \quad (5.11)$$

Where, $F < 1.5$ for one-time exceedances of daily sludge loading rate

$F < 0.9$ for short-term changes of mean sludge loading rate over interval of $0.5 \cdot SRT$

$F < 0.8$ for on-going changes of mean sludge loading rate over interval of $1.0 \cdot SRT$

5.4. Conclusions

Anaerobic sludge digestion plants can be stably operated even with high shares of flotation sludge and strong fluctuations in daily load. The decisive factor which determines process stability is the spare capacity of the AD reactor. The organic acid concentration and SMA are particularly suitable as process variables for process control. Methane yield, methane content in the biogas and pH value are just as unsuitable as fixed limits for load fluctuation of COD or sludge loading rate.

The suitability of SMA for a simple process control loop was demonstrated using the results of continuously operated reactors investigated in pilot scale. Assuming a degradation via acetate of organic matter of around 70 %, the concentration of VFA in the reactor remained below 1,000 mg HAc/L if mean acetoclastic sludge loading rates for last SRT were kept below SMA. Process disturbances (VFA > 2,000 mg HAc/L) occur when sludge loading rate exceeds SMA, as observed in the last days of each trial. A one-time exceedance of the ratio of daily sludge loading rate to SMA up to 1.5 did not necessarily affect process stability and/or cause major increase of organic acid concentration

The spare capacity for load variation of sludge digestion while maintaining sufficient process stability can only be determined using SMA as the key parameter. SMA indicates current maximum applicable COD removal rates in the reactor. Spare capacity of AD can be calculated simply using the reciprocal value of the ratio between the current COD removal rate and SMA. Based on SMA, the calculation of maximum tolerable fluctuation of sludge loading rate was additionally elaborated that could be used for a simple process control loop. This simple process control loop kept the AD process in a stable range. A more complex process control such as a digital twin based on complex models was not required.

6. Identification of sludge characteristics affecting the critical flux

This chapter is partly based on

Lutze, R., Engelhart, M. (2021). Effects of Sludge Characteristics on the Critical Flux of an AnMBR for Sludge Treatment Membrane digester for sludge treatment of municipal WWTPs - Benefits and drawbacks. *Chemie Ingenieur Technik*, volume 93, issue 9, 1375-1382, https://doi.org/10.1002/cite.202100025.

6.1. Introduction

The combination of membrane filtration and anaerobic processes for industrial and municipal wastewater treatment is well known and has been reviewed several times (e.g., Smith *et al.*, 2012; Ozgun *et al.*, 2013). However, key questions of mechanisms and minimization of fouling still remain open (Judd, 2006), but are decisive for economic viability of AnMBR (Smith *et al.*, 2012; Dereli *et al.*, 2014a; Ozgun *et al.*, 2013). Fouling induces an additional filter resistance (Smith *et al.*, 2012; Dereli *et al.*, 2014a; Ozgun *et al.*, 2013), which leads to decline in flux or necessary increase in driving force. At present, critical flux is a widely accepted method to characterise short-term membrane fouling (Le-Clech *et al.*, 2003; Fan *et al.,* 2006). Field *et al.* (1995) define critical flux as the highest flux without short-term fouling. Le-Clech *et al.* (2003) have shown that fouling also occurs in sub-critical flux operation; this fouling can be defined as long-term fouling. It is of minor importance for economic feasibility considerations, as its rate is 10-100 times lower than that of short-term fouling (Fan *et al.*, 2006; Drews, 2010). As short-term fouling significantly determines required membrane capacity and operating costs based on required TMP, critical flux can be used as a relevant design parameter. To integrate long-term fouling in the design on the basis of critical flux, a flux slightly lower than the critical value is chosen, which corresponds to approx. 60-80 % of the critical flux (Dagnew *et al.*, 2010; Judd, 2011; Dereli *et al.*, 2014a).

A lot of research concerning membrane fouling of AnMBRs treating mainly dissolved organic compounds is still being undertaken. Fouling is accelerated especially by increasing solids concentration (Liao *et al.*, 2006; Jeison and van Lier, 2008; Huang *et al.*, 2011), lower sizes of flocs (Huang *et al.*, 2011; Xiao *et al.*, 2015), increasing concentrations of colloidal matter (Choo and Lee, 1996), lack of divalent cations (Park et al, 2006) and higher concentrations of SMP or soluble EPS (Cho and Fane, 2002; Ahn *et al.*, 2006; Rosenberger *et al.*, 2006; Lin *et al.*, 2009). As fouling mechanisms are still too complex to be predicted accurately based on single parameters or their combination (Judd, 2006; Le-Clech *et al.*, 2006), researchers have started focusing on cumulative (sum) parameters such as viscosity, capillary suction time (CST) and specific resistance to filtration (SRF; Wang *et al.*, 2006; Pollice *et al.*, 2008; Laera *et al.*, 2009; Dereli *et al.*, 2014a; Dong *et al.*, 2016). However, the published results differ. Ersahin *et al.* (2014) successfully used SRF and CST to compare sludge filterability in AnMBR. Dereli *et al.* (2014a) could not detect any clear correlation between SRF or CST and fouling.

Shimizu *et al.* (1996) and Jørgensen *et al.* (2014) proposed empirical models to describe the limiting flux of aerobic MBRs based on the sludge concentration and shear stress. Both mainly

affect short-term fouling behavior, especially back transport. Proposed models describe dependencies on short-term fouling up to total solids concentrations of 12 g/L.

Application of AnMBR treating sludge differs from applications treating mostly soluble substrates. Main fractions in the anaerobic sludge are not active biomass but residual degradable and non-degradable particulate matter, which differ from aerobic MBR applications. Therefore, the validity of proposed empirical models by Shimizu *et al.* (1996) and Jørgensen *et al.* (2014) must be questioned regarding AnMBR. As the use of AnMBR for sludge treatment has not yet been investigated well, reported data regarding effects on critical flux (short-term fouling) are also limited. Increasing TS concentrations or lowering crossflow velocity/shear reduce membrane performance (Dagnew, 2010; Pileggi, 2016). Longer SRT (between SRT = 20-50 d and SRT = 15-30 d) increases the fouling potential in lab/pilot scale AnMBR (Dagnew, 2010; Dereli *et al.*, 2014a). Authors related these findings to a reduction of mean particle size of the digested sludge. Till date, the transferability of these results to other sludges have not been proven. There is also a lack of studies examining a variety of anaerobic sludges.

This chapter aims to identify key anaerobic sludge characteristics affecting critical flux (short-term fouling). Several sludges were investigated to find general key parameters and ensure transferability of results. Anaerobic sludge from digesters operated with different feedstocks, SRTs and scales was used. As key sludge characteristics, TS and VS concentrations, sum parameters such as the dynamic viscosity and CST and the applied shear rate on the membrane disc on critical flux were considered. Furthermore, an investigation was conducted on implementing an empirical model for predicting critical flux similar to proposed models for aerobic MBRs by Shimizu *et al.* (1996) and Jørgensen *et al.* (2014). Potentials for increasing critical flux are also elaborated in this chapter.

6.2. Material and Methods

6.2.1 Experimental setup

To determine critical flux, the membrane module of the pilot plant described in section 3.3.1 was used. The experimental setup included a mixing (feed) tank (as shown in Figure 45) whose contents were heated to T = 37 °C by a trace heating system. The working tank was initially filled with around 250 L sludge. The sludge was withdrawn from the feed tank with an eccentric screw pump at a flow rate of about 450 L/h, passed over the membrane unit and returned to the working tank. Flow rate was chosen based on a filtrate-to-feed-ratio of 1:10 to reduce effects of solid concentration in the filter. Volumetric flow of feed and filtrate were continuously measured using Proline Promag electromagnetic flowmeters (Endress and Hauser, Germany), and pressure in feed, concentrate and filtrate were continuously measured using Cerabar sensors (Endress and Hauser, Germany).

The membranes rotate with speeds ranging from 280 rpm to 350 rpm, which lead to crossflow velocities between 1.2-4.6 m s^{-1} at 280 rpm and between 1.5-5.7 m s^{-1} at 350 rpm as a function of the radius around the rotating shaft (see Table 10). The influence of the feed flow on the crossflow was neglected, as crossflow velocities below $1 \cdot 10^{-3}$ m s^{-1} are generated by the feed flow of 450 L h^{-1}. Characterisation of the used membranes is given in section 3.3.1 and annex A. A scheme of the membrane unit is given in Figure 17. The filtrate is withdrawn from the hollow shaft with an eccentric screw pump. Depending on experimental setup, filtrate is either

returned to the feed tank to maintain a constant TS concentration or discharged to increase TS concentration in the loop. Using additional automatic valves, the membrane can be back-washed periodically using the filtrate pump without changing its pumping direction. For a better overview, these valves are not shown in Figure 45.

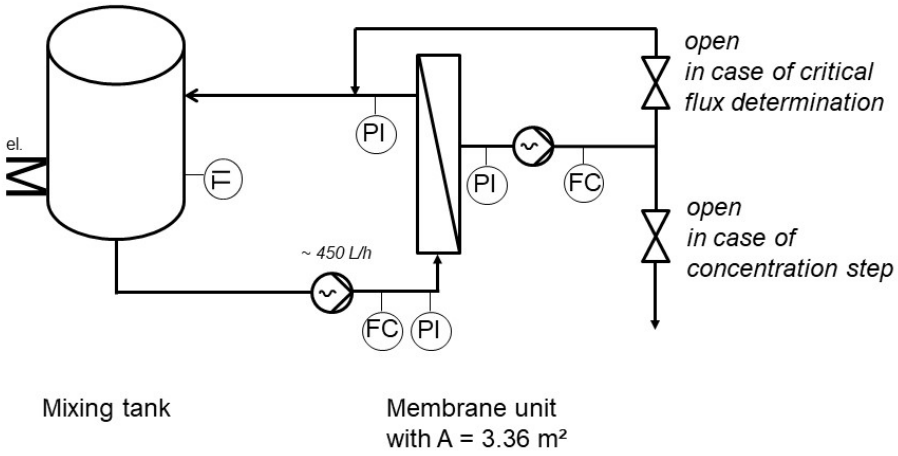

FC: Flow control, PI: Pressure indication, TI: Temperature indication

Figure 45. Simplified flow scheme of the experimental setup for critical flux investigation

6.2.2 Experimental Conditions

Sludge characteristics

Table 20 gives an overview of used sludge samples and results of sludge characterisation. All sludges were taken from digesters treating mainly municipal sewage sludge. Sludge samples from large-scale facilities are denoted LS and those from pilot-scale digesters are denoted PS. Different facilities are described by numbers ranging from 1-5. LS_2a and LS_2b were taken from the same facility but from different digesters, which were operated at different SRTs.

PS_1 and LS_1 were fed with WAS from the same municipal WWTP. PS_5 refers to anaerobic sludge from a digester fed with a mixture of flotation sludge (FS) and WAS (V_{FS}:V_{total} = 0.3; see Chapter 4). All sludge samples were taken from digesters with SRT ≥ 20 d.

Solids concentration in the reactors and sludge samples, organic share, dynamic viscosity and CST varied significantly between the samples (see Table 20). Despite different substrate compositions, three out of four digested sludges showed a similar average particle size. Sludge samples with lowest mean particle size originated from a digester operated without dosages of Fe salts to the digester. Fe salts are often used for coagulation to enhance dewatering or precipitation of H_2S in the digesters. Analyses of particle size distribution contradict findings of Houghton and Stephenson (2002), who observed larger particle diameters with increasing shares of WAS. All sludge samples were sampled at least three times on the day of the critical flux tests.

Table 20. Digested sludge characteristics used for critical flux investigations (mean±std.dev.)

Parameter	Anaerobic sludge from large-scale digesters of municipal WWTPs						
	LS_1	LS_2a	LS_2b	LS_3	LS_4	PS_1	PS_5
number of samples n [-]	12	9	9	12	9	12	12
Substrate of digestion	WAS	WAS+PrS	WAS+PrS	WAS+PrS	WAS+PrS	WAS	WAS+ FS
Supplements	+Fe-salts	+Fe-salts	+Fe-salts	none	+Fe-salts	none	none
SRT in digester [d]	30-40	~20	>30	>25	>25	~ 25	~ 20
TS [%]	2.1±0.0	2.2±0.1	2.2±0.1	3.4±0.1	2.8±0.1	2.4±0.1	2.1±0.2
VS [%]	1.4±0.1	1.5±0.0	1.4±0.0	2.0±0.0	1,7±0.1	1.5±0.0	1.5±0.1
COD/VS [g/g]	1.5±0.1	1.5±0.1	1.5±0.1	1.5±0.1	1.5±0.1	1.5±0.1	1.7±0.1
std. apparent viscosity[a] [mPa·s]	10.2±0.1	11.4±0.6	10.6±0.9	18.9±1.3	17.5±2.1	11.2±0.9	11.4±2.1
CST [s]	62±23	148±8	111±6	235±8	373±24	284±3	382±323
$COD_{supernatant}$[b] [mg/L]	460±81	780±10	838±11	1,037±210	1,441±308	1,072±96	1,500±250
$COD_{filtrate}$ [mg/L]	191±23	250±10	263±10	386±94	411±23	347±77	250±30
PO_4-$P_{filtrate}$ [mg/L]	67±3	n.d.	n.d.	103±15	47±1	132±6	62±10
Particle size distribution [µm]							
d10	19.7±0.7	18.2±0.2	17.6±0.4	12.1±0.2	18.3±0.4	20.4±0.2	23.5±3.3
d50	52.6±1.5	56.3±1.0	56.1±1.5	38.8±1.4	53.5±1.7	52.7±0.4	56.0±6.2
d90	111.6±8.0	135.8±4.3	137.9±9.0	107.3±17.2	139.6±19.0	111.5±4.1	118.1±8.6

[a] Standard condition with shear rate = 500 s^{-1} and T = 20°C were applied according to Moshage (2004);

[b] measured in supernatant after centrifugation at 3,500 rpm for 10 minutes (Hettich Universal, Germany);

Experimental procedure

Tests focused on determining critical flux. Before starting a critical flux test with sludge, TMPs while filtrating tap water were identified at filtrate flows of 7.5, 25, 50 L/h to exclude significant membrane blocking and ensure comparability of the experiments. These filtrate fluxes were chosen to appropriately cover the range studied. After this water test, the mixing tank, membrane module and all pipes were drained and replenished with digested sludge. The critical flux was then determined using the improved flux-step method described in Section 6.2.3. After determining the critical flux in the original sample, the critical flux at elevated solids concentration was determined by gradually discharging permeate from the loop. As a rule, the critical flux was investigated at four different TS concentrations within one day. Every test was performed at a rotational speed of 320 rpm as standard setting. Ultimately, the highest TS was investigated with 280 and 350 rpm as well. Each sludge sample was examined only once, but at least three samples from the same digester were taken. Finally, the pilot plant was rinsed with water, a water test was conducted and, if required, chemical cleaning was initiated.

The effects of dosage of iron salts were tested separately by adding different dosages to the original sample of sludge from WWTP #3 (LS_3). The overall experimental procedure was the same in each case.

During the tests, shear effects on particulates remained low, as the median of particle size d50 changed below ± 5 % when comparing first and last run.

6.2.3 Sampling and assays

Sludge samples were analysed for TS, VS and COD in the filtrate and supernatant, apparent dynamic viscosity, CST and particle size distribution. TS, VS and COD were analysed according to the standard procedures given in Table 12. Before analysing the COD in the supernatant, the sludge sample (feed) was centrifuged at 3,500 rpm for 10 minutes (Hettich Universal, Germany). Analysis methods for CST, apparent dynamic viscosity and particle size distribution are given in the following paragraphs. Data regarding sludge characterization of used sludge samples are summarised in Table A 6 of the annex.

Improved flux step-method for determination of critical flux

The critical flux was determined using the improved flux-step method proposed by van der Marel *et al.* (2009). The permeate flux was gradually increased in small steps (~ 1-2 L/(m²·h)). For each flux, an identical cycle was performed, where each cycle comprised filtration, degassing and backwash and a relaxation step before the start of the next flux step (see Figure 46).

The duration of the filtration step was set based on requirements for degassing and lasted for 8 minutes. Degassing is required because of accumulation of gas bubbles on the rotating discs/shaft which builds up a gas blanket on membrane surface near the hollow shaft and interferes with filtration. Build-up happens because centrifugal forces cause the solids to migrate to the outer wall of the filter housing, whereas biogas bubbles migrate towards the shaft. Therefore, the degassing phase without rotation of membranes was required regularly, to let gas bubbles ascend to the upper part of the horizontal filter housing and let them be rinsed from the filter with the concentrate flow. An integrated backwash, which is mandatory in long-term operation, reduces the cover layer on the membrane. To achieve satisfactory cake layer

reduction, the selected backflush duration was kept high (results are given in the annex D) when filtrating above the critical flux. Combined degassing and backwashing phase lasted for 30 seconds without membrane rotation. The relaxation step describes a filtration phase with low flux of 2.5 L m^{-2} h^{-1} in which reversible fouling is removed and the fouling layer is further reduced before setting a new flux stage. The relaxation phase took around 2 minutes.

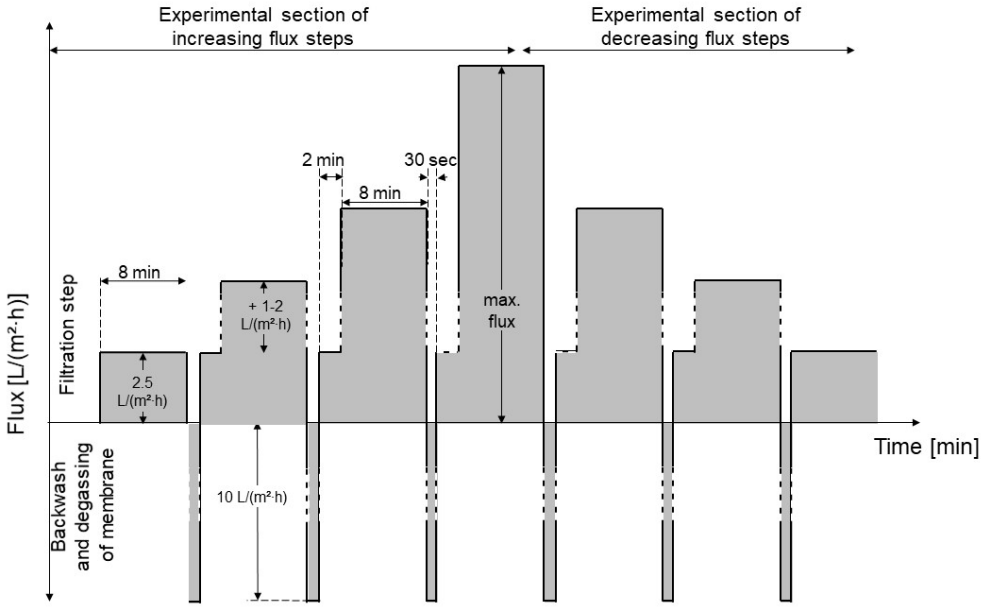

Figure 46. Applied flux-step method

During the filtration step, TMP increased over time based on cake layer formation. Afterwards, the critical flux was defined based on a method that evaluates the transition between the TMP-dependent and TMP-independent flux to assess short-term fouling potential. According to Field *et al.* (1995), it can be calculated as

$$\frac{\Delta TMP}{\Delta J} = \frac{TMP_{end\ of\ filtration\ phase\ of\ flux\ step\ n} - TMP_{end\ of\ filtration\ phase\ of\ previous\ flux\ step\ n-1}}{J_{flux\ step\ n} - J_{previous\ flux\ step\ n-1}}$$

By comparing TMP at the end of the filtration phase and the flux of a setting (flux step) with values from the previous flux step, it is possible to estimate whether the increase continues to be linear (=permeability remains constant; also see example in Figure 14). The critical flux is reached in case of a deviation of TMP increase over flux from this linearity (=reduction of permeability). In this study it was defined that this is achieved when the slope from around 10-12 (mbar·m²·h)/L has doubled at the next flux step to slopes above 25 (mbar·m²·h)/L. TMP_{end} was chosen as a significant parameter, as it is less dependent on selected duration of the filtration step, step height or defined P_{init} than other criteria (see explanation on critical flux in Section 2.2.3).

Apparent (dynamic) viscosity

Apparent (dynamic) viscosity was measured according to DIN 53019-1 (2008) by using a rotational viscometer (Rheomat R180, proRheo GmbH, Germany). The rotational viscometer functions according to the Searle principle, with the measuring fluid present in the annular gap

(constant gap) between an inner rotating and an outer fixed cylinder. Furthermore, the measuring system 11 was used (proRheo GmbH, Germany), which consists of a cylinder with an internal diameter of 32.54 mm and a measuring body width of 30 mm. The sample volume was 24 ± 1 ml. Flow curves were measured at ambient temperatures of around 20 ± 2°C. The measuring procedure was based on the method proposed by Moshage (2004). Each sludge was measured at least three times with four different shear rates in an ascending and descending ramp (80 s^{-1}, 220 s^{-1}, 360 s^{-1} and 500 s^{-1}). Each shear rate was measured for 45 seconds. Thus, each sludge had six pairs of shear stress values and a corresponding shear rate (in total 6x4 = 24 pairs of values).

As anaerobic sludge is a non-Newtonian fluid (e.g. Moshage, 2004), shear stress and dynamic viscosity depend on the shear rate. In case of the flow curve, shear stress τ is shown as a function of the shear rate $\dot{\gamma}$. For anaerobic sludge with a TS lower than 4.5 %, the flow curve can be described according to the law of Ostwald de Waele as follows (Chen, 1986):

$$\tau = K \cdot \dot{\gamma}^n \qquad (6.1)$$

Where, τ: shear stress (Pa)

K: fluid consistency factor $(Pa \cdot s)^n$

$\dot{\gamma}$: shear rate $(1/s)$

n: flow behaviour index (-)

Fluid consistency factor K and flow behaviour index n were read from the flow curve graph of shear stress vs shear rate based on potential approximation of the abovementioned measuring data (see example given in Figure 47).

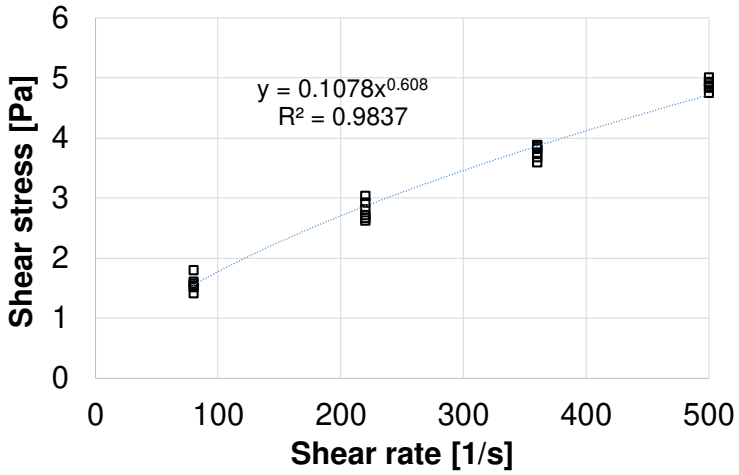

Figure 47. Example of a flow curve (shear stress over shear rate) for calculation of fluid consistency factor and flow behaviour index (sludge from WWTP 1 with a TS = 2.1 %)

Apparent viscosity, so called based on its dependency on corresponding shear rate, can be calculated as follows:

$$\eta_a = \frac{\tau}{\dot{\gamma}} = K \cdot \dot{\gamma}^{n-1} \qquad (6.2)$$

Where, η_a: apparent viscosity (Pa·s)

τ: shear stress (Pa)

K: fluid consistency factor (Pa·s)^n

$\dot{\gamma}$: shear rate (1/s)

n: flow behaviour index (-)

Conversion of apparent viscosity from 20 °C to 37 °C was based on the approach of Moshage (2004); this was further confirmed by own investigations within this study (see Figure A 4 in the annex).

Determination of area-weighted shear rate on a rotating membrane disc $\dot{\gamma}_m$

To evaluate the effect of apparent viscosity on filtration performance, the present shear on the rotating membrane disc must be considered. The relevant shear (or rather cross-flow) depends significantly on the rotational speed of the membrane and not on the flow rate by circulation of the sludge over the membrane module (Torras *et al.*, 2009; Bentzen *et al.*, 2012). According to Jørgensen *et al.* (2014), the area-weighted shear rate $\dot{\gamma}_m$ on the surface of a flat rotating membrane disc for laminar flow can be calculated as

$$\dot{\gamma}_m = 0.5133 \cdot \left(\frac{\eta_a}{\rho_s}\right)^{-0.5} \cdot (k \cdot \omega)^{1.5} \cdot \frac{r_o^3 - r_i^3}{r_o^2 - r_i^2} \qquad (6.3)$$

Where, $\dot{\gamma}_m$: shear rate on a rotating membrane disc (1/s)

η_a: apparent viscosity (Pa·s)

ρ_s: sludge density (kg/m^3); calculated according to Pileggi (2016)

k: velocity factor (-); = 0.42 (Ding et al., 2002)

ω: angular velocity (rad/s)

r_o: outer radius of membrane; = 0.156 m

r_i: inner radius of membrane; = 0.046 m

By using the abovementioned equation for apparent viscosity (expression 6.2), the shear rate can be rewritten as

$$\dot{\gamma}_m{}^{0.5n+0.5} = 0.5133 \cdot \left(\frac{K}{\rho_s}\right)^{-0.5} \cdot (k \cdot \omega)^{1.5} \cdot \frac{r_o^3 - r_i^3}{r_o^2 - r_i^2}$$

or

$$\dot{\gamma}_m = \left[0.5133 \cdot \left(\frac{K}{\rho_s}\right)^{-0.5} \cdot (k \cdot \omega)^{1.5} \cdot \frac{r_o^3 - r_i^3}{r_o^2 - r_i^2}\right]^{\frac{1}{0.5n+0.5}} \qquad (6.4)$$

Sludge density was calculated according to Pileggi (2016), using the following equation:

$$\rho_s = \frac{100 \cdot \rho_w \cdot \rho_{dry\ sludge}}{100 \cdot \rho_{dry\ sludge} + TS \cdot (\rho_w - \rho_{dry\ sludge})} \quad (6.5)$$

Where, ρ_s: sludge density (kg/m^3)

ρ_w: water density (kg/m^3)

$\rho_{dry\ sludge}$: density of dried sludge; = 2,400 kg/m^3

TS: TS concentration of the sludge (%)

After determining the area-weighted shear rate on the membrane surface (equation 6.4), present viscosity of the sludge on the membrane surface can be calculated using equation 6.2. The present viscosity of the sludge on the membrane surface is used to calculate Reynolds number at area-weighted mean radius of the membrane (r=0.113 m). If $Re < 4.5 \cdot 10^4$ (Jørgensen *et al.*, 2014), the flow is laminar and the abovementioned equation can be used to calculate the relevant shear rate on a rotating membrane disc. The radial Reynolds number is determined from the following equation (with k = 0.42 (Ding *et al.*, 2002) and ω at outer radius of membrane)

$$Re = \frac{k \cdot \omega \cdot r^2 \cdot \rho_s}{\eta} \quad (6.6)$$

Capillary suction time (CST)

Determination of CST was carried out according to DIN EN 14701-1 (2006). To homogenise the sample, it was poured four times using two 50 ml measuring cups. The sludge was then placed in a cylinder mounted on a filter paper (CST paper, HeGo Biotec GmbH, Germany). This cylinder has an inner diameter of 18 mm and a height of 25 mm. Measurement of flow time requires an emerging waterfront in the filter paper to cover the distance defined by two measurement points. Before usage, the filter paper was dried in a drying chamber at 105 °C for at least 20 minutes and then cooled down to ambient temperature in an exsiccator. CST measurements were done at least five times at an ambient temperature of around 20 ± 2 °C.

Particle size distribution

Particle size analysis was carried out using the Malvern Mastersizer 3000 (stirrer speed = 500; pump speed = 500; ultrasonic = off). Before analysis (three sludge samples were analysed; each 10 times), each sample was analysed in a dilution of approximately 500 fold in distilled water. Results were recorded as particle volume percent in 70 discrete size ranges between 0.45 and 2,000 µm (volume-related particle size distribution).

Statistical assessment

The dependence of the critical flux on influencing variables (e.g. TS, VS,...) was assessed using the Spearman rank correlation coefficient. This test can be used for assessing correlation of two variables X and Y which must not be in a linear relationship or normally distributed around the mean value of each data set (Walpole *et al.*, 2002). The requirement of the test is

that for the random variables X and Y a sample of pairs (X_1,Y_1), . . . , (X_n,Y_n) of size n exist. The procedure of the assessment starts with sorting values of X and Y by size which gives each measurement value X_i and Y_i a rank $r_{X,I}$ and $r_{Y,I}$ (Walpole *et al.*, 2002).

According to Spearman, the rank correlation coefficient can be calculated as follows:

$$r_s = 1 - \frac{6 \cdot \sum_{i=1}^{n} {d_i}^2}{n(n^2-1)} \quad (6.7)$$

Where, r_s: Spearman rank correlation coefficient

d_i: difference between the ranks assigned to X_i and Y_i

n: number of pairs of data

The value of r_s will range from -1 to +1. A value of +1 or -1 indicates perfect association. A value of zero indicates that no correlation between the parameters X and Y exists.

The null hypothesis H_0 used for the assessment of correlation was that "no correlation between X and Y exist". Mathematically, the null hypothesis states that the rank correlation coefficient $r_s = 0$. For proving the correlation between X and Y, the inconsistency of the data with the null hypothesis must be shown. This means that the null hypothesis can be rejected. The significance level p determines the probability with which the null hypothesis is falsely rejected. A significance level of 5% (p-value = 0.05) was selected according to Walpole *et al.* (2002).

For assessment, the t score was calculated as follows

$$t = \frac{r_s}{\sqrt{1-{r_s}^2}} \sqrt{n-2} \quad (6.8)$$

The calculated t-score with (n - 2) degrees of freedom were used to determine the appropriate probability that the null hypothesis is falsely rejected from common statistical tables (f.e. from Walpole *et al.*, 2002). If this value is below the selected significance level p, the null hypothesis can be rejected. This means that both parameters show a strong correlation.

6.3. Results and discussion

6.3.1 Initial observation regarding filterability as basis of the working hypothesis

The initial observation was based on investigation of filterability in terms of critical flux using two complete different anaerobic sludges. The first sludge was taken from a digester fed with pure WAS (PS_1). The second sludge was taken from a digester fed with a mixture of WAS and flotation sludge (PS_5). Major sludge characteristics are given in Table 20.

Similarities of raw sludge in terms of sludge characteristics are total solids content, volatile solids content, standard apparent viscosity and particle size distribution (see Table 20). Yet, there are major differences between both sludges in terms of colloidal matter estimated by the difference of COD in supernatant and filtrate sample (PS_1: ~ 700 mg/L; PS_5: ~ 1,300 mg/L), higher active biomass assumed in PS_5 based on higher COD removal and especially VS based removal rates (PS_1: ~ 0.1 kg COD/(kg VS·d); PS:_5 > 0.2 kg COD/(kg VS·d)) and the addition of Fe salts (PS_1: none; PS_5: input by addition in flotation unit).

Initial observations regarding filterability of two complete different anaerobic sludges from two different digester operations showed that TS content is much more decisive for critical flux than

substrate mixture or digester performance (COD loading rate) in this case (see Figure 48). The addition of flotation sludge resulted in higher COD loading rates (see Table 17), higher COD removal (see Table 17) and higher shares of active (methanogenic) biomass (see Table A 3) in the anaerobic sludge compared to the sludge fed only with WAS. The composition of the total solids in terms of active biomass differs in both sludges, but the filterability in terms of the critical flux of both anaerobic sludges is similar at even total solids contents (Figure 48). Colloidal substances also did not lead to major differences in filterability in this application with high total solids content and high apparent viscosities compared to common MBR applications. Coagulants (added during flotation process) and the extensive degradation of lipids may contribute to flux stabilization.

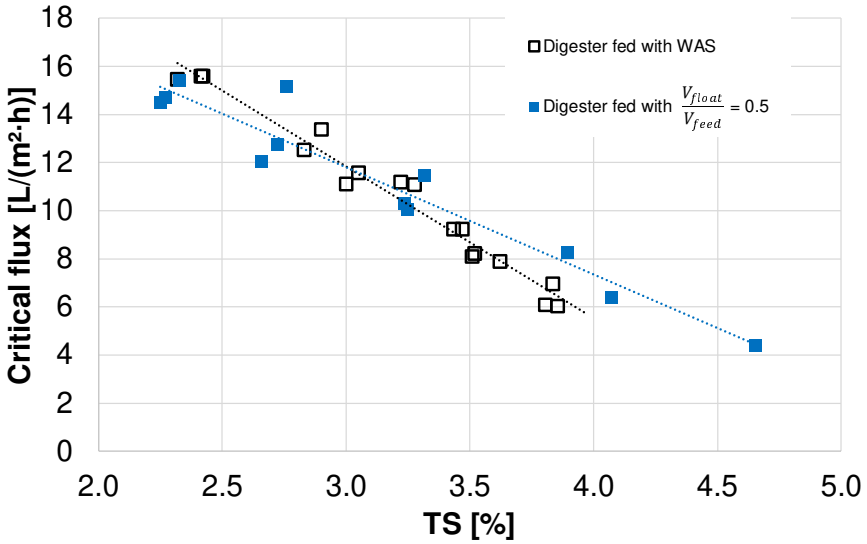

Figure 48. Critical flux of digestate of WAS (PS_1) and WAS + flotation sludge (PS_5) as feed at 320 rpm (mean crossflow velocity ≈ 3.8 m/s)

These observations result in the working hypothesis to be investigated in this chapter:

Critical flux and short-term fouling are decisively affected by high concentration of solids and increased viscosity in AnMBR applications for sludge treatment.

It is assumed that these sludge characteristics outweigh known effects of key parameters of fouling in common MBR and AnMBR applications with lower sludge concentrations, such as SMP, EPS and colloidal matter on fouling and are therefore decisive for the critical flux.

Therefore, the following section focuses on the detection of characteristic key sludge parameters influencing membrane performance (section 6.3.2). By varying these parameters for each individual sludge, the aforementioned site-specific influences fade into the background. Subsequently, an attempt is made to find a clear inter-sludge relationship between characteristic sludge parameters and filtration performance.

6.3.2 Effects of sludge characteristics on critical flux

Sludge samples of digesters treating mainly municipal sewage sludge varied significantly in solids concentration, viscosity and CST (Table 20). There was no clear correlation among sludge characteristics. Site-specific peculiarities, undefined differences of the substrates and reactor-specific differences seem to have a major influence on sludge characteristics, as already stated by DWA M-383 (2008). However, deviations in samples of each origin were low. Despite different substrate composition, anaerobic sludge samples except LS_3 showed a similar particle size distribution. These analyses contradict the findings of Houghton and Stephenson (2002), who observed larger particle diameters with increasing shares of WAS.

6.3.2.1 Solids concentration

The relationship between solids concentration and critical flux is shown in Figure 49.

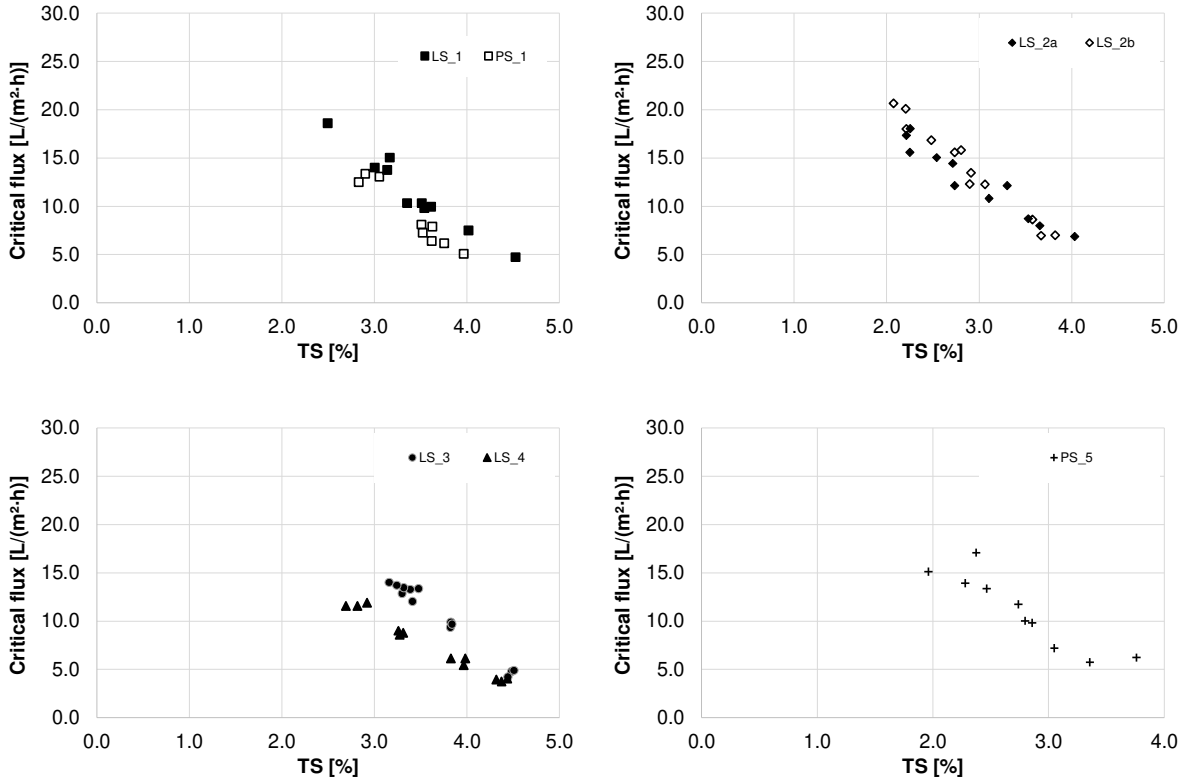

Figure 49. Critical flux in dependence of TS for each sludge at membrane rotational speed of 320 rpm

While a TS concentration of 2 % can allow for high critical fluxes above 20 L/(m²·h) (see LS_2b), critical flux drops below 5-10 L/(m²·h) for TS above 4 %. Measured critical flux roughly corresponds to values of 21 L/(m²·h) at TSS = 25 g/L,16 L/(m²·h) at TSS = 32 g/L (Dagnew, 2010) and 6-8 L/(m²·h) at TSS = 40 g/L (Pileggi, 2016). Both authors operated AnMBR for municipal sludge digestion using hollow fiber PVDF membranes. In the investigated range of TS concentrations (between 2-4.5 %), a quasi-linear relationship exists for each anaerobic sludge. The linear correlation between TS and critical flux for each single sludge sample (except PS_5) is good as regression coefficients exceed $R^2 > 0.93$. For each facility, a change of TS, for example, due to changes in the feed concentration may determine changes in critical flux. This corresponds to Jeison and Van Lier's investigations (2008), which also demonstrated a linear reduction of the critical flux as a function of TS between 25 and 50 g/L.

At a given TS, the critical flux of sludge samples from different origins varies within 5-7.5 L/(m²·h) (see Figure 50). For example, critical flux around 7.5-15 L/(m²·h) was achieved at TS = 3.0%. However, there is a statistically significant correlation between TS and critical flux. There is only a small probability that the null hypothesis "TS content is not correlated to the critical flux" results by chance, as the p-value ($p = 1.5 \cdot 10^{-25}$) is far below $p < 0.05$. For the investigated TS range, a linear model describes the dependence of critical flux on TS content as good as an exponential or logarithmic model (see Table 21). As samples without solids should not exhibit critical flux, an exponential or power law dependence is more likely in theory. Nevertheless, a precise prediction of critical flux based on the TS content of a random sludge sample is limited, as R^2 decreases to values around 0.78.

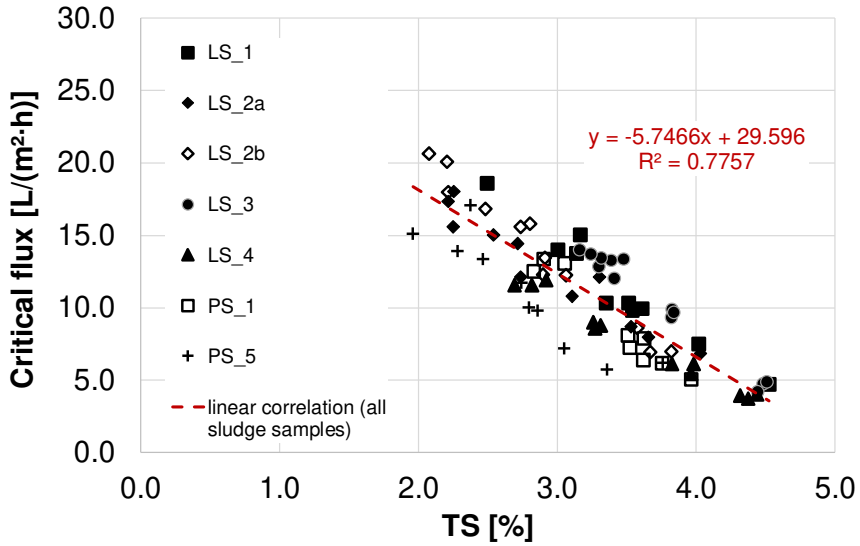

Figure 50. Correlation between critical flux and TS content for all sludge samples at membrane rotational speed of 320 rpm

Table 21. Comparison of type of dependency between TS and critical flux for an inter-sludge relationship

	Linear (y=a*x+b)	Logarithmic (y=a*ln(x))	Exponential (y=a*e^{bx})	Power (y=a*x^{b})
R^2	0.78	0.78	0.78	0.75

The relationship between VS and critical flux is similar to the relationship between TS and critical flux (see Figure 51). Correlations between VS and critical flux are also sludge-specific and cannot be translated into a precise general relationship (see Table 23). Statistically, the correlation between VS and critical flux is significant. The probability that the null hypothesis "VS content is not correlated to the critical flux" is applicable in reality is small, as the p-value ($p = 3.4 \cdot 10^{-29}$) is far below $p < 0.05$. For the investigated VS range, a linear model to predict critical flux based on VS fits as good as a logarithmic or exponential model (see Table 22). Compared to the previously introduced relationship between TS and critical, critical flux might slightly better depend on VS as regression coefficient is slightly higher. A better regression resulted from lower deviation of achieved critical flux using sludge PS_5 to other sludge samples at even VS compared to results at even TS.

Table 22. Comparison of type of dependency between VS and critical flux for an inter-sludge relationship

	Linear (y=a*x+b)	Logarithmic (y=a*ln(x))	Exponential (y=a*e^{bx})	Power (y=a*x^{b})
R^2	0.83	0.83	0.83	0.79

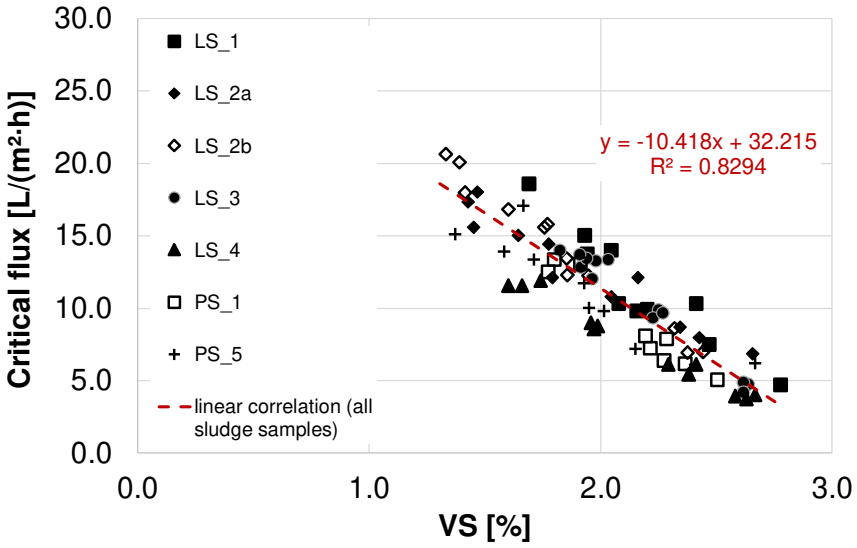

Figure 51. Correlation between critical flux and VS for all sludge samples at membrane rotational speed of 320 rpm

This indicates that in addition to the solids content, other characteristic properties of sludge also decisively affect membrane performance based on critical flux. Shimizu *et al.* (1996) and Jørgensen *et al.* (2014) proposed empirical models to describe the limiting flux of aerobic MBRs on the basis of the sludge concentration and shear stress, as both mainly affect short-term fouling behaviour, especially back transport. Shear stress is considered in Section 6.3.2.3.

6.3.2.2 Capillary suction time (CST)

CST values depend on TS and VS, as shown in Figure 52. The higher the TS or VS, the higher the CST. Standard deviations of CST measurements were always below specified values for the properties of the filtration papers (±10 % according to DBFZ (2015)). For clarity, in the following figures, standard deviations or error bars are not shown. CST values varied among sludge samples of different origins. It is especially noticeable that anaerobic sludge from digestion operated with high shares of flotation sludge from the dairy industry (PS_5) clearly showed highest CST values at even TS or VS. These poor CST values of PS_5 agree with the findings regarding poor dewaterability of digested sludge from co-digestion using lipid-rich substrates (Metcalf and Eddy, 2004; Kopp, 2006; DWA M-383, 2008; Hubert *et al.*, 2020). CST is often used as a parameter to describe the dewaterability of digested sewage sludges (DWA M-383, 2008; Kopp, 2006). It can also be assumed that the presence of degradable fats has a significant influence on the CST.

The inter-sludge relationship between CST and TS can be best described by linear and exponential law. Parameters do not show a clear mathematical correlation. Statistically, a significant

correlation exists between TS or VS and CST, as its independence is most unlikely (p-value $p = 5.0 \cdot 10^{-10} < 0.05$ for TS and CST; p-value $p = 1.3 \cdot 10^{-13} < 0.05$ for VS and CST).

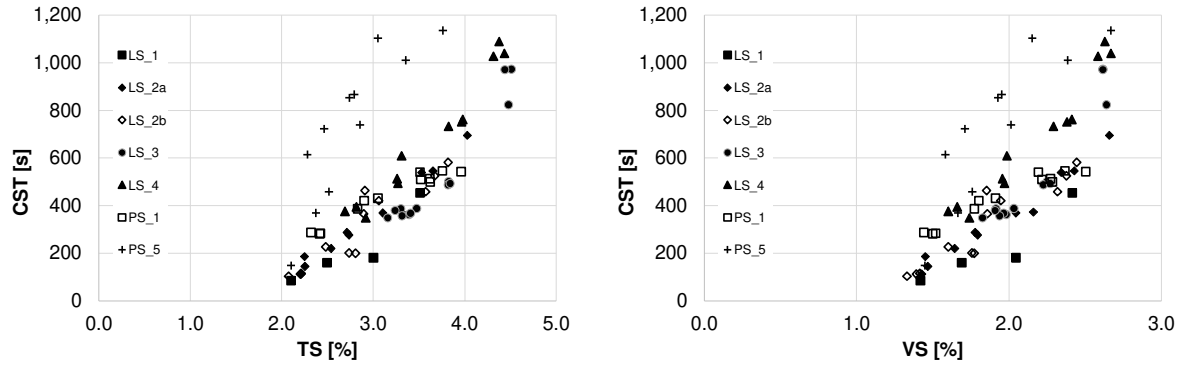

Figure 52. Capillary suction time (CST) versus total solids (TS) and volatile solids (VS) at membrane rotational speed of 320 rpm

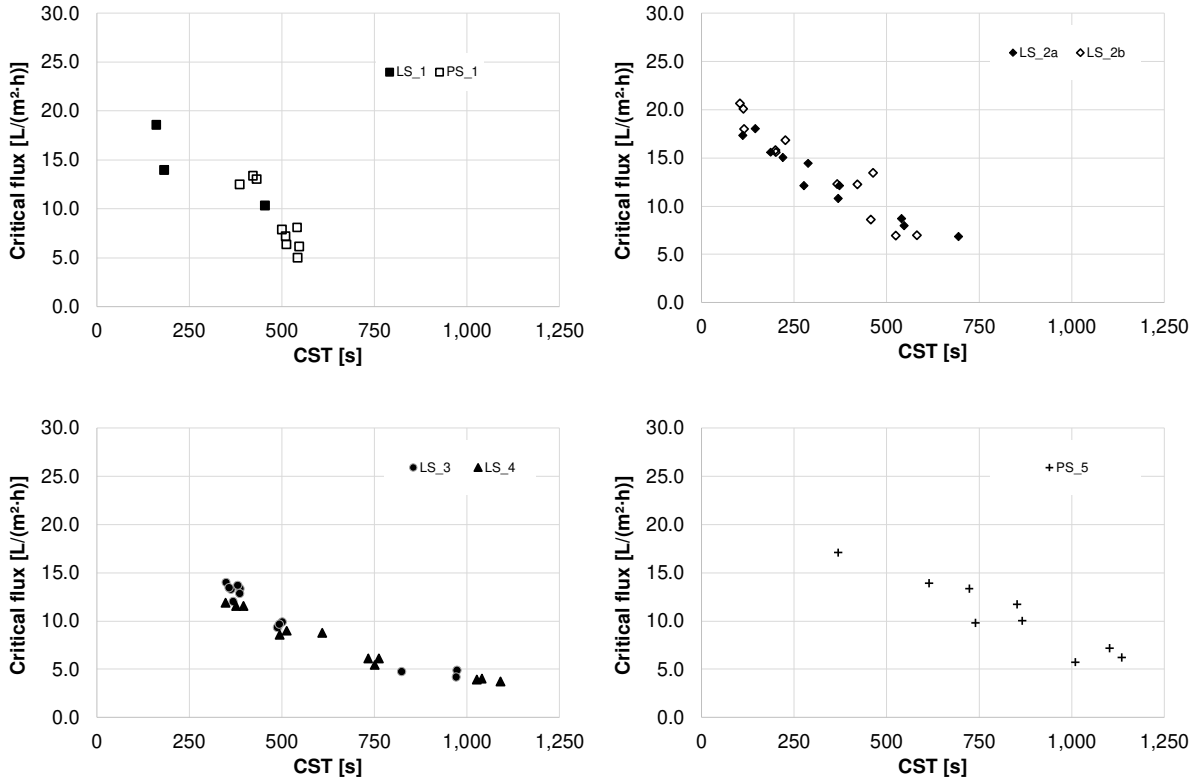

Figure 53. Critical flux in dependence of capillary suction time (CST) for each sludge at membrane rotational speed of 320 rpm

Comparing CST and critical flux for each individual sludge, sludge samples with lower CST show a better filterability and higher critical flux (see Figure 53). These trends agree with published experiences regarding aerobic membrane bioreactors (Wang *et al.*, 2006; Baumgarten, 2007) as well as known relationships between CST and short-term fouling in anaerobic MBRs (Guglielmi *et al.*, 2010; Dagnew, 2010; Dereli *et al.*, 2014a; Dong *et al.*, 2016). Although, CST successfully compares filterability of different sludges (Ersahin *et al.*, 2014), a precise prediction of critical flux based on CST has not been achieved so far.

Deviating from published experiences, the results of this study show a limited predictability of critical flux based on CST across all sludges (see Figure 54 and Table 23). The dependence of critical flux on CST is still statistically evident as null hypothesis “CST does not correlate to critical flux” is most unlikely (p value p = $3.1 \cdot 10^{-18}$ is below 0.05).

When following an exponential correlation and excluding PS_5, a good inter-sludge correlation existed between critical flux and CST, with a regression coefficient of up to R^2 = 0.89 (see Table 23). This good correlation may be due to the presence of large quantities of poorly degradable organic and non-degradable inorganic residual matter in the sludge samples compared to other studies that had high proportions of active biomass or still-degradable matter in sludge samples. The influence of different reactor sizes, mixings and loads may thus be pushed into the background.

Table 23. Comparison of type of dependency between CST and critical flux for an inter-sludge relationship

	Linear (y=a*x+b)	Logarithmic (y=a*ln(x))	Exponential ($y=a*e^{bx}$)	Power ($y=a*x^b$)
R^2 (all sludge samples)	0.68	0.76	0.70	0.69
R^2 (all sludge samples except PS_5)	0.83	0.88	0.89	0.81

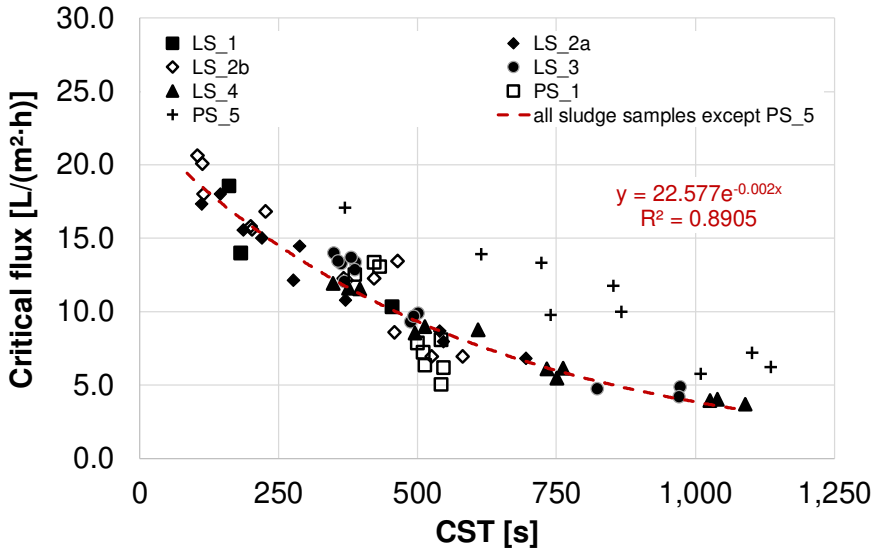

Figure 54. Correlation between CST and critical flux of investigated sludges at membrane rotational speed of 320 rpm

On including PS_5, the precise prediction of the critical flux based on CST of a random sludge becomes weaker (R^2 = 0.83; see Table 23). The relationship between CST and critical flux differs for PS_5 compared to other sludge samples. At even CST, higher critical flux was achieved for PS_5 compared to other sludge samples (Figure 54). This behaviour might be because of the different sludge compositions of PS_5. The composition of the PS_5 sludge differed from that of the other samples: It had the highest proportion of active biomass in the residual organic matter in the sludge and the highest proportion of fats compared to the other sludge samples. Obviously, this reduces the water release speed but not the filtration performance. Regarding VS content, the filtration performance of PS_5 was similar to that of the other sludges (see Figure 51); however, regarding TS, it was worse (see Figure 50).

In conclusion, CST can be considered a promising parameter for the prediction of filterability based on critical flux for anaerobic sludge from digesters treating mainly sewage sludge. Limitations of prediction result from co-digestion with lipid-rich (or other) substrates.

6.3.2.3 Apparent viscosity

Correlation between standard apparent viscosity and the other investigated sludge characteristics is provided in Figure 55. Following the example of Moshage (2004), standard apparent viscosity is characterised at a shear rate of 500 s^{-1}. In this study, it was analysed at a temperature of 20°C. Apparent viscosity is affected by TS and VS. It also affects or is affected by CST. All relationships are significant on the basis of the improbability of the null hypothesis that no relationship exists (p values are below 0.05).

The values of apparent viscosity in correlation to TS are slightly below published data in the case of aerobic sludge (Rosenberger *et al.*, 2002), equal to published data in the case of one investigated digested sludge (Füreder *et al.*, 2017; values were temperature compensated to 20°C, as suggested by Moshage (2004)) and slightly above published data in the case of digested sludge of municipal WWTPs (Moshage, 2004; Baudez *et al.*, 2013; see Figure 56).

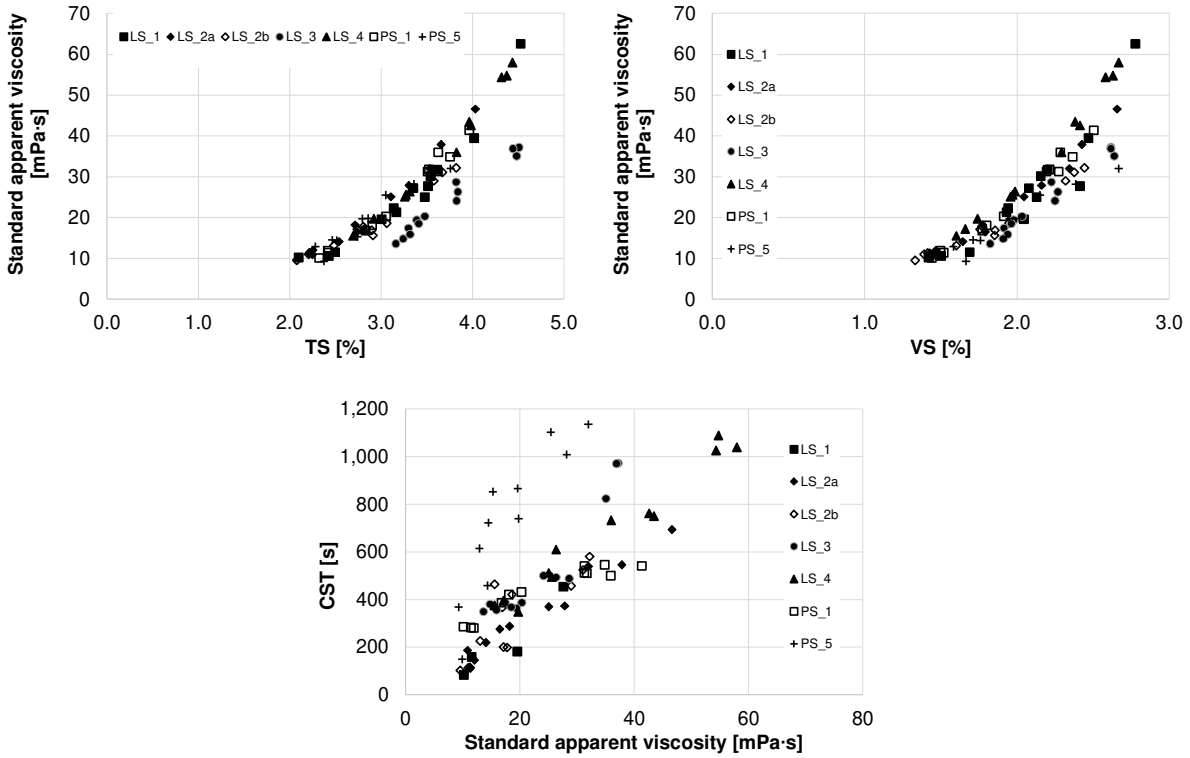

Figure 55. Dependence between standard apparent viscosity and total solids (TS), volatile solids (VS) and capillary suction time (CST) at membrane rotational speed of 320 rpm

In this study, the relationship between TS and standard apparent viscosity (and shear stress at shear rates of 500 s^{-1}) follows an exponential law, as has already been shown in published data. The relationship between standard apparent viscosity and VS seems more precise than the relationship between standard apparent viscosity and TS. A quasi-linear relation exists between the standard apparent viscosity and CST of most sludges except PS_5. Conversely, Moshage (2004) could not detect any correlation between viscosity and CST on analyzing different digested sludge samples.

Models for calculating shear stress as a function of shear rate and TS are published for activated sludge samples but not for digested sludge (Ratkovich *et al.*, 2013). Jørgensen *et al.* (2014) used a model developed by Rosenberger *et al.* (2002) with the following general equation to predict membrane performance based on shear stress:

$$\eta_a = e^{a \cdot TSS^b} \cdot \dot{\gamma}^{c \cdot TSS^d} \quad (6.9)$$

Where, η_a: apparent viscosity (mPa·s)

a-d: empirical parameters for calibration of model (see Table 24)

$\dot{\gamma}$: shear rate (1/s)

TSS: concentration of total suspended solids (g/L)

Calculations based on least-squares method deliver empirical coefficients a-d for the anaerobic sludges investigated in this study (see Table 24). Using these coefficients, a good estimate of the apparent viscosity of the MBR anaerobic sludge on the basis of TS and shear rate is provided (see Figure 56 for $\dot{\gamma}$ = 500 s^{-1}).

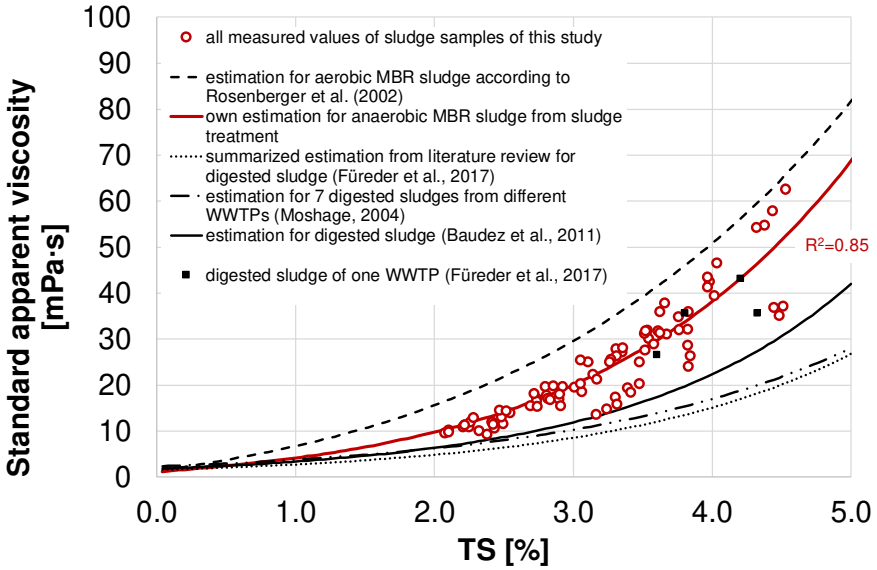

Figure 56. Comparison of empirical apparent viscosity models with data and model investigated in this study

Table 24. Values for empirical coefficients a-d for calibration of empirical apparent viscosity model

	a	b	c	d	Reference
Aerobic MBR sludge	1.9	0.43	-0.22	0.37	Rosenberger *et al.* (2002)
	0.82	0.494	-0.05	0.631	Laera *et al.* (2007)
Anaerobic MBR sludge	0.77	0.63	-0.08	0.59	own calculation

In Figure 57, the critical flux is depicted as a function of standard apparent viscosity for each sludge. Increasing viscosity reduces critical flux achieved in each case. The curves of the individual sludges are quasi-linear in a range from 10 to 30-40 mPa·s. Higher viscosity reduces critical flux only slightly for η_a > 40 mPa·s. High critical flux of 20 L/(m²·h) is achieved at low standard apparent viscosity of around 10 mPa·s (e.g., LS_2a and LS_2b) and drops to values around 5 L/(m²·h) at high standard apparent viscosity up to 60 mPa·s (e.g., LS_1, LS_3 and LS_4). Statistically, there is a significant correlation between standard apparent viscosity and

critical flux. The probability of the null hypothesis “standard apparent viscosity is not correlated to the critical flux” being true due to chance is small, as the p-value ($p = 2.1 \cdot 10^{-23}$) is far below $p < 0.05$. In addition, sludge such as PS_5 did not produce obvious outliers in this case, which was shown for TS and CST.

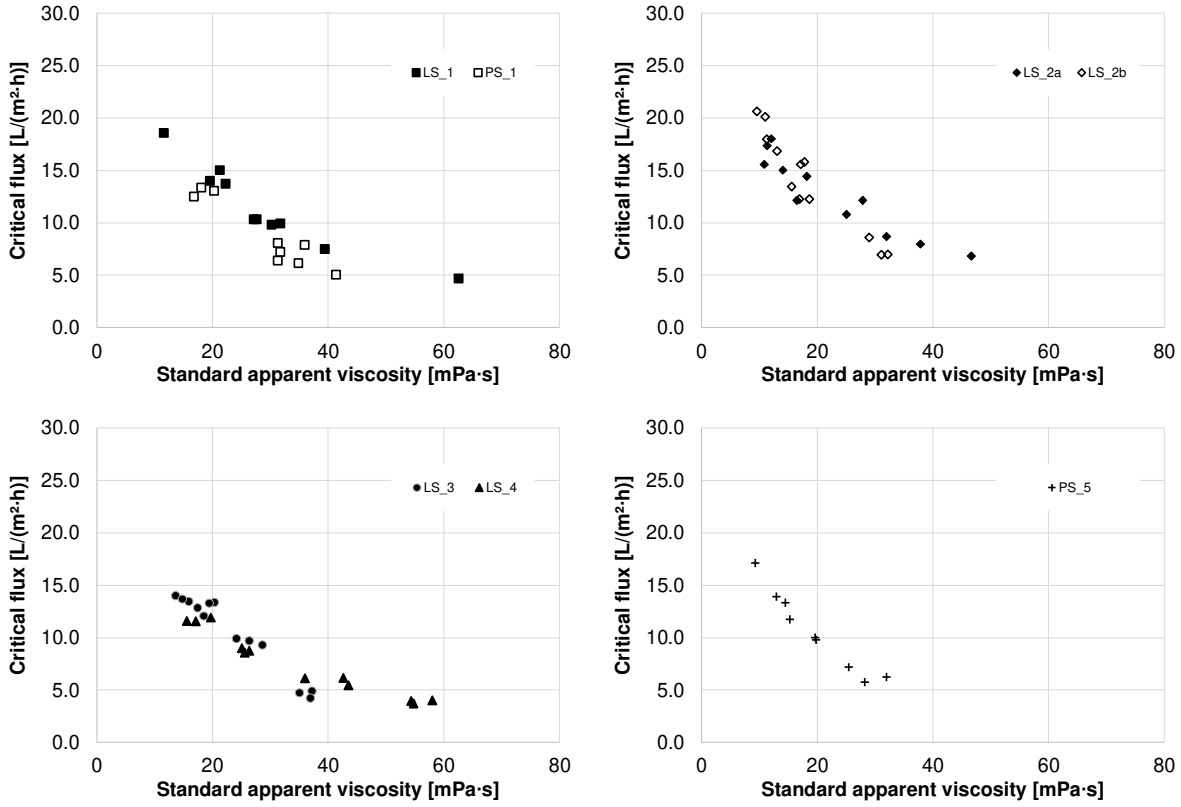

Figure 57. Critical flux affected by standard apparent viscosity at membrane rotational speed of 320 rpm

For all sludges in common, critical flux shows a definite inter-sludge correlation, with the standard apparent viscosity following a predominantly power-law dependency (see Figure 58, Table 25). The regression coefficient of this relationship is above $R^2 > 0.84$. At a given standard apparent viscosity, the critical flux of sludge samples from different origins varies slightly; within approx. 5 L/(m²·h) at standard apparent viscosities below 40 mPa·s and within approx. 1.5 L/(m²·h) at standard apparent viscosities above 40 mPa·s (see Figure 58). For example, a critical flux of around 10-15 L/(m²·h) was achieved at a standard viscosity of 20 mPa·s. Jeison and van Lier (2008) also reported a connection between sludge viscosity and critical flux. Ho and Sung (2009) assumed apparent viscosity to influence turbulences in flow by fouling. Higher viscosity reduces turbulence. Jørgensen (2014) attribute the importance of viscosity on membrane performance to its influence on mass transfer, especially on the back transport of retained particulates to the bulk.

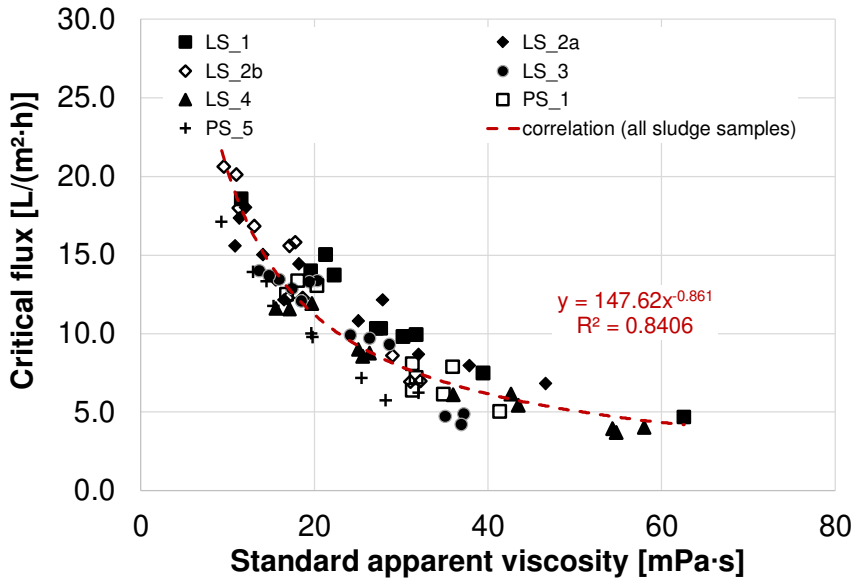

Figure 58. Correlation between standard apparent viscosity and critical flux of investigated sludges at membrane rotational speed of 320 rpm

Table 25. Comparison of type of dependency between standard apparent viscosity and critical flux for an inter-sludge relationship

	Linear (y=a*x+b)	Logarithmic (y=a*ln(x))	Exponential (y=a*e^{bx})	Power (y=a*x^{b})
R^2 (all sludge samples)	0.75	0.83	0.83	0.84

Implementation of present shear at membrane surface as basis for apparent viscosity

The accuracy of dependence between the critical flux and viscosity increases even further when the present shear at membrane surface is integrated (see Figure 59). A power-law correlation delivers the best fit with R^2=0.90 (see Table 26). Compared to all other aforementioned sludge characteristics, the measured values of critical flux deviate least at a given value. At an apparent viscosity at present shear, the critical flux of sludge samples from different origins varies slightly within 3 L/(m²·h) (see Figure 59). For example, a critical flux of around 5-8 L/(m²·h) was achieved at $\eta(\dot{\gamma}_m)$ = 20 mPa·s.

As shown, the correlation between standard apparent viscosity and critical flux can be significantly improved by integrating shear stress on the membrane surface. Therefore, shear stress and according to equations 6.4 and 6.5 solids concentration is decisive, as proposed by Shimizu *et al.* (1996) and Jørgensen *et al.* (2014). Consequently, membrane performance can be particularly optimised by increasing shear stress on the membrane (e.g. by increasing the rotational speed of membrane; see section 2.2.2 and equation 6.4) and reducing apparent viscosity of fluids (e.g. by adding $FeCl_2$; see Section 6.3.3.2).

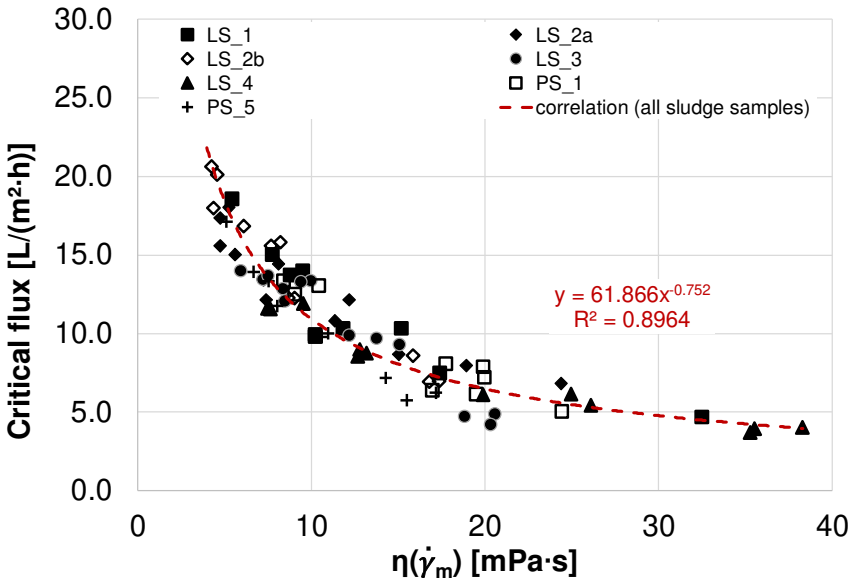

Figure 59. Correlation between apparent viscosity at present shear on membrane disc at T = 37°C and critical flux of investigated sludges at membrane rotational speed of 320 rpm

Table 26. Comparison of type of dependency between present apparent viscosity on membrane disc and critical flux for an inter-sludge relationship

	Linear (y=a*x+b)	Logarithmic (y=a*ln(x))	Exponential (y=a*e^{bx})	Power (y=a*x^{b})
R^2 (all sludge samples)	0.74	0.88	0.84	0.90

6.3.3 Potentials for improving critical flux

6.3.3.1 Rotation of membrane

Crossflow velocity is mainly set by membrane rotation but varies according to distance from the rotating hollow shaft (see Table 10). In principle, increasing rotational speed boosts back transport of retained particulates to bulk stream and reduces cake layer formation on the membrane surface (also see Section 2.2.2). During filtration, increasing crossflow velocities noticeably reduce TMPs at similar flux (see example in Figure 60).

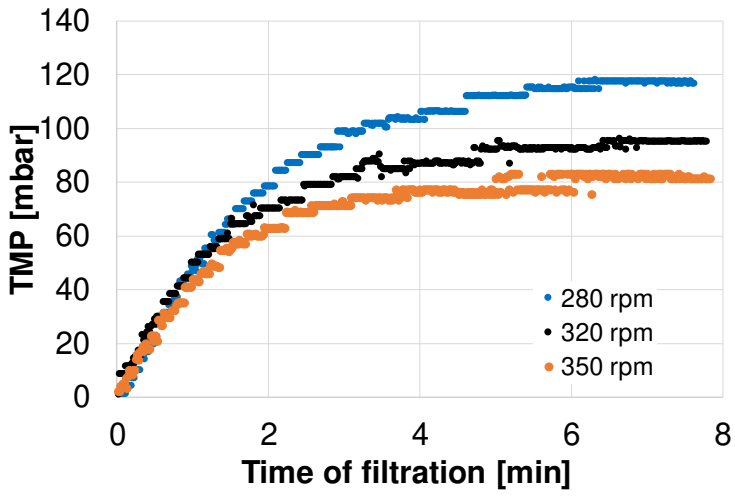

Figure 60. Development of transmembrane pressure (TMP) over time during filtration at different membrane rotational velocities applying a flux of J = 7 L/(m²·h) (PS_2b with a TS = 3.8%)

In addition to lowering TMP, rotational speed also influences critical flux (see Figure 61). At TS concentrations of more than 3.5 %, an improvement of 20 % in critical flux was observed after increasing the rotational speed from a standard speed of 320 rpm (Mohr, 2011) to 350 rpm. This corresponds to increases of mean cross-flow velocity from 3.8 to 4.1 m/s. A reduction to 280 rpm (mean cross-flow velocity of 3.3 m/s) led to losses of about 20 %. Changes of critical flux related to changes of crossflow velocity cannot be described via the sludge parameters TS, VS and CST. These parameters remain unchanged when the membrane operation is changed and, consequently, always correlate only with a defined operational setting of the membrane module.

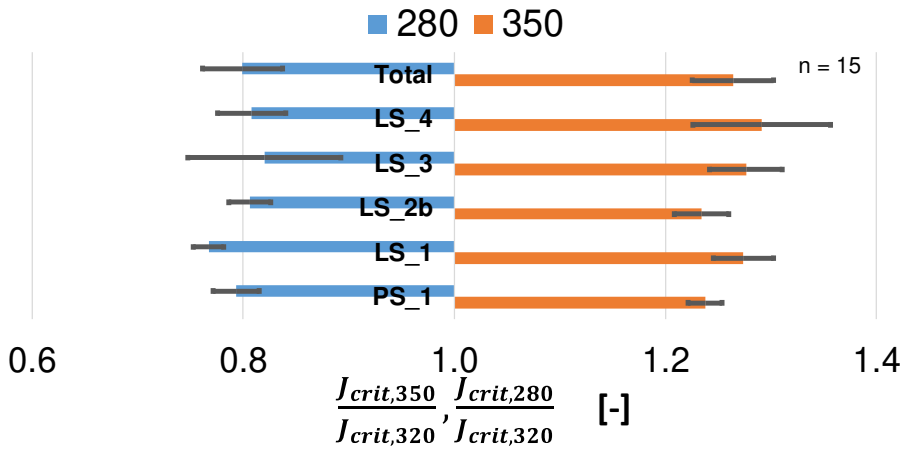

Figure 61. Critical flux in dependence of membrane rotation compared to standard setting of 320 rpm for different sludge samples with total solid contents > 3.5 %

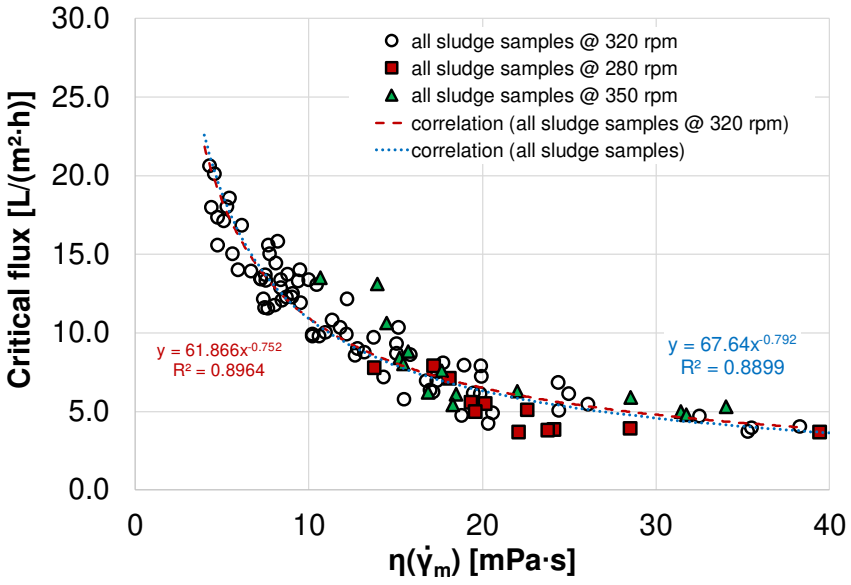

Figure 62. Correlation between apparent viscosity at present shear on membrane disc at T = 37°C and critical flux at different rotation speed of the membrane

However, this does not apply to the apparent viscosity when shear stress present directly at the membrane is considered. Changes in crossflow velocity result in altered apparent viscosities at present shear on the membrane surface. The critical flux at rotational speeds of the membrane other than standard follow the correlation curve between critical flux and apparent

viscosity at present shear on the membrane surface at 320 rpm (see Figure 62). Thus, previously described dependencies can be transferred to a rotational range of the membrane discs between 280-350 rpm.

6.3.3.2 Addition of ferrous chloride ($FeCl_2$)

As mentioned in Section 2.3, ferric and ferrous chloride often induce a shift to higher fluxes in (An)MBR applications, treating mainly soluble organic matter (e.g., Kim and Lee, 2003; Holbrook *et al.*, 2004; Itonaga *et al.* 2004; Baumgarten, 2007; Waeger *et al.*, 2010). In sludge digestion, ferric and ferrous chloride is often used to reduce soluble as well as gaseous H_2S (e.g., Wilén *et al.*, 2003; Jin *et al.*, 2004). It was also used in sludge of facilities LS_1, LS_2 and LS_4. In this work, sludge samples of LS_3 with TS ≈ 3.2 % and TS ≈ 4.5 % were dosed with various amounts of ferric chloride (20 % $FeCl_2$) and the effects on sludge properties (see Table 27) and membrane filtration performance were investigated.

Table 27. Changes in sludge characteristics after dosing of ferric chloride in digested sludge of two different total solid concentrations using sludge from location LS_3 (mean±std.dev; no. of samples n = 3)

Parameter	Original sample	$FeCl_2$ 20 % addition		
		V_{spec}≈0.75 L/m³	V_{spec}≈1.5 L/m³	V_{spec}≈2.25 L/m³
TS [%]	3.2±0.1	3.2±0.1	3.2±0.1	3.3±0.2
VS [%]	1.9±0.1	1.9±0.1	1.9±0.1	1.9±0.1
TS specific dosage [mL $FeCl_2$ 20 %/kg TS]	0	25±2	50±5	70±10
$\eta(\dot{\gamma}_m)$ [mPa·s][a]	6.8±0.7	6.7±0.1	5.9±0.6	5.9±0.3
CST [s]	232±74	206±72	204±47	202±11
$COD_{supernatant}$ [mg/L]	990±276	959±115	942±65	922±59
$COD_{filtrate}$ [mg/L]	381±101	387±71	358±52	339±41
PO_4-$P_{filtrate}$ [mg/L]	98±9	70±4	52±8	41±9
TS [%]	4.6±0.1	4.6±0.1	4.5±0.1	4.6±0.1
VS [%]	2.7±0.1	2.6±0.0	2.6±0.0	2.7±0.0
TS specific dosage [mL $FeCl_2$ 20 %/kg TS]	0	20±2	36±4	54±5
$\eta(\dot{\gamma}_m)$ [mPa·s][a]	25.4±6.0	20.6±1.4	19.9±2.2	18.8±1.1
CST [s]	452±111	431±109	406±96	376±77
$COD_{supernatant}$ [mg/L]	1,688±405	1,698±217	1,768±150	1,700±150
$COD_{filtrate}$ [mg/L]	459±132	457±85	506±75	467±45
PO_4-$P_{filtrate}$ [mg/L]	109±11	86±9	68±5	54±6

[a] According to Jørgensen *et al.* (2014); temperature was adapted as given by Moshage (2004); rotational speed of membranes = 320 rpm

Sludge samples with TS content of 3.2 % showed only slight fluctuations in CST, but apparent viscosity at present shear $\eta(\dot{\gamma}_m)$ was reduced significantly from 6.8 mPa·s to 5.9 mPa·s. As expected, the phosphorus concentration also decreased from 98 mg/L to 41 mg/L based on precipitation processes. In samples with high TS of around 4.6 %, CST and apparent viscosity at present shear on membrane disc and phosphorus concentration decreased significantly. However, effect of Fe dosage on COD concentration in supernatant and filtrate was negligible. This contradicts the observations of Lee *et al.* (2001), Holbrook *et al.* (2004), and Itonaga *et al.* (2004), who found a reduction in colloidal matter on adding ferric chloride in aerobic MBRs. Possibly, in sludge digestates with higher TS than that of aerobic MBRs, the effects of iron

cations as a coagulant for floc enhancement and encapsulation of colloidal matter are not pronounced, as particle size distribution also remains unvaried by iron dosage (see Figure 63).

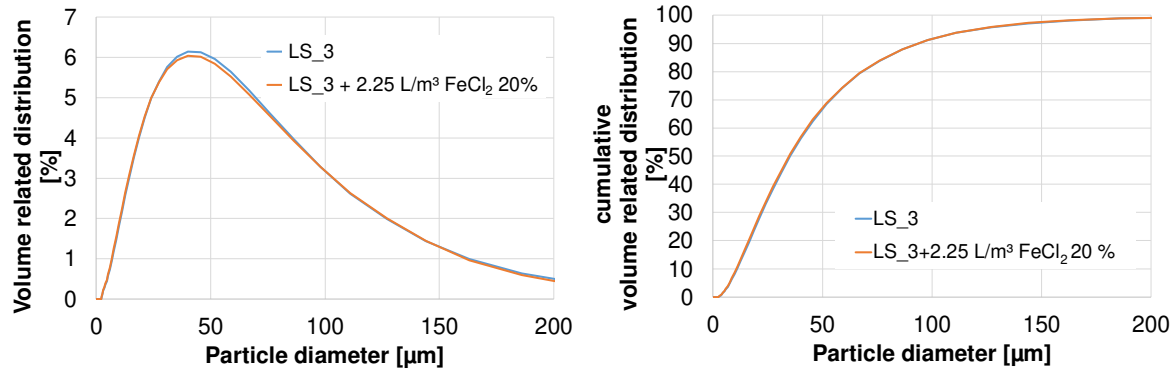

Figure 63. Comparison of particle size distribution of LS_3 due to $FeCl_2$ dosages

Possibly, iron cations have neutralised the negative charge of the particulate biomass (Wilen *et al.*, 2003, Jin *et al.*, 2004). A more compact structure of the hydrogel system and an improved balance of charge might have reduced the apparent dynamic viscosity. Further, iron prefers to react with sulfide and subsequently with phosphate (e.g., Xiao *et al.*, 2013; Zhang *et al.*, 2013; Flores-Alsina *et al.*, 2016). The slight observed reduction of phosphate concentration by addition of iron could have significantly reduced the hydrogel and made it more compact. Kopp (2006) relates this to changed interaction between proteins and phosphate compounds within the hydrogel structure around the cells. In hydrogel systems, a compartment around biomass cells is defined where EPS produced by bacteria are present (Madigan *et al.*, 2003).

The addition of Fe^{2+} salts also showed a positive influence on membrane filtration performance in terms of critical flux (see Figure 64). Increasing Fe^{2+} dosages improved critical flux from J_{crit} =13.5 L/(m²·h) up to J_{crit} = 17 L/(m²·h) in sludge samples with TS = 3.2 %. At TS ≈ 4.6 %, critical flux increased from J_{crit} =5 L/(m²·h) to J_{crit} ≥ 7 L/(m²·h). Both results confirm that findings of previous research regarding aerobic MBRs (Lee *et al.,* 2001; Holbrook *et al.,* 2004; Itonaga *et al.*, 2004) can be transferred to AnMBRs.

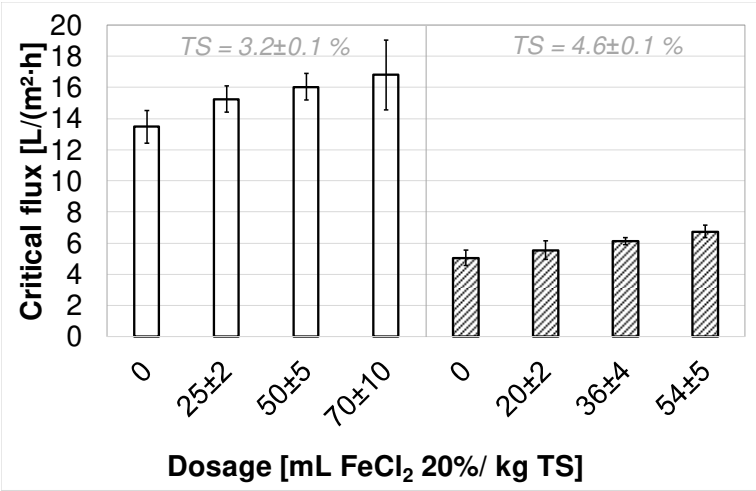

Figure 64. Change in critical flux as a function of iron dosage (n = 3)

In line with Chapter 6.3.2.1, improvements in critical flux should be linked to changes of apparent viscosity at present shear on the membrane surface (see Figure 64 and Figure 65a). Results fit the previously elaborated correlation between critical flux and apparent viscosity at present shear on the membrane surface. CST value is not a suitable parameter to explain the increase of J_{crit} due to the addition of Fe^{2+} salts (see Figure 65b).

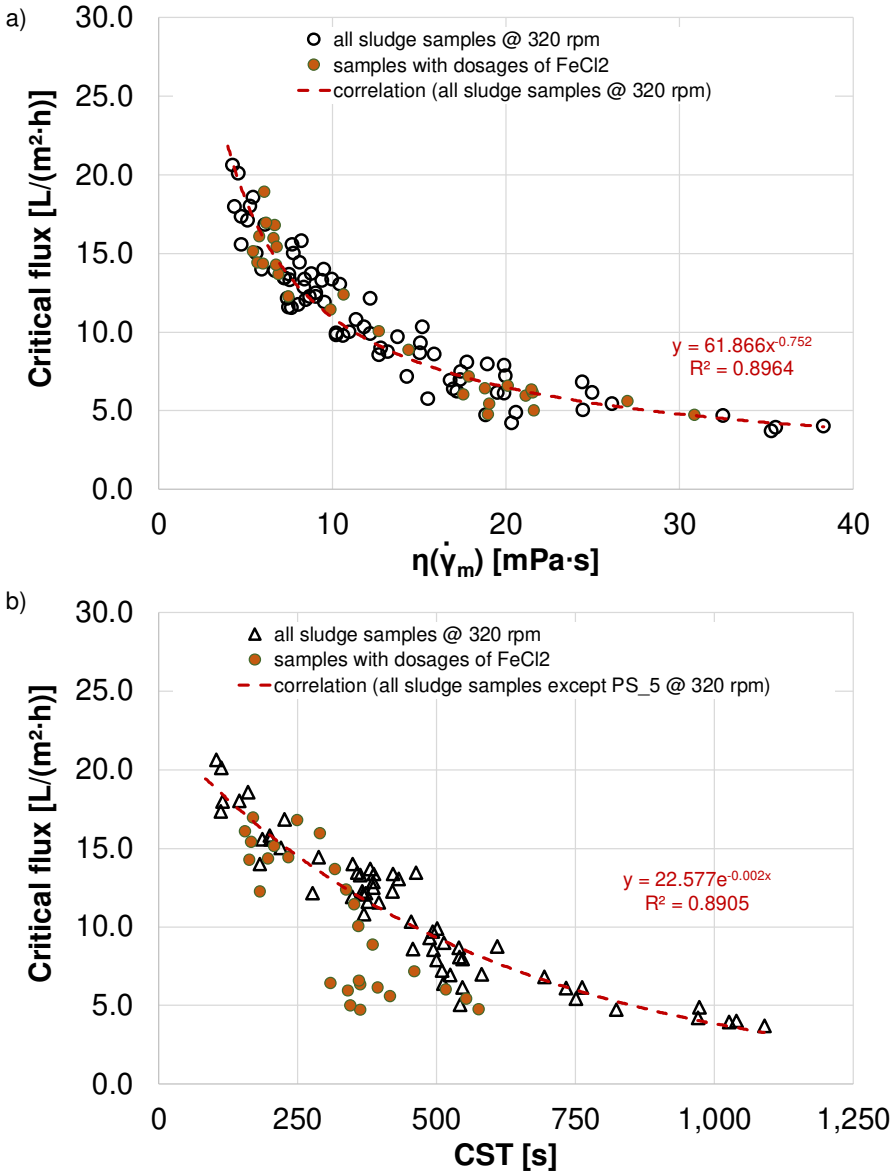

Figure 65. Critical flux as function of present dynamic viscosity (a) and CST (b) at membrane rotational speed of 320 rpm

6.3.3.3 Sludge retention time (SRT)

The influence of SRT on critical flux was investigated using digested sludge from a site comprising three large-scale digesters operated in series. Digested sludge from the first digester at SRT ≈ 20 days (LS_2a) was compared with digested sludge from the final digester with a total SRT ≥ 35 days (LS_2b). Sludge characteristics such as TS, standard dynamic viscosity (T = 20 °C; shear rate = 500 s^{-1}), CST and particle size distribution however did not vary significantly (see Table 20 and Figure 66).

Small differences in viscosity (see Figure 66) at even TS between both sludges were only observed at higher TS concentration above 3.0 %. For sludge samples with TS > 3 %, apparent viscosity declined with increased SRT which is in accordance to findings of Moshage (2002) and Füreder *et al.* (2017). However, Moshage (2002) and Füreder *et al.* (2017) attributed this to a decrease in VS/TS ratio which was not found in samples of LS_2a and LS_2b (LS_2a: VS/TS ~ 0.65±0.02; LS_2b: VS/TS ~ 0.64±0.02). Based on these unchanged ratios although SRT has been extended, only slightly higher removal of organic matter can be assumed which was not expected but explains similarity of the samples. While Dagnew (2010) and Dereli *et al.* (2014a) both reported a reduction of median particle size with increased SRT (i.e., Dagnew (2010) reported variation from SRT = 15 d to 30 d, and Dereli *et al.* (2014a) reported variation from SRT = 20 d to 50 d), the median particle size of sludge samples LS_2a and LS_2b were within standard deviation: Median particle size of LS_2a was 56.3±1.0 µm and of LS_2b was around 56.1±1.5 µm. Possibly, high shear forces caused by mixing in small scale (pilot scale) might have been the reason for their findings, as in large-scale mixing, the shear effects are much less pronounced.

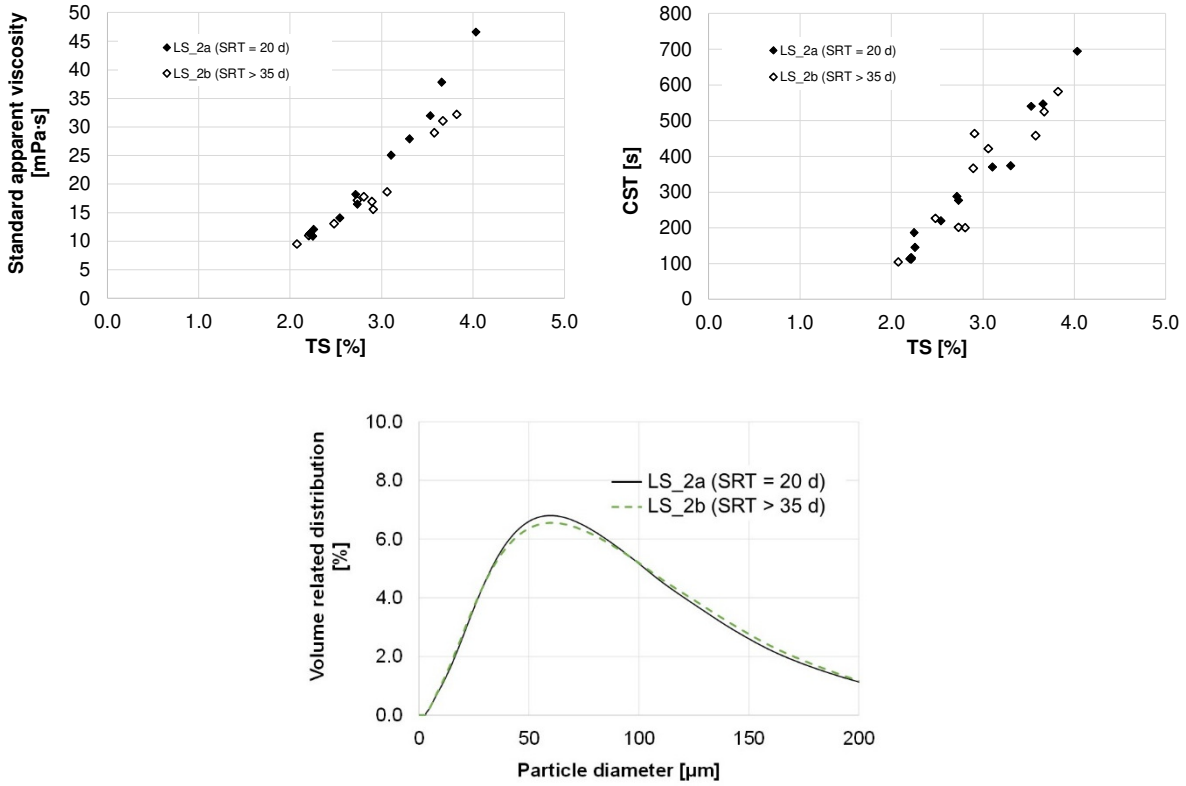

Figure 66. Comparison of sludge properties of LS_2a (SRT = 20d) and LS_2b (SRT > 35 d)

The similarity of sludge properties also becomes evident in critical flux performance. An extension of SRT from 20 d to more than 35 d had no significant effect on the filterability and the fouling potential, which is why the dependency of critical flux on the TS (see Figure 49), standard dynamic viscosity (see Figure 57) and CST (see Figure 53) of both samples shows a similar trend. Claims of Dagnew (2010) and Dereli *et al.* (2014a) that HRT and SRT significantly influence the filtration performance cannot be confirmed, at least not for HRT and SRT with extensive substrate degradation.

6.4. Consolidation of the results in an empirical model to predict the critical flux

As mentioned in Section 2.2.2, the net radial flux of material towards the membrane is the combination of a convective flux and back transport fluxes of retained compounds into the bulk stream (Bacchin *et al.*, 2006). This leads to a concentration increase of non-permeating compounds on the membrane (concentration polarization). The most common model to describe concentration polarization in ultrafiltration of macromolecular solutions is the gel polarization model, which is based on the film theory of mass transfer (Porter, 1972; Zeman and Zydney, 1996; Cheryan, 1998). The model assumes that back transfer is mainly affected by diffusion.

The limiting flux is hereby proportional to a diffusion coefficient D. The diffusion expressed by the diffusion coefficient can be Brownian diffusion (D_B), shear-induced diffusion (D_S) or both (Jørgensen *et al.*, 2014) depending especially on the particle size of the foulant. If particle sizes are larger than 0.1 µm, Brownian diffusion does not significantly affect the back transport (Fane, 1984). Therefore, back transport can mainly be described by shear-induced diffusion as proposed by Zydney and Colton (1986; see Section 2.2.2; expression 2.19). Simply put, the limiting flux is proportional to the shear-induced diffusion coefficient. Additionally, the diffusion coefficient has a linear relationship to the shear rate. Therefore, it can be assumed that the limiting flux is also proportional to the shear rate.

$$J_{lim} \sim D_s \sim \dot{\gamma}_m \tag{6.10}$$

Applying hydrodynamic models (see Section 2.2.2; expression 2.22) based on Darcy's law suggested by Altmann and Ripperger (1997), Melin and Rautenbach (2007) and Schipolowski (2007), the flux is also proportional to the shear rate and consequently connected to the apparent viscosity by a power-law relationship:

$$J = \frac{TMP}{(R_m + R_{ads} + R_{gel\,layer}) \cdot \eta_{filtrate}} \sim \frac{1}{R} \sim \frac{1}{\frac{\eta_{feed}}{\tau_w}} \sim \frac{\tau_w}{\eta_{feed}} \sim \frac{K \cdot \dot{\gamma}_m{}^n}{K \cdot \dot{\gamma}_m{}^{n-1}} \sim \dot{\gamma}_m \tag{6.11}$$

As the shear rate relates to the apparent viscosity by a power law relationship (see expression 6.3), this must also refer to the relationship between the (limiting) flux and the apparent viscosity.

The correlation between critical flux and apparent viscosity at present shear rate on membrane surface is given in Figure 67. It shows a power-law relationship between critical flux and apparent viscosity and meets theoretical expectations (given in expression 6.10 and 6.11). The graph in Figure 67 includes all results from investigations at different rotational velocities of the membrane (see Section 6.3.2 and 6.3.3.1) and dosages of ferrous chloride (see Section 6.3.3.2). Findings concerning type of relationship between critical flux and apparent viscosity (power-law) or present shear rate on membrane surface (linear) agree with Jørgensen *et al.* (2014) who reported a linear correlation between shear rates and flux at shear rates above 500 s^{-1} using aerobic MBR sludge with a TSS concentration of 12 g/L.

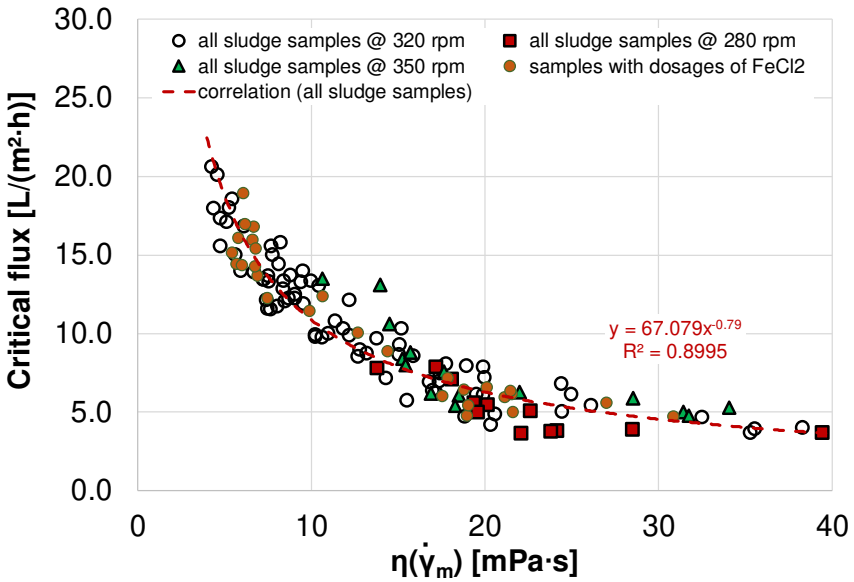

Figure 67. Correlation between apparent viscosity at present shear on membrane disc at T = 37°C and critical flux of all investigated sludges

The empirical relationship observed in this study has the following expression:

$$J_{crit} = 67.079 \cdot (\eta_a(\dot{\gamma}_m))^{-0.79} \quad (6.12)$$

For prediction of critical flux, measurements of apparent viscosity as well as geometric and flow-related parameters of the membrane module must be considered. Using calculation for shear rate on the membrane disc proposed by Jørgensen *et al.* (2014) (equation 6.4) and integrating found empirical relationship between apparent viscosity at shear rate on membrane disc and critical flux (expression 6.12), critical flux can be calculated for a rotating membrane disc as follows:

$$J_{crit} = 67.079 \cdot \left[K \cdot \dot{\gamma}_m{}^{n-1}\right]^{-0.79} \quad (6.13)$$

$$\text{with } \dot{\gamma}_m = \left[0.5133 \cdot \left(\frac{K}{\rho_s}\right)^{-0.5} \cdot (k \cdot \omega)^{1.5} \cdot \frac{r_o^3 - r_i^3}{r_o^2 - r_i^2}\right]^{\frac{1}{0.5n+0.5}} \quad (6.4)$$

$$J_{crit} = f(\eta_a, \rho_s, \omega, \text{geometry of rotating disc})$$

Where, J_{crit}: critical flux ($L/(m^2 \cdot h)$)

$\dot{\gamma}_m$: shear rate on a rotating membrane disc ($1/s$)

η_a: apparent viscosity ($Pa \cdot s$)

K: fluid consistency factor ($Pa \cdot s)^n$

n: flow behaviour index (-)

ρ_s: sludge density (kg/m^3); calculated according to Pileggi (2016)

k: velocity factor (-); = 0.42 (Ding *et al.*, 2002)

ω: angular velocity (rad/s)

r_o: outer radius of membrane; = 0.156 m

r_i: inner radius of membrane; = 0.04 m

A comparison of actual data with calculated values of critical flux using the aforementioned empirical equation shows a good match (see Figure 68a). Around 95 % of the calculated critical flux values had a deviation of less than ±2.4 L/(m²·h) from actual measured values, and 90 % of the values had a deviation of less than ±2.1 L/(m²·h).

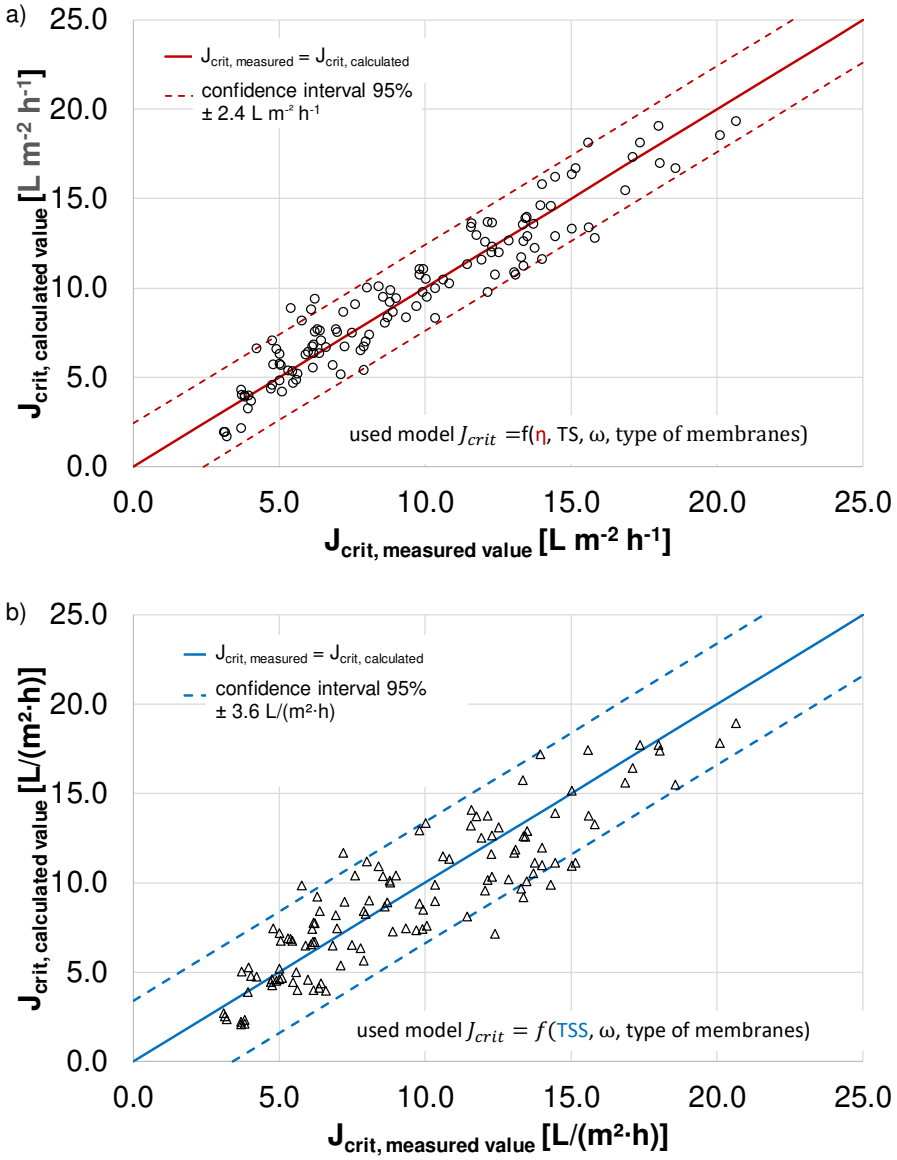

Figure 68. Comparison of measured and calculated values for critical flux using model with measured parameters of apparent dynamic viscosity (a) and calculated viscosities based on TSS (b)

The measurement effort to predict the expected critical flux of a sludge sample can be reduced at the expense of accuracy by integrating the empirical apparent viscosity model proposed by Rosenberger *et al.* (2002; equation 6.9) in the found empirical relationship (expression 6.10). In this work, empirical parameters for calculating apparent viscosity were determined for anaerobic digested sludge (see Table 24). This resulted in a critical flux equation that only depends on the known dimensions of the membrane module, selection of the rotational speed and TSS concentration.

Hence, critical flux can also be predicted in a simplified manner as follows:

$$J_{crit} = 67.079 \cdot \left[e^{a \cdot TSS^b} \cdot \dot{\gamma}_m{}^{c \cdot TSS^d} \right]^{-0.79} \quad (6.14)$$

$$\text{with } \dot{\gamma}_m = \left[0.5133 \cdot \left(\frac{0.001 \cdot e^{a \cdot TSS^b}}{\rho_s} \right)^{-0.5} \cdot (k \cdot \omega)^{1.5} \cdot \frac{r_o^3 - r_i^3}{r_o^2 - r_i^2} \right]^{\frac{1}{0.5 \cdot c \cdot TSS^d + 1.0}} \quad (6.15)$$

$J_{crit} = f(TSS, \omega, \text{type of membranes})$

Where, J_{crit}: critical flux (L/(m²·h))

a-d: empirical parameters for calibration of model (see Table 24)

TSS: concentration of total suspended solids (g/L)

ρ_S: sludge density (kg/m³); calculated according to Pileggi (2016)

k: velocity factor (-); = 0.42 (Ding *et al.*, 2002)

ω: angular velocity (rad/s)

r_o: outer radius of membrane; = 0.156 m

r_i: inner radius of membrane; = 0.04 m

Comparing actual data with values predicted for critical flux using the simplified empirical calculation based on TSS, the accuracy was found to be only slightly worse than with measured dynamic viscosities (see Figure 68b). Around 95 % of the modelled critical flux values had a deviation of less than ±3.6 L/(m²·h) from actual measured values, and 90 % of the values had a deviation of less than ±3.2 L/(m²·h).

6.5. Conclusions

In AnMBR applications that mainly treat particulate organic matter (such as WAS, primary sludge and flotation sludge) at TS concentrations between 2-4.5 %, critical flux from 4 L/(m²·h) to 20 L/(m²·h) resulted.

Critical flux was mainly influenced by the apparent dynamic viscosity as decisive sludge parameter. A significant correlation between the critical flux and the standard apparent viscosity at shear rates of 500 s^{-1} ($R^2 > 0.84$) using different anaerobic sludges and concentrations was observed following a power-law relationship in investigations at 320 rpm. The characteristic sludge parameters TS, VS and CST did not exhibit a clear correlation to the critical flux but showed correct tendencies.

The correlation between apparent viscosity and critical flux can be significantly improved by integrating the present shear rate on the membrane surface ($R^2 = 0.9$). Consequently, an empirical equation (model) was developed to predict the critical flux based on apparent viscosity involving present shear rate on membrane disc. It was found that 95 % of calculated values showed a deviation of less than ±2.4 L/(m²·h) from actual measured values of critical flux.

To further reduce the measurement effort for prediction of the expected critical flux of a sludge sample, an empirical calculation of the apparent viscosity on the basis of TSS concentration was integrated into the previously developed equation. This resulted in a critical flux model that now depends on TSS instead of the apparent dynamic viscosity. The accuracy of this

simplified model is only slightly reduced, as 95 % of the calculated critical flux values only deviated within a range of ±3.6 L/(m²·h) from actual measured values.

Filtration performance can be improved by increasing rotational speed of membrane and adding Fe-salts (here, $FeCl_2$) to the sludge, as both affect apparent viscosity at present shear on membrane disc. An increase of mean cross-flow velocity from 3.8 to 4.1 m/s (rotational speed from 320 rpm to 350 rpm) improves critical flux by 20 %. A dosage of 70 L/ t TS $FeCl_2$ 20 % improves the critical flux up to 30 %. Increased critical flux was also represented by the model. Extending SRT above 20 d neither reduces the apparent dynamic viscosity nor increases the critical flux significantly.

Although these empirical equations (models) for predicting the critical flux apply to a large number of investigated sludges, they were only investigated in one system. The transferability to other disc geometries and other membrane materials is still to be tested. The distance between the discs also certainly has an effect on the flux, which could be taken into account but whose influence could not be investigated within this study. As an outlook, it would be interesting if the models developed based on present shear on the membrane can be transferred to other membranes or sludge samples in the frame of AnMBR applications.

7. Economical Assessment of AnMBRs for Sludge Treatment

In the following sections, a simplified comparison of AnMBR with CSTR from an economic point of view is introduced. First, energy costs of membrane operation are considered in regard to total solids concentration and flux. Second, capital costs and return on investment of two cases are estimated. The two cases considered in this study are:

- The treatment of WAS on a municipal WWTP (see chapter 3 and chapter 7.1)
- The treatment of a substrate mixture of WAS and flotation sludge from the dairy industry (see chapter 5).

As a decisive factor for operating costs an energy-based comparison of both systems is conducted. Capital costs are compared without depreciation. Other costs like downstream sludge dewatering expenditure as well as diverse, difficult to estimate site-specific factors, such as costs for land use, costs for groundwork, ancillary building costs and additional benefits in the operation of the AnMBR which offer higher process stability are not taken into account. In the case of implementation of AnMBR for sludge treatment in the dairy industry, costs for sludge disposal are included although these are also highly site-specific and subject to large variations. However, the inclusion shortens the duration of the return on investment considerably, which is why it should not be omitted at this point.

7.1. Energy costs of membrane operation of rotating discs

Additional energy demand for rotation of membranes in pilot scale varied as a function of total solids concentration as well as rotational velocity. At a membrane rotational speed of 350 rpm energy consumption varied from 3 kWh_{el}/d in solid free tap water, 4 kWh_{el}/d at TS ≈ 4 % and up to 5 kWh_{el}/d at TS > 5 % (Figure 69a). The given values are based on a membrane operation cycle with a filtration length of 8 minutes followed by a 30 sec break of rotation for degassing and backwashing. The relationship between energy demand and total solids concentration is exponential. Particularly, increases of TS over 3.5 % boost the energy demand (Figure 69a). Higher concentrations of solids also impair the filterability in terms of critical flux (Figure 69; also see chapter 0). The critical flux shown was calculated with the elaborated expression to predict critical flux based on TSS, rotation velocity and type of membrane module (chapter 6.4; equation 6.12 with 6.13). When evaluating the filtrate yield as a function of effort (energy input for rotation and required membrane surface based on the critical flux), it becomes clear that especially lower TS concentrations improve the efficiency of the investigated membrane module Figure 69b). This is especially due to the strong exponential increase of critical flux at reduced TS-concentrations, which changes much more depending on the TS than the energy demand.

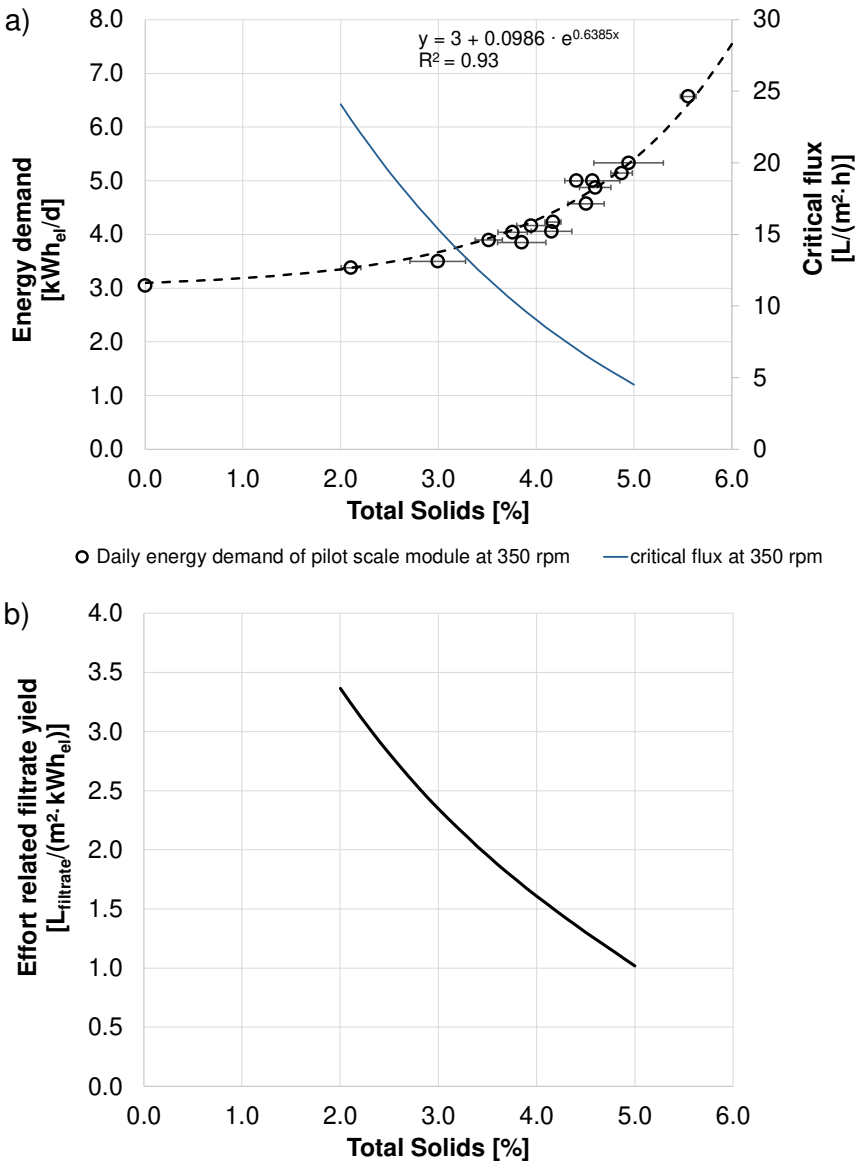

Figure 69. Daily energy demand and critical flux for the operated membrane unit in pilot scale with A = 3.36 m², membrane rotational speed of 350 rpm (a) and effort related filtrate yield based on energy demand and membrane surface required (b)

In large scale, design of the membrane module and aggregates would be similar, but membrane module size would be extended to 10 m² by elongating the hollow shaft. Concerning ball bearings and axial face seals, equal energy demands of around 3.0 kWh_{el}/d were assumed for the membrane units in pilot and large scale when operated in water (dynamic viscosity ~ 1.0 mPa·s). Higher energy demands based on higher torques of membranes in viscous fluids must be considered in case of upscaling.

Here, a simplified linear increase was assumed:

$$E_{large\ scale} = (E_{pilot\ scale} - E_0) \cdot \frac{A_{large\ scale}}{A_{pilot\ scale}} + E_0 \qquad (7.1)$$

Where, $E_{large\ scale}$: daily energy consumption for rotation of membrane module in large scale (kWh_{el}/d)

$E_{pilot\ scale}$: daily energy consumption for rotation of membrane module in pilot scale (kWh_{el}/d)

E_0: daily energy consumption for rotation of membrane module in clear water (kWh_{el}/d) (=3.0 kWh_{el}/d)

$A_{large\ scale}$: membrane surface of module in large scale (m^2); here $A_{large\ scale}$ = 10.0 m^2

$A_{pilot\ scale}$: membrane surface of module in pilot scale (m^2); here $A_{pilot\ scale}$ = 3.36 m^2

Overall, a reduction of specific energy demand for rotation of membranes from pilot scale to large scale around 50 % might be achievable (Table 28). In addition, the energy consumption can be set in relation to the filtration performance by taking into account the daily produced filtrate volume per module. Filtrate related energy consumption is therefore additionally dependent on operational long-term flux the so-called sustainable flux. Assuming a sustainable flux in the range of (0.6-0.8)·J_{crit} according to Dagnew (2010), Dereli *et al.* (2014a) and Judd (2011), Table 28 summarises the dependence of the filtrate flow related energy demand on rotational speed for the membrane unit when filtrating a sludge with a TS content of 3.5 %. A reduction of the rotation speed to lower the energy demand leads to the contrary effect as much more membrane surface is required for filtration of a specific filtrate volume which is due to lower critical flux achieved at reduced rotation velocity. The energy expenditure per produced filtrate volume therefore increases when the rotation speed is reduced. Consequently, a filtration at 350 rpm is more favorable than applying lower rotational speeds.

Table 28. Energy demand for rotation of filter in pilot scale and large scale at total solid contents around 3.5 % and various rotational speeds

long-term flux in operation	Energy demand [kWh_{el}/m^3 filtrate] at TS ≈ 3.5 %					
	3.36 m² Pilot Scale			10 m² Large Scale		
	280 rpm	320 rpm	350 rpm	280 rpm	320 rpm	350 rpm
0.6·J_{crit}[a]	9.7	8.2	6.9	4.7	4.2	3.3
0.8·J_{crit}[b]	7.3	6.1	4.9	3.5	3.1	2.3
J_{crit}[c]	5.8	4.9	4.1	2.8	2.5	1.9

[a] sustainable flux with J = 0.6·J_{crit};
[b] sustainable flux with J = 0.8·J_{crit};
[c] J_{crit} was calculated with the formula for predicting critical flux based on TSS = 3.5%, rotational speed = 350 rpm and type of membrane module developed in chapter 6.4; 280rpm: 6 L/(m²·h); 320 rpm: 9 L/(m²·h); 350 rpm: 12 L/(m²·h)

Figure 70 provides specific energy demands for a membrane module in large scale with A = 10 m², when operated with a rotational speed of 350 rpm. Due to integration of sustainable flux, the relationship between (specific) energy demand and total solids concentration compared is even more unfavorable. Therefore, a TS = 3.5 % seems to be a limit for an energetically reasonable operation of membranes.

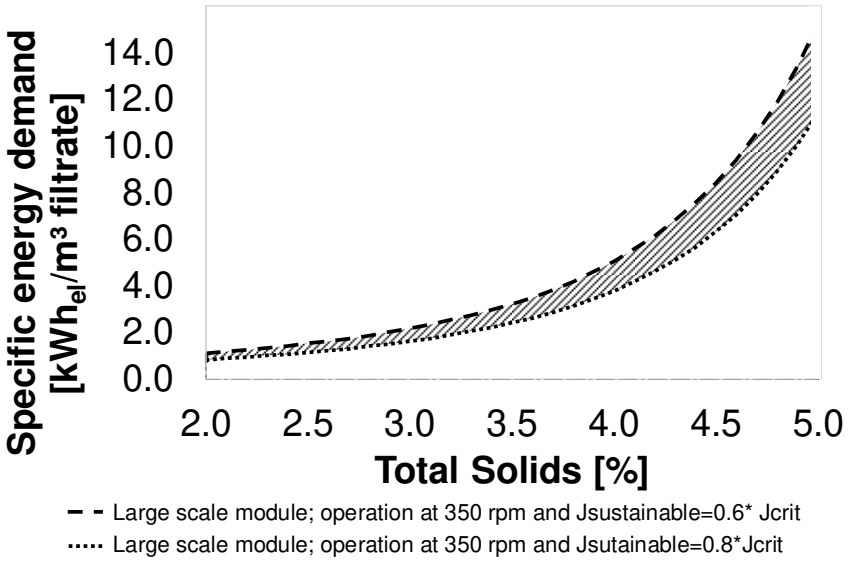

Figure 70. Calculated specific energy demand for a membrane unit in large scale with A = 10 m², operated with a sustainable flux at membrane rotational speed of 350 rpm

7.2. Comparison of AnMBR and CSTR treating WAS

Exemplarily, 100 m³/d WAS with 4 % TS, 3 % VS and a maximum COD removal of 45 % are to be treated. Substrate characteristics are given in Table 16. Maximum methane yield and disintegration constant k_{dis} are given in Table 18. AnMBR and CSTR are compared both in terms of equal HRT and SRT. Mass flows are given in Figure 71 and Figure 72. Calculation of COD degradation, methane flow and outlet values can be found in Table A 8 in the annex. Mixing of digester was assumed to be realised by a screw conveyor (DWA-A 216, 2015). Circulation for heating was assumed to require a daily exchange of digester volume (DWA-A 216, 2015). The installation of the membrane module could be realised in the heating circuit. Therefore, no additional pumps for feeding are required, because feed flow (approx. ten times of filtrate flow) is smaller than required flow for heating flow (approx. daily exchange of digester volume).

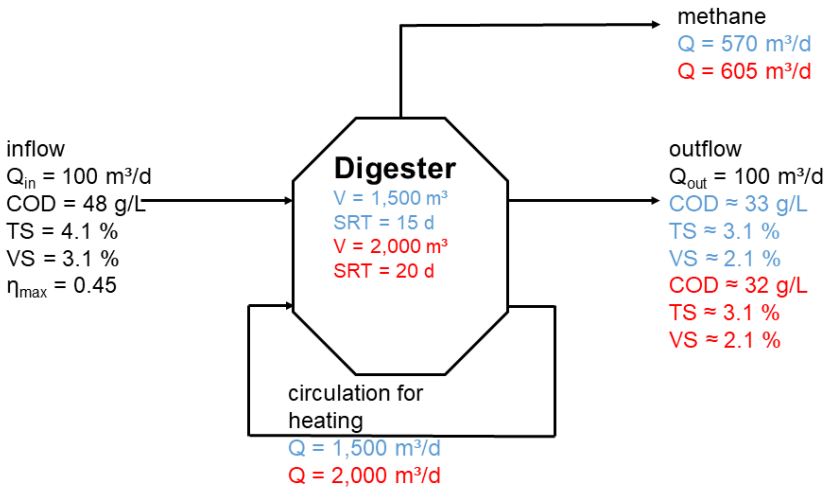

Figure 71. Expected flows of CSTR operated with SRT = 15 d (in blue) and SRT = 20 d (in red)

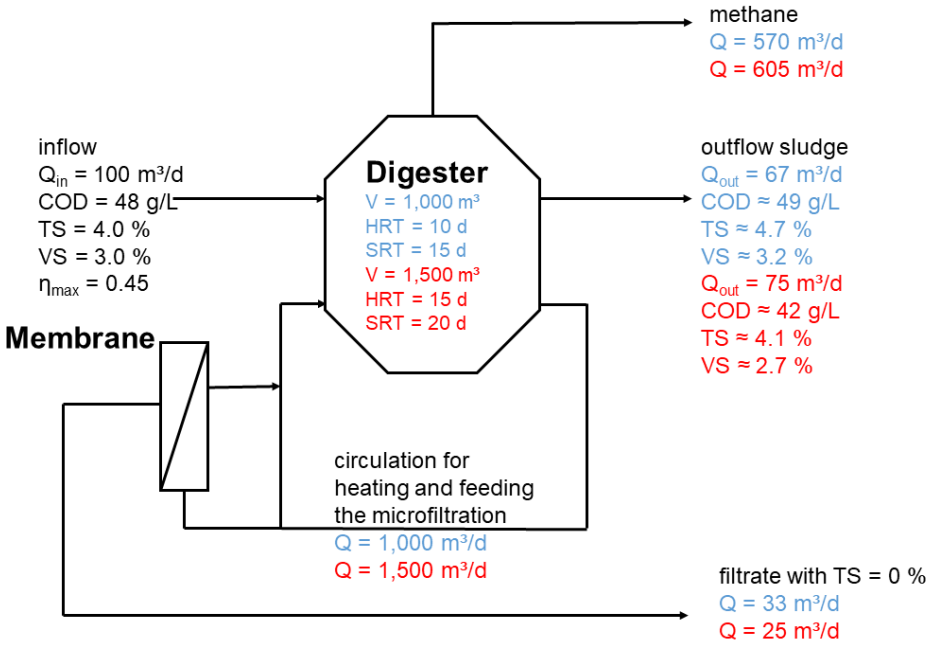

Figure 72. Expected flows of AnMBR operated with HRT = 10 d and SRT = 15 d (in blue) and with HRT = 15 d and SRT = 20 d (in red)

These mass balances are the fundamentals for the energy balance given in Table 29. Electric energy requirements for sludge circulation for heating purposes and feeding of the membrane modules are calculated in consideration of a specific energy requirement of the sludge pump, a minimum flow required, and the total pump head based on head loss in piping and additional head loss of the membrane module. Calculation is given in Table 29. Specific energy consumption of sludge pumps used on WWTPs are around 4.5 W/(m³·m) (DWA-A 216, 2015). A pressure head loss of 2.5 m water column was assumed in CSTRs. Additional head losses of 1 m WC were considered in AnMBRs as head losses of 0.5 m WC were observed in pilot scale independent from TS content. The effect of variation in TS content between 3.2-4.7 % on head loss over a length of 100 m at a velocity of 1.0 m/s are negligible because values differ just slightly (0.4-0.8 m water column) (Reichel, 2015) and are much lower than assumed head loss according to DWA-A 216 (2015).

Table 29. Energy Balance - CSTR and AnMBR for treating 100 m³/d WAS

Energy[1] in kWh/d	CSTR HRT = 15 d SRT = 15 d	AnMBR HRT = 10 d SRT = 15 d	CSTR HRT = 20 d SRT = 20 d	AnMBR HRT = 15 d SRT = 20 d
E_{mixing}[2]	-110	-70	-140	-110
$E_{heating\ circuit}$[3]	-17	-15	-22	-24
$E_{membrane\ rotation}$[4,5]		-260[4]		-100[5]
$E_{methane}$[6]	1,980	1,980	2,120	2,120
Net electric energy[7]	1,853	1,635	**1,958**	1,886
Heat loss[8]	-210	-160	-240	-210
Total energy balance[9]	1,643	1,475	**1,718**	1,676

[1] Energy consumptions are negative values while energy gains are positive values
[2] $E_{mixing} = V_{digester} \cdot e_{spec} \cdot 24$ h/d / 1000 with e_{spec} = 3 W/m³ using a screw conveyor (DWA-A 216, 2015)
[3] $E_{heating\ circuit} = Q_{circulation} \cdot e_{spec.,\ sludge\ pump} \cdot H$
with $Q_{circulation} = 1.0 \cdot V_{reactor}$ (DWA-A216. 2015); $e_{spec.,\ sludge\ pump}$ = 4.5 Wh/(m³·m) (DWA-A 216, 2015), assumed total pump head H = 2.5 m WC in CSTRs based on DWA-A 216 (2015); additional head loss of 1 m WC in AnMBRs
[4] $E_{membrane\ rotation} = Q_{filtrate} \cdot e_{spec.,\ membrane}$
with $e_{spec.,\ membrane}$ = 7.9 kWh/m³ filtrate for 350 rpm and J = 0.8·Jcrit=4.6 L/(m²·h) (see Figure 70);
[5] $E_{membrane\ rotation} = Q_{filtrate} \cdot e_{spec.,\ membrane}$
with $e_{spec.,\ membrane}$ = 4.1 kWh/m³ filtrate for 350 rpm and J = 0.8·Jcrit=6.8 L/(m²·h) (see Figure 70);
[6] caloric value methane H_{CH4} = 10 kWh/m^3_N, η_{CHP} = 0.35
[7] Net electric energy = $P_{external\ circulation} + P_{membrane} + P_{methane}$
[8] Heat loss = $A_{reactor\ surface} \cdot U \cdot \Delta T$
with reactor design: cylindrical with height H to diameter D ~ 1 (DWA-M 368 (2014)) and an additional free board for gas of 2 m in height;
CSTR with HRT = 15 d: $V_{reactor,water}$ = 1,500m³, $V_{reactor,total}$ = 1,800 m³, D = 12.5 m, H = 14.5 m;
AnMBR with HRT 10 d: $V_{reactor,water}$ = 1,000 m³, $V_{reactor,total}$ = 1,250 m³, D = 11 m, H = 13 m;
CSTR with HRT = 20 d: $V_{reactor,water}$ = 2,000 m³, $V_{reactor,total}$ = 2,300 m³ D = 13.75 m, H = 15.5 m;
AnMBR with HRT = 15 d: $V_{reactor,water}$ = 1,500m³, $V_{reactor,total}$ = 1,800 m³, D = 12.5 m, H = 14.5 m;
coefficient of heat transmission U = 0.4 W/(m²·K) (DWA-A 216, 2005);
Temperature difference $\Delta T = T_{reactor} - T_{ambient\ temperature}$ = 37 °C - 10 °C
[9] Total Energy Balance = Net electric energy + Heating loss

It is shown that at similar SRT, increased electrical expenses of AnMBR membrane operation (see Table 29) cannot be compensated by lower electric energy requirements for mixing based on smaller reactor volumes. Nevertheless, more electric energy is generated by CHP units burning methane than required for mixing and membrane operation. CSTR with a SRT of 20 d might have slight advantages from an energetic point of view compared to the other digesters. Taking heat losses for a total energy balance into account AnMBR does not differ significantly from the standard process CSTR at similar SRT. Energetic disadvantages of AnMBR are even smaller in case of higher losses of pressure in the pipes or higher pump heads required. This is consistent with the experience of Dagnew (2010) and Dvorak *et al.* (2016), who state advantages of AnMBR in particular when SRT are extended compared to the CSTR.

Table 30. Simplified estimation of capital costs for CSTR and AnMBR treating 100 m³/d WAS

Capital costs in euro[1]	CSTR HRT = 15 d SRT = 15 d	AnMBR HRT = 10 d SRT = 15 d	CSTR HRT = 20 d SRT = 20 d	AnMBR HRT = 15 d SRT = 20 d
Digester[2]	1,875,000	1,425,000	2,254,000	1,872,000
Membranes[3]		2,700,000		1,350,000
Additional[4]		50,000		50,000
Total	**1,875,000**	4,175,000	2,254,000	3,272,000
Break-even specific membrane costs at similar SRT with		660 €/m²		1,100 €/m²

[1] Depreciation and amortization were not considered; life time = 30 years
[2] Digester costs: life time = 30 years, specific costs were calculated according to AbwAnlZuwV HE (2006) in combination with person equivalent specific sludge mass given in DWA-M 368 (2014) (see annex)
CSTR with HRT = 15 d: $V_{reactor,total}$ = 1,800 m³, specific costs = 1,040 €/m³;
AnMBR with HRT 10 d: $V_{reactor,total}$ = 1,250 m³, specific costs = 1,140 €/m³;
CSTR with HRT = 20 d: $V_{reactor,total}$ = 2,300 m³, specific costs = 980 €/m³;
AnMBR with HRT = 15 d: $V_{reactor,total}$ = 1,800 m³, specific costs = 1,040 €/m³;
[3] Membrane costs ~ 4,500 €/m² (Mohr, 2011); AnMBR with SRT = 15d: J_{net} = 4.6 L/(m²·h) for SRT = 15 d and with SRT = 20d: Jnet = 6.8 L/(m²·h); life time = 15 years
[4] additional costs are measuring technology for membrane operation and a CIP tank; total costs of 50,000 €

In a simplified evaluation of the capital costs, disadvantages of the AnMBR become obvious. 80 percent of the critical flux were expected as net flux. On the basis of these net fluxes and specific membrane costs of around 4,500 €/m² (Mohr, 2011), the AnMBR is significantly more expensive than the CSTR in terms of invest (Table 30). Specific membrane costs must be reduced down to around 1,100 €/m² for SRT = 20 d or below 660 €/m² for SRT = 15 d in order to equalise capital costs between AnMBR and CSTR treating WAS operated at similar SRT.

7.3. Comparison of AnMBR and CSTR treating WAS and flotation sludge

Sludge treatment of the dairy industry as described in Chapter 4, needs to cope with 20 m³/d of WAS and 20 m³/d of flotation sludge. Substrate characteristics are given in Table 16. Maximum methane yield and disintegration constant k_{dis} are given in Table 18. AnMBR and CSTR are compared both in terms of equal HRT and SRT. A CSTR with a SRT of 15 days is considered as standard and compared to an AnMBR operated with reduced HRT = 12 d, and a CSTR and an AnMBR with extended sludge retention times of SRT = 20 d. Mass flows are given in Figure 73 and Figure 74. Calculation of COD degradation, methane flow and outlet values are given in Table A 9 in the annex. Required circulation for heating of digester was assumed to require a daily exchange of digester volume (DWA-A 216, 2015). Mixing of digester was assumed to be realised by screw conveyors. Following assumptions made in previous chapter 7.2, the installation of the membrane module could be realised in the heating circuit. Therefore, no additional pumps for feeding are required, because feed flow (approx. ten times of filtrate flow) is smaller than required flow for heating flow (approx. daily exchange of digester volume).

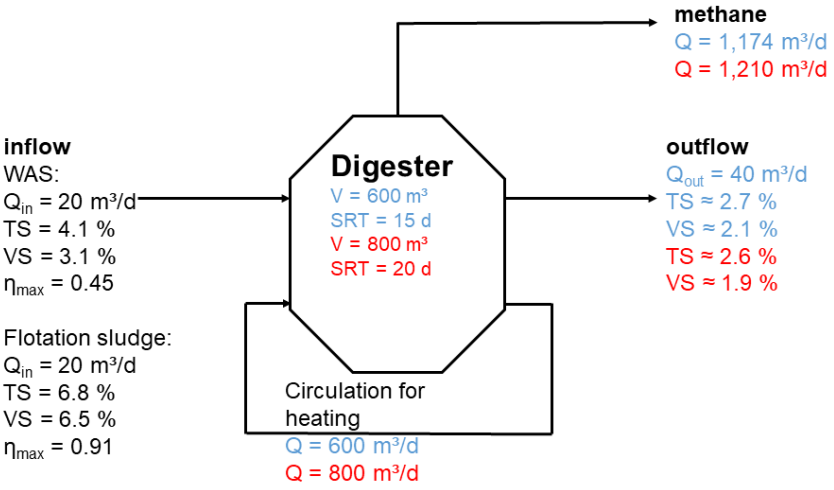

Figure 73. Expected flows of CSTRs operated with SRT = 15 d (in blue) and SRT = 20 d (in red) treating 20 m³/d of WAS and 20 m³/d of flotation sludge from the dairy industry

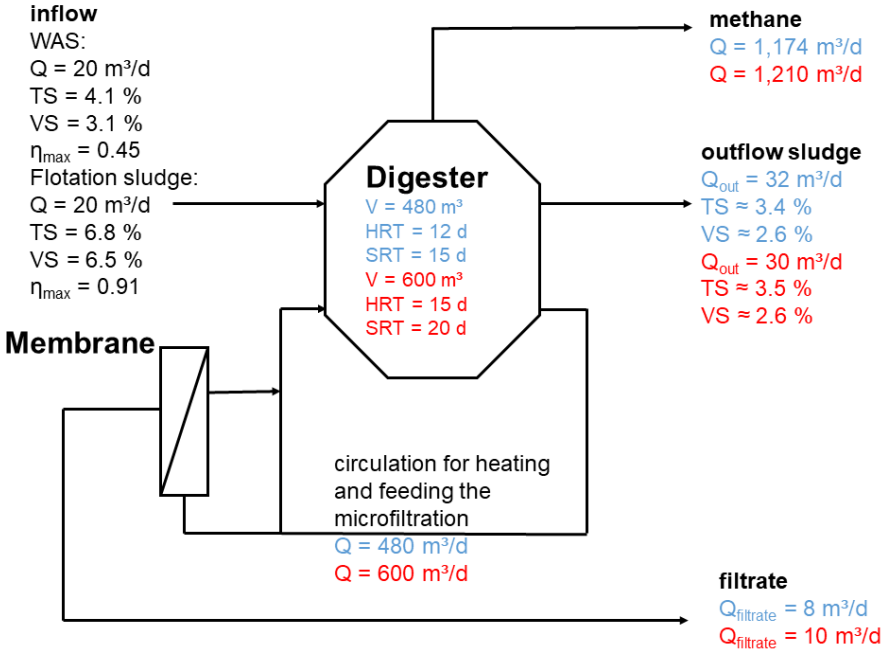

Figure 74. Expected flows of AnMBR operated with HRT = 12 d and SRT = 15 d (in blue) and with HRT = 15 d and SRT = 20 d (in red) treating 20 m³/d of WAS and 20 m³/d of flotation sludge from the dairy industry

These mass balances are the fundamentals for the energy balance given in Table 31. Assumptions concerning electric energy requirements for sludge circulation, pressure losses are equal to the ones provided in the previous chapter 7.2. Comparing AnMBR with CSTR at similar SRT, membrane operation consumes slightly more energy than saved for heating (Table 31). Overall, consumed energy is negligible as energy generated in terms of methane is much higher. Reactors operated with SRT = 20 d are more energy efficient than reactors with SRT = 15 d because higher COD removal and methane generation is achieved by extending SRT. Extending sludge retention time from 15 to 20 days by implementation of a membrane does not lead to a strong change in the energy balance (Table 31). Additional energy expenditure for operation of the membrane is compensated by extra generated methane.

Table 31. Energy Balance - CSTR and AnMBR treating 20 m³/d of WAS and 20 m³/d of flotation sludge from the dairy industry

Energy[1] in kWh/d	CSTR HRT = 15 d SRT = 15 d	AnMBR HRT = 12 d SRT = 15 d	CSTR HRT = 20 d SRT = 20 d	AnMBR HRT = 15 d SRT = 20 d
E_{mixing}[2]	-43	-35	-58	-43
$E_{heating\ circuit}$[3]	-8	-8	-9	-9
$E_{membrane}$[4,5]		-18[4]		-24[5]
$E_{methane}$[6]	4,110	4,110	4,240	4,240
Net electric Energy[7]	4,059	4,049	**4,173**	4,164
Heating loss[8]	-114	-102	-138	-114
Total energy balance[9]	3,945	3,947	4,035	**4,050**

[1] Energy consumptions are negative values while energy gains are positive values
[2] $E_{mixing} = V_{digester} \cdot e_{spec} \cdot 24$ h/d / 1000 with e_{spec} = 3 W/m³ using a screw conveyor (DWA-A 216, 2015)
[3] $E_{heating\ circuit} = Q_{circulation} \cdot e_{spec.,\ sludge\ pump} \cdot H$
with $Q_{circulation}$ = 1.0 · $V_{reactor}$ (DWA-A216. 2015); $e_{spec.,\ sludge\ pump}$ = 4.5 Wh/(m³·m) (DWA-A 216, 2015), assumed total pump head H = 2.5 m WC in CSTRs based on DWA-A 216 (2015); additional head loss of 1 m WC in AnMBRs
[4] $E_{membrane} = Q_{filtrate} \cdot e_{spec.,\ membrane}$
with $e_{spec.,\ membrane}$ = 2.0 kWh/m³ filtrate for 350 rpm and J = 0.8·Jcrit=10.5 L/(m²·h) (see Figure 70)
[5] $E_{membrane} = Q_{filtrate} \cdot e_{spec.,\ membrane}$
with $e_{spec.,\ membrane}$ = 2.4 kWh/m³ filtrate for 350 rpm and J = 0.8·Jcrit=9.5 L/(m²·h) (see Figure 70)
[6] caloric value methane H_{CH4} = 10 kWh/m³$_N$, η_{CHP} = 0.35
[7] Net electric energy = $P_{external\ circulation} + P_{membrane} + P_{methane}$
[8] Heat loss = $A_{reactor\ surface} \cdot U \cdot \Delta T$
with reactor design: cylindrical with height H to diameter D ~ 1 (DWA-M 368 (2014)) and additional freeboard for gas of 2m in height,
CSTR with HRT = 15 d: $V_{reactor,water}$ = 600 m³, $V_{reactor,total}$ = 700 m³, D = 9 m, H = 11 m;
AnMBR with HRT = 12 d: $V_{reactor,water}$ = 480 m³, $V_{reactor,total}$ = 600 m³, D = 8.5 m, H = 10.5 m;
CSTR with HRT = 20 d: $V_{reactor,water}$ = 800 m³, $V_{reactor,total}$ = 950 m³, D = 10 m, H = 12 m;
AnMBR with HRT = 15 d: $V_{reactor,water}$ = 600 m³, $V_{reactor,total}$ = 700 m³, D = 9 m, H = 11 m;
coefficient of heat transmission U = 0.4 W/(m²·K) (DWA-A 216, 2005);
Temperature difference $\Delta T = T_{reactor} - T_{ambient\ temperature}$ = 37 °C - 10 °C
[9] Total Energy Balance = Net electric energy + Heating loss

However, it is clear from the previous chapter 7.2 that the AnMBR has disadvantages in terms of capital costs compared to the CSTR. Treating a mixture of WAS and flotation sludge, economic disadvantages are not as strong as for the treatment of WAS. Required specific membrane costs at similar SRT are around 2,600 €/m² which are 50 % of the specific membrane cost of 4,500 €/m² according to Mohr (2011) (Table 32). Less drawbacks result from the lower membrane surface required and higher volume-related costs of digesters.

Lower membrane surface needs to be installed due to higher achievable net flux during operation. It was assumed that a net flux around 10 L/(m²·h) can be achieved at expected TS around 3.5 % in the reactor (see Figure 74, Table A 9 and expression 6.14 in chapter 6.4).

Table 32. Simplified estimation of capital costs for CSTR and AnMBR treating 20 m³/d of WAS and 20 m³/d of flotation sludge from the dairy industry

Capital costs in euro[1]	CSTR HRT = 15 d SRT = 15 d	AnMBR HRT = 12 d SRT = 15 d	CSTR HRT = 20 d SRT = 20 d	AnMBR HRT = 15 d SRT = 20 d
Digester[2]	910,000	820,000	1,159,000	910,000
Membranes[3]		300,000		390,000
Additional[4]		25,000		25,000
Total	**910,000**	1,145,000	1,159,000	1,325,000
Break-even specific membrane costs at even SRT with		980 €/m³		2,600 €/m²
Return on investment[5] with sludge disposal costs of 50 €/ t TS[6]	3.5 years	4.3 years	4.2 years	4.7 years

[1] Depreciation and amortization were not considered; life time = 30 years
[2] Digester costs: life time = 30 years, specific costs were calculated according to AbwAnlZuwV HE (2006) in combination with person equivalent specific sludge mass given in DWA-M 368 (2014) (see annex)
CSTR with HRT = 15 d: $V_{reactor,total}$ = 700 m³, specific costs = 1,300 €/m³;
AnMBR with HRT 12 d: $V_{reactor,total}$ = 600 m³, specific costs = 1,360 €/m³;
CSTR with HRT = 20 d: $V_{reactor,total}$ = 950 m³, specific costs = 1,220 €/m³;
AnMBR with HRT = 15 d: $V_{reactor,total}$ = 700 m³, specific costs = 1,300 €/m³;
[3] Membrane costs ~ 4,500 €/m² (Mohr, 2011); life time = 15 years;
AnMBR with SRT = 15d: J_{net} = 10.5 L/(m²·h); AnMBR with SRT = 20 d: Jnet = 9.5 L/(m²·h);
[4] additional costs are measuring technology for membrane operation and a CIP tank; total costs of 25,000 €
[5] Return on investment = Capital costs /(yearly savings electric energy+yearly savings sludge disposal) with electricity costs of 0.15 €/kWh_{el};
[6] sludge disposal costs can vary between 25 €/ t TS for use in agricultural up to 130 €/ t TS sludge for incineration (Schumacher and Nebocat, 2009)

Sludge treatment of residues from dairy industry is economical feasible. Basically, for all systems, a return on investment period (ROI) of less than 5 years seems achievable, if investment costs are offset with savings from power generation and lower expenses for sludge disposal. For all systems, these periods can be significantly reduced with lower specific digester and/or membrane costs. With regard to operation at similar SRT, CSTRs are currently the economically most promising option. However, in this scenario reduced membrane costs and additional "soft factors" like hardly calculable potential for higher process stability of the AnMBR (see chapter 5) may also provide economic advantages for its implementation.

7.4. Conclusions

Although these fundamental considerations were made with many uncertainties and therefore can only show general tendencies, viability of the AnMBR system in both previously introduced cases compared to CSTR depends on the applied flux, costs for digester and especially the development of the specific membrane costs.

Higher volume-related costs of digesters allow higher maximum allowed specific membrane costs for achieving profitability of AnMBR. Higher volume-related costs are mostly encountered in applications with smaller reactor volumes or lower sludge mass to be treated (see Figure 75 and cost function of digesters provided in the annex E).

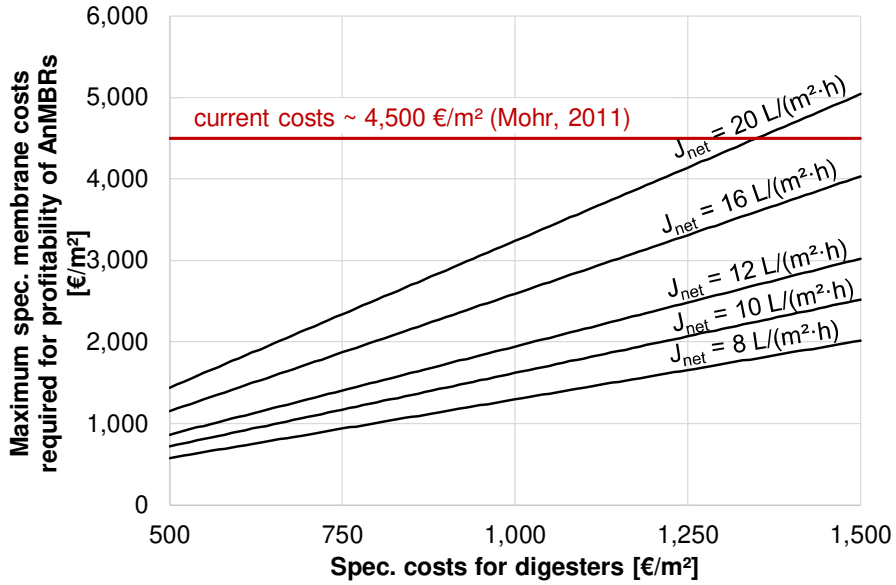

Figure 75. Maximum specific membrane costs required for viability of AnMBRs compared to CSTRs in dependence of specific digester costs and net flux at even SRT, decoupling factor of 1.5 and a lifetime of membranes of 15 years

Membrane operation with higher net flux results in case of lower TS concentration of the anaerobic sludge. This effect is especially pronounced in applications treating high shares of fully degradable substrates such as flotation sludge.

Specific membrane costs possibly will drop with increasing number of installations (Churchhouse and Wildgoose, 1999, Mohr, 2011). For aerobic MBR systems, specific costs for hollow fiber membranes used in MBRs declined to a level of 20 % of the original price over a period of 10 years after the number of installed systems increased (Churchhouse and Wildgoose, 1999). This decline is in a range required for viability of AnMBR in both previously introduced cases. Costs of the membrane can also be reduced if the lifetime of membranes can be significantly extended over 15 years as expected.

As general conclusion, AnMBRs are economically most viable in applications facing

- operation at low TS,
- high shares of fully degradable substrates (or high shares of soluble substrates) and
- small scale applications.

8. Final Conclusions and Outlook

8.1. Final conclusions

A mixture of WAS and lipid-rich flotation sludge from the dairy industry with high COD-related shares of lipids (> 0.9) was successfully treated using CSTRs and an AnMBR in pilot scale. The application was challenging owing to potential inhibition of methanogens. An AnMBR using rotating ceramic discs as membranes for particulate-rich sludge digestion was successfully operated for more than four years in pilot scale.

During pilot trials, over the test duration, the membranes showed no significant aging effect in terms of reduction in permeability after chemical cleaning. Shear forces resulting from cross-flow velocities applied to reduce cake layer formation on the membrane surface apparently did not negatively affect the activity or decay of acetoclastic methanogens. Therefore, an AnMBR equipped with rotating ceramic discs is basically suited for application as sludge digester. AnMBR provides the following benefits over conventional fill-and-draw CSTRs:

- reduction of reactor volumes at similar COD removal,
- extension of SRT and increase of COD removal at similar HRT (= digester volume) and
- improvement of process stability and spare capacities for organic load.

COD removal kinetics

Common models following substrate first-order kinetics approach, as used e.g. in ADM1 (Batstone *et al.*, 2002), are suitable to describe degradation kinetics, COD removal and methane yields in AnMBR used for sludge treatment. SRT decisively determines COD removal. Hence, COD removal of an AnMBR corresponds to the performance of a CSTR at even SRT. COD removal is improved in AnMBR compared to CSTR when SRT is extended by membrane filtration. Therefore, an AnMBR could be operated with higher OLR than a CSTR. Additional effects boosting COD removal such as increased substrate degradability, higher disintegration constants or higher biomass related constants were not observed in the pilot scale investigation of the AnMBR.

Treatment of lipid-rich sludge

Achieved COD loading rates, lipid-related loading rates and shares of flotation sludge exceeded design recommendations of Dereli *et al.* (2014b), DWA M-368 (2014) and Mata-Alvarez *et al.* (2014). CSTRs could be operated with a maximum $OLR_{COD,deg}$ = 8.3 kg COD/(m³·d) corresponding to OLR_{FS} = 2.7 kg VS/(m³·d) at SRT = 15 d. Similar maximum tolerable OLR of $OLR_{COD,deg}$ = 7.7 kg COD/(m³·d) corresponding to OLR_{FS} = 2.5 kg VS/(m³·d) was achieved in CSTR operated at SRT = 11 d. Using an AnMBR with HRT = 10 d and SRT = 15 d, an OLR of 11.2 kg COD_{deg}/(m³·d) or 3.8 kg VS_{FS}/(m³·d) did not lead to process instabilities. Specific lipid loading rates up to 0.18 kg lipid/(kg VS·d) were observed. Applicable specific lipid load was slightly higher than recommendations, which range from 0.04-0.13 kg lipid/(kg VS·d) according to Dereli *et al.* (2014) and Szabo-Corbacho *et al.* (2019). Furthermore, the treatment of high

shares of easily degradable substrates (flotation sludge) did not negatively influence degradation of slowly degradable substrates such as WAS.

Process limitations could not be observed from methane generation and only limited from concentrations of organic acids but on the basis of SMA measurements. Emerging inhibition and emerging process instabilities were clearly shown when measured safety factors SF were compared with safety factors calculated from non- or, at least, low-inhibited operation phases (SF_0). Consequently, regular monitoring of SMA during operation of high-solid digestion with industrial readily degradable substrates is recommended. Process stability and maximum tolerable organic loads depended mainly on residual lipid concentration in the anaerobic sludge. The digestion process remained stable up to a residual degradable lipid content of 150 mg lipid/g TS, although inhibition of acetoclastic methanogens started at 50 mg lipid/g TS. Values were in the range proposed by other authors (e.g., Ziels *et al.*, 2016; Szabo-Corbacho *et al.*, 2019). As a limiting value, the degradable lipid content of the anaerobic sludge generally should remain between 50-100 mg lipid/g TS. Lower degradable lipid content in the anaerobic sludge can be achieved with elevated SRT or reduced shares of lipid-rich substrates.

This study shows that common design criteria such as the OLR or the lipid-related sludge load do not assure a stable or efficient digestion process. Owing to the limitations on the applicability of existing design parameters, a generally valid design criterion for lipid-rich digestion – the maximum degradable lipid content in the anaerobic sludge – was elaborated. This criterion refers to the current state of knowledge on LCFA inhibition: inhibition of methanogens is initiated by the LCFA concentration related to the TS content in the sludge (Hwu *et al.*, 1996; Pereira *et al.*, 2002; Ziels *et al.*, 2016). The elaborated expression of the maximum degradable lipid content in the anaerobic sludge covers all influencing parameters such as SRT, kinetic coefficients k_{dis}/k_{hyd}, lipid share and inorganic/inert solids in the reactor.

Anaerobic sludge digestion plants may also be operated at strong fluctuations of daily load. The organic acid concentration and SMA are particularly suitable as process variables for a simple process control loop. Methane yield, methane content in the biogas and pH value are just as unsuitable as fixed limits to counteract load fluctuations of COD or sludge loading rates. The suitability of SMA for process control was demonstrated using results of continuously operated reactors investigated in pilot scale. Assuming that around 70 % of organic matter gets degraded via acetate, concentration in the reactor remains below 1,000 mg HAc/L as long as mean acetoclastic sludge loading rate for last SRT remains below the SMA. Process disturbances (VFA > 2,000 mg HAc/L) occurred when sludge loading rate exceeded SMA, as observed in the last 20 days of each trial. The decisive factor for coping with these fluctuations was the spare loading capacity of the AD reactor. Spare capacities for load variations of sludge digestion maintain sufficient process stability and can be expressed also using SMA as a key parameter.

Based on these fundamental investigations, AnMBR provides advantages either in the decrease of reactor volumes without neglecting process stability by reducing HRT at even SRT or in increase of removal performance and process stability without raising reactor volume by extending SRT. COD removal and process stability of an AnMBR correspond to that of a CSTR operated at even SRT. RT improves process stability against substrate overload and accumulation of organic acids when SRT is extended. AnMBR shows advantages over CSTR due to lower sludge loads and higher spare loading capacities (e.g., defined as SF) at equal COD

loading rates. In the investigated case of co-digestion of flotation sludge from dairy industry with WAS, higher process stability was observed in AnMBR at similar fluctuations of daily load.

Membrane performance

In the field of sludge digestion, membrane performance in terms of the critical flux depends in particular on the apparent dynamic viscosity as decisive sludge characteristic parameter. A higher apparent viscosity reduces the flux. The characteristic sludge parameters TS, VS and CST did not exhibit a clear correlation to the critical flux but showed correct tendencies. The correlation between apparent viscosity and critical flux can be significantly improved by integrating the present shear rate on the membrane surface (R^2 = 0.9). For the tested membrane module configuration the relationship between the apparent viscosity at present shear on membrane surface and the critical flux can be represented empirically on the basis of measured data (see Section 6.4 for detailed information):

$$J_{crit} = 67.079 \cdot (\eta_a(\dot{\gamma}_m))^{-0.79}$$

95 % of modelled values using this expression showed a deviation of less than ±2.4 L/(m²·h) from actual measured values of critical flux. To further reduce the measurement effort spent in predicting the expected critical flux of a sludge sample, an empirical apparent viscosity calculation was integrated into the abovementioned equation. This resulted in a critical flux equation that only depends on TSS as well as geometric and flow-related parameters of the membrane module. The accuracy of this simplified equation is only slightly less, as 95 % of the modelled critical flux values deviated within a range of ±3.6 L/(m²·h) from actual measured values.

Filtration performance can be improved by increasing the rotational speed of the membrane and adding Fe salts (here $FeCl_2$) to the sludge, as they affect shear stress on the membrane disc and apparent dynamic viscosity, respectively. An increase of rotational speed from 320 rpm to 350 rpm improved critical flux by 20 % (increase of mean cross-flow from 3.8 m/s to 4.1 m/s). A dosage of 70 L/ t TS $FeCl_2$ 20 % improved the critical flux up to 30 %. Increased critical flux values were also represented by the model equation. In the study, a maximum critical flux of approx. 17 L/(m²·h) was achieved when filtrating sludge with TS ≈ 3 %. These results agree with the findings of Badenova AG & Co. KG (2005), which used similar membranes, and are slightly higher than the results of Dagnew (2010), who achieved a flux of 16 L/(m²·h) at TSS = 32 g/L using tubular PVDF membranes in long-term investigations. At TS ≈ 4.0 % and TS ≈ 4.6 %, maximum critical fluxes of around 14 L/(m²·h) and 8 L/(m²·h) were observed, respectively.

The treatment of lipid-rich substrates had no negative effect on the critical flux compared to the effect of treatment with WAS at the same TS content.

Economic viability

The economic viability and, consequently, large-scale implementation of AnMBR for sludge digestion particularly depend on the capital costs. Capital costs are predominantly determined by the membrane flux. Increasing energy requirements for membrane operation can be compensated by advantages of lower heat loss based on smaller digester volumes or higher methane yields at similar digester volumes. In AnMBR, the energy demand for membrane rotation

is around 1.0–2.5 kWh_{el}/m^3 filtrate at a TS concentration of 3.5 % and corresponding critical flux of around 12 $L/(m^2 \cdot h)$.

Based on these boundary conditions, a clear economic viability of AnMBR using rotating disc filters can only be achieved by decreasing the specific membrane costs to around 1,500 €/m². The specific membrane costs of investigated rotating membranes were in the range of 4,500 €/m² (Mohr, 2011). AnMBRs for sludge digestion are economically most viable in applications facing operation at low TS, high shares of fully degradable substrates (or high shares of soluble substrates) and small-scale applications.

8.2. Outlook

AnMBRs are an attractive option for sludge treatment as long as high flux can be achieved. Higher flux can be achieved especially at lower viscosities (respectively TS) of the anerobic sludge in the reactor.

On municipal WWTPs, a combination with thermal pressure hydrolysis as a disintegration process to boost the COD removal of organic matter has not been investigated so far. Thermal pressure hydrolysis as pretreatment significantly reduces dynamic viscosity of feed, which would favor operation at higher flux.

Concerning sludge-treatment in industrial sites, transfer of design and process control criteria elaborated in this work to other applications treating lipid-rich substrates or membrane types would be interesting.

AnMBRs also present an attractive option for anaerobic industrial wastewater treatment, where possible inhibition of microorganisms requires long SRT or wastewater constituents exclude pellet growth required for common high-rate performance reactors (such as EGSB, UASB). Concerning inhibition, applications involve the treatment of lipid-rich substrates, saline residues (e.g. kitchen wastes), nitrogen-rich substrates (e.g. slaughterhouse wastes) and sulphate-rich wastes (e.g. residuals from starch industry). Concerning prevention of pellet formation, treatment of whey, mono substrates and wastewater with high TSS concentration are of interest.

Regarding critical flux, further investigations on the influence of substrates on the sludge properties and the effects of membrane material and module configuration and, consequently, the critical flux are conceivable. Effects on long-term fouling rates especially by dosing of divalent cations also need further investigation. It would also be fascinating to investigate the influence of moving particles on the reduction of cake layers on the membrane surface in rotating membrane modules, as introduced for ceramic tube modules by Düppenbecker (2018), who applied AnMBRs to treat municipal wastewater.

References

Ahn, J., Do, T., Kim, S., Hwang, S. (2006) The effect of calcium on the anaerobic digestion treating swine wastewater. *Biochem. Eng. J.* 30(1), 33–38.

Ahring, B., Angelidaki, I., Johansen, K. (1992) Anaerobic treatment of manure together with industrial waste. *Water Sci. Technol.* 25(7), 311–318.

Alferes, J., García-Heres, J. L., Roca, E., Garcia, C., Irizar, I. (2008) Integration of equalisation tanks within control strategies for anaerobic reactors. Validation based on ADM1 simulations. *Water Sci. Technol*. 57(5), 747–752.

Altmann, J., Ripperger, S. (1997) Particle deposition and layer formation at the crossflow microfiltration. J. Membr. Sci. 124(1), 119–128.

Alves, M., Mota Vieira, J., Alvares Pereira, R., Pereira, M., Mota, M. (2001) Effect of lipids and oleic acid on biomass development in anaerobic fixed-bed reactors. Part I: biofilm growth and activity. Water Res. 35(1), 255–263.

Alves, M., Periera, M., Sousa, D., Cavaleiro, A., Picavet, M., Smidt, H., Stams, A. (2009) Waste lipids to energy: How to optimize methane production from long-chain fatty acids (LCFA). *Microb. Biotechnol.* 2(5), 538–550.

An, Y., Wang, Z., Wu, Z., Yang, D., Zhou, Q. (2009) Characterization of membrane foulants in an anaerobic non-woven fabric membrane bioreactor for municipal wastewater treatment. *Chem. Eng. J*. 155, 709–715.

Angelidaki, I., Ahring, B. (1992) Effects of free long-chain fatty acids on thermophilic anaerobic digestion. *Appl. Microbiol. Biotechnol.* 37, 808–812.

Angelidaki, I., Ellegard, L., Ahring, B (1993) A mathematical model for dynamic simulation of anaerobic digestion of complex substrates: Focusing on ammonia inhibition. *Biotechnol. and Bioeng.* 42, 159–166.

Angelidaki, J., Alves, M., Bolzonella, D., Borzacconi, J., Campos, A., Kalyuzhnyi, P., Jenicek, P., van Lier, J. (2009) Defining the biomethane potential (BMP) of solid organic wastes and energy crops: A proposed protocol for batch assays. *Water Sci. Technol*. 59, 927–934.

Bacchin, P., Aimar P., Field R. W. (2006) Critical and sustainable fluxes: Theory, experiments and applications. *J. Membr. Sci*. 281, 42–69.

Badenova A. G. & Co. K. G. (2005) Innovative Schlamm- und Filtratwasserbehandlung zur Reduzierung der Emissionen in der Biosphäre. *Abschlussbericht zur Fördermaßnahme*. https://www.badenova.de/mediapool/media/dokumente/unternehmensbereiche_1/stab_1/innovationsfonds/abschlussberichte/2005_6/2005-14-AZV-Wutoeschingen.pdf, (last visit: 06.05.2019).

Baker, R. (2012) *Membrane Technology and Applications*. 3rd edition, Wiley, Chichester, UK.

Batstone, D. J., Keller, J., Angelidaki, I., Kalyuzhnyi, S., Pavlostathis, S. G., Rozzi, A., Sanders, W., Siegrist, H., Vavilin, V. (IWA Task Group on Modelling of Anaerobic Digestion Processes) (2002) *Anaerobic Digestion Model No. 1 (ADM1)*. IWA Publishing, London.

Batstone, D., Lu, Y., Jensen, P. (2015) Impact of dewatering technologies on specific methanogenic activity. *Water Res*. 82, 78–85.

Battimelli, A., Carrere, H., Delgenes, J. (2009) Saponification of fatty slaughterhouse wastes for enhancing biodegradability. *Bioresour. Technol.* 100(15), 3695–3700.

Baudez, J., Slatter, P., Eshtiaghi, N. (2013) The impact of temperature on the rheological behaviour of anaerobic digested sludge. *Water Res.* 45, 5675–5680.

Baumgarten, S. (2007) Membranbioreaktoren zur industriellen Abwasserreinigung. *Ph.D. Thesis, RWTH Aachen,* Aachen, Germany.

Bayerische Landesanstalt für Landwirtschaft (LfL) (2013) *Gruber-Tabelle zur Fütterung der Milchkühe, Zuchtrinder, Schafe, Ziegen*. http://www.lfl.bayern.de/cms07/publikationen/informationen/d_36967. (last visit: 20.03.2017).

Bayerisches Landesamt für Umwelt (LfU) (2007) *Biogashandbuch Bayern – Materialienband.* https://www.lfu.bayern.de/energie/biogashandbuch/doc/deckblatt.pdf. (last visit: 29.04.2019).

Beccari, M., Majone, M., Torrisi, L. (1998) Two-reactor system with partial phase separation for anaerobic treatment of olive oil mill effluents. *Water Sci. Technol.* 38, 53–60.

Becker, P., Koster, D., Popov, M. N., Markossian, S., Antranikian, G., Markl, H. (1999) The biodegradation of olive oil and the treatment of lipid-rich wool scouring wastewater under aerobic thermophilic conditions. *Water Res.* 33, 653–660.

Bentzen, T., Ratkovich, N., Madsen, J., Jensen, J., Bak, S., Rasmussen, M. (2012) Analytical and numerical modelling of Newtonian and non-Newtonian liquid in a rotational crossflow MBR. *Water Sci. Technol.* 66(11), 2318–2327.

Berg, S., Berg, M., Lüdtke, M., Söhr, S., Baresel, C. (2016) Extended Sludge Retention Time in a Full Scale Anaerobic Digester at Himmerfjärden WWTP. *IWA "Holistic Sludge Management 2016", 07. June–09. June 2016*, Malmö, Sweden.

Bernard, O., Polit, M. Hadj-Sadok, Z., Pengov, M., Dochain, D., Estaben, M., Labat, P. (2001) Advanced monitoring and control of anaerobic wastewater treatment plants: Software sensors and controllers for an anaerobic digester. *Wat. Sci. Technol*. 43(7), 175–182.

Bharambe, G., Kabouris, J., Bustamante, H., van Rys, D., Cesca. J., Murthy, S. (2015) Anaerobic digestion with recuperative thickening minimises biosolids quantities and odours in Sydney. *OZWater, 12. May–14. May 2015, Adelaide*, Australia.

Bischofsberger, W., Dichtl, N., Rosenwinkel, K., Seyfried, C., Böhnke, B. (2005) *Anaerobtechnik.* Springer Verlag, Berlin.

Blatt, W., Dravid, A., Michaels, A., Nelsen, L. (1970) Solute polarization and cake formation in membrane ultrafiltration: Causes, consequences, and control techniques. In: Flinn, J. E. (ed.) *Membr. Sci. and Technol. Plenum*, 47–91.

Boe, K., Batstone, D.J., Angelidaki, I. (2007) An innovative online VFA monitoring system for the anaerobic process, based on headspace gas chromatography. *Biotechnol. and Bioeng.* 96 (4), 712–721.

Borowski, S., Kubacki, P. (2015) Co-digestion of pig slaughterhouse waste with sewage sludge. *Waste Manage.* 40, 119–126.

Bowen W., Jenner, F. (1995) Theoretical descriptions of membrane filtration of colloids and fine particles: An assessment and review. *Adv. in Colloid and Interface Sci*. 56, 141–200.

Brond, S., Faxa, J., Bovbjerg, J., Soholm, J., Ploumann, J., Vollertsen, J. (2016) Application of membrane filtration in combination with municipal anaerobic digesters. *IWA "Holistic Sludge Management 2016", 07. June–09. June 2016*, Malmö, Sweden.

Cervantes, J., Pavlostathis, S., van Haandel, A. (2006) *Advanced Biological Treatment Process for Industrial Wastewaters: Principles and Applications*. IWA Publishing, London.

Chang, I., Lee, C. (1998) Membrane filtration characteristics in membrane coupled activated sludge system–the effect of physiological states of activated sludge on membrane fouling. *Desalination* 120, 221–233.

Chen, J., Ortiz, R., Steele, T., Stuckey, D. (2014) Toxicants inhibiting anaerobic digestion: A review. *Biotechnol. Adv.* 32, 1523–1534.

Chen, R., Nie, Y., Hu, Y., Miao, R., Utashiro, T., Li, Q., Xu, M., Li, Y. (2017) Fouling behaviour of soluble microbial products and extracellular polymeric substances in a submerged anaerobic membrane bioreactor treating low strength wastewater at room temperature. *J. Membr. Sci.* 531, 1–9.

Chen, Y. (1986) Rheological properties of sieved beef-cattle manure slurry: Rheological model and effects of temperature and solids concentration. *Agricultural Wastes* 1., Nr.1.

Chen, Y., Cheng, J., Creamer, K. (2008) Inhibition of anaerobic digestion process: A review. *Bioresour. Technol.* 99(10), 4044–4064.

Chen, Y., Hashimoto, A. (1980) Substrate utilization kinetic model for biological treatment processes. *Biotechnol. Bioeng.* 14, 2081–2095.

Cheryan, M. (1998) *Ultrafiltration and Microfiltration Handbook*. 2nd edition, CRC Press, Boca Raton, USA.

Cho, B., Fane, A. (2002) Fouling transients in nominally sub-critical flux operation of a membrane bioreactor. *J. Membr. Sci.* 209, 391–403.

Choo, K., Lee, C. (1996) Membrane fouling mechanisms in the membrane-coupled anaerobic bioreactor. *Water Res.* 30, 1771–1780.

Choo, K., Kang, I., Yoon, S., Park, H., Kim, J., Adiya, S., Lee, C. (2000) Approaches to membrane fouling control in anaerobic membrane bioreactors. *Water Sci. Technol.* 41(10), 363–371.

Christian, S., Grant, S., McCarthy, P., Wilson, D., Mills, D. (2010) The first two years of full-scale anaerobic membrane bioreactor (AnMBR) operation treating high strength industrial wastewater. *Proceedings of IWA 12th World Congress on Anaerobic Digestion*, Guadalajara, Mexico.

Churchhouse, S., Wildgoose, D. (1999) Membrane bioreactors hit the big time – from lab to full-scale installation. In Proceedings: *International Meeting on Membrane Bioreactors for Wastewater Treatment*, University of Cranfield, UK.

Cirne, D., Paloumet, X., Bjornsson, L., Alves, M., Matthiasson, B. (2007) Anaerobic digestion of lipid-rich waste – Effects of lipid concentration. *Renew. Energ.* 32(6), 965–975.

Cobbledick, J., Aubry, N., Zhang, V., Rollings-Scattergood, S., Latulippe, D. R. (2016) Lab-scale demonstration of recuperative thickening technology for enhanced biogas production and dewaterability in anaerobic digestion processes. *Water Res.* 95, 39–47.

Conklin, A., Bucher, R., Stensel, H., Ferguson, J. (2007) Effects of oxygen exposure on anaerobic digester sludge. *Water Environ. Res.* 79(4), 396–405.

Contois, D. (1959) Kinetics of bacterial growth: Relationship between population density and specific growth rate of continuous cultures. *J. gen. Microbiol.* 21,40–50.

Creamer, K., Chen, Y., Williams, C., Cheng, J. (2010) Stable thermophilic anaerobic digestion of dissolved air flotation (DAF) sludge by co-digestion with swine manure. *Bioresour. Technol.* 101, 3020–3024.

Cussler, E. (2009) *Diffusion: Mass Transfer in Fluid Systems*. 3rd edition, Cambridge University Press, New York, USA.

Dagnew, M. (2010) Characterization of anaerobic membrane digesters for stabilization of waste activated sludge*. Ph.D. Thesis*, *University of Waterloo,* Ontario, Canada.

Dagnew, M., Parker, W., Seto, P. (2010) A pilot study of anaerobic membrane digesters for concurrent thickening and digestion of waste activated sludge (WAS). *Water Sci. Technol.* 61, 1451–1458.

Dagnew, M., Parker, W., Seto, P. (2012) Anaerobic membrane bioreactors for treating waste activated sludge: Short term membrane fouling characterization and control tests. *J. Membr. Sci.* 421–422, 103–110.

Dagnew, M., Pickel, J., Parker, W., Seto, P. (2013) Anaerobic membrane bio-reactors for waste activated sludge digestion: Tubular versus hollow fiber membrane configurations. *Environ. Prog. Sustain. Energy* 32(3), 598–604.

Davidsson, A., Lovstedt, C., la Cour Jansen, J., Gruvberger, C., Aspegren, H. (2008) Co-digestion of grease trap sludge and sewage sludge. *Waste Manage.* 28(6), 986–992.

DBFZ Deutsches Biomasseforschungszentrum gemeinnützige GmbH (2015) *Schriftenreihe des BMU-Förderprogramms "Energetische Biomassenutzung", Band 7, Messmethodensammlung Biogas.*

De Lemos Chernicharo, C. (2007) *Anaerobic Reactors, Biological Wastewater Treatment Series, Volume 4.* IWA Publishing, London.

Dereli, R., Ersahin, M., Ozgun, H., Ozturk, I., Jeison, D., van der Zee, F., van Lier, J. (2012) Potentials of anaerobic membrane bioreactors to overcome treatment limitations induced by industrial wastewaters. *Bioresour. Technol*. 122, 160–170.

Dereli, R., Grelot, A., Heffernan, B., van der Zee, F., van Lier, J. (2014a) Implications of changes in solids retention time on long term evolution of sludge filterability in anaerobic membrane bioreactors treating high strength industrial wastewater. *Water Res.* 59, 11–22.

Dereli, R., van der Zee, F., Heffernan, B., Grelot, A., van Lier, J. (2014b) Effect of sludge retention time on the biological performance of anaerobic membrane bioreactors treating corn-to-ethanol thin stillage with high lipid content. *Water Res.* 49, 453–464.

Deveci, H. (2002) Effect of solids on viability of acidophilic bacteria. *Miner. Eng.* 15(12), 1181–1189.

Diez, V., Ramos, C. Cabezas, J. (2012) Treating wastewater with high oil and grease content using an anaerobic membrane bioreactor (AnMBR). Filtration and cleaning assays. *Water Sci. Technol.* 65(10), 1847–1853.

Ding, L., Al-Akoum, O., Abraham, A., Jaffrin, M. (2002) Milk protein concentration by ultrafiltration by rotating disk modules. *Desalination*, 144, 307–311.

Dolfing J. (1988) Acetogenesis. In Zehnder, A. (ed.) *Biology of Anaerobic Microorganisms*, Wiley.

Dong, Q., Parker, W., Dagnew, M. (2016) Long term performance of membranes in an anaerobic membrane bioreactor treating municipal wastewater. *Chemosphere* 144, 249–256.

Drews, A. (2010) Membrane fouling in membrane bioreactors – Characterization contradictions, cause and cures. *J. Membr. Sci*. 363, 1–28.

Duarte, A., Andersen, G. (1982) Inhibition modelling in anaerobic digestion. *Water Sci. Technol. 14*, 749–763.

Düppenbecker, B. (2018) Upgrading of anaerobic municipal wastewater treatment by means of low-energy mirco- and ultrafiltration. *Ph.D. Thesis*, *Verein zur Förderung des Instituts IWAR der TU Darmstadt e.V.* (249).

Dvorak, L., Gomez, M., Dolina, J., Cernin, A. (2016) Anaerobic membrane bioreactors – a mini review with emphasis on industrial wastewater treatment: Applications, limitations and perspectives. *Desalination Water Treat.* 57(41), 19062–19076.

DWA-A 216 (2015) Arbeitsblatt DWA-A 216, Energiecheck und Energieanalyse – Instrumente zur Energieoptimierung von Abwasseranlagen (Energy assessment and energy analysis – instruments for an energy optimization of wastewater treatment plants). *Deutsche Vereinigung für Wasserwirtschaft, Abwasser und Abfall e.V, Hennef,* Germany (in German).

DWA-M 366 (2013) DWA Merkblatt M 366, Maschinelle Schlammentwässerung. *Deutsche Vereinigung für Wasserwirtschaft, Abwasser und Abfall e.V, Hennef,* Germany (in German).

DWA-M 368 (2004) DWA Merkblatt M 368, Biologische Stabilisierung von Klärschlamm (Biological stabilization of sewage sludge). *Deutsche Vereinigung für Wasserwirtschaft, Abwasser und Abfall e.V, Hennef,* Germany (in German).

DWA-M 383 (2008) DWA Merkblatt M 383 Kennwerte der Klärschlammentwässerung. *Deutsche Vereinigung für Wasserwirtschaft, Abwasser und Abfall e.V, Hennef,* Germany (in German).

Eastman, J., Ferguson, J. (1981) Solubilization of particulate organic carbon during the acid phase of anaerobic digestion. *J. Wat. Poll. Cont. Fed.* 53, 352–366.

Edwards, J., Othmann, M., Crossin, E., Burn. S. (2017) Anaerobic co-digestion of municipal waste and sewage sludge: A comparative life cycle assessment in the context of a waste provision. *Bioresour. Technol.* 223, 237–249.

Engelhart, M., Schaum, C., Lutze, R., Rühl, J., Schebek, L., Seier, M., Dornburg, A., Dörner, F., Vukovic, N., Klinger, J., Jakob, M., John, M., Gilbert, E., Feit, E., Schließmann, U., Mohr, M., Sievers, M., Bormann, H., Niedermeiser, M., Franck, J., Edens, G., Wittstock, R., Ansmann, T., Dierich, A., Mohajeri, S., Westenberg, D. (2018) Abwasserbehandlung der Zukunft – Energiespeicher in der Interaktion mit technischer Infrastruktur im Spannungsfeld von Energieerzeugung und –verbrauch (ESITI) – Schlussbericht, https://bmbf.nawam-

erwas.de/sites/default/files/180307_abschlussbericht_gesamt_final.pdf (last visit: 09.05.2019)

Ersahin, M., Ozgun, H., Tao, Y., van Lier, J. (2014) Applicability of dynamic membrane technology in anaerobic membrane bioreactors. *Water Res.* 48, 420–429.

Escalante, H., Castro, L., Amaya, M., Jaimes, L., Jaimes-Estevez, J. (2018) Anaerobic digestion of cheese whey: Energetic and nutritional potential for the dairy sector in developing countries. *Waste Manage.* 71, 711–718.

Esposito, G., Frunzo, L., Panico, A., Pirozzi, F. (2011) Modelling the effect of the OLR and of MSW particle size on the performances of an anaerobic co-digestion reactor. *Process Biochem*. 46, 557–565.

Fan, F., Zhou, H., Husain, H. (2006) Identification of wastewater sludge characteristics to predict critical flux for membrane bioreactor processes. *Water Res.* 40, 205–212.

Fane, A. (1984) Ultrafiltration of suspensions. *J. Membr. Sci*. 20, 249–259.

Feng, Y., Behrendt, J., Wendland, C., Otterpohl, R. (2006) Parameters analysis of the IWA Anaerobic Digestion Model No. 1 (ADM1) for the anaerobic digestion of blackwater with kitchen refuse. *Water Sci. Technol.* 54(4), 139–147.

Fernandez, B., Porrier, P., Chamy, R. (2001) Effect of inoculum-substrate ratio on the start-up of solid waste anaerobic digesters. *Water Sci. Technol*. 44(4), 103–108.

Field, R., Pearce, G. (2011) Critical, sustainable and threshold fluxes for membrane filtration with water industry application. *Adv. in colloid and interface sci.* 164, 38–44.

Field, R., Wu, D., Howell, J., Gupta, B. (1995) Critical flux concept for microfiltration fouling. *J. Membr. Sci*., 100, 259–272.

Flores-Alsina, X., Solon, K., Mbamba, C., Tait, S., Gernaey, K., Jeppsson, U., Batstone, D. (2016) Modelling phosphorus (P), sulphur (S) and iron (Fe) interactions for dynamic simulations of anaerobic digestion processes. *Water Res*. doi: 10.1016/j.watres.2016.03.012.

Fonouni, M., Etemadi, H., Yegani, R., Zarin, S. (2017) Fouling characterization of TiO_2 nanoparticle embedded polypropylene membrane in oil refinery wastewater treatment using membrane bioreactor. *Desailination and Water Treat.* 90, 99–109.

Fuchs, W., Binder, H., Mavrias, G., Braun, R. (2003) Anaerobic treatment of wastewater with high organic content using a stirred tank reactor coupled with a membrane filtration unit. *Water res.* 37, 902–908.

Füreder, K., Svardal, K., Krampe, J., Kroiss, H. (2017) Rheology and friction loss of raw and digested sewage sludge with high TSS concentrations: A case study. *Water Sci. and Technol*. Bonus issue 1, 276–286.

Gallert, C., Winter, J., Svardal, K. (2015) Grundlagen anaerober Prozesse. In Rosenwinkel, K. *et al.* (ed.) *Anaerobtechnik*. Springer Verlag.

Garcia-Gen, S. (2015) Modelling, optimisation and control of anaerobic co-digestion processes. *Ph.D. Thesis, Universidad de Santiago de Compostela, Departamento de Ingenierıa Quımica.*

García-Gen, S., Sousbie, P., Rangaraj, G., Lema, J. M., Rodríguez, J., Steyer, J.-P. (2015) Kinetic modelling of anaerobic hydrolysis of solid wastes, including disintegration processes. *Waste Manage.* 35, 96–104. doi: 10.1016/j.wasman.2014.10.012.

Ghyoot, W., Verstraete, W. (1997) Coupling membrane filtration to anaerobic primary sludge digestion. *Environ. Technol.* 18(6), 569–580.

Girault, R., Bridoux, G., Nauleau, F., Poullain, C., Buffet, J., Peu, P. (2012) Anaerobic co-digestion of waste activated sludge and greasy sludge from flotation process: Batch versus CSTR experiments to investigate optimal design. *Bioresour. Technol.* 105,1–8.

Grady, C., Daigger, G., Lim, H. (1999) *Biological Wastewater Treatment*. 2nd edition, Marcel Dekker, Inc.

Grepmeier, M. (2002). Experimentelle Untersuchungen an einer zweistufigen fuzzygeregelten anaeroben Abwasserreinigungsanlage mit neuartigem Festbettmaterial. *Ph.D. Thesis*, *Technische Universität München*, Munich, Germany.

Guglielmi, G., Saroj, D., Chiarani, D., Andreottola, G. (2007). Sub-critical fouling in a membrane bioreactor for municipal wastewater treatment: Experimental investigation and mathematical modelling. *Water Research* 41, 3903-3914.

Guglielmi, G., Chiarani, D., Saroj, D., Andreottola, G., (2010) Sludge filterability and dewaterability in a membrane bioreactor for municipal wastewater treatment. *Desalination* 250(2), 660–665.

Gujer, W., Zehnder, A. (1983) Conversion Processes in anaerobic digestion. *Water Sci. and Technol.* 15(8–9), 127–167.

Hamawand, I. (2015) Anaerobic digestion process and bio-energy in meat industry: A review and a potential. *Renew. Sust. Energ. Rev.* 44, 37–51.

Hanaki, K., Matsuo, T. and Nagase, M. (1981) Mechanisms of inhibition caused by long chain fatty acids in anaerobic digestion process. *Biotech. Bioeng.* 23, 1591–1610.

Harris, P., Schmidt, T., McCabe, B. (2017) Evaluation of chemical, thermobaric and thermochemical pre-treatment on anaerobic digestion of high-fat cattle slaughterhouse waste. *Bioresour. Technol.* 244, 605–610.

He, P., Lü, F., Shao, L., Pan, X. Lee, D. (2007) Kinetics of enzymatic hydrolysis of polysaccharide-rich particulates. *J. Chin. Inst. Chem. Eng.* 38, 21–27.

Henderson, C. (1973) The effects of fatty acids on pure cultures of rumen bacteria. *J. Agricul. Sci*. 81, 107–112.

Henze, M., Harremoes, P., Cour Jansen, J. (2002) *Wastewater Treatment*. 3rd edition, *Springer Verlag*, Berlin, Germany.

Ho, C. Zydney, A. (2006) Overview of fouling phenomena and modeling approaches for membrane bioreactors. *Sep. Sci. and Technol.* 41, 1231–1251.

Ho, J., Sung, S. (2009) Effects of solid concentration and cross-flow hydrodynamics on microfiltration of anaerobic sludge. *J. Membr. Sci.* 345, 142–147.

Holbrook, R., Higgins, M., Murthy, S., Fonseca, A., Fleischer, E., Daigger, G., Grizzard, T., Love, N., Novak, J. (2004) Effect of alum addition on the performance of submerged membranes for wastewater treatment. *Water Environ. Res.* 76(6).

Houghton, J., Stephenson, T. (2002) Particle size analysis of digested sludge. *Water Res.* 36(18), 4643–4647.

Hu, Y., Kobayashi, T., Zhen, G., Shi, C., Xu, K. (2018) Effects of lipid concentration on thermophilic anaerobic co-digestion of food waste and grease waste in a siphon-driven self-agitated anaerobic reactor. *Biotechnol. Rep.* 19, e0002 69.

Huang, Y. H., Huang, G. H., Chou, S. and Cheng, S. S. (2000) Hydrogen as a quick indicator of organic shockloading in UASB. *Wat. Sci. Technol.*,42 (3–4), 43–50.

Huang, Z., Ng, H., Ong, S. (2009) The Impact of sludge retention time (SRT) on submerged anaerobic membrane bioreactor for low-strength wastewater treatment. *WEFTEC 2009*, 2761–2770.

Huang, Z., Ong, S., Ng, H. (2011) Submerged anaerobic membrane treatment bioreactor for low-strength wastewater treatment: Effect on HRT and SRT on treatment performance and membrane fouling. *Water Res.*, 45, 705–713.

Hubert, C., Steiniger, B., Schaum, C. (2020) Residues from the dairy industry as co-substrate for flexibilization of digester operation. *Water Environ. Res*. 92, 534–540.

Hwu, C., Donlon, B., Lettinga, G. (1996) Comparative toxicity of oleic acid to anaerobic sludges from various origins. *Wat. Sci. Tech.* 34, 351–358.

Inanc, B., Matsui, S., Ide, S. (1999) Propioniuc acid accumulation in anaerobic digestion of carbohydrates: An investigation on the role of hydrogen gas. *Water Sci. Technol.* 40(1), 93–100.

Ince, O., Anderson, G. Kasapgil, B. (1995) Control of organic loading rate using the specific methanogenic activity test during start-up of an anerobic digestion system. *Wat. Res.* 29(1), 349–355.

Itonaga, T., Kimura, K., Watanabe, Y. (2004) Influence of suspension viscosity and colloidal particles on permeability of membrane used in membrane bioreactor (MBR). *Water Sci. Technol.* 50, 301–309.

Jahn, L., Baumgartner, T., Svardal, K., Krampe, J. (2016) The influence of temperature and SRT on high-solid digestion of municipal sewage sludge. *Water Sci. Technol.* 74 (4), 836–843.

Jeison, D., van Lier, J. (2008) Feasibility of thermophilic anaerobic submerged membrane bioreactors (AnSMBR) for wastewater treatment. *Desalination* 231, 227–235.

Jensen, P., Yap, S., Boyle-Gotla, A., Janoschka, J., Carney, C., Pidou, M., Batstone, D. (2015) Anaerobic membrane bioreactors enable high rate treatment of slaughterhouse wastewater. *Biochem. Eng. J.* 97, 132–141.

Jimenez, J., Latrille, E., Harmand, J., Robles, A., Ferrer, J., Gaida, D., Wolf, C., Mairet, F., Bernard, O., Alcarez-Gonzalöez, V., Mendez-Acosta, H., Zitomer, D., Totzke, D., Spanjers, H., Jacobi, F., Guwy, A., Dinsdale, R., Premier, G., Mazhegrane, S., Ruiz-Filippi, G., Seco, A., Ribeiro, T., Pauss, A., Steyer, J. P. (2015) Instrumentation and control of anaerobic digestion processes: A review and some research challenges. *Rev. Environ. Sci. Biotechnol.* 14, 615–648.

Jin, B., Wilén, B., Lant, P. (2004) Impacts of morphological, physical and chemical properties of sludge flocs on dewaterability of activated sludge. *Chem. Eng. J.* 98, 115–126.

Jørgensen, M., Pedersen, M., Christensen, M., Christensen, M. (2014) Dependence of shear and concentration on fouling in a membrane bioreactor with rotating membrane discs. *AIChE J*. 60(2), 706–715.

Jørgensen, M., Pedersen, M., Christensen, M., Keiding, K. (2012) Shear effects on fouling layer compressibility in a high pressure membrane bioreactor. *Proceedings of WFC11.*

Josse, J., Scattergood, S., Scherson, Y. (2017) Municipal Digester Repowering demonstration (MDRD) project. *Final Project Report, California Energy Commission.*

Judd, S. (2006) *The MBR Book: Principles and Applications of Membrane Bioreactors in Water and Wastewater Treatment*. Elsevier, Oxford.

Judd, S. (2011) *The MBR Book: Principles and Aapplications of Membrane Bioreactors in Water and Wastewater Treatment.* 2nd edition, *Elsevier*, ISBN 978-0-08-096682-3.

Kabouris, J., Tezel, U., Pavlostathis, S., Engelmann, M., Dulaney, J., Todd, A., Gillette, R. (2009) Mesophilic and thermophilic anaerobic digestion of municipal sludge and fat, oil, and grease. *Water Environ. Res.* 81, 476–485.

Kafle, G., Kim, S., Sung, K. (2013) Ensiling of fish industry waste for biogas production: A lab scale evaluation of biochemical methane potential (BMP) and kinetics. *Bioresour. Technol.* 127, 326–336.

Kang, I., Yoon, S., Lee, C. (2002) Comparison of the filtration characteristics of organic and inorganic membranes in a membrane coupled anaerobic bioreactor. *Water Res*. 36, 1803–1813.

Karode, S., Kumar, A. (2001) Flow visualization through spacer filled channels by computational fluid dynamics - I. Pressure drop and shear rate calculations for flat sheet geometry. *J. Membr. Sci*. 193, 69–84.

Kayawake, E., Narukami, Y., Yamagata, M. (1991) Anaerobic digestion by a ceramic membrane enclosed reactor. *J. Ferment. Bioeng.* 71, 122–125.

Khongnakorn, W., Choksuchart, S., Wisniewski, C. (2008) Physico-chemical Characteristics and Dewatering apitude of sMBR sludge. *J. Applied Membrane Science & Technology*, Vol. 7, 33-40.

Kim, J., Lee, C. (2003) Effect of powdered activated carbon on the performance of an aerobic membrane bioreactor: Comparison between cross-flow and submerged membrane systems. *Water Environ. Res.* 75(4), 300–307.

Kim, J., Lee, C., Choo,K. (2007) Control of struvite precipitation by selective removal of NH_4^+ with dialyzer/zeolite in an anaerobic membrane bioreactor*. Appl. Microbiol. Biotechnol.* 75, 187–193.

Kim, S., Han, S., Shin, H. (2004) Kinetics of LCFA inhibition on acetoclastic methanogenesis, propionate degradation and b-oxidation. *J. Environ. Sci. Health. A Tox. Hazard Subst. Environ. Eng.* 39, 1025–1037.

Kopp, J. (2006) Neue Verfahren zur Verbesserung der Klärschlammeigenschaften, *39. Essener Tagung für Wasser- und Abfallwirtschaft*. In: *GWA* 202 (60), 1–13.

Koster, I., Cramer, A. (1986) Inhibition of methanogenesis from acetate in granular sludge by long chain fatty acids. *Appl. Microbiol. Biotech.* 53, 403–409.

Kraume, M., Wedi, D., Schaller, J., Iversen, V., Drews, A. (2009) Fouling in MBR – what use are lab investigation for full scale operation? *Desalination*, 236, 94–103.

Krebber, K. (2013) Optimierung der Energiebilanz von Membranbioreaktoren. *Ph.D. Thesis, RWTH Aachen,* Aachen, Germany.

Kroiss, H., Svardal, K. (2015) Einflussfaktoren auf die anaeroben biologischen Abbauvorgänge. In Rosenwinkel, K. *et al.* (ed.) *Anaerobtechnik*. Springer Verlag.

Kujawski, O., Steinmetz, H. (2009) Development of instrumentation systems as a base for control of digestion process stability in full-scale agricultural and industrial biogas plants. *Water Sci. Technol.* 60(8), 2055–2063.

Kuozeli-Katsiri, A., Kartsonas, N., Priftis, A. (1988) Assessment of the toxicity of heavy metals to the an-aerobic digestion of sewage sludge. *Environ. Technol. Lett.* 9, 261–270.

Laera, G., Giordano, C., Pollice, A., Saturno, D., Mininni, G. (2007) Membrane bioreactor sludge rheology at different solid retention times. *Water Res.* 41(18), 4197–4203.

Laera, G., Pollice, A., Saturno, D., Giordano, C., Sandulli, R. (2009) Influence of sludge retention time on biomass characteristics and cleaning requirements in a membrane bioreactor for municipal wastewater treatment. *Desalination* 236 (1e3), 104–110.

Le-Clech, P., Chen, V., Fane, A. (2006) Fouling in membrane bioreactors used in wastewater treatment. *J. Membr. Sci.* 284, 17–53.

Le-Clech, P., Jefferson, B., Chang, I. ,Judd, S. (2003) Critical flux determination by the flux-step method in a submerged membrane bioreactor. *J. Membr. Sci*. 227, 81–93.

Lee, J., Kim, J., Kang, I., Cho, M., Park, P., Lee, C. (2001) Potential and limitations of alum or zeolite addition to improve the performance of a submerged membrane bioreactor. *Water Sci. Technol.* 43, 59–66.

Leighton, D., Acrivos, A. (1987) The shear-induced migration of particles in concentrated suspensions. *J. Fluid Mech.* 181, 415–439.

Lensch, D. (2017) Möglichkeiten zur Intensivierung der Klärschlammfaulung durch Prozessoptimierung und Vorbehandlung. *Ph.D. Thesis, TU Darmstadt, Verein zur Förderung des Instituts IWAR der TU Darmstadt e.V.* (241).

Li, Y., Jin, Y., Borrion, A., Li, H., Li, J. (2017) Effects of organic composition on the anaerobic biodegradability of food waste. *Bioresour. Technol.* 243, 836–845.

Liao, B., Kraemer, J, Bagley, D. (2006) Anaerobic membrane bioreactors: Applications and research directions. *Crit. Rev. Environ. Sci. Technol.* 36(6), 489–530.

Liebetrau, J. (2006) Regelungsverfahren für die anaerobe Behandlung von organischen Abfällen. *Ph.D. Thesis*, *Manuskripte zur Abfallwirtschaft Bauhaus-Universität Weimar*, Band 9.

Lim, A., Bai, R. (2003) Membrane fouling and cleaning in microfiltration of activated sludge wastewater. *J. Membr. Sci*. 216(1–2), 279–290.

Lin, H., Xie, K., Mahendran, B., Bagley, D., Leung, K., Liss, S., Liao, B. (2009) Sludge properties and their effects on membrane fouling in submerged anaerobic membrane bioreactors (SAnMBRs). *Water Res.* 43, 3827–3837.

Linke, B, Mumme, J., Mähnert, P., Schönberg, M., Plogties, V. (2011) Grundlagen und Verfahren der Biogasgewinnung. *Biogas in der Landwirtschaft: Leitfaden für Landwirte im Land Brandenburg*, 12–28, Potsdam.

Lokshina, L., Vavilin, V., Salminen, E., Rintala, J. (2003) Modeling of anaerobic degradation of solid slaughterhouse waste. *Appl. Biochem. Biotechnol*. 109(1–3), 15–32.

Londong, J., Rosenwinkel, K. (2013) Industrieabwasserbehandlung: Rechtliche Grundlagen, Verfahrenstechnik, Abwasserbehandlung ausgewählter Industriebranchen, Produktionsintegrierter Umweltschutz. *Bauhaus Universität Weimar.*

Luostarinen, S., Luste, S., Sillanpää, M. (2009) Increased biogas production at wastewater treatment plants through co-digestion of sewage sludge with grease trap sludge from a meat processing plant. *Biores. Technol*. 100, 79–85.

Luste, S., Luostarinen, S., (2010) Anaerobic co-digestion of meat-processing byproducts and sewage sludge – effect of hygienization and organic loading rate. *Bioresour. Technol.* 101, 2657–2664.

Lyko, S., Wintgens, T., Alhalbouni, D., Baumgarten, S., Tacke, D., Drensla, K., Janot, A., Dott, W., Pinnekamp, J., Melin, T. (2008) Long-term monitoring of a full-scale municipal membrane bioreactor – characterisation of foulants and operational performance. *J. Membr. Sci.* 317 (1–2), 78–87.

Madigan, M., Martinko, J., Parker, J. (2003) Brock Biology of microorganisms. 10th edition, *Pearson Education,* USA.

Maillacheruvu, K., Parkin, G. (1996) Kinetics of growth, substrate utilization and sulfide toxicity for propionate, acetate, and hydrogen utilizers in anaerobic systems. *Water Environ. Res.* 68, 1099–1106.

Manison, P. (2013) Sustainable ceramic membranes for wastewater applications. https://www.waterworld.com/articles/iww/print/volume-13/issue-4/features/filtration-efficiency.html, (last visit: 29.04.2019).

Mata-Alvarez, J. (2015) *Biomethanization of the Organic Fraction of Municipal Solid Wastes*. IWA Publishing, London.

Mata-Alvarez, J., Dosta, J., Romero-Güiza, M., Fonoll, X., Peces, M., Astals, S. (2014) A critical review on anaerobic co-digestion achievements between 2010 and 2013. *Renew. Sust. Energ. Rev.* 36, 412–427.

McCarty, P. (1964) Anaerobic waste treatment fundamentals. *Public Works* 95(11), 91–94.

Meabe, E., Deleris, S., Soroa, S. Sancho, L. (2013) Performance of anaerobic membrane bioreactor for sewage sludge treatment: Mesophilic and thermophilic processes. *J. Membr. Sci.* 446, 26–33.

Melin, T., Rautenbach, R. (2007) *Membranverfahren: Grundlagen der Modul- und Anlagenauslegung 3. Auflage*. Springer Verlag, Berlin, Heidelberg.

Meng, F., Chae, S., Drews, A., Kraume, M., Shin, H., Yang, F. (2009) Recent advances in membrane bioreactors (MBRs): Membrane fouling and membrane material. *Water Res.* 43, 1489–1512.

Metcalf and Eddy (2004) *Wastewater Engineering – Treatment and Reuse*. 4th edition, McGraw-Hill.

Mohr, M., (2011) Betrieb eines anaeroben Membranbioreaktors vor dem Hintergrund der Zielstellung des vollständigen Recyclings kommunalen Abwassers und seiner Inhaltsstoffe. *PhD. Thesis*, *Fraunhofer Verlag*, Stuttgart.

Monteggia, L. (1991) The use of a specific methanogenic activity for controlling anaerobic reactors. *Ph.D. Thesis, The University of Newcastle upon Tyne*, UK.

Moshage, U. (2004) Rheologie kommunaler Klärschlämme – Messmethoden und Praxisrelevanz. *PhD Thesis*. *Veröffentlichungen des Institutes für Siedlungswasserwirtschaft TU Braunschweig*, Heft 72.

Moukazis, I., Pellera, F., Gidarakos, E. (2018) Slaughterhouse by-products treatment using anaerobic digestion. *Waste Manage.* 71, 652–662.

Mulder, M. (1996) *Basic Principles of Membrane Technology*. 2nd edition, Springer Netherlands.

Murto, M., Björnsson, L., Mattiasson, B., (2004) Impact of food industrial waste on anaerobic co-digestion of sewage sludge and pig manure. *J. Environ. Manage*. 70, 101–107.

Nakao, S., Nomura, T., Kimura, S. (1979) Characteristics of macromolecular gel layer formed on ultrafiltration tubular membrane. *AIChE J*. 25(4), 615–622.

Negri, E., Mata-Alvarez, J., Sans, C., Cecchi, F. (1993) A mathematical model of volatile fatty acids (VFA) production in a plug-flow reactor treating the organic fraction of municipal solid waste (MWS). *Wat. Sci. Tech.* 27(2), 201–208.

Nguyen, D., Gadhamshetty, V., Nitayavardhana, S., Khanal, S. (2015) Automatic process control in anaerobic digestion: A critical review. *Bioresour. Technol.* (193), 513–522.

Nielsen, H., Uellendahl, H., Ahring, B. (2007) Regulation and optimization of the biogas process: Propionate as a key parameter. *Biomass Bioenergy* 31, 820–830.

Noutsopoulos, C., Mamais, D., Antoniou, K., Avramides, C., Oikonomopoulos, P., Fountoulakis, I. (2013) Anaerobic co-digestion of grease sludge and sewage sludge: The effect of organic loading and grease sludge content. *Bioresour. Technol.* 131, 452–459.

Ochando-Pulido, J., Stoller, M., Bravi, M., Martinez-Ferez, A., Chianese, A. (2012) Batch membrane treatment of olive vegetation wastewater from two-phase olive oil production process by threshold flux based methods. *Sep. Purif. Technol.* 101, 34–41.

Oh, S., Martin, A. (2010) Long chain fatty acids degradation in anaerobic digester: Thermodynamic equilibrium consideration. *Process Biochem.* 45, 335–345.

Olsson, G., Nielsen, M., Yuan, Z., Lynggard-Jensen, A., Steyer, J. (2005) *Instrumentations, Control and Automation in Wastewater Systems*. IWA Publishing, London.

Ozgun, H., Dereli, R. Ersahin, M., Kinaci, C., Spanjers, H., van Lier, J. (2013) A review of anaerobic membrane bioreactors for municipal wastewater treatment: Integration options, limitations and expectations. *Sep. Purif. Technol.* 118, 89–104.

Padmasiri, S.I., Zhang, J., Fitch, M., Norddahl, B., Morgenroth, E., Raskin, L. (2007) Methanogenic population dynamics and performance of an anaerobic membrane bioreactor (AnMBR) treating swine manure under high shear conditions. *Water Res.* 41 (1), 134–144.

Pages-Diaz, J., Pereda-Reyes, I., Sanz, J., Lundin, M., Taherzadeh, M., Horvath, I. (2018) A comparison of process performance during the anaerobic mono- and co-digestion of slaughterhouse waste through different operational modes. *J. Environ. Sci. (China)* 65, 1491–56.

Palatsi, J., Laureni, M., Andrés, M., Flotats, X., Nielsen, H. Angelidaki, I. (2009) Strategies for recovering inhibition caused by long chain fatty acids on anaerobic thermophilic biogas reactors. *Bioresour. Technol.*100, 4588–4596.

Park, C., Abu-Orf, M., Novak, J. (2006) The digestibility of waste activated sludges. *Water Environ. Res*. 78, 31–40.

Parkin, G., Speece, R., Yang, C., Kocher, W. (1983) Response of methane fermentation systems to industrial toxicants. *J. Water Pollut. Control*. 44–53.

Pavlostathis, S. (1985). A kinetic model for anaerobic digestion of waste activated sludge. *Ph.D. Thesis, Cornell University, USA*.

Pavlostathis, S. Gossett, J. (1986) A kinetic-model for anaerobic digestion of biological sludge. *Biotechnol. Bioeng.* 28(10), 1519–1530.

Pavlostathis, S. G., Giraldo-Gomez E. (1991) Kinetics of anaerobic treatment: A critical review. *Crit. Rev. in Environ. Sci. Technol*. 21, 411–490.

Pereira, M., Cavaleiro, A. Mota, M., Alves, M. (2003) Accumulation of long chain fatty acids onto anaerobic sludge under steady state and shockloading conditions: Effect on acetogenic and methanogenic activity. *Water Sci. Technol.* 48, 33–40.

Pereira, M., Pires, O., Mota, M., Alves, M. (2002) Anaerobic degradation of oleic acid by suspended and granular sludge: Identification of palmitic acid as a key intermediate. *Water Sci. and Technol.* 45(10), 139–144.

Pereira, M., Pires, O., Mota, M., Alves, M. (2005) Anaerobic biodegradation of oleic and palmitic acids: Evidence of mass transfer limitations caused by long chain fatty acid accumulation onto the anaerobic sludge. *Biotechnol. Bioeng.* 92(1), 15–23.

Pierkiel, A., Lanting, J. (2005) Membrane-coupled anaerobic digestion of municipal sewage sludge. *Water Sci. Technol.* 52(1–2), 253–258.

Pileggi, V. (2016) Investigation of the performance of an anaerobic membrane bioreactor in the treatment of mixed municipal sludge under ambient, mesophilic and thermophilic operating conditions. *Ph. D. Thesis, University of Waterloo, Waterloo, Canada*.

Pileggi, V., Parker, W. (2017) AnMBR digestion of mixed WRRF sludges: Impact of digester loading and temperature. *J. Water Process Eng*. 19, 74–80.

Pind, P., Angelidaki, I., Ahring, B. (2003) Dynamics of the anaerobic process: Effects of volatile fatty acids. *Biotechnol. Bioeng*. 82, 791–799.

Pitk, P., Kaparaju, P., Palatsi, J., Affes, R., Vilu, R. (2013) Co-digestion of sewage sludge and sterilized solid slaughterhouse waste: Methane production efficiency and process limitations. *Bioresour. Technol.* 134, 227–232.

Poggio, D., Walker, M., Nimmo, W., Ma, L., Pourkashanian, M. (2016) Modelling the anaerobic digestion of solid organic waste – Substrate characterization method for ADM1 using a combined biochemical and kinetic parameter estimation approach. *Waste Manage.* 53, 40–54.

Polizzi, C., Alatrite-Mondragon, F., Munz, G. (2017) Modelling the disintegration process in anaerobic digestion of tannery sludge and fleshing. *Front. Environ. Sci.* https://doi.org/10.3389/fenvs.2017.00037.

Pollice, A., Laera, G., Saturno, D., Giordano, C., (2008) Effects of sludge retention time on the performance of a membrane bioreactor treating municipal sewage. *J. Membr. Sci.* 317,65–70.

Porter, M. C. (1972) Concentration polarization with membrane ultrafiltration. *Industrial & Engineering Chemistry Product Research and Development*, 11, 234–248.

Ratkovich, N., Horn, W., Helmus, F., Rosenberger, S., Naessens, W., Nopens, I., Bentzen, T. (2013) Activated sludge rheology: A critical review on data collection and modelling. *Water Res.* 47, 463–482.

Reipa, A. (2003) Kostenreduzierung für Kommunen und Verbände durch effiziente *Erzeugung und Verwertung von Faulgas als Primärenergie sowie Reduzierung der Faulschlammmenge, Teilprojekt: Co-Vergärung, Schlussbericht zum Forschungsvorhaben, Emschergenossenschaft//Lippeverband Emscher Gesellschaft für Wassertechnik mbH, Essen*.

Rinzema, A., Alpenhaar, A., Lettinga, G. (1989) The effect of lauric acid shock loads on the biological and physical performance of granular sludge in UASB reactors digesting acetate. *J. Chem. Tech. Biotech.* 46, 257–266.

Rinzema, A., Boone, M., van Knippenberg, K., Lettinga, G. (1994) Bactericidal effect of long chain fatty acids in anaerobic digestion. *Water Environ. Res.* 66, 40–49.

Ripperger S. (1993) Berechnungsansätze zur Crossflow-Filtration (Calculation of crossflow filtration). *Chemie Ingenieur Technik* 65, 533–540.

Roediger, H., Roediger, M., Kapp, H. (1990) Anaerobe alkalische Schlammfaulung. *Oldenbourg Verlag*, München.

Rodriguez-Abalde, A., Flotats, X., Fernandez, B. (2017) Optimization of the anaerobic co-digestion of pasteurized slaughterhouse waste, pig slurry and glycerine. *Waste Manage.* 61, 521–528.

Rojas, C., Uhlenhut, F., Schlaak, M., Borchert, A., Steinigeweg, S. (2010) Simulation des anaeroben Prozesses bei der Biogaserzeugung. *Chemie Ingenieur Technik* 83(3), 306–321.

Romero-Flores, A., Li, B., Manning, E., Higgins, M., Al-Oman, A., Murthy, S., Riffat, R., De Cliuppeleir, H. (2017) Impact of recuperative thickening on anaerobic digestion of thermally hydrolysed sludge. In Proceedings: *IWA Specialist Conference on Sludge Management "Sludge Tech 2017", 09.–13.07.2017,* London, UK.

Rosenberger, S., Kubin, K., Kraume, M. (2002) Rheology of activated sludge in membrane bioreactors. Eng. Life Sci. 2(9), 269–275.

Rosenberger, S., Laabs, C., Lesjean, B., Gnirss, R., Amy, G., Jekel, M., Schrotter, J. C. (2006) Impact of colloidal and soluble organic material on membrane performance in membrane bioreactors for municipal wastewater treatment. *Water Res. 40*(4), 710–720.

Roy, F., Albagnac, G., Samain, E. (1985) Influence of calcium addition on growth of syntrophic cultures degrading long-chain fatty acids. *Appl. Environ. Microbiol.* 49, 702–705.

Rozzi, A., Verstraete, W. (1981) Calculation of active biomass and sludge production vs waste composition in anaerobic contact processes. *Trib. Cebedeau 455* (34), 421–427.

Rühl, J. (2016) Dataset for CSTRs operated with SRT = 12 d and SRT = 20 d in the year 2015 and 2016 within the frame of ESiTi project.

Rusdi, R., Ochs, A., von Munch, E. (2005) Determining the hydrolysis rate constants of several organic substrates used in co-digestion to enable mathematical modelling with ADM1. In: Ahring, B. K., Hartmann, H. (ed.) *Proceedings of the Fourth International Symposium on Anaerobic Digestion of Solid Waste, vol. 1. Copenhagen, Denmark*, 569–575.

Salama, E., Saha, S., Kurade, M., Dec, S., Chang, S., Jein, B. (2019) Recent trends in anaerobic co-digestion: Fat, oil, and grease (FOG) for enhanced biomethanation. *Prog. Energy Combust. Sci.* 70, 22–42.

Sanders, W. (2001) Anaerobic hydrolysis during digestion of complex substrates. *Ph.D. Thesis, Wageningen Universiteit*, *Wageningen, The Netherlands.*

Sanders, W., Geerink, M., Zeemann, G., Lettinga, G. (2000) Anaerobic hydrolysis kinetics of particulate substrates. *Water Sci. Technol.* 41(3), 17–24.

Schaum, C., Lensch, D., Bolle, P. Y., Cornel, P. (2015) Sewage sludge treatment: Evaluation of the energy potential and methane emissions with COD balancing. *J. Water Reuse Desalination* 05.4, 437–445.

Schipolowski, T. (2007) Experimentelle und theoretische Untersuchungen zur Auslegung von Ultrafiltrationsverfahren. *Ph.D. Thesis, Tu Berlin,* Berlin, Germany.

Schlattmann, M. (2011) Weiterentwicklung des „Anaerobic Digestion Model (ADM1)“ zur Anwendung auf landwirtschaftliche Substrate. *Ph.D. Thesis, Technische Universität München*, München, Germany.

Schnürer, A. (2016) Biogas production: Microbiology and technology*. Adv. Biochem. Engin./Biotechnol*. 156, 195–234.

Schreff, D. (2020, August 8th) Überlegungen zum wirtschaftlichen Einsatz der anaeroben Schlammstabilisierung in Kläranlagen. http://www.ib-schreff.de/fileadmin/Daten/Publikationen/ibSchreff_tah_faulung.pdf.

Schumacher, W., Nebocat, G. (2009) Kosten der Ersatzbrennstoffverbrennung in Monoverbrennungsanlagen. In: *Energie aus Abfall*, Band 6, TK Verlag.

Schwinge, J., Neal, P., Wiley, D., Fane, A. (2002) Estimation of foulant deposition across the leaf of a spiral-wound module. *Desalination* 146, 203–208.

Sheu, C., Freese, E. (1972) Effect of fatty acids on growth and envelope proteins of *Bacillus subtilis*. *J. Bacteriol.* 111, 516–524.

Shimizu, Y., Okuno, Y. I., Uryu, K., Ohtsubo, S., Watanabe, A. (1996) Filtration characteristics of hollow fiber microfiltration membranes used in membrane bioreactors for domestic wastewater treatment. *Water Res*. 30, 2385–2392.

Shin, H., Kim, S., Lee C., Nam, S. (2003) Inhibitory effects of long-chain fatty acids on VFA degradation and ß-oxidation. *Water Sci. Technol.* 47, 139–149.

Siegrist, H., Vogt, D., Garcia-Heras, J., Gujer, W. (2002) Mathematical model for meso- and thermophilic anaerobic sewage sludge digestion. *Environ. Sci. Technol*. 36, 1113–1123.

Silvestre, G., Rodriguez-Abalde, F., Fernandez, B., Flotats, X., Bonimati, A. (2011) Biomass adaptation over anaerobic co-digestion of sewage sludge and trapped grease waste. *Bioresour. Technol.* 102, 6830–6836.

Singh, K., Burke, D., Grant, S. (2010) Anaerobic flat sheet membrane bioreactor treating food processing wastewater: Pilot-scale performance. *Proceedings of IWA 12th World Congress on Anaerobic Digestion*, Guadalajara, Mexico.

Sipma, J., Osuna, M., Emanuelsson, M., Castro, P. (2010) Biotreatment of industrial wastewaters under transient-state conditions: Process stability with fluctuatons of

organic load, substrates, toxicants, and environmental parameters. *Crit. Rev. Environ. Sci. Technol.* 40(2), 147–197.

Smith, A. L., Stadler, L. B., Love, N. G., Skerlos, S. J., Raskin, L. (2012) Perspectives on anaerobic membrane bioreactor treatment of domestic wastewater: A critical review. *Bioresour. Technol.* 122, 149–159.

Sobeck D., Higgins M. (2002) Examination of three theories for mechanisms of cation-induced bioflocculation. *Water Res.* 36(3), 527–538.

Sötemann, S., Ristow, N., Wentzel, M., Ekama, G. (2005) A steady state model for anaerobic digestion of sewage sludges. *Water SA* 31(4).

Stoller, M., Ochando-Pulido, J., Chianese, A. (2013) Comparison of critical and threshold fluxes on ultrafiltration and nanofiltration by treating 2-phase or 3-phase olive mill wastewater. *Chem. Eng. Trans.* 32, 397–402.

Strathmann, H. (2011) *Introduction to Membrane Science and Technology*. Wiley-VCH, Weinheim, Germany.

Stuckey, D. (2012) Recent developments in anaerobic membrane reactors. *Bioresour. Technol*. 122, 137–148.

Suto, P., Gray, D., Larsen, E., Hake, J. (2006) Innovative anaerobic digestion investigation of fats, oils, and grease. *WEF Biosolids and Residuals Conference Proceedings*, 858–879.

Szabo-Corbacho, M., Pacheco-Ruiz, S., Miguez, D., Hooijmans, C., Garcia, H., Brdjanovic, D., van Lier, J. (2019). Impact of solids retention time on the biological performance of an AnMBR treating lipid-rich synthetic dairy wastewater. *Environ. Technol*. doi: 10.1080/09593330.2019.1639829.

Tang, J., Wang, X., Hu, Y., Ngo, H., Li, Y. (2017) Dynamic membrane-assisted fermentation of food wastes for enhancing lactic acid production. *Bioresour. Technol.* 234, 40–47.

Tolksdorf, J., Lu, D., Cornel, P. (2016) First implementation of a SEMIZENTRAL Resource Recovery Center. *J. Water Reuse Desalination.* doi: 10.2166/wrd.2016.129.

Torpey, W., Melbinger, N. (1967) Reduction of digested sludge volume by controlled recirculation. *J. Water Pollut. Control* 39, 1464–1474.

Torras, C., Pallares, J., Garcia-Valls, R., Jaffrin, M. (2009) Numerical simulation of the flow in a rotating disk filtration module. *Desalination* 235(1–3), 122–138.

Usack, J., Gerber Van Doren, L., Posmanik, R., Labatut, R., Tester, J., Angenent, L. (2018) An evaluation of anaerobic co-digestion implementation on New York State dairy farms using an environmental and economic life-cycle framework. *Appl. Energy* 211, 28–40.

Valentini, A., Garuti, G., Rozzi, A., Tilche, A. (1997) Anaerobic degradation kinetics of particulate organic matter: A new approach. *Wat. Sci. Tech*. 36(6–7), 239–246.

Van der Marel, P., Zwijnenburg, A., Kempermann, A., Wessling, M., Temmink, H., van der Meer, W. (2009) An improved flux-step method to determine the critical flux and the critical flux for irreversibility in a membrane bioreactor. *J. Membr. Sci.* 332, 24–29.

Vavilin, V., Angelidaki, I. (2005) Anaerobic degradation of solid material: Importance of initiation centers for methanogenesis, mixing intensity, and 2D distributed model. *Biotechnol. Bioeng*. 89(1), 113–122.

Vavilin, V., Fernandez, B., Palatsi, J. Flotats, X. (2008) Hydrolysis kinetics in anaerobic degradation of particulate organic material: An overview. *Waste Manage*. 28, 939–951.

Vavilin, V., Rytov, S., Lokshina, L. (1996) A description of hydrolysis kinetics in anaerobic degradation of particulate organic matter. *Bioresour. Technol.* 56, 229–237.

VDI Verein Deutscher Ingenieure (2006) *Vergärung organischer Stoffe, Substratcharakterisierung, Probenahme, Stoffdatenerhebung, Gärversuche (Fermentation of organic materials – Characterization of the substrate, sampling, collection of material data, fermentation tests*). 4630. Beuth Verlag GmbH, Berlin (in German).

Veeken, A., Hamelers, B. (2000) Effect of substrate-seed mixing and the leachate recirculation on solid state digestion of biowaste. *Water Sci. Technol.* 41(3), 255–262.

Waeger, F., Delhaye, T., Fuchs, W. (2010) The use of ceramic microfiltration and ultrafiltration membranes for particle removal from anaerobic digester effluents. *Sep. Purif. Technol.* 73(2), 271–278.

Walpole, R., Myers, R., Myers, S., Ye, K. (2002) Probability & Statistics for Engineers & Scientiest. *Prentice Hall, 7th edition*, Upper Saddle River, USA.

Wan, C., Zhou, Q., Li, Y. (2011) Semi-continuous anaerobic co-digestion of thickened waste activated sludge and fat, oil and grease. *Waste Manage.* 31(8), 1752–1758.

Wang, K., Martin Garcia, N., Soares, A., Jefferson, B., McAdam, E. (2018) Comparison of fouling between aerobic and anaerobic MBR treating municipal wastewater. *H_2Open Journal* 1(2), 131–159.

Wang, L., Aziz, T., de los Reyes III, F. (2013) Determining the limits of anaerobic codigestion of thickened waste activated sludge with grease interceptor waste. *Water Res*. 47, 3835–3844.

Wang, Z., Wu, Z., Yu, G., Liu, J., Zhou, Z., (2006) Relationship between sludge characteristics and membrane flux determination in submerged membrane bioreactors. *J. Membr. Sci.* 284 (1e2), 87–94.

Ward, A., Hobbs, P., Holliman, P., Jones, D. (2008) Optimisation of the anaerobic digestion of agricultural resources. *Bioresour. Technol*. 99, 7928–7940.

WEF/ASCE (2009) Design of municipal wastewater treatment plants, Volume 3: Solids processing and management, WEF manual of practice no. 8/ASCE manuals and reports on engineering practice no. 76, 5. Auflage. *WEF Press, Water Environment Federation (Alexandria/Virginia), American Society of Civil Engineers/Environmental and Water Resources Institute (Reston/Virginia)*, McGraw-Hill, USA.

Weichgrebe, D. (2015) Kompendium Biogas. Habilitationsschrift, *Veröffentlichung des ISAH*, Heft 155.

Wichern. M. (2010) Simulation biochemischer Prozesse in der Siedlungswasserwirtschaft. *Oldenbourg Industrieverlag*.

Wilén, B., Jin, B., Lant, P. (2003) Relationship between flocculation of activated sludge and composition of extracellular polymeric substances. *Water Sci. Technol.* 47(12), 95–103.

Xiao, X., Huang, Z., Ruan, W., Yan, L., Miao, H., Ren, H., Zhao, M. (2015) Evaluation and characterization during the anaerobic digestion of high-strength kitchen waste slurry via a pilot-scale anaerobic membrane bioreactor. *Bioresour. Technol.* 193, 234–242.

Xiao, X., Sheng, G. P., Mu, Y., Yu, H. (2013) A modeling approach to describe ZVI-based anaerobic system. *Water Res.* 47(16), 6007–6013.

Xiao, X., Shi, W., Huang, Z., Ruan, W., Miao, H., Ren, H., Zhao, M. (2017) Process stability and microbial response on membrane bioreactor treating high-strength kitchen waste slurry under different organic loading rates. *Int. Biodeterior. Biodegradation* 121(2017), 35–43.

Yamaguchi, T., Harada, H., Hisano, T., Yamazaki, S., Tseng, I. (1999) Process behavior of UASB reactor treating a wastewater containing high strength sulfate. *Water Res.* 33, 3182–3190.

Yamato, N., Kimura, K., Miyoshi, T., Watanabe, Y. (2006) Difference in membrane fouling in membrane bioreactors (MBRs) caused by membrane polymer materials. *J. Membr. Sci*. 280, 911–919.

Yang, S., Nghiem, L. D., Bustamante, H., van Rys, D., Murthy, S. N. (2015) Recuperative thickening: A possible tool to improve anaerobic digestion of wastewater sludge. *OZWater, 12. May–14. May 2015*, *Adelaide,* Australia.

Yoon, S., Kang, I., Lee, C. (1999) Fouling of inorganic membrane and flux enhancement in membrane-coupled anaerobic bioreactor. *Sep. Sci. Technol.* 34(5), 709–724.

Zehnder, A. (1978) Ecology of methane formation. In Mitchell, R. (ed.) *Wat,.Poll. Micr.*, 2, 349–376, *John Wiley and Sons Inc*.

Zeman, L., Zydney, A. (1996) *Microfiltration and Ultrafiltration: Principles and Applications.* Marcel Dekker, New York, USA.

Zhang, J., Padmasiri, S., Fitch, M., Norddahl, B., Raskin, L., Morgenroth, E. (2007) Influence of cleaning frequency and membrane history on fouling in an anaerobic membrane bioreactor. Desalination, 207(1–3), 153–166.

Zhang, J., Zhang, Y., Chang, J., Quan, X., Li, Q. (2013) Biological sulfate reduction in the acidogenic phase of anaerobic digestion under dissimilatory Fe (III)-reducing conditions. *Water Res.* 47(6), 2033–2040.

Zhao, X., Li, L., Wu, D., Xiao, T., Ma, Y., Peng, X. (2019) Modified anaerobic digestion model No. 1 for modelling methane production from food waste in batch and semi-continuous anaerobic digestions. *Bioresour. Technol.* 271, 109–117.

Ziels, R., Karlsson, A., Beck, D., Ejlertsson, J., Yekta, S., Bjorn, A., Stensel, D., Svensson, B. (2016) Microbial community adaption influences long-chain fatty acid conversion during anaerobic codigestion of fats, oils, and grease with municipal sludge. *Water Res.* 103, 372–382.

Zitomer D., Bachman, T., Vogel, D. (2005) Thermophilic anaerobic digester with ultrafilter for solids stabilization. *Water Sci. Technol.* 52, 525–530.

Zonta, Z., Alves, M., Flotats, X., Palatsi, J. (2013) Modeling inhibitory effects of long chain fatty acids in the anaerobic digestion process. *Water Res.* 47,1369–1380.

List of Figures

List of Tables

Nomenclature

A	Surface of particulate matter (m^2)
A	Exponent of A-order kinetics
AD	Anaerobic digestion
ADM1	Anaerobic Digestion Model No. 1
AnMBR	Anaerobic membrane reactor
$B_{VS,COD}$	COD sludge loading rate (kg COD/kg VS·d)
BM	Biomass
BMP	Biomethane potential (L CH_4/kg COD)
c	Concentration (g/L or mg/L)
CapEx	Capital expenditure
CFV	Crossflow velocity (m/s)
CHP	Combined Heat and Power
COD	Chemical oxygen demand
CST	Capillary suction time (s)
CSTR	Continuous stirred-tank reactor; also used as index
D	Diffusion coefficient of solute (m^2/h)
D(Φ)	Hydrodynamic diffusion coefficient (-)
D_B	Brownian diffusion coefficient (m^2/s)
D_S	Shear-induced diffusion coefficient
dx	thickness of infinitesimal boundary layer segment (m)
E	Electric energy consumption (kWh_{el}/d)
$E_{spec.,membrane}$	Specific energy concumption of the membrane (kWh_{el}/m^3 filtrate)
E_0	Electric energy consumption in clear water (kWh_{el}/d)
EGSB	Expanded granular sludge bed
EPS	Extracellular polymeric substances
F	Empirical factor substituting COD removal in transient state (-)
F(TMP)	Pressure-depending factor (1/(m·s))
f_{ch}	COD related share of carbohydrates of total COD (-)
f_{li}	COD related share of lipids of total COD (-)
f_{pr}	COD related share of proteins of total COD (-)
FOG	Fat, oil and grease
FS	Flotation sludge; also used as index
HRT	Hydraulic retention time
IC50	Half maximum inhibitory concentration (g/L)
J	Flux (L/(m^2·h))

J_{crit}	Critical flux (=$J_{critical}$) (L/(m²·h))
J_{lim}	Limiting flux (L/(m²·h))
$J_{sustainable}$	Sustainable flux (L/(m²·h))
K	Hydrolysis constant in half-order biomass kinetics $(m^3/kg)^{0.5}/d$)
K	Fluid consistency factor (Pa·s)
k	velocity factor (-)
K'	Hydrolysis constant (m/d)
K_b	Boltzman constant (J/K)
K_b	Equilibrium constant in two-Phase model
k_d	Decay rate (1/d)
k_{dis}	Disintegration constant (1/d)
$K_{H,A}$	Hydrolysis constant in A-order biomass kinetics $((m^3/kg)^A/d)$
k_{hyd}	Hydrolysis constant (1/d)
$k_{hyd,exp}$	Exponential factor for hydrolysis constant
$k_{hyd,max}$	Maximum hydrolysis constant (1/d)
K_S	Half-saturation coefficient for S (g/L)
k_{SBK}	Surface-based hydrolysis constant (kg/(m³·d))
K_x	Half-saturation coefficient for X (g/L)
LCFA	Long-chain fatty acids
LS	Large scale
m	Flow behavior index (-)
M	Substrate mass (kg)
M_{VS}	mass of volatile solids in the batch or reactor (g or kg VS)
MF	Microfiltration
MWCO	Molecular weight cutoff (Da)
n	COD conversion via acetate pathway (-)
n	flow behavior index (-);
OLR	Organic loading rate (kg COD/(m³·d)
OpEx	Operational expenditure
P_x	Biomass production (Kg VS/d)
PE	Population equivalent
PrS	Primary sludge
PS	Pilot scale
Q	Volume flow (m³/d or L/d)
r	Radius (m)
R_{ads}	Resistance of membrane by adsorption (1/m)
Re	Reynolds number (-)

r_i	Inner radius of membrane (m)
R_m	Resistance of membrane (1/m)
r_o	Outer radius of membrane (m)
ROI	Return on Investment (a)
RT	Recuperative thickening; also used as index
S	Substrate concentration (mostly soluble) (g/L)
SBR	Sequencing batch reactor
SF	Safety factor [-]
SLR	Sludge loading rate (kg COD/(kg VS·d)
SMA	Specific methanogenic activity (g COD-CH_4/(g VS·d))
SMP	Soluble microbial products
SRT	Sludge retention time (d)
t	Time (d)
T	Temperature (°C or K)
THP	Thermal Hydrolysis Process
TMP	Transmembrane pressure (bar)
TS	Total solids (%)
TSS	Total suspended solids (g/L)
UASB	Upflow anaerobic sludge bed reactors
UF	Ultrafiltration
UL	Upper limit of hydrolytic biomass concentration
V’	Flow (m^3/d)
V_{CH4}	Cumulated methane volume (m^3)
$V_{reactor}$	Volume of a reactor (m^3)
VFA	Volatile fatty acid
VS	Volatile solids (%)
WAS	Waste activated sludge; also used as index
WWTP	Wastewater treatment plant
X	Concentration of particulate matter (g/L)
X_0	Initial concentration of substrate X (g/L)
X_{BM}	Concentration of biomass (g/L)
$X_{BM,hyd}$	Concentration of hydrolytic biomass (g/L)
$X_{BM,hyd,UL}$	Upper limit of concentration of hydrolytic biomass (g/L)
$X_{BM,methanogens}$	Concentration of methanogenic biomass (g/L)
Y_{max}	Maximum yield of biomass (g VSS/g COD)
Y_{CH4}	Methane yield (L CH_4/kg COD_{added})
$Y_{CH4,max}$	Maximum methane yield (L CH_4/kg COD_{added})

Greek letters

$\dot{\gamma}$	Shear rate (1/s)
$\dot{\gamma}_m$	Shear rate on membrane surface (1/s)
δ	Thickness of the boundary layer (m)
η	Dynamic viscosity (Pa·s)
η_a	Apparent viscosity (Pa·s)
η_{COD}	COD removal (-)
μ_{max}	Maximum specific growth rate of biomass (1/d)
ρ_s	Sludge density (kg/m³)
ρ_w	Water density (kg/m³)
τ	Shear stress
τ_W	Wall shear stress (Pa)
ω	Specific foulant mass on membrane surface (kg/m²)
ω	Angular velocity (rad/s)
Φ	Volume fraction of particles relative to concentration (-)

Additional Indices used with several symbols

in	Inlet
li	Lipid
max	Maximum
min	Minimum
out	Outlet
res	Residual
deg	Degradable

Appendix

Appendix A Fundamentals of anaerobic digestion

Derivation of a formulae for the degree of degradation using a CSTR based on a general mass balance

The degradation performance of a CSTR can be described by starting on the basis of a general mass balance. For the steady state, the substance mass in the reactor doesn't change which is why the storage term can be set to zero. Consequently,

$$Storing = Transport + Reaction$$

$$0 = Transport + Reaction$$

The transport term respectively the concentration change in the inlet and outlet can be simplified by taking equal volume flows into account

$$V \cdot \frac{dc}{dt} = V' \cdot (c_{in} - c_{out})$$

Where, V: volume (L)

c: concentration (mg/L)

V': volume flow (L/h)

The temporal change of the concentration, the reaction, can be represented by including a reaction rate r in a volume as follows

$$Reaction = r \cdot V$$

For a first-order reaction as commonly used in anaerobic sludge treatment with $r = k_{dis} \cdot c_{out}$, the outflow concentration can now be calculated as follows by using above mentioned equations

$$c_{out} = \frac{c_{in}}{1 + k_{dis} \cdot t}$$

Where, c_{out}: outflow concentration (mg/L)

c_{in}: inflow concentration (mg/L)

k_{dis}: disintegration constant for substrate first order kinetics Volume flow (1/d)

t: reaction time (d)

By extension and conversion of above equation, the degree of degradation η for a steady state following a substrate first order reaction can be determined as follows

$$\eta = 1 - \frac{c_{out}}{c_{in}} = \frac{k_{dis} \cdot t}{1 + k_{dis} \cdot t}$$

Appendix B Investigations on kinetics in AnMBR and CSTR

Detailed description of AnMBR pilot plant

Continuous digestion tests were performed using an anaerobic membrane digester in a pilot scale (constructed by EnviroChemie GmbH, Germany). A simplified flow scheme is given in Figure A 1.

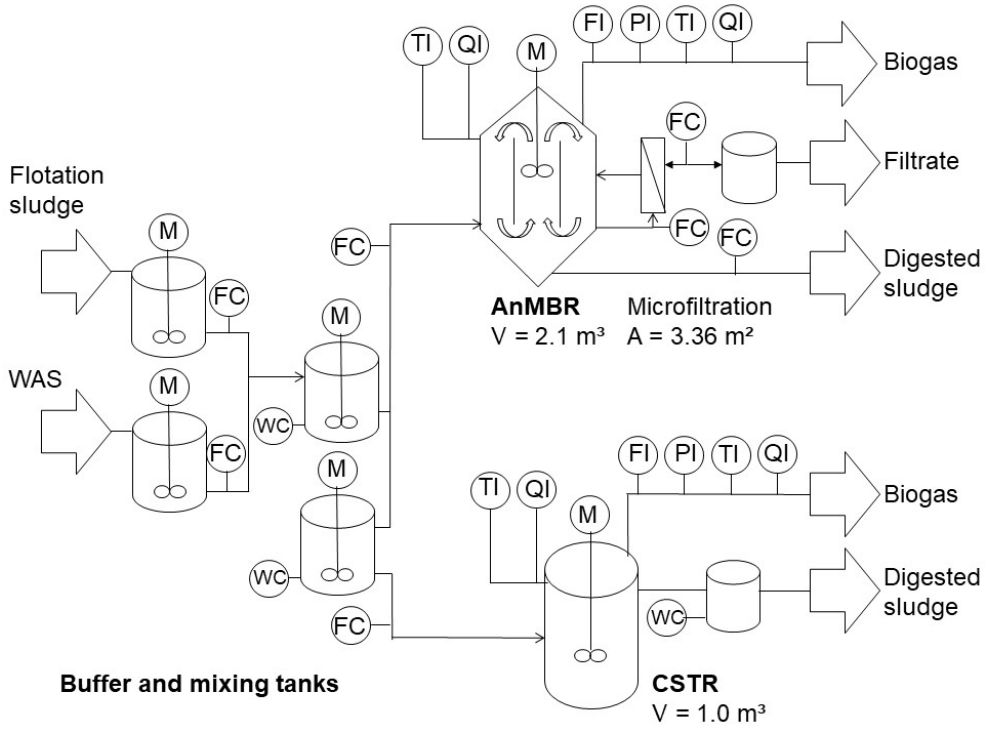

FC: Flow control, FI: Flow indication, PI: Pressure indication,

TI: Temperature indication, QI: pH indication (in digester); CH_4, CO_2 indication (in digester gas)

Figure A 1. Simplified flow scheme of the anaerobic membrane digester and CSTR used for anaerobic digestion of WAS and flotation sludge in pilot scale

Buffer tanks

Buffer tanks had a volume of 1.5 m³ each and were continuously mixed. Both were manually filled with flotation sludge and WAS approx. twice per week. From these tanks, it was pumped to a mixing tank. This mixing tank had a volume of 400 L, was continuously mixed and was placed on a scale (WC measurement). Scale allowed to set a reproducible gravimetric ratio of WAS and flotation sludge as measurement of flows were considered as not precise enough. This mixture was prepared several times a day depending on required volume of inlet to anaerobic digester.

In case of feeding the AD with WAS as the only substrate, mixing tank was used as well but flotation sludge was not added.

Feeding the AD

The mixed sludge is pumped from the mixing tank into the anaerobic digester (V = 2 m³) by use of an eccentric screw pump. This screw pump was capable to pump up to 400 L/h which

is why this pump was set to run for a couple of minutes each hours to achieve a quasi-continuous feeding. The manipulated value used here was a given mass per day and cycle. The reactor was fed 20 times per day (20 cycles). Additionally, volumetric flow of feed was measured using Proline Promag electromagnetic flowmeters (Endress and Hauser, Germany),

Anaerobic digester of AnMBR

The pilot plant has a digester volume of 2.1 m^3, is fully automated and was operated at mesophilic conditions with temperatures around 37±1 °C. A slow-running agitator and a guide tube mounted inside the vessel ensure complete mixing by aiming to create a loop. Additional, an external circulation by a pump was used for feeding the membrane module and a double-pipe heat exchanger before returning this flow back to the reactor. The circulation flow was around 400 L/h which should additionally ensure complete mixing.in the anaerobic digester. The circulation line also contained a measuring section for measuring pH and temperature (Memosens CPS171D, Endress and Hauser, Germany).

The hourly difference from inlet and filtrate flow was pumped out of the reactor using an eccentric screw pump on the basis of measured water level in the reactor. This also ensured a constant used reactor volume.

Membrane module

The microfiltration membrane unit allows decoupling of SRT and HRT. It consists of rotating ceramic disc filters (Filter ceramic disc 312, Kerafol GmbH, Germany) with a nominal pore size of 0.2 µm, an outer diameter of 312mm, an inner diameter of 91 mm and a thickness of 5.85 mm mounted on a hollow shaft ($A_{Membrane}$ = 3.36 m^2; see Figure 17 and Figure 18). Each membrane had a membrane surface of 0.14 m^2 which is why 24 membranes were installed on the hollow shaft. For reducing fouling on the membrane, a rotating hollow shaft was used in this study. Rotational velocities between 250-350 rpm were applied. Corresponding crossflow velocities are given in Table 10. As filtrate flow was maximum around 50 L/h and feed around 400 L/h, no significant increase of concentration over the membrane module occurred as the ratio of feed to filtrate was approx. 8:1. Volumetric flow of feed and filtrate were continuously measured using Proline Promag electromagnetic flowmeters (Endress and Hauser, Germany), and pressure in feed, concentrate and filtrate were continuously measured using Cerabar sensors (Endress and Hauser, Germany).

The membrane module was operated with a set filtrate flow and a required filtrate volume per day for keeping a specific SRT/HRT ratio in the reactor. Transmembrane pressure (TMP) changed over the duration of filtration. During filtration, gas formed in the filter and accumulated along the shaft during rotation. This interfered the filtration process which is why rotation of the filter was stopped regularly (each 8-10 minutes) for about 30 seconds for degassing. Additional, membrane was backwashed with filtrate each hour for 60 seconds with a flow around 10-20 L/h.

Filtrate was generally discharged while concentrate was pumped back to the reactor.

When a maximum TMP of 500 mbar was reached, chemical cleaning of the membrane had to be performed using acid and caustic cleaners provided by EnviroChemie. Chemical cleaning was required approx. 1-2 times per year and followed this procedure:

- Rinsing of membrane module with tap water
- Caustic cleaning with pH > 12 at Temperatures > 40 °C for approx. 2 hours
- Rinsing of membrane module with tap water
- Measurement of clear water flux for evaluating success of cleaning
- Acid cleaning with pH < 2 at Temperatures > 40 °C for approx. 2 hours
- Rinsing of membrane module with tap water
- Measurement of clear water flux for evaluating success of cleaning
- As option an additional caustic cleaning was repeated
- *Caustic cleaning with pH > 12 at Temperatures > 40 °C for approx. 2 hours*
- *Rinsing of membrane module with tap water*
- *Measurement of clear water flux for evaluating success of cleaning*

Biogas measurement

Biogas was collected from top of the reactor and flow was continuosly measured using a drum gas meter (Type TG1, Dr. Ing. Ritter Apparatebau GmbH & Co. KG, Germany). Afterwards, gas was cooled to 5 °C for drying and CH_4 and CO_2 were measured continuously by BlueSens gas sensor (BlueSens gas sensor GmbH, Germany; also see Table 12). Gas flow rates were normalised according to VDI 4630 (2006).

CSTRs

CSTR had a volume of 1 m^3 and were fed with a mixture from mixing tank of the AnMBR pilot plant. Concerning sensor and biogas measurement, plant was constructed in the same way. Mixing was ensured by an agitator. Heating was done by heat tracing around the reactor. The feeding was also carried out with an eccentric screw pump (also approx. 20 times per day for a couple of minutes), whereby the effluent of these reactors hydrostatically overflowed. This ensured the same volume used over duration of tests. Inlet and outlet were also measured by scales.

Compilation of BMP tests of waste activated sludge for determination of k_{dis} and $Y_{CH4,max}$

Table A 1. Results of BMP tests of waste activated sludge

Sample	k_{dis}		$Y_{CH4,max}$		
	mean	std.dev.	mean	std.dev.	n
1	0.20	0.02	168	5	5
2	0.19	0.01	160	4	3
3	0.19	0.02	170	10	8
4	0.21	0.01	115	13	3
5	0.19	0.02	157	5	2
Total	**0.20**	**0.02**	**154**	**22**	

Retention of COD of fine particulates smaller than 0.45 µm, ammonium and phosphate

Retention of COD of fine particulates smaller than 0.45 µm is about 60 % with high variation during reactor operation of more than 15 months (Figure A 2). As expected, ammonium and phosphate are not retained by the membrane.

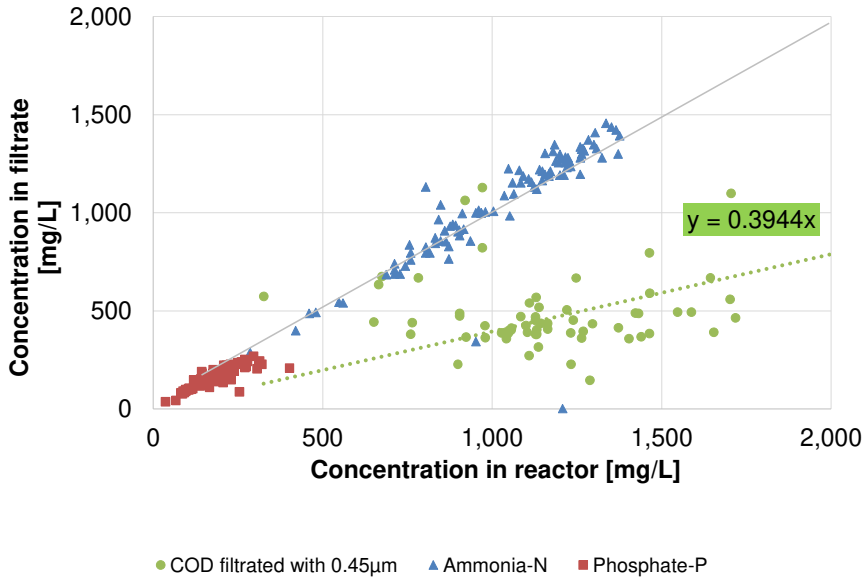

Figure A 2. Retention of COD, Ammonium, and phosphorus by membrane (nominal pore size of 0.2 µm)

Appendix C Investigations on AD treating lipid-rich substrates

Compilation of BMP tests of flotation sludge for determination of k_{dis} and $Y_{CH4,max}$

Table A 2. Results of BMP tests of flotation sludge

Sample	k_{dis}		$Y_{CH4,max}$		
	mean	std.dev.	mean	std.dev.	n
1	0.47	0.11	330	3	3
2	0.56	0.10	300	3	3
3	0.51	0.05	328	10	5
4	0.53	0.08	328	13	3
5	0.49	0.04	309	5	4
Total	**0.51**	**0.03**	**320**	**15**	

Data basis for the calculation of SF used in Figure 30

Table A 3. Data basis for the calculation of SF used for showing dependencies on SRT and share of flotation sludge

SRT	SRT/ HRT	COD_{FS}/ COD_{total}	mean acetate conversion	SMA	SF
[d]	[-]	[-]	[kg COD/ kg VS·d]	[kg COD/ kg VS·d]	[-]
CSTR with SRT = 10 d					
10.2	1.0	0.37	0.09	0.27 ± 0.01	3.01 ± 0.08
9.5	1.0	0.40	0.11	0.31 ± 0.01	2.75 ± 0.09
9.5	1.0	0.50	0.14	0.33 ± 0.02	2.43 ± 0.14
9.5	1.0	0.47	0.14	0.32 ± 0.02	2.33 ± 0.17
10.0	1.0	0.73	0.27	0.48 ± 0.04	1.78 ± 0.16
10.0	1.0	0.74	0.29	0.45 ± 0.03	1.55 ± 0.10
10.0	1.0	0.74	0.30	0.47 ± 0.02	1.56 ± 0.08
10.0	1.0	0.81	0.36	0.55 ± 0.06	1.53 ± 0.16
10.0	1.0	0.81	0.35	0.48 ± 0.02	1.35 ± 0.07
10.0	1.0	0.82	0.34	0.48 ± 0.01	1.41 ± 0.04
CSTR with SRT = 20 d					
20.0	1.0	0	0.02	0.08 ± 0.02	3.22 ± 0.15
20.0	1.0	0	0.02	0.07 ± 0.01	3.04 ± 0.27
20.0	1.0	0	0.02	0.08 ± 0.01	3.14 ± 0.41
20.0	1.0	0.80	0.18	0.38 ± 0.03	2.11 ± 0.17
20.0	1.0	0.87	0.19	0.50 ± 0.03	2.63 ± 0.18
20.0	1.0	0.88	0.19	0.50 ± 0.02	2.61 ± 0.13
AnMBR with SRT = 15 d					
15.0	1.5	0.50	0.11	0.31 ± 0.03	2.89 ± 0.31
15.0	1.5	0.49	0.12	0.35 ± 0.04	2.94 ± 0.35
15.0	1.5	0.68	0.11	0.27 ± 0.02	2.55 ± 0.23
15.0	1.5	0.72	0.17	0.33 ± 0.02	1.98 ± 0.15
15.0	1.5	0.82	0.26	0.52 ± 0.05	2.00 ± 0.21
15.0	1.5	0.90	0.29	0.49 ± 0.09	1.68 ± 0.30

Calculation of SF from provided data by Dereli *et al.* (2014b)

Table A 4. Calculation of SF from provided data by Dereli *et al.* (2014b)

	Reactor R 20	Reactor R 30	Calculation
SRT [d]	20	30	
B_{VS} [kg COD/(kg VSS·d)]	0.53	0.47	
COD removal [%]	73	80	
COD removal rate [kg $COD_{removed}$/(kg VSS·d)]	0.39	0.38	$= B_{VS} \cdot \frac{COD\ removal}{100\%}$
COD removal rate via acetate [kg $COD_{removed\ via\ acetate}$/(kg VSS·d)]	0.273	0.266	$= COD\ removal\ rate\ \cdot 0.7$
SMA [kg $COD_{removed\ via\ acetate}$/(kg VSS·d)]	0.42	0.45	from figure 6 (Dereli et al., 014b)
SF [-]	1.5	1.7	$= \frac{SMA}{COD\ removal\ rate\ via\ acetate}$

Data basis for comparison of different design approaches provided in Table 19

The relevant design parameter of each case is given in bold numbers. It is decisive for the sludge retention time in the digester respectively its required volume or its size.

Table A 5. Calculation of COD removal and outlet concentrations for a CSTR and AnMBR treating WAS and flotation sludge from a dairy industry at a Temperature of 37°C used for comparison of different design approaches

Parameter	Unit							
SRT	d	9	34	39	13	18	20	15
Design parameters								
Tech. Degree of degradation $\eta_{COD,\ degradable}$=1-$B_{COD,deg,out}/B_{COD,deg.,in}$	-	**0.80**	0.94	0.94	0.85	0.88	0.90	0.87
Degr. COD Loading rate	kg COD/ (m³·d)	10.7	**2.9**	2.5	7.4	5.4	5.9	6.4
FOG related loading rate[d]	kg VS_{FOG}/ (m³·d)	3.6	0.95	**0.83**	**2.5**	1.8	1.6	2.2
lipid related loading rate	kg VS_{li}/ (kg VS·d)	0.14	0.05	0.05	0.11	**0.09**	0.08	0.10
degradable lipid content of the anaerobic sludge	kg VS_{li}/ kg TS	0.16	0.06	0.06	0.13	0.11	**0.10**	0.11
Mass Balance Mixture								
Inflow Q_{in} $= Q_{WAS} + Q_{FS}$	m³/d	40	40	40	40	40	40	40
COD concentration inlet $= B_{COD,in}/Q_{in}$	g/L	118	118	118	118	118	118	118
TS concentration inlet $= B_{TS,in}/Q_{in}$	g/L	55	55	55	55	55	55	55
VS concentration inlet $= B_{VS,in}/Q_{in}$	g/L	48	48	48	48	48	48	48

Parameter	Unit							
SRT	d	9	34	39	13	18	20	15
inlet COD mass flow $B_{COD,in}$ $= B_{COD,WAS} + B_{COD,FS}$	kg/d	4,720	4,720	4,720	4,720	4,720	4,720	4,720
Inlet deg. COD mass flow $B_{COD,deg,in}$ $= B_{COD,deg,WAS} + B_{COD,deg,FS}$	kg/d	3,852	3,852	3,852	3,852	3,852	3,852	3,852
Inlet lipid load[e] $= B_{COD,WAS} \cdot c_{lipid,WAS} + B_{COD,FS} \cdot c_{lipid,FS}$	kg/d	1,230	1,230	1,230	1,230	1,230	1,230	1,230
inlet TS mass flow $B_{TS,in}$ $= B_{TS,WAS} + B_{TS,FS}$	kg/d	2,180	2,180	2,180	2,180	2,180	2,180	2,180
inlet VS mass flow $B_{VS,in}$ $= B_{VS,WAS} + B_{VS,FS}$	kg/d	1,920	1,920	1,920	1,920	1,920	1,920	1,920
COD removal η_{COD} $= 1 - (B_{COD,out}/B_{COD,in})$	-	0.60	0.73	0.74	0.65	0.68	0.69	0.65
Outflow sludge Q_{out}	m³/d	40	40	40	40	40	40	40
COD concentration in outflow $= B_{COD,out}/Q_{out}$	g/L	47	32	31	42	38	37	40
TS concentration in outflow $= B_{TS,out}/Q_{out}$	g/L	30	24	23	28	26	26	27
VS concentration in outflow $= B_{VS,out}/Q_{out}$	g/L	23	17	16	21	20	19	21
outlet COD mass flow $B_{COD,out}$ $= B_{COD,out,WAS} + B_{COD,out,FS}$	kg/d	1,875	1,289	1,231	1,663	1,521	1,470	1,610
outlet deg. COD mass flow $B_{COD,deg,out}$ $= B_{COD,deg,out,WAS} + B_{COD,deg,out,FS}$	kg/d	770	227	219	566	446	394	483
residual degradable lipid[e] $= B_{COD,WAS,deg.out} \cdot c_{lipid,WAS} + B_{COD,FS,deg} \cdot c_{lipid,FS}$	kg/d	201	57	56	146	113	102	124
outlet TS mass flow $B_{TS,out}$ $= B_{TS,out,WAS} + B_{TS,out,FS}$	kg/d	1,200	940	916	1,108	1,051	1,037	1,085
outlet VS mass flow $B_{VS,out}$ $= B_{VS,out,WAS} + B_{VS,out,FS}$	kg/d	940	683	656	848	791	777	825

Parameter	Unit							
SRT	d	9	34	39	13	18	20	15
WAS								
Inflow $Q_{in,WAS}$	m³/d	20	20	20	20	20	20	20
COD concentration WAS	g/L	48	48	48	48	48	48	48
TS concentration WAS	g/L	41	41	41	41	41	41	41
VS concentration WAS	g/L	31	31	31	31	31	31	31
COD/VS	g COD/g VS	1.55	1.55	1.55	1.55	1.55	1.55	1.55
COD mass flow WAS $B_{COD,WAS}$	kg/d	960	960	960	960	960	960	960
COD mass flow degradable	kg/d	432	432	432	432	432	432	432
TS mass flow WAS $B_{TS,WAS}$	kg/d	820	820	820	820	820	820	820
VS mass flow WAS $B_{VS,WAS}$	kg/d	620	620	620	620	620	620	620
COD removal[a] $\eta_{COD,WAS}$ $= \eta_{COD,max,WAS} \cdot k_{dis,WAS} \cdot SRT/(1 + k_{dis,WAS} \cdot SRT)$	-	0.28	0.39	0.40	0.33	0.35	0.36	0.34
degr. COD removal $\eta_{COD,deg.WAS}$ $= k_{dis,WAS} \cdot SRT/(1 + k_{dis,WAS} \cdot SRT)$	-	0.64	0.87	0.89	0.72	0.76	0.8	0.75
Biomass production[b] $P_{x,WAS}$ $= Y \cdot \eta_{COD,WAS} \cdot B_{COD,WAS}/(1 + k_{d,WAS} \cdot SRT)$	kg VS/d	15	13	12	12	15	15	16
outlet COD mass flow $B_{COD,out,WAS}$ $= (1 - \eta_{COD,WAS}) \cdot B_{COD,WAS} + P_{x,WAS} \cdot 1.42 kg\ COD/kg\ VS$	kg/d	715	604	593	660	645	635	657
outlet degr. COD mass flow $B_{COD,deg,out,WAS}$ $= \left(1 - \eta_{COD,deg,,WAS}\right) \cdot B_{COD,deg.,WAS}$	kg/d	155	56	48	121	104	86	108
outlet TS mass flow $B_{TS,out,WAS}$ $= (B_{TS,WAS} - B_{VS,WAS}) + B_{VS,out,WAS}$	kg/d	660	590	583	626	618	617	625
outlet VS mass flow $B_{VS,out,WAS}$ $= (1 - \eta_{COD,WAS}) \cdot B_{COD,WAS}/(COD/VS) + P_{x,WAS}$	kg/d	460	390	383	426	418	417	425

Parameter	Unit							
SRT	d	9	34	39	13	18	20	15
Flotation Sludge								
Inflow $Q_{in,FS}$	m³/d	20	20	20	20	20	20	20
COD concentration FS	g/L	188	188	188	188	188	188	188
TS concentration FS	g/L	68	68	68	68	68	68	68
VS concentration FS	g/L	65	65	65	65	65	65	65
COD/VS	g COD/g VS	2.9	2.9	2.9	2.9	2.9	2.9	2.9
COD mass flow FS $B_{COD,FS}$	kg/d	3,760	3,760	3,760	3,760	3,760	3,760	3,760
COD mass flow degradable	kg/d	3,420	3,420	3,420	3,420	3,420	3,420	3,420
TS mass flow FS $B_{TS,FS}$	kg/d	1,360	1,360	1,360	1,360	1,360	1,360	1,360
VS mass flow FS $B_{VS,FS}$	kg/d	1,300	1,300	1,300	1,300	1,300	1,300	1,300
COD removal[c] $\eta_{COD,FS}$ $= \eta_{COD,max,FS} \cdot k_{dis,FS} \cdot SRT/(1 + k_{dis,FS} \cdot SRT)$	-	0.75	0.86	0.87	0.79	0.82	0.83	0.80
degr. COD removal $\eta_{COD,deg.FS}$ $= k_{dis,FS} \cdot SRT/(1 + k_{dis,FS} \cdot SRT)$	-	0.82	0.95	0.95	0.87	0.90	0.91	0.89
Biomass production[b] $P_{x,FS}$ $= Y \cdot \eta_{COD,FS} \cdot B_{COD,FS}/(1 + k_{d,FS} \cdot SRT)$	kg VS/d	155	112	105	150	140	137	146
outlet COD mass flow $B_{COD,out,FS}$ $= (1 - \eta_{COD,FS}) \cdot B_{COD,FS} + P_{x,FS} \cdot 1.42 kg\ COD/kg\ VS$	kg/d	1,160	685	638	1,003	876	835	950
outlet degr. COD mass flow $B_{COD,deg,out,FS}$ $= \left(1 - \eta_{COD,deg,,FS}\right) \cdot B_{COD,deg.,FS}$	kg/d	615	171	171	445	342	308	375
outlet TS mass flow $B_{TS,out,FS}$ $= (B_{TS,FS} - B_{VS,FS}) + B_{VS,out,FS}$	kg/d	540	355	333	482	433	420	460
outlet VS mass flow $B_{VS,out,FS}$ $= (1 - \eta_{COD,FS}) \cdot B_{COD,FS}/(COD/VS) + P_{x,FS}$	kg/d	480	293	273	422	373	360	400

[a] $\eta_{COD,max,WAS}$ = 0.45; $k_{dis,WAS}$ = 0.20 d^{-1} (see Table 18)
[b] expression and constants Y=0.07 gVS/gCSB, k_d=0.03 d^{-1} according to Metcalf and Eddy (2004)
[c] $\eta_{COD,max,FS}$ = 0.91; $k_{dis,WAS}$ = 0.51 d^{-1} (see Table 18)
[d] assuming that flotation sludge can be classified as FOG as FOG is commonly used for food leftovers and is not only related to fats
[e] lipid content of WAS: 0.07 g /g COD_{in}; lipid content of flotation sludge: 0.31 g/ g CO_{in} (see Table 16)

Appendix D Investigations on critical flux

Backwash length and filtration length

Within the determination of the critical flux, backwashing times of 30 seconds were used, although in order to initiate a cleaning of the covering layer, these are not necessary in length. However, the membrane design limits the backwash in terms of pressure and pressure change. Even with a backwash, a maximum pressure of 0.5 bar must be maintained for this module and pressure surges should also be avoided, which is why backwash was carried out with a low back flux of 6.0 L/(m²·h) in this case. Backwash times between 10 and 60 seconds were studied to test a minimum backwash duration required at a duration of the filtration cycle of 8 minutes. The Figure A 3 shows the TMP profile at a constant flux operated at the critical flux of 6 L/(m²·h) over the duration of the filtration. It turns out that with backwash times of 30 and 60 seconds, the transmembrane pressure remains constant at the end of the filtration and no increase is evident. Increases of TMP at the end of filtration over cycles occur at backwash times of 10 and 15 seconds and indicate an incomplete removal of the cake layer on the membrane surface during the backwash step. Therefore, a minimum backwash duration of 15 seconds is recommended when filtrating at J_{crit}. From this, the net flux for the examined settings according to *Judd* (2011) can be determined as follows

$$J_{net} = J_{gross} \cdot \frac{t_{filtration} - t_{backwash}}{t_{filtration} + t_{backwash}} = 0.94 \cdot J_{gross}$$

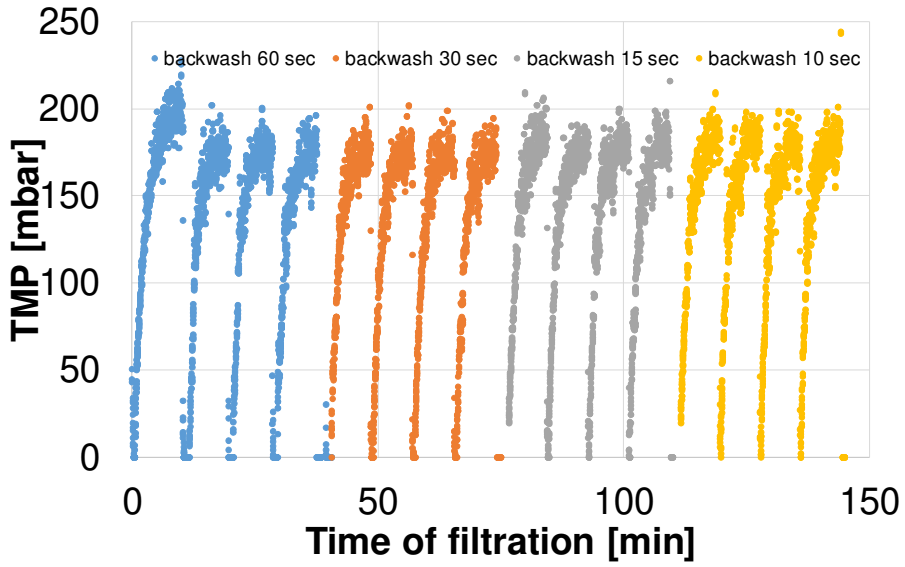

Figure A 3. TMP over time during cake buildup after different backwash length by filtration of PS2 with a TS = 3.8 % at J_{crit} = 6 L/(m²·h)

Consideration of the temperature when determining the dynamic viscosity

Moshage (2004) determines the change of the dynamic viscosity as a function of the temperature for digested sludge as follows

$$\eta_{a,Tx} = \eta_{T=20°C} \cdot e^{-0.0142 \cdot (T_x - 20)}$$

Where, γ: shear rate (1/s)

$\eta_{a,Tx}$: apparent dynamic viscosity at Temperature T = x°C (Pa·s)

$\eta_{a,T=20°C}$: apparent dynamic viscosity at T = 20°C (Pa·s)

b: empirical parameter; b = 0.0142 °C^{-1}

T_x: Temperature x [°C]

Own measurements show a similar dependence for digested sludge at different shear rates (figure below) and confirm results of *Moshage* (2004). In this work, the parameter b according to *Moshage* (2004) is used for temperature compensation, because it is based on more data compared to own measurements.

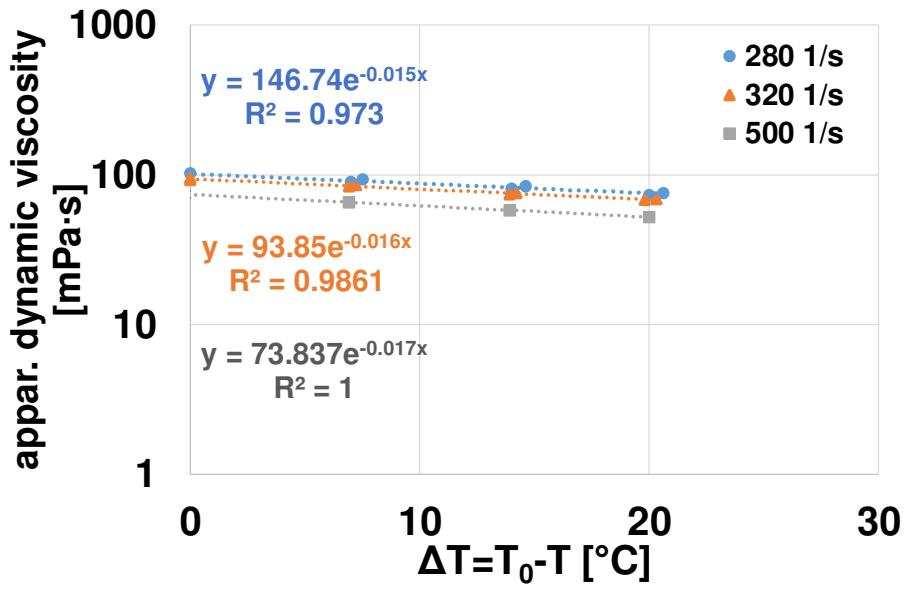

Figure A 4. Apparent dynamic viscosity as a function of temperature differences with T = 25 °C under different shear rates

Sludge characterisation of samples for critical flux determination

Table A 6. Sludge characterisation of samples for critical flux determination

				Data from flow curves			
WWTP	TS	VS	Std. dyn. Viscosity[1]	Consistency factor K	Flow exponent m	R^2	CST
#	%	%	mPa·s	mPa·s	-		s
	2.1	1.4	10.2±0.2	108	0.61	0.97	85±6
LS_1	2.5	1.7	11.6±0.8	124	0.61	0.89	161±9
	3.0	2.0	19.6±0.9	382	0.52	0.96	182±7

				Data from flow curves			
WWTP	TS	VS	Std. dyn. Viscosity[1]	Consistency factor K	Flow exponent m	R^2	CST
#	%	%	mPa·s	mPa·s	-		s
	3.5	2.4	27.7±1.7	512	0.53	0.95	454±17
	2.1	1.3					
	2.4	1.5	10.6±0.3	131	0.57	0.95	47±3
	3.1	1.9	22.3±0.4	554	0.46	0.98	97±25
	3.4	2.1	27.2±0.9	759	0.44	0.98	140±5
	3.2	1.9	21.3±0.5	589	0.44	0.98	63±4
	3.6	2.2	31.7±0.5	714	0.44	0.99	88±4
	3.5	2.2	30.2±3.5	656	0.48	0.89	81±1
	3.5	2.1	25.0±0.4	714	0.44	0.99	115±7
	4.0	2.5	39.4±1.5	1,592	0.38	0.97	175±21
	4.5	2.8	62.6±1.0	2,962	0.35	0.99	268±4
	2.1	1,3	9.5±0.4	96	0.62	0.94	104±5
	2,5	1,6	13.1±0.8	164	0.59	0.94	227±9
	2,9	1,9	16.9±0.6	205	0.60	0.95	367±24
	3,6	2,3	29.0±0.8	620	0.50	0.99	458±7
	2,2	1,4	11.3±0.8	228	0.51	0.95	115±18
LS_2b	2,7	1,8	17.2±0.4	362	0.50	0.99	202±34
	3,1	1,9	18.6±0.8	318	0.54	0.96	421±13
	3,7	2,4	31.1±2.0	791	0.48	0.96	525±26
	2,2	1,4	11.0±0.7	167	0.55	0.93	113±10
	2.8	1,8	17.8±0.8	368	0.51	0.96	200±4
	2,9	1,9	15.6±0.8	232	0.56	0.96	464±42
	3,8	2,4	32.2±0.9	905	0.46	0.98	581±25
	2,3	1,5	10.9±0.6	117	0.61	0.90	187±12
	2,7	1,8	16.5±0.3	243	0.55	0.98	277±23
	3,5	2,3	32.0±1.1	943	0.44	0.98	540±59
	2,3	1,5	12.1±0.8	158	0.58	0.93	146±5
	2,7	1,8	18.2±0.4	305	0.53	0.97	288±11
LS_2a	3,1	2,0	25.1±0.6	593	0.48	0.99	370±42
	3,7	2,4	37.8±1.6	1,284	0.42	0.98	547±21
	2,2	1,4	11.4±0.4	156	0.57	0.94	112±8
	2,5	1,6	14.1±0.2	227	0.53	0.94	220±20
	3,3	2,2	27.9±1.5	782	0.44	0.97	373±15
	4,0	2,7	46.6±1.3	1,722	0.40	0.97	695±53
	3,5	2,0	20.3±1.2	394	0.52	0.95	388±7
	3,8	2,2	24.1±0.6	539	0.50	0.96	501±18
	4,5	2,6	35.1±1.7	1,179	0.43	0.97	823±25
	3,3	1,9	17.4±1.1	344	0.52	0.93	387±24
	3,8	2,2	28.6±2.0	762	0.47	0.93	488±31
	4,5	2,6	37.2±1.4	1,240	0.43	0.98	973±47
	3,4	2,0	19.4±1.2	419	0.50	0.89	363±12
	3,8	2,3	26.3±0.5	628	0.49	0.98	493±12
	4,4	2,6	36.9±1.2	1,180	0.44	0.98	971±8
	3,4	2,0	18.5±0.9	434	0.49	0.95	368±10
LS_3	3,2	1,8	13.7±0.3	224	0.54	0.91	349±8

				Data from flow curves			
WWTP	TS	VS	Std. dyn. Viscosity[1]	Consistency factor K	Flow exponent m	R^2	CST
#	%	%	mPa·s	mPa·s	-		s
	3,3	1,9	15.9±0.2	286	0.53	0.97	357±21
	3,2	1,9	14.8±0.5	154	0.62	0.91	381±18
LS_4	2,8	1,7	17.2±0.3	385	0.49	0.96	396±22
	3,3	2,0	26.4±1.0	756	0.46	0.97	610±42
	4,0	2,4	42.6±1.8	1,648	0.41	0.98	762±28
	4,4	2,6	54.8±0.5	2,246	0.40	0.99	1,090±85
	2,9	1,7	19.7±0.2	377	0.52	0.97	348±35
	3,3	2,0	25.5±0.4	714	0.46	0.99	495±21
	3,8	2,3	36.0±1.8	1,168	0.44	0.97	733±23
	4,4	2,7	58.0±0.9	2,472	0.39	0.99	1,040±57
PS_1	2,7	1,6	15.6±0.5	237	0.56	0.97	376±40
	3,3	2,0	25.0±0.5	612	0.48	0.99	513±40
	4,0	2,4	43.5±0.5	1,478	0.43	0.99	751±33
	4,3	2,6	54.3±1.0	2,073	0.41	0.99	1,027±50
	2.4	1.5	12.0±0.4	311	0.46	0.80	282±73
	2.9	1.8	18.1±0.4	347	0.52	0.94	422±52
	3.5	2.2	31.3±3.8	657	0.51	0.89	542±13
	3.6	2.3	31.3±0.6	792	0.48	0.99	513±28
	2.3	1.4	10.1±0.5	95	0.63	0.85	287±13
	2.8	1.8	16.8±0.2	193	0.61	0.92	387±31
	3.5	2.2	31.7±0.6	773	0.50	0.89	510±27
	3.8	2.4	34.9±2.3	965	0.46	0.96	547±42
PS_5	2.4	1.5	11.4±0.6	87	0.67	0.87	283±15
	3.1	1.9	20.3±1.2	322	0.55	0.93	432±60
	3.6	2.3	35.9±1.9	1,122	0.44	0.97	500±69
	4.0	2.5	41.3±1.2	1,292	0.44	0.99	542±7
	2.3	1.6	12.9±0.5	99	0.67	0.91	615±67
	2.5	1.7	14.5±0.5	130	0.64	0.91	723±24
	2.8	2.0	19.7±0.9	208	0.62	0.91	866±99
	3.1	2.2	25.5±1.4	378	0.56	0.95	1,103±132
	2.1	1.4	9.9±0.6	83	0.65	0.87	149±5
	2.5	1.8	14.4±0.8	153	0.62	0.94	459±17
	2.9	2.0	19.8±0.4	249	0.59	0.95	740±11
	3.4	2.4	28.2±0.9	538	0.52	0.98	1,010±56
	2.0	1.4	n.d.	n.d.	n.d.	n.d.	n.d.
	2.4	1.7	9.3±4.6	119	0.61	0.95	369±53
	2.7	1.9	15.3±0.3	146	0.63	0.96	853±30
	3.8	2.7	32.0±0.4	856	0.47	0.99	1,135±118

[1] Standard conditions with shear rate = 500 s^{-1} and T = 20°C were applied according to Moshage (2004); values are measuring data and not calculated data using K and m;

Appendix E Economical comparison of AnMBR and CSTR

Data of energy consumption of membrane module in pilot scale

Table A 7. Data of energy consumption of membrane module in pilot-scale

membrane rotation rpm	TS %	number of samples n -	energy consumption of module kWh_{el}	Time period of investigation d	Note
280	3.48±0.14	24	2.8	42	used for calculation in Table 28
320	3.47±0.18	14	3.5	30	used for calculation in Table 28
350	2.11±0.10	6	3.4	21	
350	2.99±0.29	11	3.5	15	
350	3.51±0.14	11	3.9	19	used for calculation Table 28
350	3.76±0.15	14	4.0	23	
350	3.85±0.25	17	3.9	30	
350	3.95±0.15	6	4.2	9	
350	4.16±0.21	12	4.1	17	
350	4.17±0.08	10	4.2	13	
350	4.41±0.05	7	5.0	10	
350	4.51±0.18	3	4.6	8	
350	4.57±0.28	7	5.0	15	
350	4.60±0.16	6	4.9	16	
350	4.89±0.11	8	5.1	15	
350	4.95±0.35	5	5.3	10	
350	5.55±0.08	5	6.6	8	

Calculation of COD removal and methane flow for a CSTR and AnMBR treating WAS

Table A 8. Calculation of COD removal and methane flow for a CSTR and AnMBR treating WAS at a Temperature of 37°C

Parameter	Unit	CSTR		AnMBR	
HRT | SRT	d|d	15 | 15	20 | 20	10 | 15	15 | 20
Inflow Q_{in}	m³/d	100	100	100	100
COD concentration inlet	g/L	48	48	48	48
TS concentration inlet	g/L	41	41	41	41
VS concentration inlet	g/L	31	31	31	31
COD/VS	g COD/g VS	1.55	1.55	1.55	1.55
inlet COD mass flow $B_{COD,in}$	kg/d	4,800	4,800	4,800	4,800
inlet TS mass flow $B_{TS,in}$	kg/d	4,100	4,100	4,100	4,100
inlet VS mass flow $B_{VS,in}$	kg/d	3,100	3,100	3,100	3,100
COD removal[a] η_{COD} $= \eta_{COD,max} \cdot k_{dis} \cdot SRT/(1 + k_{dis} \cdot SRT)$	-	0.34	0.36	0.34	0.36
Methane flow Q_{CH4} $= B_{COD,in} \cdot \eta_{COD} \cdot 0.35 m^3/kg\ COD$	m³/d	567	605	567	605

COD-methane $B_{COD,CH4}$ $= Q_{CH4}/(0.35m^3/kg\ COD)$	kg COD/d	1,620	1,728	1,620	1,728
Biomass production[b] P_x $= Y \cdot B_{COD,CH4}/(1 + k_d \cdot SRT)$	kg VS/d	78	76	78	76
Outflow sludge Q_{out}	m³/d	100	100	67	75
Outflow filtrate $Q_{filtrate}$	m³/d	-	-	33	25
COD concentration in outflow $= B_{COD,out}/Q_{out}$	g/L	33	32	49	42
TS concentration in outflow $= B_{TS,out}/Q_{out}$	g/L	31	31	47	41
VS concentration in outflow $= B_{VS,out}/Q_{out}$	g/L	21	21	32	27
outlet COD mass flow $B_{COD,out}$ $= B_{COD,in} - B_{COD,CH4} + P_x \cdot 1.42kg\ COD/kg\ VS$	kg/d	3291	3180	3291	3180
outlet TS mass flow $B_{TS,out}$ $= (B_{TS,in} - B_{VS,in}) + B_{VS,out}$	kg/d	3130	3058	3130	3058
outlet VS mass flow $B_{VS,out}$ $= (B_{COD,in} - B_{COD,CH4})/(COD/VS) + P_x$	kg/d	2130	2058	2130	2058

[a] $\eta_{COD,max}$ = 0.45; k_{dis} = 0.20 d^{-1} (see Table 18)
[b] expression and constants Y=0.07 gVS/gCSB, k_d=0.03 d^{-1} according to Metcalf and Eddy (2004)

Calculation of specific costs for digesters according to AbwAnlZuwV HE (2006)

First the conversion of the reactor volumes into person equivalents of a corresponding digestion on municipal sewage treatment plant is carried out. It was assumed that 1 population equivalent (PE) requires approximately 0.0375 m³ of digestion volume. This was calculated as follows:

$$\frac{V_{reactor}}{1PE} = \frac{m'_{PE} \cdot SRT}{c_{TS}} = \frac{60g\ TS/(PE \cdot d) \cdot 25d}{40g\ TS/L} = 0.0375m^3/PE$$

Where, m'_{PE}: generated TS per person [g TS/(PE·d)]; = 60 g TS/(PE·d) (DWA-M 368, 2014)

c_{TS}: TS concentration inflow [g TS/L]; = 40 g/L assumed

SRT: Sludge retention time [d]; =25 d (DWA-M 368, 2014)

Specific costs of the digester can be calculated with the cost functions according to AbwAnlZuwV HE (2006) as follows

$$\text{Specific costs} = 450 \cdot X^{-0.23}$$

Where, specific costs: PE related digesters costs [€/PE]

PE: Population equivalent [PE]

Volume related digester costs can be calculated by combining both expressions

$$\text{Specific costs} = \frac{450 \cdot X^{-0.23}}{0.0375m^3/PE}$$

Calculation of COD removal and methane flow for a CSTR and AnMBR treating WAS and flotation sludge from dairy industry

Table A 9. Calculation of COD removal, methane flow and outlet concentrations for a CSTR and AnMBR treating WAS and flotation sludge from a dairy industry at a T=37°C

Parameter	Unit	CSTR		AnMBR	
HRT | SRT	d | d	15 | 15	20 | 20	12 | 15	15 | 20
Total					
Inflow Q_{in} $= Q_{WAS} + Q_{FS}$	m³/d	40	40	40	40
COD concentration inlet $= B_{COD,in}/Q_{in}$	g/L	118	118	118	118
TS concentration inlet $= B_{TS,in}/Q_{in}$	g/L	55	55	55	55
VS concentration inlet $= B_{VS,in}/Q_{in}$	g/L	48	48	48	48
inlet COD mass flow $B_{COD,in}$ $= B_{COD,WAS} + B_{COD,FS}$	kg/d	4,720	4,720	4,720	4,720
inlet TS mass flow $B_{TS,in}$ $= B_{TS,WAS} + B_{TS,FS}$	kg/d	2,180	2,180	2,180	2,180
inlet VS mass flow $B_{VS,in}$ $= B_{VS,WAS} + B_{VS,FS}$	kg/d	1,920	1,920	1,920	1,920
COD removal η_{COD} $= (B_{COD,CH4}/B_{COD,in})$	-	0.71	0.73	0.71	0.73
Methane flow Q_{CH4} $= Q_{CH4,WAS} + Q_{CH4,FS}$	m³/d	1,174	1,211	1,174	1,211
COD-methane $B_{COD,CH4}$ $= Q_{CH4}/(0.35m^3/kg\ COD)$	kg COD/d	3,346	3,466	3,346	3,466
Biomass production[b] P_x $= P_{x,WAS} + P_{x,FS}$	kg VS/d	162	152	162	152
Outflow sludge Q_{out}	m³/d	40	40	32	30
Outflow filtrate $Q_{filtrate}$	m³/d	-	-	8	10
COD concentration in outflow $= B_{COD,out}/Q_{out}$	g/L	40	37	50	49
TS concentration in outflow $= B_{TS,out}/Q_{out}$	g/L	27	26	34	35
VS concentration in outflow $= B_{VS,out}/Q_{out}$	g/L	21	19	26	26
outlet COD mass flow $B_{COD,out}$ $= B_{COD,out,WAS} + B_{COD,out,FS}$	kg/d	1,610	1,470	1,610	1,470
outlet TS mass flow $B_{TS,out}$ $= B_{TS,out,WAS} + B_{TS,out,FS}$	kg/d	1,085	1,037	1,085	1,037
outlet VS mass flow $B_{VS,out}$ $= B_{VS,out,WAS} + B_{VS,out,FS}$	kg/d	825	777	825	777
WAS					
Inflow $Q_{in,WAS}$	m³/d	20	20	20	20
COD concentration WAS	g/L	48	48	48	48

Parameter	Unit	CSTR		AnMBR	
HRT | SRT	d | d	15 | 15	20 | 20	12 | 15	15 | 20
TS concentration WAS	g/L	41	41	41	41
VS concentration WAS	g/L	31	31	31	31
COD/VS	g COD/g VS	1.55	1.55	1.55	1.55
COD mass flow WAS $B_{COD,WAS}$	kg/d	960	960	960	960
TS mass flow WAS $B_{TS,WAS}$	kg/d	820	820	820	820
VS mass flow WAS $B_{VS,WAS}$	kg/d	620	620	620	620
COD removal[a] $\eta_{COD,WAS}$ $= \eta_{COD,max,WAS} \cdot k_{dis,WAS} \cdot SRT/(1 + k_{dis,WAS} \cdot SRT)$	-	0.34	0.36	0.34	0.36
Methane flow $Q_{CH4,WAS}$ $= B_{COD,WAS} \cdot \eta_{COD,WAS} \cdot 0.35 m^3/kg\ COD$	m³/d	114	121	114	121
COD-methane $B_{COD,CH4,WAS}$ $= Q_{CH4,WAS}/(0.35 m^3/kg\ COD)$	kg COD/d	326	346	326	346
Biomass production[b] $P_{x,WAS}$ $= Y \cdot B_{COD,CH4,WAS}/(1 + k_{d,WAS} \cdot SRT)$	kg VS/d	16	15	16	15
outlet COD mass flow $B_{COD,out,WAS}$ $= B_{COD,WAS} - B_{COD,CH4,WAS} + P_{x,WAS} \cdot 1.42 kg\ COD/kg\ VS$	kg/d	657	635	667	635
outlet TS mass flow $B_{TS,out,WAS}$ $= (B_{TS,WAS} - B_{VS,WAS}) + B_{VS,out,WAS}$	kg/d	625	617	625	617
outlet VS mass flow $B_{VS,out,WAS}$ $= (B_{COD,WAS} - B_{COD,CH4,WAS})/(COD/VS) + P_{x,WAS}$	kg/d	425	417	425	417
Flotation Sludge					
Inflow $Q_{in,FS}$	m³/d	20	20	20	20
COD concentration FS	g/L	188	188	188	188
TS concentration FS	g/L	68	68	68	68
VS concentration FS	g/L	65	65	65	65
COD/VS	g COD/g VS	2.9	2.9	2.9	2.9
COD mass flow FS $B_{COD,FS}$	kg/d	3,760	3,760	3,760	3,760
TS mass flow FS $B_{TS,FS}$	kg/d	1,360	1,360	1,360	1,360
VS mass flow FS $B_{VS,FS}$	kg/d	1,300	1,300	1,300	1,300
COD removal[c] $\eta_{COD,FS}$ $= \eta_{COD,max,FS} \cdot k_{dis,FS} \cdot SRT/(1 + k_{dis,FS} \cdot SRT)$	-	0.80	0.83	0.80	0.83
Methane flow $Q_{CH4,FS}$ $= B_{COD,FS} \cdot \eta_{COD,FS} \cdot 0.35 m^3/kg\ COD$	m³/d	1,060	1,090	1,060	1,090
COD-methane $B_{COD,CH4,FS}$ $= Q_{CH4,FS}/(0.35 m^3/kg\ COD)$	kg COD/d	3,020	3,120	3,020	3,120
Biomass production[b] $P_{x,FS}$ $= Y \cdot B_{COD,CH4,FS}/(1 + k_{d,FS} \cdot SRT)$	kg VS/d	146	137	146	137
outlet COD mass flow $B_{COD,out,FS}$ $= B_{COD,FS} - B_{COD,CH4,FS} + P_{x,FS} \cdot 1.42 kg\ COD/kg\ VS$	kg/d	950	835	950	835
outlet TS mass flow $B_{TS,out,FS}$ $= (B_{TS,FS} - B_{VS,FS}) + B_{VS,out,FS}$	kg/d	460	420	460	420
outlet VS mass flow $B_{VS,out,FS}$ $= (B_{COD,FS} - B_{COD,CH4,FS})/(COD/VS) + P_{x,FS}$	kg/d	400	360	400	360

[a] $\eta_{COD,max,WAS}$ = 0.45; $k_{dis,WAS}$ = 0.20 d^{-1} (see Table 18)
[b] expression and constants Y=0.07 gVS/gCSB, k_d=0.03 d^{-1} according to Metcalf and Eddy (2004)
[c] $\eta_{COD,max,FS}$ = 0.91; $k_{dis,WAS}$ = 0.51 d^{-1} (see Table 18)

Zum Autor:

Herr Robert Lutze hat an der Technischen Universität Berlin „Technischer Umweltschutz“ studiert. Nach seinem Abschluss als Diplom-Ingenieur im Jahr 2008 war er als Projektingenieur in der Abteilung Forschung & Entwicklung der EnviroChemie GmbH tätig und befasste sich in den kommenden Jahren schwerpunktmäßig mit biologischen Verfahren zur Industrieabwasserreinigung. Von 2013 bis 2019 war Robert Lutze wissenschaftlicher Mitarbeiter an der Technischen Universität Darmstadt, Fachgebiet Abwassertechnik des Instituts IWAR. Hier forschte er zu anaeroben Membranbioreaktoren zum Einsatz in der Klärschlammbehandlung im Kontext einer bedarfsgerechten Biogaserzeugung. Im Rahmen dieser Untersuchungen entstand die vorliegende Dissertation.

Zum Inhalt:

Der schonende Umgang mit den weltweit verfügbaren Ressourcen ist eine zentrale Herausforderung für Wirtschaft und Gesellschaft. Eine Mitbehandlung der bei der industriellen Abwasserreinigung (insbesondere der Lebensmittelverarbeitung) anfallenden Schlämme in einer anaeroben Faulung zur Biogaserzeugung vor Ort anstelle einer externen Entsorgung kann energetische Vorteile bieten.

Der Betrieb einer anaeroben Faulung mit großen Anteilen von Flotatschlamm, welcher vor allem aus Lipiden besteht, ist jedoch eine Herausforderung und wesentlicher Untersuchungsgegenstand dieser Studie. Abweichend von konventionellen Faulungen als Durchlaufreaktoren zur Schlammbehandlung, können anaerobe Membranbioreaktoren (AnMBRs) eine nachhaltige technologische Lösung bei der Schlammfaulung fettreicher Substrate auf industriellen Kläranlagen darstellen. Sie ermöglichen einen weitgehenden Abbau organischer Substanz und eine ausreichende Prozessstabilität bei reduziertem Reaktorvolumen.

In dieser Studie wurden die Kinetik des biologischen Abbauprozesses und die Prozessgrenzen bei Behandlung von fetthaltigen Substraten in einem anaeroben Membranbioreaktor im Vergleich mit konventionellen Faulungen in Ausschwemmreaktoren untersucht. Die Auswirkungen der Scherbeanspruchung durch den Membranbetrieb auf die Biomasseaktivität und die Membranleistung wurden ebenfalls betrachtet. Dimensionierungshilfen beim Einsatz fetthaltiger Substrate und wirtschaftliche Einsatzbereiche von AnMBRs zur Schlammbehandlung wurden abgeleitet.

ISBN 978-3-940897-69-5